FORCED CONVECTION HEAT TRANSFER TO WATER WITH AIR INJECTION THROUGH ONE POROUS HEATED WALL OF A RECTANGULAR DUCT

Grant Earl Sims

1969

Imperial College of Science and Technology

ABSTRACT

A study was made of forced convection heat-transfer to water and air-water mixtures in a horizontal rectangular duct with air injection through one porous heated wall. The main independent variables were the rate of air injection through the porous wall, the liquid velocity in the duct and the amount of air mixed with the water upstream of the heated test section; the method of mixing the upstream air and water was also varied. The dependent variables reported were the heat-transfer coefficient and the flow pattern.

The conditions analyzed here were those for which the heat-transfer coefficient increased with increasing rate of air injection through the porous heat-transfer surface (analogous in saturated nucleate boiling to the heat-transfer coefficient increasing with vapour formation rate, i.e. with heat flux). For these conditions, the heat-transfer coefficients were correlated using the concept (analogous to Chen's for forced-convection saturated boiling) that the heat-transfer coefficient was comprised of two contributions, one associated with the forced convection flow and one with the bubbling at the heat-transfer surface. The quantities appearing in the correlating equation were found empirically.

As part of this study, a quantitative comparison of the heat-transfer coefficients in pool barbotage and saturated nucleate pool boiling was presented. This comparison took into account the

vapour formation rate near the heating surface in boiling and the absence of "latent heat transport" in barbotage. A "heat-transfer-coefficient-through-the-liquid" α_f was defined which took into account the same mechanisms in boiling and barbotage. It was concluded that, at the same dimensionless vapour/gas flow rates, the dimensionless α_f in boiling and barbotage were closely comparable in magnitude.

ACKNOWLEDGMENTS

The author gratefully acknowledges the help he has received over the course of this investigation, especially from the following persons: Professor B. W. Martin, formerly of Imperial College and now at The University of Wales Institute of Science and Technology, the author's supervisor without whose guidance and encouragement this work would not have been possible; Professor D. B. Spalding who suggested the problem and offered advice at many stages; Mr. D. G. Martin of Imperial College, Dr. B. W. A. Ricketson and Mr. A. T. Jeffs of the Rocket Propulsion Establishment with whom many valuable discussions were held.

I am especially grateful to the Ministry of Aviation for financial support during this study.

Thanks are due also to Mr. Kasi Nathan for help in constructing the apparatus.

TABLE OF CONTENTS

LIST OF FIGURES

LIST OF TABLES

NOMENCLATURE

a	Height of channel normal to heated surface, ft
a'	Empirical constant, see equation (D.37)
A	Area, ft^2
A_R	Aspect ratio, defined in Section 6.3
b	Width of channel and of heated surface, ft
b'	Empirical constant, see equation (D.37)
B	Empirical constant, see equations (6.45) and (6.46)
C	Coefficient of discharge for orifice
C_D	Correction for pipe size (orifice calculation)
C_p	Specific heat at constant pressure, Btu/lb degF
C_{Re}	Correction for Reynolds number (orifice calculation)
d	Diameter of tube, ft
d_e	Equivalent diameter of flow channel, defined in equation (6.3), ft
d_{or}	Diameter of orifice, ft or in.
d_{pipe}	Diameter of pipe in which orifice was installed, ft
D	Bubble diameter, ft
E	Velocity of approach factor, see beneath equation (E.2)
E	DC emf in any thermocouple signal, μV
E_{ac}	AC emf in any thermocouple signal, V
E_{dc}	DC emf in any thermocouple signal, μV
E_{ref}	DC emf at the terminals of the two reference wires, μV

E_{std}	Voltage read on standard voltmeter, V
E_{th}	Thermal emf in any thermocouple signal, μV
ΔE	Voltage drop between two points on heater Δx apart in distance, V
$\Delta E_{overall}$	Overall voltage drop between the two ends of the heater, V
f	Frequency of bubble formation, 1/h
F	Upstream turbulence factor
F_C	Reynolds number factor (of Chen)
F_E	Ratio of the local to the overall heat generation rate
F_v	Vapour content of air and vapour mixture, lb vapour/lb air
Fr^*	Special form of Froude number, defined in equation (6.42)
g	Acceleration due to gravity, ft/h^2
g_o	Constant in Newton's Second Law of Motion, 4.17×10^8 lb ft/lbf h^2
G	Mass velocity, lb/ft^2h
h	Enthalpy, Btu/lb
h	Pressure drop across orifice, in. water
h_{fg}	Latent heat of vaporization, Btu/lb
I	Current in the porous heater, amps
I_{std}	Current read on standard ammeter, amps
k	Thermal conductivity, Btu/ft h degF
K	Flow coefficient (orifice calculation), defined above equation (E.3)
K_T	Dimensionless group used in correlating saturated nucleate pool boiling data, defined in equation (6.29)

K_T^*	Dimensionless group used in correlating barbotage data, defined in equation (6.35)
Ku	Kutateladze number, defined in equation (2.24)
Ku^*	Modified form of the Kutateladze number, defined in equation (2.34)
L	Length of porous heater, ft
m	Orifice constant, defined beneath equation (E.2)
$\dot{m}$	Mass flow rate, lb/h
$\dot{m}''$	Mass flux, lb/ft^2h
M	Used for convenience, defined in equation (D.25)
n	Number of bubble sources on the heating surface
N_1	Dimensionless group, defined in equation (2.46)
Nu_{SP}	Single-phase Nusselt number, defined in equation (6.2)
Nu_{bub}^*	Special form of Nusselt number, defined in equation (6.32)
$Nu_{bub,f}^*$	Special form of Nusselt number, defined in equation (6.40)
Nu_f^*	Special form of Nusselt number, defined in equation (2.41)
Nu_{tot}^*	Special form of Nusselt number, defined in equation (2.43)
p	Porosity, defined in Table 2.4
P	Pressure, psi
Pr	Prandtl number
ΔP_{chan}	Pressure drop in the flow channel between inlet to, and exit from, the porous heated section, psi
$\dot{q}''$	Heat flux, Btu/ft^2h

$\dot{q}''_{net}$	Net heat flux, defined in equation (D.32), Btu/ft^{2}h
$\dot{q}'''$	Volumetric heat generation rate, Btu/ft^{3}h
Q	Volumetric flow rate, ft^3/h
R	Result, as used in Section E.1
Re	Reynolds number, defined in equation (6.4)
R_{ref}	Resistance of the heater between the two reference wires, ohms
R_{TC}	Resistance of the heater between the points of electrical contact of the two wires of a thermocouple
Re_{or}	Reynolds number based on orifice diameter (orifice calculation)
S	Suppression factor (of Chen)
S_α	Empirical constant, see equation (D.37)
T	Temperature, °F
u	Velocity, ft/h or ft/s
v	Variable, as used in Section E.1
V	Volume of bubble, ft^3
$\dot{V}''_g$	Barbotage-rate or gas volume injected through porous heater per unit time and unit heater area, ft^3/ft^{2}h or ft^3/ft^{2}s
W	Mass flow rate, lb/h
x	Position along heater, ft
X_{tt}	Martinelli flow parameter, defined in equation (6.8)
y	Distance from the heating surface, ft

y_F Thickness of the liquid film at the base of a bubble in boiling, in.

y_T Thermal boundary layer thickness, in.

Y Proportionality constant used in estimating the evaporation correction to the heat flux

z Distance through the porous heater, ft

Z Factor in orifice calculation, defined beneath equation (E.2)

Greek Symbols

α Heat-transfer coefficient, Btu/ft^{2}h degF

$\bar{\alpha}$ Mean heat-transfer coefficient, Btu/ft^{2}h degF

β Volumetric quality

γ Latent heat fraction, defined in equation (2.18)

δ Thickness of the porous heater, ft

ε Correction for expansion (orifice calculation)

ζ Ratio of the heat-transfer-coefficient-through-the-liquid to the total heat-transfer coefficient in boiling, see equation (2.12)

μ Dynamic viscosity, lb/ft h

μ_R Ratio of liquid viscosities evaluated at bulk temperature to that evaluated at wall temperature

ρ Density, lb/ft^3

$\rho_{k=0}$ Density of porous material when $k_{eff} = 0$, lb/ft^3

ρ_{or} Gas density at the high-pressure orifice tapping, lb/ft^3

σ	Surface tension, lbf/ft
Ψ	Bubble effectiveness factor
Ψ_o	Bubble effectiveness factor for zero inlet-quality tests
Ψ^+	Ratio Ψ/Ψ_o
ω	Product of bubble break-off diameter and frequency, ft/h
ω	Uncertainty interval, as used in Section E.1

Subscripts

a	Air
A	Conditions at the A-surface (a plane an arbitrary distance above the heating surface)
ac	Electrical ac current or potential
app	Apparent
b	Bubble break-off conditions
B	Bulk conditions
bub	Maximum obtainable due to bubbling for fixed fluid properties and bubbling rate
cr	Critical
D	Conditions at one bubble-detachment height above heating surface
dc	Electrical dc current or potential
diff	Indicates diffusion mechanism
e	Conditions at exit from the heated porous section
eff	Effective, based on bulk volume

elec	Electrical
f	Refers to heat transfer, or heat-transfer coefficient, through the liquid
f	Liquid
g	Gas (barbotage) or vapour (boiling)
i	Conditions at inlet to the heated porous section
in	Conditions on entering the control volume
LH	Refers to mechanism of latent heat transport
mac	Due to macroconvection
mean	Conditions at the mean pressure and mean bulk temperature within the heat-transfer section
meas	Measured
Metal	Refers to solid metal
mic	Due to microconvection
o	Refers to tests with zero inlet-quality
O	Conditions at the O-surface (bottom face of porous element)
out	Conditions on leaving the control volume
p	Projected (area)
PB	Pool boiling
plen	Conditions in the plenum chamber
pred	Predicted
S	Conditions at the S-surface (solid-liquid interface)
sat	Refers to saturation vapour content

SP	Single phase
T	Total cross-section
tot	Total (for heat transfer and heat-transfer coefficient)
TP	Two phase, but restricted to conditions of zero barbotage and finite inlet-quality
tr	Transition condition beyond which any finite barbotage-rate causes a reduction in the heat-transfer coefficient
v	Vapour
x	Local value (along the porous heater)
∞	Conditions at some very large distance from the heating surface
1,2,3,4	Refers to various locations in the flow circuitry, see Fig. 3.2

CHAPTER 1 INTRODUCTION

1.1 Background

Boiling heat transfer is a very important method of heat removal, particularly in systems, such as nuclear reactors and liquid propellant rocket motors, which involve high heat-flux densities. However, boiling is a complex phenomenon affected by many variables [94].

Because of this complexity, several authors [1,27,28,49,63] have sought to improve the understanding of heat transfer across bubble-stirred boundary layers by simulating nucleate boiling using "barbotage" or electrolysis to produce bubbles on the heat-transfer surface. (The term "barbotage" used here is defined as the bubbling of a gas through a drilled or porous heat-transfer surface into a liquid.) Barbotage systems are attractive for the study of bubble-stirred boundary layers mainly because, in contrast with boiling, the bubble generation rate is independent of the rate of heat transfer and can be accurately controlled and measured [89].

As with boiling, barbotage systems may be divided first into two categories, namely (i) "free convection" or "pool" systems in which the porous heat-transfer surface is located in a pool of liquid and (ii) "forced-convection" systems in which the porous heat-transfer surface is situated in a wall past which the liquid or gas and liquid mixture is forced. Further subdivision is possible [19].

The experiments described in this thesis are of forced-convection barbotage. A study is made of heat transfer to water and air-water mixtures flowing in a horizontal rectangular duct having one porous wall (the bottom) through which air is bubbled. A rectangular channel with air injection through one wall was chosen for the following reasons.

(i) The geometry simulates that of a rocket motor cooling channel. The present project forms part of a larger study [42,43,81] dealing with this geometry (boiling work is currently in progress).

(ii) The use of transparent side-walls (as in the present apparatus) permits flow patterns to be observed along the porous heat-transfer section. This is in contrast to a tube in which such observations are not possible.

(iii) No previous barbotage results for this geometry have so far appeared in the literature.

When considering barbotage as an analog of boiling, various aspects may be examined; these may be purely hydrodynamic or may include heat transfer. Zuber [92], Wallis [88], and more recently Kudirka [48], have noted the similarities in appearance of the bubbling flow regimes in barbotage and saturated nucleate pool boiling; the similarity of initiation [92,86] and of growth rates and growth times [86] have also been pointed out.

In boiling a hydrodynamic crisis has been postulated [50] to occur at the critical heat flux (burnout). In barbotage, a

similar hydrodynamic crisis has been postulated [54] and studied [1,54,58,80,87].

With regard to heat transfer, a first step toward understanding the connection between barbotage and boiling is to compare the heat-transfer coefficients in both these phenomena [63,27,80,49]. Part of the present study deals in considerable detail with this comparison, to which the following paragraphs give some background. (Although the investigation of Mixon, Chon and Beatty [63], involving electrolytic gas evolution at the heat-transfer surface, does not strictly fall within the definition of barbotage, the following discussion occurs as if it did.)

In making heat-transfer comparisons between boiling and barbotage the following aspects should be considered.

(i) The boiling results used should be for saturated, as opposed to subcooled, nucleate boiling. This is because the hydrodynamic similarities [92,86,89,48] (particularily bubble growth rate and departure [86]) in boiling and barbotage refer to saturated boiling conditions. In highly-subcooled boiling, the bubbles grow and collapse on the heating surface [33] without detaching at all, a behaviour unlike that of a barbotage bubble. Most previous comparisons have used saturated nucleate boiling results [27,80,49].

(ii) A significant variable in both barbotage and boiling is the rate of vapour/gas formation [63]. It is later argued that the relevant vapour formation rate for use in the comparisons is that

near the heating surface (perhaps it is obvious). Unfortunately, this rate is usually not known (with the exception noted later) in saturated nucleate boiling. In general, previous comparisons were based on using a vapour formation rate which would exist if all the heat flux produced vapour [27,80,49]. It is especially a recent paper by Rallis and Jawurek [68], giving vapour formation rates near the heating surface in the saturated nucleate pool boiling of water over a wide range of heat fluxes, which allows an improvement to be made over previous comparisons. Use is made of this new information in the comparisons performed in the present work.

(iii) It is desirable to plot both the boiling and the barbotage data on dimensionless coordinates which accommodate fluid property differences. Earlier comparisons were on dimensional coordinates [63,27] while later comparisons [80,49] were on dimensionless coordinates, the first presentation of this type being in Ref. 80.

(iv) It has been recognized [63,27,49] that, as a means of transferring heat, the "latent heat transport" [68] which occurs in boiling has no counterpart in barbotage. To date no attempt has been made to quantitatively account for this difference. The present work makes a first attempt. It is necessary however to have knowledge of the latent heat transport in saturated nucleate boiling; measurements of vapour formation rates also provide information on latent heat transport. It is largely the recent work of Rallis and Jawurek [68] which provides this.

Unfortunately, the information on vapour formation rate and latent heat transport, which are necessary for the present method of comparison, are available only for pool (as opposed to forced convection) systems in saturated nucleate boiling. For this reason, the heat-transfer comparisons in the present work are restricted (with one exception appearing in Section 6.10) to pool barbotage and saturated nucleate pool boiling.

1.2 Purpose and Scope

The purpose of the present investigation is:

(i) to present a quantitative method of comparing the heat-transfer coefficients in pool barbotage and saturated nucleate pool boiling which takes account of (a) the vapour formation rate near the surface in boiling and (b) the different heat-transfer mechanisms which exist in barbotage and boiling;

(ii) to measure and correlate the heat-transfer coefficient between one heated porous wall of a rectangular duct and an air-water mixture flowing within the duct.

The main dependent variables observed are the heat-transfer coefficient and the flow pattern; the main independent variables are the barbotage-rate $\dot{V}''_g$ (rate of air injection through the porous heating surface), the water flow rate and the amount of air introduced upstream of the heated porous test section. A minor independent variable was the method of introducing the air into the water upstream of the test section. The range of variables is given in detail in Table 4.2.

The conditions of greatest interest here are those for which the heat-transfer coefficient increases with increasing barbotage-rate $\dot{V}''_g$ (analogous in boiling to the increase in the heat-transfer coefficient with increasing vapour formation rate; i.e. with heat flux). The heat-transfer coefficient is correlated for this region.

1.3 Layout of Thesis

A review of the previous forced convection barbotage investigations is presented in Section 1.4.

Chapter 2 presents the method of comparing the heat-transfer coefficients in pool barbotage and saturated nucleate pool boiling. The main result of the comparisons is shown in Figs. 2.5 and 2.7.

The remainder of the body of the thesis is divided into five parts, thus

Apparatus

Procedure

Flow Pattern Observations

Presentation and Discussion of Heat-Transfer Results

Summary and Conclusions.

In the chapter on flow observations the main results take the form of: the flow map Fig. 5.3, the tabulated flow pattern

boundaries Table 5.1 and the discussion in Section 5.5.

The experimental results for the heat-transfer coefficient are presented in Figs. 6.2 to 6.13 while a summary of the correlating equations is given in Section 6.6.1.

In order to assist the discussions which occur in this thesis, Fig. 1.1 shows a schematic diagram, the contents of which are classified according to (i) boiling or barbotage and (ii) pools or forced convection. The figure indicates the location in the thesis of discussion of the various "links" or relations between the subjects in the rectangles.

The number of each figure, equation and table begins with the number of the chapter, or the letter of the appendix, in which it appears.

1.4 Review of the Forced Convection Barbotage Heat-Transfer Literature

An excellent review of the pool-barbotage literature has recently been presented by Duffield [19]. The present review is therefore limited to forced convection barbotage. However, later in this thesis, extensive use is made of the pool-barbotage heat-transfer results of Akturk [1] and of Gose, Acrivos and Petersen [27]; details of their experiments will be given where their results are first used. Similarily, topics will be discussed such as saturated nucleate pool boiling and two-phase two-

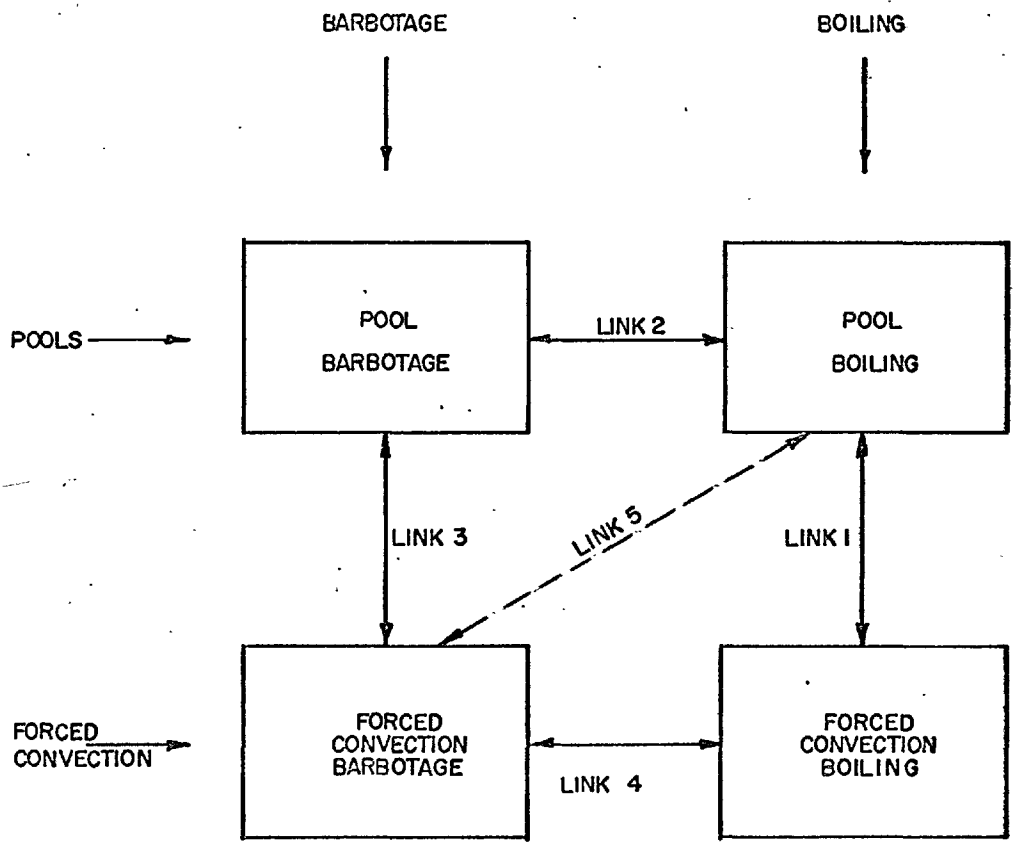

LINK	1	DISCUSSED	IN	REFS.	52 AND 8
LINK	2	DISCUSSED	IN	CHAP.	2
LINK	3	DISCUSSED	IN	SEC.	6.7
LINK	4	DISCUSSED	IN	SEC.	6.10
LINK	5	DISCUSSED	IN	SEC.	6.10

FIG. 1.1 "LINKS" BETWEEN POOLS AND FORCED CONVECTION, BOILING AND BARBOTAGE

component forced convection flow patterns. The relevant literature will be discussed at appropriate points throughout the thesis. Attention is further restricted in the present section to forced convection barbotage in enclosed channels and to investigations with heat transfer. This then excludes: the theoretical analysis of Hirata and Nishiwaki [36] for barbotage from a flat porous plate to a liquid of infinite extent flowing past the plate, and the studies in channels in which purely hydrodynamic quantities (pressure drop [89,62] and velocity and density profiles [90]) were of interest.

The investigations of direct interest are those of Gose, Petersen and Acrivos [28], Gose, Acrivos and Petersen [27] and Kudirka, Grosh, and McFadden [49]. Details of these investigations are summarized in Table 1.1.

The previous investigations were in vertical, round tubes [28,27,49] with upward flow of the liquid or gas-liquid mixture. The gas-liquid systems used were nitrogen-water [28], air-water [27,49] and air-ethylene glycol [27,48]. Provision was made for mixing gas with the liquid upstream of the heated porous test section in the most recent investigation [49]. The earliest investigation [28] was considered to be of a preliminary nature [27].

Gose et al. [27] observed that the effect of barbotage was approximately "linearly additive" to the effect of single-phase forced convection, i.e. for a given barbotage rate and liquid, the

Table 1.1 Details of Previous Forced Convection Barbotage Experiments

	Gose, Petersen and Acrivos [28]	Gose, Acrivos and Petersen [27]	Kudirka, Grosh and McFadden [49]
Geometry of heat-transfer tube	Vertical round porous tube, 7/8-in. ID (2-in. OD) and 6-in. long; liquid flow upward.	Vertical round porous tube, 7/8-in. ID (2-in. OD) and 6-in. long; liquid flow upward.	Vertical round porous tube, 5/8-in. ID (7/8-in. OD) and 11-in. long; liquid flow upward.
Description of porous tube	Sintered bronze; porosity of inner surface 25%; pore diameter 7-13 μ (0.000276 - 0.000512 in.)	Sintered bronze; porosity of inner surface 0.128%; mean pore diameter 0.000625 in.; 4170 pores/in.^{2}	Machined from Oilite bronze-cored bar stock, etched in dilute nitric acid; pore density on outside of tube possibly about 700/in.^{2}
Gas-liquid	Nitrogen-water	Air-water Air-ethylene glycol	Air-water Air-ethylene glycol
Liquid-velocity range, ft/s	0.11 - 3.0	0.3 - 9.9	1.0 - 9.0
Reynolds number range	749 - 20,500	380 - 50,000	380 - 45,000
Range of barbotage rates, V''_g, ft/s	0 - 0.045	0 - 0.185	0 - 0.62
Gas velocity along channel upstream of the heated test section, ft/s	Zero	Zero	0 - 76 at location of reported heat-transfer coefficients
Heat-transfer coefficients reported	Mean	Mean	Local at a location 14 diameters from the beginning of the heated section

absolute increase in the heat-transfer coefficient over that for single-phase flow was approximately the same regardless of the value of the heat-transfer coefficient in the absence of barbotage. Kudirka et al. [49] found that the effect of barbotage was "algebraically additive", i.e. the magnitude of the effect of barbotage on the heat-transfer coefficient depended not only on the barbotage rate and the liquid, but also on the factors affecting the heat-transfer coefficient in the absence of barbotage (liquid velocity and gas velocity along the channel).

Another method of gas production at the heat-transfer wall was studied by Metais [61]. He measured heat-transfer coefficients in vertical and horizontal tubes in which water, saturated with air at entry to the tube, was heated, so liberating air at the walls of the tube. The maximum rate of air liberation was approximately 2 or 3 orders of magnitude less than the smallest finite barbotage rate in the previous [27,28,49] and the present barbotage experiments. Maximum changes in the heat-transfer coefficients over those for deaerated water (no air liberation at the tube wall) were only 20% (compared with, in some cases in the present investigation, changes of some hundreds of per cent in the heat-transfer coefficient with finite barbotage over that with zero barbotage). For these reasons, the work of Metais is not treated further in this thesis.

CHAPTER 2 COMPARISON OF HEAT-TRANSFER COEFFICIENTS IN POOL BARBOTAGE AND SATURATED NUCLEATE POOL BOILING

2.1 Introductory Remarks*

This chapter presents a quantitative comparison between heat-transfer coefficients in pool barbotage and saturated nucleate pool boiling. The main considerations presented in the chapter are arranged as follows. First, an examination is made of heat-transfer mechanisms, noting particularily that latent heat transport occurs in boiling, but not in barbotage. A "heat-transfer-coefficient-through-the-liquid" α_f is then defined which accounts for the same heat-transfer mechanisms in boiling and barbotage; this is used as the basis of comparison. Next, vapour formation rates and latent heat transport in boiling are estimated from published data; this information is used in the comparison. Finally, the comparison is made of the dimensionless α_f in boiling and barbotage at the same dimensionless vapour/gas flow rates; this represents the main result of this chapter and is shown in Figs. 2.5 and 2.7.

The present comparisons are restricted to:

(i) heat-transfer coefficients,

(ii) saturated, as opposed to subcooled, nucleate pool boiling on smooth surfaces,

(iii) pool or free convection systems, as opposed to forced convection,

---

*The author gratefully acknowledges many helpful discussions with Dr. P. L. Duffield in connection with the material presented in this chapter.

(iv) horizontal heaters.

There are many equations presented in this chapter; for this reason the important equations are summarized in Table 2.5.

2.2 Heat Transfer Mechanisms

2.2.1 Boiling Heat Transfer Mechanisms

The cyclic distributions of heat and mass fluxes and temperatures which occur during the formation and departure of vapour bubbles are replaced here by a simple one-dimensional system involving only time and area means of these quantities; this is done for both boiling and barbotage. This replacement allows a simple treatment of the problem (only a simple treatment is justified in the present state of knowledge); further, the measured heat-transfer coefficients which are compared are indeed time and area means. Semeria [77] presents an excellent review of boiling heat-transfer analyses based on the bubble cycle.

The system is shown in Fig. 2.1a in which a control volume extends from the horizontal heating surface (S-surface) to a plane A-A (A-surface) at an arbitrary distance above the heating surface. For the most general case shown, A-A is contained within the thermal boundary layer. Also shown is a plane D-D (D-surface) located at the "bubble detachment height" (defined as the height of the bubble at the moment it detaches from the heating surface); the significance of the D-surface will be seen later. There are no fluxes

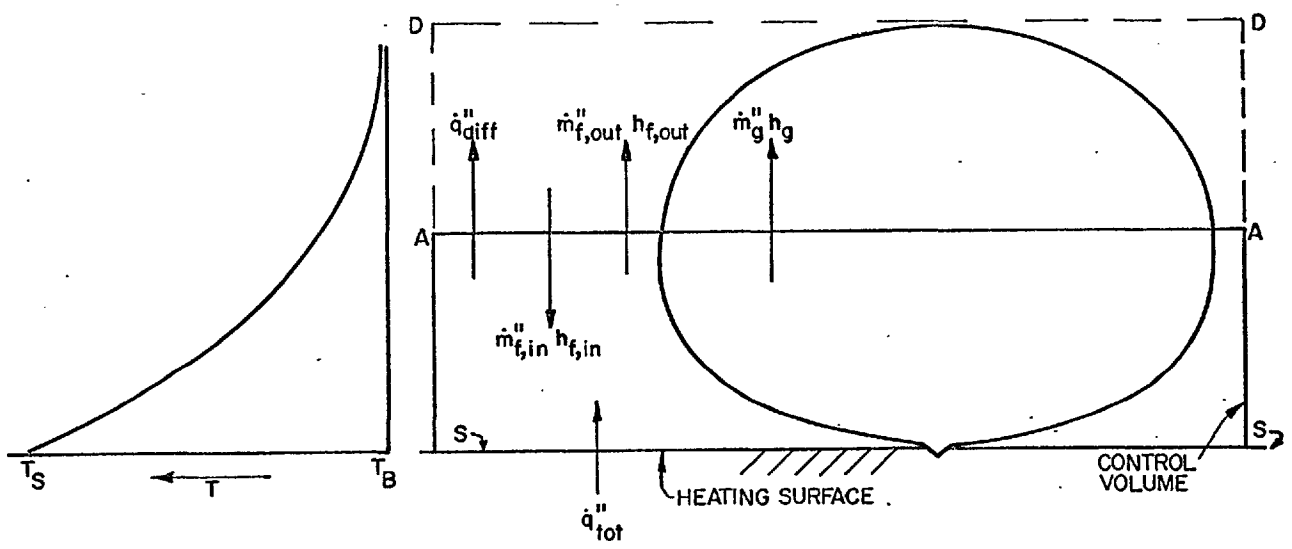

FIG. 2.1a ENERGY FLUXES IN BOILING

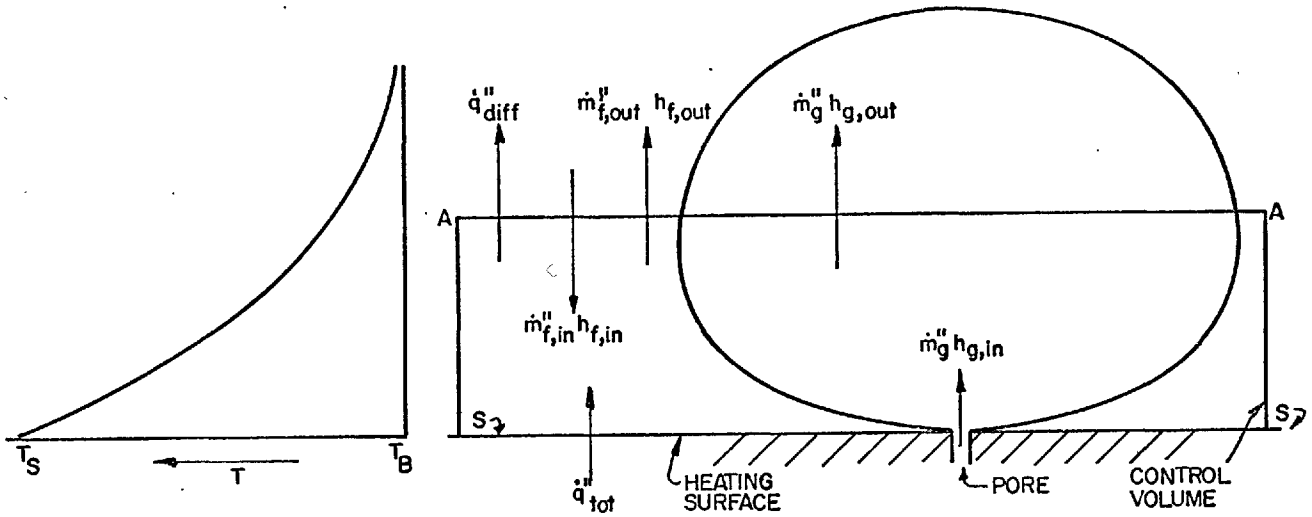

FIG. 2.1b ENERGY FLUXES IN BARBOTAGE

FIG. 2.1 ENERGY FLUXES IN BOILING AND BARBOTAGE

through the sides of the control volume.

An energy balance applied to the control volume yields

$$\dot{q}''_{tot} = \dot{q}''_{diff} + \dot{m}''_{f,out}\, h_{f,out} - \dot{m}''_{f,in}\, h_{f,in} + \dot{m}''_{g}\, h_{g} \qquad (2.1)$$

where the "dot" over the symbol signifies per unit time and the "double prime" superscript signifies per unit area of heating surface;

$\dot{q}''_{tot}$ is the total heat flux crossing the S-surface; in boiling experiments it is the usual heat flux measured;

$\dot{q}''_{diff}$ is the heat flux through the A-surface due to the presence of the temperature gradient; it includes both molecular and eddy diffusion;

$\dot{m}''_{f,in}$ and $\dot{m}''_{f,out}$ are the mass fluxes of liquid entering and leaving the control volume respectively; they are caused by the action of the bubbles and by density gradients in the liquid;

$\dot{m}''_{g}$ is the mass flux of the vapour passing out through the A-surface;

$h_{f,in}$ and $h_{f,out}$ are the mean enthalpies of the liquid entering and leaving the control volume respectively; due to the presence of the superheated liquid they may have values greater than that of the bulk saturated liquid; in general, of course, $h_{f,out} > h_{f,in}$;

h_{g} is the enthalpy of the saturated vapour;

h_{fg} is the latent heat of vaporisation (used below).

From mass continuity

$$\dot{m}''_{f,in} = \dot{m}''_{f,out} + \dot{m}''_{g} \tag{2.2}$$

and from thermodynamics

$$h_g - h_{f,in} \simeq h_{fg} \tag{2.3}$$

Substitution of equations (2.2) and (2.3) in (2.1) yields

$$\dot{q}''_{tot} = \dot{q}''_{diff} + \dot{m}''_{f,out} (h_{f,out} - h_{f,in}) + \dot{m}''_{g} h_{fg} \tag{2.4}$$

In the above equation, the term $\dot{m}''_{g} h_{fg}$ is called the "latent heat transport" for which the symbol $\dot{q}''_{LH}$ is used, i.e.

$$\dot{q}''_{LH} \equiv \dot{m}''_{g} h_{fg} \tag{2.5}$$

The remaining two terms on the right-hand side of equation (2.4) represent the heat transfer through the liquid, for which a symbol $\dot{q}''_{f}$ is defined by

$$\dot{q}''_{f} \equiv \dot{q}''_{diff} + \dot{m}''_{f,out} (h_{f,out} - h_{f,in}) \tag{2.6}$$

Equation (2.4) may be rewritten as

$$\dot{q}''_{tot} = \dot{q}''_{f} + \dot{q}''_{LH} \tag{2.7}$$

It is important to note that the relative magnitude of the terms in equation (2.7) vary:

(i) with distance y from the heating surface for a fixed $\dot{q}''_{tot}$ (Fig.2.2a illustrates this qualitatively), and

(ii) with the intensity of bubbling, i.e. with $\dot{q}''_{tot}$, for a fixed distance from the heating surface.

2.2.2 Barbotage Heat Transfer Mechanisms

The barbotage system is shown in Fig. 2.1b. An energy balance together with the mass continuity equation written for the control volume yields

$$\dot{q}''_{tot} = \dot{q}''_{diff} + \dot{m}''_{f,out} (h_{f,out} - h_{f,in}) \qquad (2.8)$$

where all the symbols are as for boiling. The quantities $h_{f,in}$ and $h_{f,out}$ may have values greater than that of the bulk liquid due to the presence of liquid moved bodily from the thermal boundary layer. In equation (2.8) the gas-enthalpy term has been neglected as it is small compared with the other terms.

If the same definition of $\dot{q}''_f$ as for boiling, equation (2.6), is used, then equation (2.8) becomes

$$\dot{q}''_{tot} = \dot{q}''_f \qquad (2.9)$$

In barbotage then, the heat transferred through the liquid $\dot{q}''_f$ is the total heat flux. The ratio $\dot{q}''_f/\dot{q}''_{tot}$ is shown in Fig. 2.2a for comparison with the same quantity in boiling. A significant difference between barbotage and boiling is seen; namely, the ratio $\dot{q}''_f/\dot{q}''_{tot}$ is constant and equal to one for barbotage while for

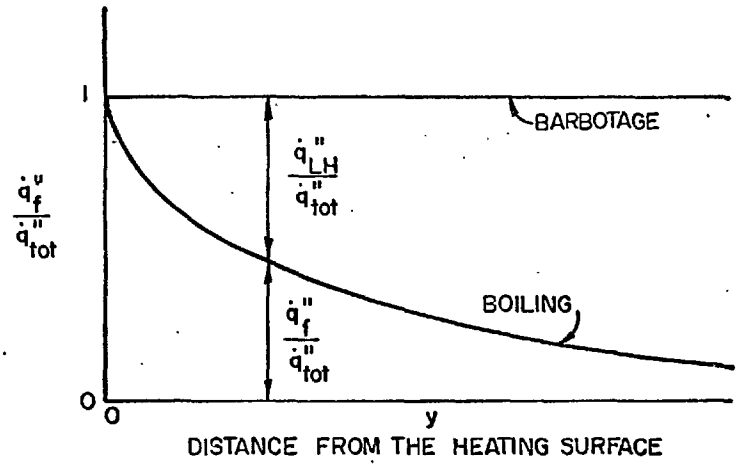

FIG. 2.2a QUALITATIVE RELATION BETWEEN HEAT-FLUX TERMS AND DISTANCE FROM THE HEATING SURFACE

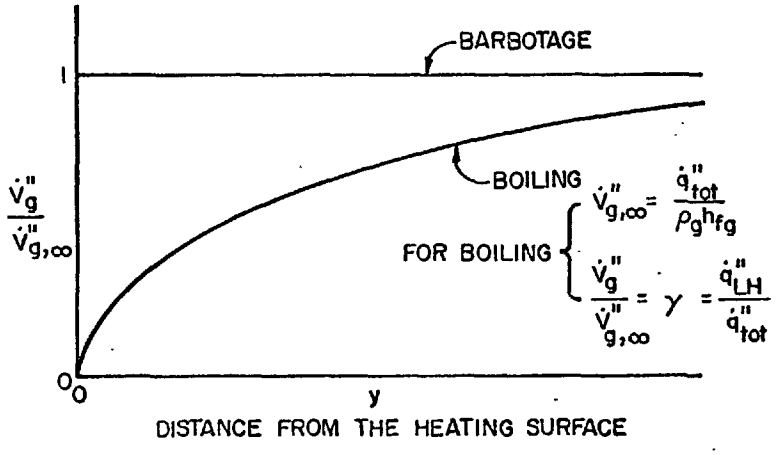

FIG. 2.2b QUALITATIVE RELATION BETWEEN VAPOUR OR GAS VELOCITY AND DISTANCE FROM THE HEATING SURFACE

FIG. 2.2 QUALITATIVE RELATIONS OF $\dot{q}''_f/\dot{q}''_{tot}$ vs. y AND $\dot{V}''_g/\dot{V}''_{g,\infty}$ vs. y FOR BOILING AND BARBOTAGE

boiling it varies with the distance from the heated wall.

2.3 Basis of Comparison of Heat-Transfer Coefficients

2.3.1 The Heat-Transfer-Coefficient-Through-the-Liquid

A "heat-transfer-coefficient-through-the-liquid" α_f is now defined; it is the reciprocal of the total resistance to the flow of heat through the thermal boundary layer in the liquid. The resistance to the flow of heat through the liquid in an incremental length of thermal boundary layer dy is $- dT/\dot{q}''_f$ while the resistance across the whole boundary layer is

$$-\int_{T_S}^{T_B} \frac{dT}{\dot{q}''_f}$$

where T_S is the temperature at the liquid-solid interface and T_B is the bulk liquid temperature (saturation temperature in boiling). Therefore, α_f is defined as

$$\alpha_f \equiv \frac{1}{-\int_{T_S}^{T_B} \frac{dT}{\dot{q}''_f}} = \frac{1}{\int_{T_B}^{T_S} \frac{dT}{\dot{q}''_f}} \qquad (2.10)$$

This definition is used for both boiling and barbotage and is the basis of the comparisons of the heat-transfer coefficients.

2.3.2 Boiling Heat-Transfer Coefficients

In boiling $\dot{q}''_f$ varies through the thermal boundary layer

and in general the function $\dot{q}''_f \sim T$ is unknown. There are, however, two limiting cases for α_f. Before listing the limits it is useful to define the following quantities:

$$\alpha_{tot} \equiv \frac{\dot{q}''_{tot}}{T_S - T_B} \tag{2.11}$$

$$\zeta \equiv \frac{\alpha_f}{\alpha_{tot}} \tag{2.12}$$

$$\gamma_D \equiv \frac{\dot{q}''_{LH,D}}{\dot{q}''_{tot}} \tag{2.13}$$

The quantity α_{tot} is, of course, the usual heat-transfer coefficient reported for boiling experiments; ζ has been introduced for convenience. The symbol $\dot{q}''_{LH,D}$ is the latent heat transport crossing the D-surface; γ_D therefore represents the fraction of the total heat flux crossing the D-surface as latent heat.

The two limits of α_f are:

$$\left.\begin{aligned} &\text{upper limit} \quad , \quad \alpha_f = \alpha_{tot} \qquad\qquad\quad ,\text{i.e.} \quad \zeta = 1 \\ &\text{lower limit} \quad , \quad \alpha_f = \left(1 - \frac{\dot{q}''_{LH,D}}{\dot{q}''_{tot}}\right) \alpha_{tot} \quad ,\text{i.e.} \quad \zeta = 1 - \gamma_D \end{aligned}\right\} \tag{2.14}$$

A discussion of the physical conditions which would exist for each of these limits is given in Section 2.6. At the present time it is very difficult, if not impossible, to determine to which limit the real α_f is closer.

2.3.3 Barbotage Heat-Transfer Coefficients

In barbotage, $\dot{q}''_f$ is uniform through the thermal boundary layer and equal to $\dot{q}''_{tot}$. Equation (2.10) for this case is

$$\alpha_f = \frac{\dot{q}''_f}{T_S - T_B} = \frac{\dot{q}''_{tot}}{T_S - T_B} \tag{2.15}$$

which is the usual definition of the heat-transfer coefficient in barbotage.

2.4 Definition of Vapour and Gas Velocities

2.4.1 Boiling Vapour Velocity

If the mass flux of vapour crossing any plane is $\dot{m}''_g$, then the vapour velocity $\dot{V}''_g$ crossing that plane is

$$\dot{V}''_g = \frac{\dot{m}''_g}{\rho_g} \tag{2.16}$$

where ρ_g is the vapour density. Combination of equations (2.16) and (2.5) yields

$$\dot{V}''_g = \frac{\dot{q}''_{LH}}{\rho_g h_{fg}} \tag{2.17}$$

Generally $\dot{m}''_g$ or $\dot{V}''_g$, and hence $\dot{q}''_{LH}$, as functions of y are unknown. However, sufficient information is available to obtain these quantities at one "bubble detachment height" y_D above the heating surface.

It is convenient for later use to define a ratio γ, to be called the "latent heat fraction", by

$$\gamma \equiv \frac{\dot{q}''_{LH}}{\dot{q}''_{tot}} \tag{2.18}$$

A symbol $\dot{V}''_{g,\infty}$, representing the vapour velocity which would obtain if all the heat flux $\dot{q}''_{tot}$ produced vapour (e.g. at some very large distance from the heating surface), is defined by

$$\dot{V}''_{g,\infty} \equiv \frac{\dot{q}''_{tot}}{\rho_g h_{fg}} \tag{2.19}$$

Substitution of (2.17) and (2.19) in (2.18) gives

$$\gamma = \frac{\dot{V}''_g}{\dot{V}''_{g,\infty}} \tag{2.20}$$

Fig. 2.2b indicates qualitatively how $\dot{V}''_g/\dot{V}''_{g,\infty}$, i.e. γ or $\dot{q}''_{LH}/\dot{q}''_{tot}$, might vary with distance y from the heating surface for otherwise fixed conditions. Combination of (2.17) and (2.18) yields a relation to be used later:

$$\dot{V}''_g = \gamma \frac{\dot{q}''_{tot}}{\rho_g h_{fg}} \tag{2.21}$$

At the D-surface (one "bubble detachment height" above the heating surface):

$$\gamma_D \equiv \frac{\dot{q}''_{LH,D}}{\dot{q}''_{tot}} = \frac{\dot{V}''_{g,D}}{\dot{V}''_{g,\infty}} \tag{2.22}$$

$$\dot{V}''_{g,D} = \gamma_D \frac{\dot{q}''_{tot}}{\rho_g h_{fg}} \tag{2.23}$$

where $\dot{V}''_{g,D}$ is the vapour velocity crossing the D-surface.

2.4.2 Barbotage Gas Velocity

In barbotage the gas velocity $\dot{V}''_g$ is defined as the gas volume injected through the heating surface per unit time and projected area of heating surface; $\dot{V}''_g$ is uniform with respect to y.

The ratio $\dot{V}''_g/\dot{V}''_{g,\infty}$ for barbotage is shown in Fig. 2.2b in order to illustrate the second significant difference between boiling and barbotage ($\dot{V}''_{g,\infty}$ in barbotage may be interpreted as the gas velocity at some large distance from the heating surface). The ratio $\dot{V}''_g/\dot{V}''_{g,\infty}$ for barbotage is uniform and equal to one while for boiling it varies with y.

In summary, two significant differences between boiling and barbotage are seen to be that, in barbotage (i) $\dot{V}''_g$ and (ii) $\dot{q}''_f$ are uniform with respect to y, while in boiling both these quantities vary with y.

2.5 The Latent Heat Fraction at the D-Surface in Saturated Nucleate Pool Boiling

2.5.1 General Remarks

In making comparisons between barbotage and boiling, it is necessary to know the vapour generation rate in boiling, which, however, is a function of the distance from the heated wall. It is therefore necessary to decide at which position in the pool $\dot{V}''_g$ should be used for the purpose of the comparisons. The choice is limited as there is some knowledge of $\dot{V}''_g$ at only two positions, namely:

(i) at very large distances from the heating surface where

$$\dot{V}''_{g,\infty} = \frac{\dot{q}''_{tot}}{\rho_g h_{fg}} \tag{2.19}$$

i.e. where all the heat flux has produced vapour, and

(ii) at the D-surface (coincident with the top of the bubble at the moment of detachment), where

$$\dot{V}''_{g,D} = \gamma_D \frac{\dot{q}''_{tot}}{\rho_g h_{fg}} \tag{2.23}$$

It seems reasonable that the vapour generation rate which most influences the heat-transfer coefficient is that near the heating surface, i.e. the growing and departing bubbles cause vigorous agitation of the thermal boundary layer, so markedly affecting the heat-transfer coefficient. For this reason, the relevant vapour generation rate in the comparisons is taken as $\dot{V}''_{g,D}$.

In previous quantitative comparisons [27,80,49] between barbotage and saturated nucleate pool boiling heat-transfer coefficients, the vapour velocity was taken as $\dot{q}''_{tot}/\rho_g h_{fg}$. In the absence of a knowledge of, or assumptions concerning γ_D, this would be the only alternative. It is especially a recent publication [68] which has given information on γ_D so making the present comparisons possible.

2.5.2 Choice of Coordinates

The coordinates for presenting the information on latent heat transport, or vapour velocity, at the D-surface are (i) the

dimensionless ratio γ_D as ordinate, and (ii) as abscissa, the dimensionless group to be called the Kutateladze number Ku and defined as

$$Ku \equiv \frac{\dot{q}''_{tot}}{h_{fg}\,\rho_g^{\frac{1}{2}}[\sigma g_o g(\rho_f - \rho_g)]^{\frac{1}{4}}} \qquad (2.24)$$

where:

$\dot{q}''_{tot}$, h_{fg} and ρ_g have been previously defined,

g is the gravitational acceleration,

g_o is the constant in Newton's Second Law of Motion,

σ is the surface tension of the liquid-vapour interface,

ρ_f is the density of the liquid.

The Kutateladze number Ku is chosen to non-dimensionalize $\dot{q}''_{tot}$ for the following reason. For saturated pool boiling on horizontal heating surfaces the critical heat flux $\dot{q}''_{tot,cr}$ (burnout) is determined by the Kutateladze relation [50]

$$Ku_{cr} \equiv \frac{\dot{q}''_{tot,cr}}{h_{fg}\,\rho_g^{\frac{1}{2}}[\sigma g_o g(\rho_f - \rho_g)]^{\frac{1}{4}}} = 0.16 \pm 0.03 \qquad (2.25)$$

which is the maximum limiting value of Ku for nucleate boiling of all liquids*. The degree of development of nucleate boiling is most clearly seen then if data are plotted in terms of Ku; for all liquids γ_D is expected to increase with Ku reaching a maximum value when Ku is in the vicinity of 0.16.

*Strictly speaking, the term "all liquids", as used in this work, refers to liquids wetting the heat-transfer surface (by far the more common case in boiling heat transfer).

Unfortunately the available information on γ_D is limited; certain assumptions to be discussed in Section 2.5.3 are necessary when applying the $\gamma_D \sim$ Ku function in the comparisons.

2.5.3 Sources of Experimental Data

Measurements of vapour formation in saturated pool boiling are very limited. The data of Rallis and Jawurek [68] are directly usable; Yamagata et al. [91] present data which can be used after some inference; other possible sources [16,76] are also treated. The investigations of Gunther and Kreith [33] and Rohsenow and Clark [71] are excluded as they refer to subcooled conditions. The result of plotting the data is shown in Fig. 2.3, which is later used in the comparison of boiling and barbotage heat-transfer coefficients. Each source of γ_D information is treated in more detail below.

The most important source of information is the work of Rallis and Jawurek [68]. The system investigated was the saturated nucleate pool boiling of water at atmospheric pressure on a horizontal wire. Over a wide range of heat fluxes cine photography was used to obtain measurements of $\dot{V}''_{g,b}$ the rate of formation of vapour bubbles up to the moment of detachment or "break-off" from the heating surface; this was obtained from

$$\dot{V}''_{g,b} = \frac{n}{A} \overline{fV_b} \qquad (2.26)$$

where:

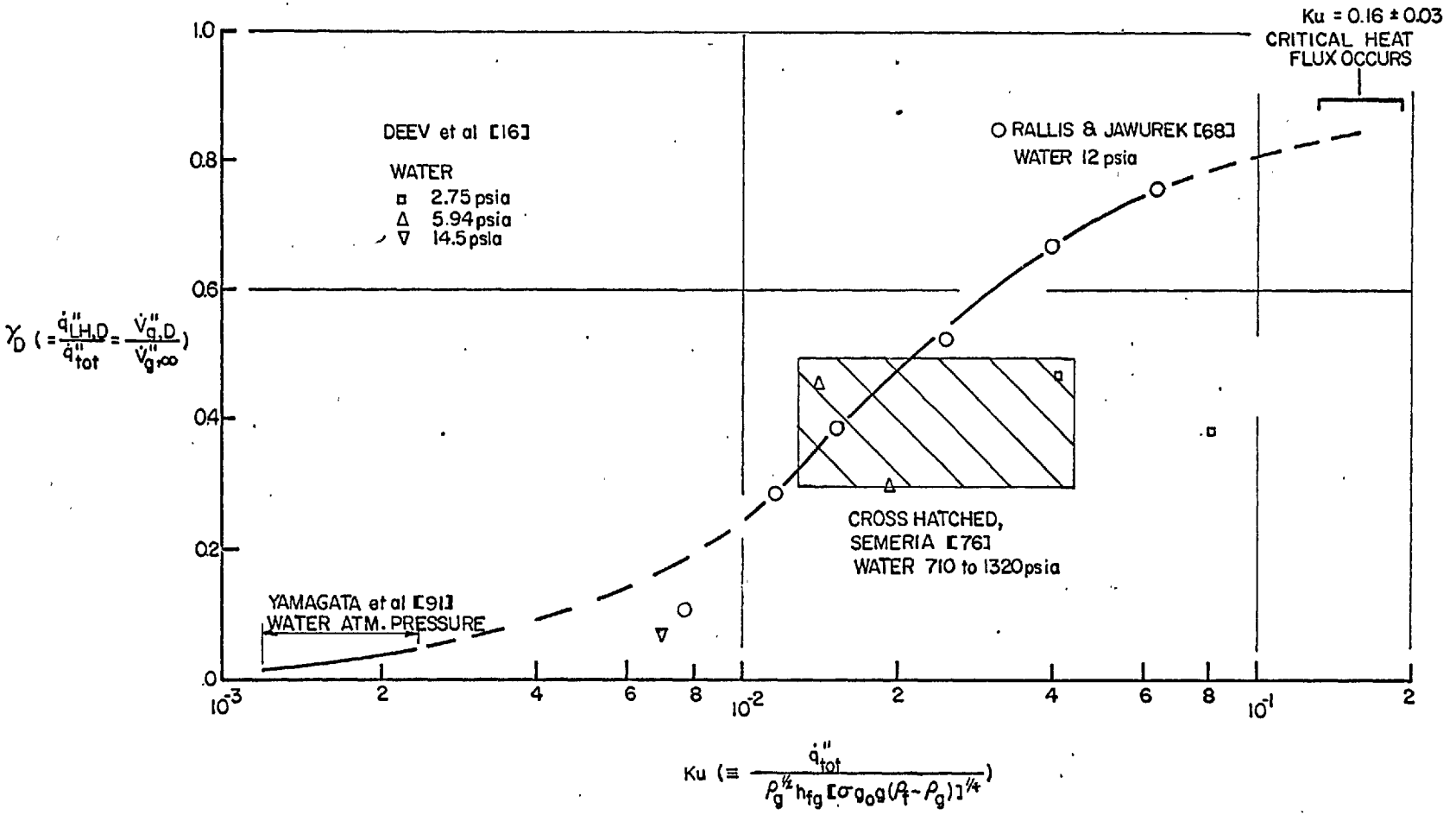

FIG. 2.3 VARIATION OF LATENT HEAT FRACTION WITH KUTATELADZE NUMBER FOR SATURATED NUCLEATE POOL BOILING

n is the number of bubble sources on the heating surface,

A is the area of the heat-transfer surface,

$\overline{fV_b}$ is the arithmetic mean of products $f \cdot V_b$ for all nucleating sites,

f is frequency of bubble formation,

V_b is the bubble volume at detachment or "break-off". The authors [68] are then able to calculate $\dot{q}''_{LH,b}$ from

$$\dot{q}''_{LH,b} = \dot{V}''_{g,b}\ \rho_g\ h_{fg} \tag{2.27}$$

where $\dot{q}''_{LH,b}$ is the rate at which energy is required to form bubbles up to the moment of detachment from the heating surface [71,68]; it is the "usual" definition of latent heat transport.

In the present work the term "latent heat transport", $\dot{m}''_g\ h_{fg}$ or $\dot{V}''_g\ \rho_g\ h_{fg}$, is qualified by specifying the y-plane at which $\dot{m}''_g$ or $\dot{V}''_g$ occurs. Because the bubbles grow little in rising a distance of one bubble detachment height from the heating surface [84], it is possible to write:

$$\left.\begin{aligned} &\dot{V}''_{g,b} \simeq \dot{V}''_{g,D} \\ &\dot{q}''_{LH,b} \simeq \dot{q}''_{LH,D} \\ &\frac{\dot{q}''_{LH,b}}{\dot{q}''_{tot}} \simeq \frac{\dot{q}''_{LH,D}}{\dot{q}''_{tot}} \quad \text{or} \quad \frac{\dot{q}''_{LH,b}}{\dot{q}''_{tot}} \simeq \gamma_D \\ &\frac{\dot{V}''_{g,b}}{\dot{V}''_{g',\infty}} \simeq \frac{\dot{V}''_{g,D}}{\dot{V}''_{g',\infty}} \quad \text{or} \quad \frac{\dot{V}''_{g,b}}{\dot{V}''_{g',\infty}} \simeq \gamma_D \end{aligned}\right\} \tag{2.28}$$

The Rallis and Jawurek [68] results, presented as $\frac{\dot{q}''_{LH,b}}{\dot{q}''_{tot}}$ vs. $\dot{q}''_{tot}$ in the original work, are plotted in Fig. 2.3 in the form of γ_D vs. Ku.

Further information on vapour velocity leaving the heating surface can be inferred from the investigation of Yamagata et al.[91]. The system investigated was the saturated nucleate pool boiling of water at atmospheric pressure on a smooth horizontal plate. These authors present experimental data which are described by the equation (see Fig. 21 of Ref. 91)

$$\alpha_{tot} = C_1 \, \dot{q}''^{2/3}_{tot} \tag{2.29}$$

In their Fig. 24, Yamagata et al. present the same data on different coordinates, through which they draw the line

$$\alpha_{tot} = C_2 (n \, \overline{D_b^3 f})^{0.23} \tag{2.30}$$

where:

$\overline{D_b^3 f}$ is the mean value of $D_b^3 \cdot f$,

D_b is the bubble diameter at detachment.

Combination of equations (2.29), (2.30), (2.26), (2.27) and (2.19) together with a knowledge of the heat-transfer surface area yields

$$\frac{\dot{q}''_{LH,b}}{\dot{q}''_{tot}} = \frac{\dot{V}''_{g,b}}{\dot{V}''_{g,\infty}} = C_3 \, (\dot{q}''_{tot})^{1.90} \tag{2.31}$$

where:

$C_1 = 2.81$
$C_2 = 229$
$C_3 = 3.72 \times 10^{-10}$

} for α_{tot} in Kcal / m^2 h deg C,
$\dot{q}''_{tot}$ in Kcal / m^2 h,
$n \overline{D_b^3 f}$ in mm^3/ s.

For distilled water at atmospheric pressure (the relevant test conditions), equation (2.31), combined with (2.28), becomes

$$\gamma_D = 4020 \, Ku^{1.90} \qquad (2.32)$$

This equation, over the range for which it applies, is plotted in Fig. 2.3.

The information on water-surfactant solutions given by Yamagata et al. cannot be used here as the dynamic surface tension, as opposed to the static surface tension, of the solutions is unknown [72,73]. The calculation of Ku requires a knowledge of the dynamic surface tension (which is equal to the static surface tension for pure liquids).

Semeria [76] also provides some relevant information. In his paper, which deals with different bubble types found in boiling water on horizontal wires, tubes and flat plates, Semeria reports that in his experiments at 50 to 93 kg/cm^2 pressure (710 to 1320 psia) and heat fluxes from 40 to 130 W/cm^2 (130,000 to 430,000 Btu/ft^2h), 30 to 50% of the surface heat flux was transported by the latent heat of vaporisation of the coalescing bubbles leaving the heating surface. The information is plotted in Fig. 2.3; it appears as an "area" on the figure .

Deev et al. [16] report n, $\bar{f}$, $\bar{D}_b$ and $\dot{q}''_{tot}$ for a total of five data points for water boiling at three different pressures on a horizontal flat surface. It is possible to obtain an approximate value of γ_D for these points using

$$\gamma_D \simeq \frac{\dot{q}''_{LH,b}}{\dot{q}''_{tot}} = \frac{1}{\dot{q}''_{tot}} \left(n \bar{f} \frac{\pi \bar{D}_b^3}{6}\right) \frac{\rho_g h_{fg}}{A} \qquad (2.33)$$

where:

$\bar{D}_b$ is the mean break-off or detachment diameter of the bubbles,

$\bar{f}$ is the mean frequency of bubble formation.

Rallis and Jawurek [68] have pointed out that, for purposes of calculating vapour generation rates, the use of $\bar{D}_b$ and $\bar{f}$ as in equation (2.33) is inferior to the use of $\overline{fD_b^3}$ or $\overline{fV_b}$ as in equations (2.26) or (2.30). However, because of the general paucity of data in which any combination of n, f and D_b is reported in the same work, the Deev et al. data is included here on Fig. 2.3.

2.5.4 Presentation and Discussion of the $\gamma_D \sim Ku$ Function

The information available(from papers in which some combination of n, f and D_b or V_b is reported in the same work) for determining the $\gamma_D \sim Ku$ function is presented in Fig. 2.3. All the data is for water at various pressures. The fluid properties for the Semeria [76] and Rallis and Jawurek [68] data are different, yet the data are in close correspondence on the figure. Four of the five data points at three different pressures (one of which is atmospheric

pressure) of Deev et al. [16] are in reasonable agreement with the Semeria and the Rallis and Jawurek data.

In determining the function to be used in the present work, cognizance is taken of the relative importance of the different sources of data; these are, in descending order of importance: Rallis and Jawurek [68], Yamagata et al. [91], Semeria [76] and Deev et al. [16]. The $\gamma_D \sim$ Ku function is obtained by: following the Yamagata et al. data in the low Ku region, joining (dashed line) the Yamagata et al. data to the Rallis and Jawurek data, following the smoothed Rallis and Jawurek data and then extrapolating (dashed line) these latter data to the region of the critical Kutateladze number.

It is apparent that the $\gamma_D \sim$ Ku function is based on a limited amount of data. For this reason, three separate assumptions, each to be used in turn in the comparisons of the heat-transfer coefficients, are made concerning the validity of the data. All assumptions refer to smooth surfaces. It is assumed that the $\gamma_D \sim$ Ku function represents:

Case 1 - all liquids regardless of fluid properties,

Case 2 - water and organic liquids at atmospheric pressure,

Case 3 - water at atmospheric pressure.

Case 1 has been included in order to keep the comparisons as general as possible. Even if subsequent evidence shows that γ_D is a function not only of Ku, but also of one (or more) fluid property groups, then at least the method of comparing heat-transfer

coefficients for the most general case will have been illustrated in this work. It may well turn out that γ_D is also a function of heater geometry; it is likely that γ_D will depend on surface roughness.

Case 2 is more restrictive than Case 1; it has been included as all the existing barbotage data, against which boiling heat-transfer coefficients can be compared, are for water and organic liquids at atmospheric pressure.

Case 3 has been included as there can be little argument as to the validity of this assumption. The $\gamma_D \sim$ Ku function of Fig. 2.3 follows the Yamagata et al. [91] data and the Rallis and Jawurek [68] data, both of which investigations are for water at atmospheric pressure (for the latter work, atmospheric pressure was 12 psia).

It will be seen in Section 2.7 how each of the above cases is combined with an appropriate equation representing boiling heat transfer.

2.6 Limiting Values of ζ ($\equiv \alpha_f/\alpha_{tot}$) in Boiling

The basis of heat-transfer comparisons in the present work is the heat-transfer-coefficient-through-the-liquid α_f defined in equation (2.10) as

$$\alpha_f \equiv \frac{1}{-\int_{T_S}^{T_B} \frac{dT}{q''_f}} = \frac{1}{\int_{T_B}^{T_S} \frac{dT}{q''_f}} \qquad (2.10)$$

In order to determine α_f, a knowledge of the function $\dot{q}''_f \sim T$ is necessary; in general this function is unknown.

Combination of equations (2.7) and (2.17) yields

$$\dot{q}''_f = \dot{q}''_{tot} - \dot{V}''_g \rho_g h_{fg}$$

The function $\dot{q}''_f \sim T$ could therefore be determined by knowing (i) $\dot{V}''_g \sim y$ (this would give $\dot{q}''_f \sim y$) and (ii) $T \sim y$. Measurements of $T \sim y$ are available for a few cases in saturated [40,59] or nearly-saturated [29] nucleate pool boiling while no measurements of $\dot{V}''_g \sim y$ in the region of interest (where T is varying with y) are known to the author. It is therefore necessary to work with the two limiting cases of α_f or $\zeta (\equiv \frac{\alpha_f}{\alpha_{tot}})$ which are found to be

$$\left.\begin{aligned} &\text{upper limit} \quad , \quad \alpha_f = \alpha_{tot} \quad , \text{ i.e. } \zeta = 1 \\ &\text{lower limit} \quad , \quad \alpha_f = \left(1 - \frac{\dot{q}''_{LH,D}}{\dot{q}''_{tot}}\right) \alpha_{tot} \quad , \text{ i.e. } \zeta = 1 - \gamma_D \end{aligned}\right\} \quad (2.14)$$

The limiting cases would be obtained under certain combinations of the following:

(i) the ratio of the thermal boundary layer thickness y_T to the bubble detachment height y_D,

(ii) the ratio of y_T to the thickness of the liquid film at the base of the bubble y_F [64,69],

(iii) the y-location at which vapour is generated.

Evidence concerning y_T, y_F and y_D for saturated water boiling at atmospheric pressure is presented in Table 2.1 which is an enlarged version of a table originally prepared by Duffield [20]. The conclusions to be drawn from the table are:

$y_T < y_D$ always and possibly $y_T << y_D$,

$y_T > y_F$ always and possibly $y_T >> y_F$.

The lower limit, $\zeta = 1 - \gamma_D$, would be obtained if:

$y_T < y_D$,

$y_T >> y_F$,

all the vapour is generated at the film [64].

The upper limit, $\zeta = 1$, would be obtained if:

$y_T << y_D$,

either $y_T > y_F$ or $y_T >> y_F$,

all the vapour is generated from the top of the bubble [93].

The physical conditions attending these two limiting cases are depicted in Fig. 2.4 and listed in Table 2.2 together with the resulting $\dot{q}''_f$, α_f and ζ.

2.7 Comparison of Heat-Transfer-Coefficients-Through-the-Liquid in Pool Barbotage and Pool Boiling

2.7.1 General Remarks

The comparisons will be effected by plotting on the same graph of dimensionless coordinates both boiling and barbotage heat-

Table 2.1 Evidence on the Relative Magnitudes of y_F, y_T and y_D in Saturated* Nucleate Pool Boiling at Atmospheric Pressure*

Author(s)	y_F 10^{-3}in	y_T 10^{-3}in	y_D 10^{-3}in	$\frac{y_T}{y_D}$	Comment **
Moore and Mesler [64]	~0.08				Calculated; $\dot{q}''_{tot}$ = 135,000 to 202,000
Sharp [78]	~0.01 or 0.02				Measured+; 0.1 atm press., T_B = 85 deg F
Madsen [57]	0.6-1.7				Calculated; $\dot{q}''_{tot}$ = 52,000 to 87,000
Grant and Patten [29]		30-35			At initiation of boiling; 11 deg F Subcooling
Marcus and Dropkin [59]		6-36			Function of α_{tot}; $\dot{q}''_{tot}$ = 1,000 to 40,000
Yamagata et al. [91]		28-59			Function of α_{tot}; $\dot{q}''_{tot}$ < 14,000
Gaertner [24]			130		++Mean value, independent of $\dot{q}''_{tot}$ for $\dot{q}''_{tot}$ = 10,000 to 70,000
Jacob and Linke [41]			110		++Mean, low $\dot{q}''_{tot}$
Semeria [75]			77 110		
Cole [12]			600		++Mean, at $\dot{q}''_{tot,cr}$
Behar and Semeria [4]				$\frac{1}{6}$ to $\frac{1}{4}$	Measured on Schlieren photograph

*Unless otherwise stated.

**$\dot{q}''_{tot}$ in Btu/ft^{2}h

+Included because of the lack of measured y_F's.

++Using bubble break-off dia. = y_D.

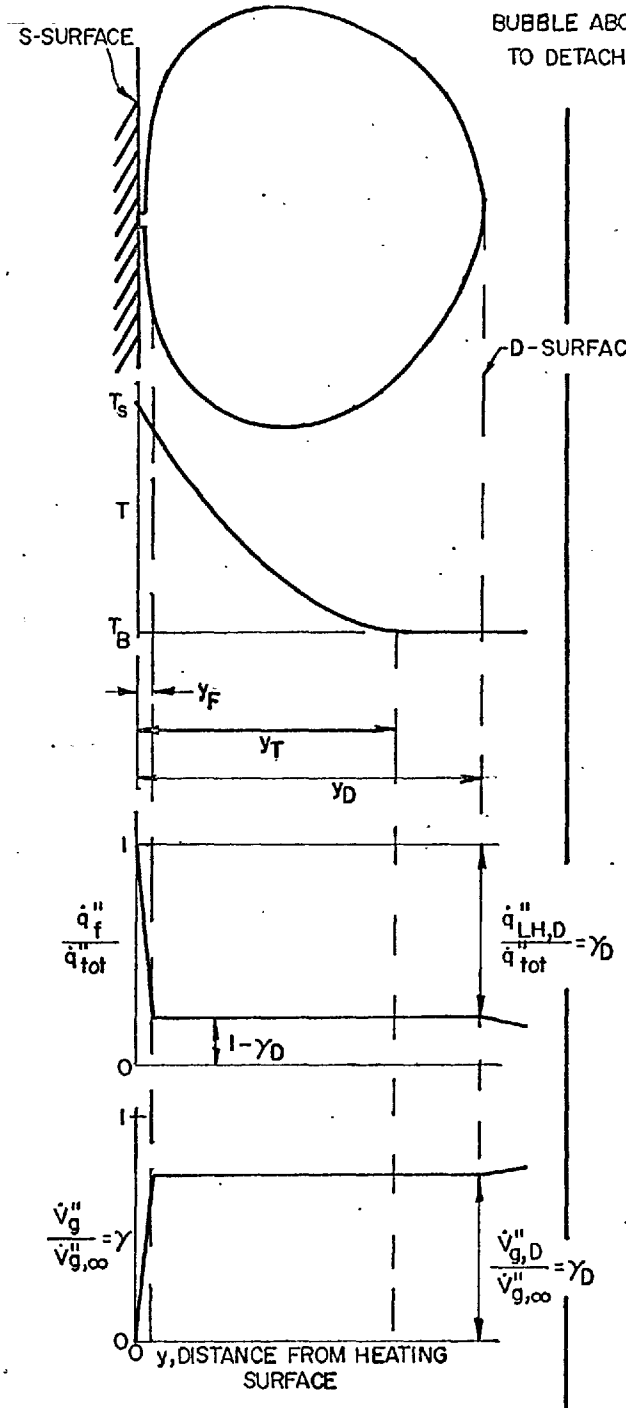

CONDITIONS:

(i) $y_T < y_D$

(ii) $y_T \gg y_F$

(iii) ALL VAPOUR GENERATED AT y_F

FIG. 2.4a CONDITIONS FOR LOWER LIMIT OF ζ: $\zeta = 1-\gamma_D$

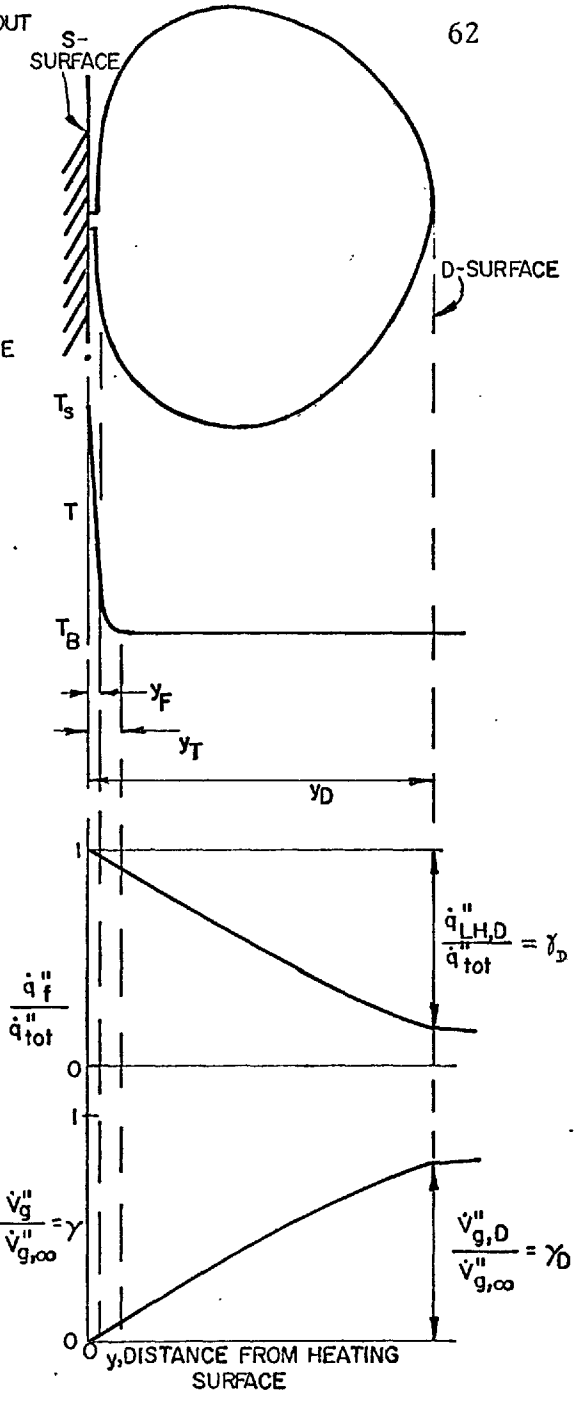

CONDITIONS:

(i) $y_T \ll y_D$

(ii) $y_T > y_F$ or $y_T \gg y_F$

(iii) ALL VAPOUR GENERATED AT TOP OF BUBBLE

FIG. 2.4b CONDITIONS FOR UPPER LIMIT OF ζ: $\zeta = 1$

FIG. 2.4

FIG. 2.4 LIMITING CASES FOR $\zeta (\equiv \frac{\alpha_f}{\alpha_{tot}})$ IN BOILING

Table 2.2 Conditions Attending the Limiting Cases for $\zeta(\equiv \frac{\alpha_f}{\alpha_{tot}})$ in Boiling

		Lower Limit $\zeta = 1 - \gamma_D$	Upper Limit $\zeta = 1$
Physical Conditions	(i) $y_T \sim y_D$	$y_T < y_D$	$y_T << y_D$
	(ii) $y_T \sim y_F$	$y_T >> y_F$	$y_T > y_F$ or $y_T >> y_F$
	(iii) Where the vapour is generated.	All generated at y_F from the liquid film.	All generated from the top of the bubble.
	Depicted in Fig.	2.4a	2.4b
Resulting Relations	$\dot{q}''_f$	$\simeq$ Const.	$\simeq$ Const.
		$\simeq \dot{q}''_{tot} - \dot{q}''_{LH,D}$	$\simeq \dot{q}''_{tot}$
	α_f, from equation (2.10)	$\frac{\dot{q}''_{tot} - \dot{q}''_{LH,D}}{T_S - T_B}$	$\frac{\dot{q}''_{tot}}{T_S - T_B}$
	ζ, from equations (2.11), (2.12) and (2.22)	$1 - \frac{\dot{q}''_{LH,D}}{\dot{q}''_{tot}}$	1
		$= 1 - \gamma_D$	

transfer data. It was mentioned earlier that in making the comparisons, it would be necessary to use information on the latent heat fraction at the D-surface γ_D in conjunction with the boiling data. Because the information, on which the $\gamma_D \sim Ku$ function was based, was limited, three different assumptions in varying degrees of restriction were made concerning the function's applicability (Section 2.5.4).

Now, to represent the boiling data, equations are used below; the applicability of the equations correspond with the applicability of the $\gamma_D \sim Ku$ function. This is illustrated in Table 2.3. This table shows three cases of comparison which are performed below. The barbotage data used in each comparison is also indicated in the table.

There is more detailed discussion below on the dimensionless coordinates, the boiling equations and the barbotage data used in the comparisons. The final result of the comparisons is shown in Figs.2.5 and 2.7.

2.7.2 Dimensionless Coordinates Employed

The coordinates for the comparison are:

(i) as the abscissa, a non-dimensionalized $\dot{V}''_g$,

(ii) as the ordinate, non-dimensionalized α_f.

Both $\dot{V}''_g$ and α_f are made dimensionless by the use of fluid properties.

In more detail, the abscissa is chosen as Ku^* a modified form of the Kutataledze number defined by

Table 2.3 Comparison Cases

Comparison		Boiling		Barbotage
Case	Presented in Fig.	Applicability of $\gamma_D \sim Ku$ function, Fig. 2.3	Applicability of boiling equation	Data used ($\dot{V}''_g < \dot{V}''_{g,cr}$)
Case 1 Most general case	2.5	Case 1. All liquids regardless of fluid properties.	Case 1. All liquids regardless of fluid properties. Equation (2.42) and hence (2.47).	Case 1. All existing data for horizontal porous plates. See Table 2.4.
Case 2	2.7	Case 2. Water and organic liquids at atmospheric pressure.	Case 2. Water and organic liquids at atmospheric pressure. Equation (2.49) and hence (2.50).	Case 2. As above for Case 1. All existing barbotage data is for water and organic liquids at atmospheric pressure.
Case 3 Most restricted case	2.7	Case 3. Water at atmospheric pressure.	Case 3. Water at atmospheric pressure. Same equation as for Case 2. above.	Case 3. Water at atmospheric pressure. (Injected gas: air).

$$Ku^* \equiv \frac{\dot{V}''_g \rho_g^{\frac{1}{2}}}{[\sigma g_o \, g(\rho_f - \rho_g)]^{\frac{1}{4}}} \tag{2.34}$$

This definition applies to both boiling and barbotage. As explained previously (Section 2.5.1), the relevant $\dot{V}''_g$ for boiling is taken to be $\dot{V}''_{g,D}$. For boiling, from equations (2.34), (2.23) and (2.24) there results

$$Ku^* = \gamma_D \, Ku \tag{2.35}$$

Similarily, it is possible to write

$$Ku^*_{cr} = \gamma_D \, Ku_{cr} \tag{2.36}$$

where Ku^*_{cr} is the value of Ku^* at the critical heat flux (burnout).

The reasons for choosing Ku^* as the abscissa are given below.

(i) The use of Ku^* gives a common upper limit on the abscissa for boiling and barbotage. The argument is as follows. In obtaining the criterion for the critical heat flux for boiling on horizontal heaters ($Ku_{cr} = 0.16 \pm 0.03$), Kutateladze [50] postulated that the critical heat flux is due to a hydrodynamic crisis. The value of Ku^*_{cr} corresponding to $Ku_{cr} \simeq 0.16$ may be obtained from Fig. 2.3 as

$$\begin{aligned} Ku^*_{cr} &= \gamma_D \, Ku_{cr} \\ &\simeq (0.85)(0.16) \\ &\simeq 0.14 \end{aligned}$$

Similarily in barbotage, the existence of a hydrodynamic crisis similar to that in boiling has been postulated [54], the substantiation appearing in Refs. 1, 54, 58, 80 and 87. In heat-transfer barbotage, this crisis occurs at the critical gas injection velocity $\dot{V}''_{g,cr}$ where a maximum occurs in a plot of $\alpha_f \sim \dot{V}''_g$ [1,80] (see sketch below).

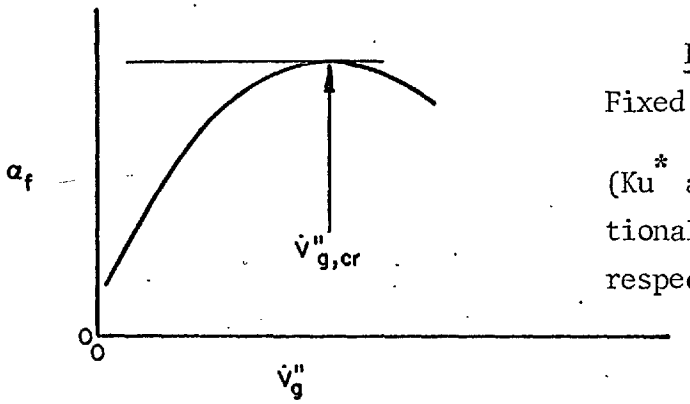

Barbotage

Fixed: liquid, gas porous plate.

(Ku^* and Ku^*_{cr} are proportional to $\dot{V}''_g$ and $\dot{V}''_{g,cr}$ respectively).

SKETCH ILLUSTRATING LOCATION OF $\dot{V}''_{g,cr}$

For barbotage Ku^*_{cr} is therefore defined as

$$Ku^*_{cr} \equiv \frac{\dot{V}''_{g,cr}\,\rho_g^{\frac{1}{2}}}{[\sigma g_o\, g(\rho_f - \rho_g)]^{\frac{1}{4}}} \qquad (2.37)$$

In heat-transfer barbotage the values of Ku^*_{cr} obtained for horizontal heaters are:

Akturk [1], 0.08 to 0.095,

Gose et al. [27] as calculated in [80], 0.13 to 0.23†.

It is therefore considered acceptable here to use a value of about

† Except for the Oil 69 data of Gose et al.

0.14 to represent Ku^*_{cr} for heat-transfer barbotage.

In summary then Ku^* is a measure in both boiling and barbotage of the proximity of the bubbling rate to the hydrodynamic crisis, $Ku^* \simeq 0.14$ being the approximate value at which the crisis occurs. The present comparisons of α_f are restricted to bubbling rates less than the critical; this then gives a common upper limit for boiling and barbotage on the abscissa.

(ii) It can be shown that it is necessary to use Ku^* as the abscissa if (a) it is desired to represent boiling on the comparisons graph by a unique line independent of fluid properties for a given value of $\zeta(\equiv \alpha_f/\alpha_{tot})$ and (b) it is assumed (as it is here) that γ_D is a function of Ku only (or of Ku^* only since $Ku^* = \gamma_D\, Ku$).

The ordinate follows from the equation used to represent boiling. This will become clearer in Section 2.7.3 immediately below.

2.7.3 Equations Representing Boiling

Case 1 - Boiling equation representing all liquids boiling on smooth surfaces.

Some boiling correlations may be arranged in the form

$$\alpha_{tot} = \phi\left(\frac{\dot{q}''_{tot}}{\rho_g h_{fg}}\ ,\ \text{fluid properties}\right) \qquad (2.38)$$

where $\phi(\quad)$ means "some function of". The above equation may be manipulated into

$$\alpha_f = \phi(\dot{V}''_{g,D} , \gamma_D , \zeta , \text{fluid properties}) \qquad (2.39)$$

or in dimensionless form

$$Nu^*_f = \phi(Ku^* , \gamma_D , \zeta , \text{dimensionless fluid property groups}) \qquad (2.40)$$

where a special form of Nusselt number is defined by

$$Nu^*_f \equiv \frac{\alpha_f}{k_f} \sqrt{\frac{\sigma g_o}{g(\rho_f - \rho_g)}} \qquad (2.41)$$

and k_f is the thermal conductivity of the liquid. It is then possible to plot both barbotage data and the boiling equation on coordinates of

$$\frac{Nu^*_f}{\phi(\text{dimensionless fluid property groups})} \text{ vs. } Ku^*$$

The Tolubinskii-Sagan [74] relation is used here to represent boiling for a combination of the following reasons.

(i) It can be written in terms of variables or fluid properties which have meaning in barbotage as well as boiling. An example of a property used in some boiling equations, e.g. [55,56,14,39,22], but having no meaning in barbotage is, T_{sat} the saturation temperature of the liquid. Another example is h_{fg} when it does not appear in combination as $\dot{q}''_{tot} / \rho_g h_{fg}$, e.g. [15, 55, 38].

(ii) There is no constant to fix which depends on surface-fluid combination.

(iii) It contains no linear dimension which relates to heater size.

By far the majority of investigators agree that heater size has little effect on the heat-transfer coefficient.

(iv) It fits boiling data having a wide range of fluid properties.

(v) It is extremely simple.

The Tolubinskii-Sagan [74]† relation is

$$Nu^*_{tot}\, Pr_f^{0.2} = 41.3 \left(\frac{q''_{tot}}{\rho_g\, h_{fg}\, D_b\, f}\right)^{0.6} \tag{2.42}$$

where a form of Nusselt number is defined as

$$Nu^*_{tot} \equiv \frac{\alpha_{tot}}{k_f} \sqrt{\frac{\sigma g_o}{g(\rho_f - \rho_g)}} \tag{2.43}$$

and Pr_f is the liquid Prandtl number. The product $D_b f$, for which the symbol ω is used below, is given by the empirical relation††

$$\omega = D_b f = 918 \left(\frac{\rho_g'}{\rho_g}\right)^{1.1} \quad \text{ft/h} \tag{2.44}$$

where ρ_g' is the vapour density at one atm abs pressure.

---

†Tolubinskii [83] proposed the following equation for the correlation of heat-transfer data in saturated nucleate pool boiling:

$$Nu^*_{tot}\, Pr_f^{0.3} = 54 \left(\frac{q''_{tot}}{\rho_g\, h_{fg}\, D_b\, f}\right)^{0.6} \tag{2.44a}$$

Sagan [74], subsequently investigating the effect of the Prandtl number over a very wide range ($1.7 \leqslant Pr_f \leqslant 1540$), modified the Tolubinskii equation to that of equation (2.42), which is therefore called the Tolubinskii-Sagan equation.

††Both Tolubinskii [83] and Sagan [74] used this relation for ω or $D_b f$.

Alegbraic manipulation of equation (2.42) yields

$$\frac{\zeta \, Nu^*_{tot}}{N_1^{0.6} \, Pr_f^{-0.2}} = 41.3 \, \frac{\zeta}{\gamma_D^{0.6}} \, (\gamma_D \, Ku)^{0.6} \tag{2.45}$$

where

$$N_1 \equiv \frac{[\sigma g_o \, g(\rho_f - \rho_g)]^{\frac{1}{4}}}{\omega \, \rho_g^{\frac{1}{2}}} \tag{2.46}$$

Now $\zeta \equiv \dfrac{\alpha_f}{\alpha_{tot}} = \dfrac{Nu^*_f}{Nu^*_{tot}}$

and $Ku^* = \gamma_D \, Ku$

Equation (2.45) may therefore be written as

$$\frac{Nu^*_f}{N_1^{0.6} \, Pr_f^{-0.2}} = 41.3 \, \frac{\zeta}{\gamma_D^{0.6}} \, (Ku^*)^{0.6} \tag{2.47}$$

which is the equation used to represent boiling in the comparisons on coordinates of $\dfrac{Nu^*_f}{N_1^{0.6} \, Pr_f^{-0.2}}$ vs. Ku^*. Equation (2.47) is plotted in Fig. 2.5 for the two limits of $\zeta = 1$ and $\zeta = 1 - \gamma_D$; values of γ_D were obtained from Fig. 2.3.

Case 2 - Equation representing water and organic liquids boiling at atmospheric pressure on smooth surfaces.

When a restriction to atmospheric pressure is allowed, it is possible to obtain a variation of the Tolubinskii-Sagan equation which has certain advantages over the original equation.

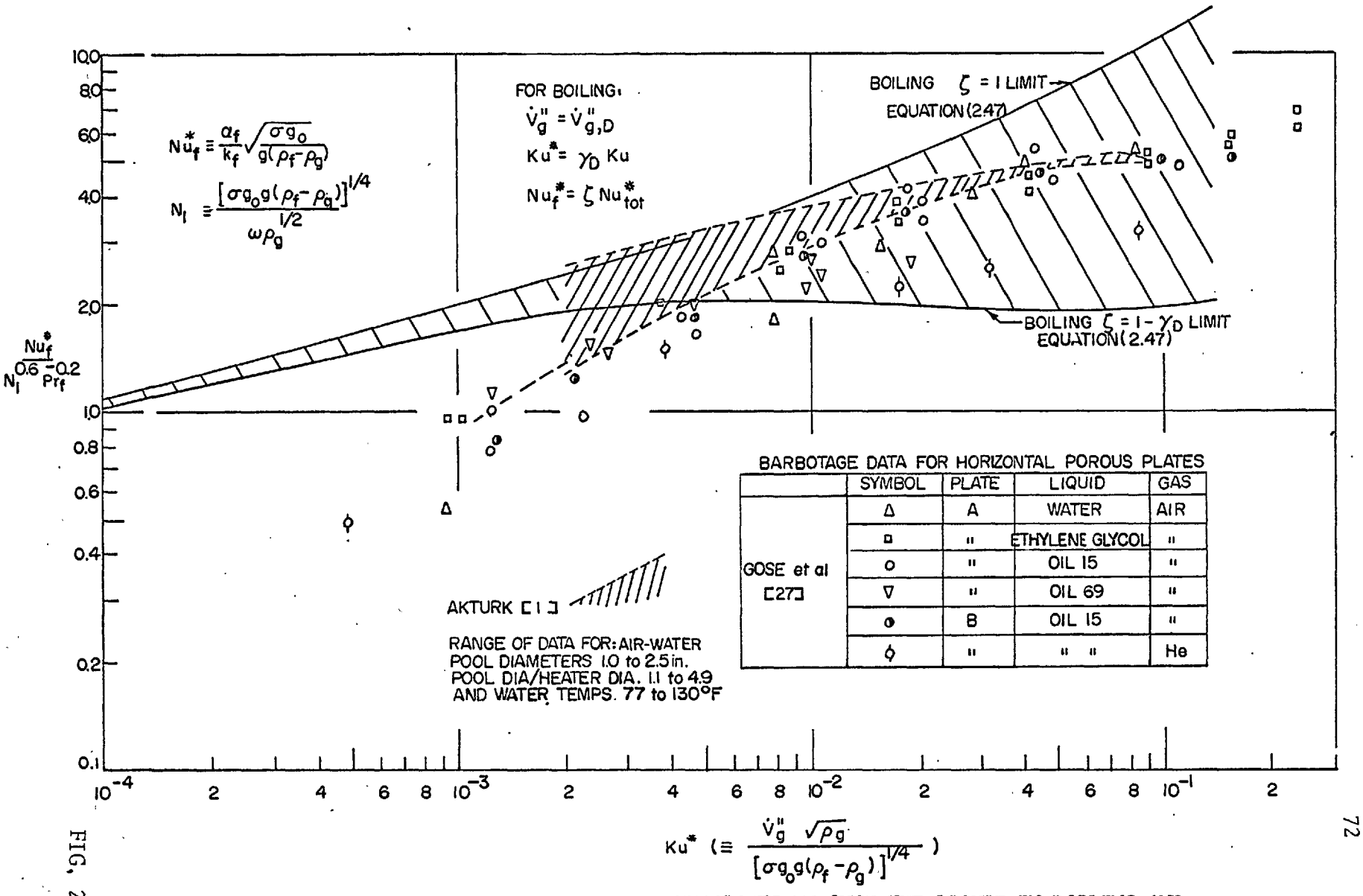

FIG. 2.5 COMPARISON OF HEAT-TRANSFER-COEFFICIENTS-THROUGH THE-LIQUID IN BOILING AND BARBOTAGE, MOST GENERAL CASE

(i) Instead of using equation (2.44), which involves a dimensional constant, for $D_b f$, the Zuber [92] relation is used*. The latter relates $D_b f$ to fluid properties and a dimensionless constant. The resulting final equation therefore relates the heat-transfer coefficient to heat flux and fluid properties only.

(ii) A very simple dimensionless grouping results for the ordinate on the comparisons graph.

The Zuber [92] relation for $D_b f$ is

$$D_b f = 0.59 \left[\frac{\sigma g_o \, g(\rho_f - \rho_g)}{\rho_f^2} \right]^{1/4} \tag{2.48}$$

Substitution of (2.48) in (2.42) yields

$$Nu^*_{tot} \, Pr_f^{0.2} = 56.7 \, (Ku \sqrt{\frac{\rho_f}{\rho_g}})^{0.6} \tag{2.49}$$

Now, the liquids of special interest here are water and organics since these are the liquids which were used in the barbotage experiments. In order to test whether equation (2.49) does indeed represent boiling of these liquids at atmospheric pressure, Fig. 2.6 presents this equation together with representative boiling data including all the widely-quoted Cichelli and Bonilla [11] data at atmospheric pressure. It is concluded that the agreement is satisfactory for the present purpose.

Equation (2.49) may be manipulated further to yield

---

*The Zuber relation quoted as equation (2.48) applies only at atmospheric or near-atmospheric pressure. A test of the relation against water data at 1 to 5 atm abs pressure [95] verifies this statement.

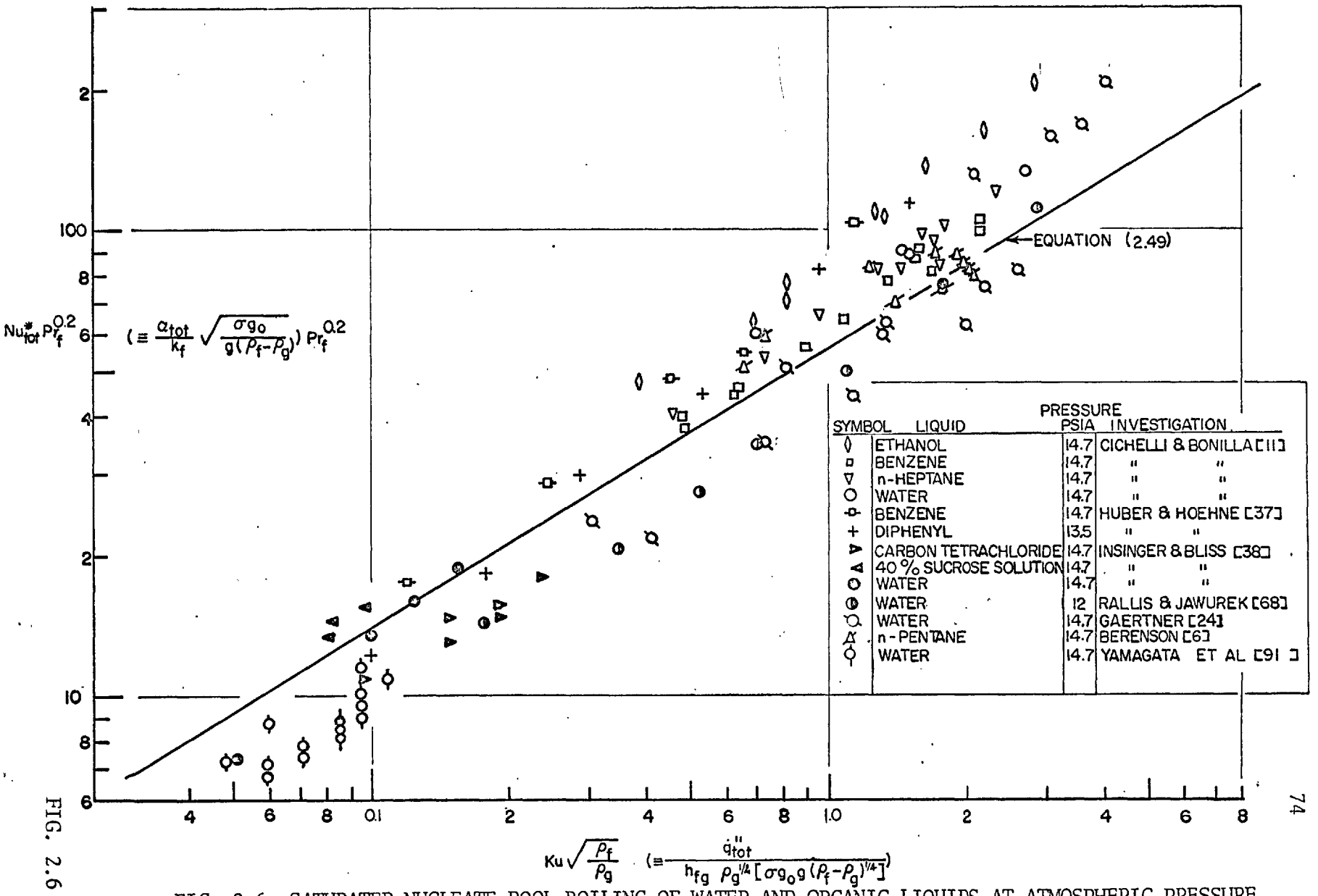

FIG. 2.6 SATURATED NUCLEATE POOL BOILING OF WATER AND ORGANIC LIQUIDS AT ATMOSPHERIC PRESSURE

$$\frac{Nu^*_f}{Pr_f^{-0.2}\left(\frac{\rho_f}{\rho_g}\right)^{0.3}} = 56.7 \frac{\zeta}{\gamma_D^{0.6}} (Ku^*)^{0.6} \qquad (2.50)$$

This equation, used to represent boiling of water and organic liquids at atmospheric pressure, is plotted in Fig. 2.7 for the two limits of $\zeta = 1$ and $\zeta = 1 - \gamma_D$; γ_D was obtained from Fig. 2.3.

Case 3 - Equation representing boiling of water at atmospheric pressure on a smooth surface.

Equation (2.49) and hence (2.50) represent the saturated nucleate boiling of water at atmospheric pressure (see Fig. 2.6).

2.7.4 Barbotage Data Used in the Comparisons

There are two important sources of heat-transfer barbotage data for horizontal porous surfaces: Akturk [1] and Gose et al. [27]*. The relevant details of these experiments are given in Table 2.4. The results obtained by Mixon et al. [63] for heat transfer at a surface with electrolytic gas evolution are not included here as the range of their Ku^* (maximum $Ku^* \simeq 3 \times 10^{-6}$) is well below the minimum Ku^* ($\simeq 1.4 \times 10^{-5}$) information available in boiling.

*Gose et al. performed experiments with drilled plates as well as porous plates (the term "porous" here describes metal plates manufactured by sintering metal powders while "drilled" describes solid metal plates with holes drilled through them). The drilled plates are unlike boiling heat-transfer surfaces in that the number of bubble generation sites does not vary with the amount of gas leaving the heat-transfer surface; nor with drilled plates does any phenomenon occur which corresponds to the critical heat flux in boiling [80]. For these reasons, the Gose et al. drilled plate data are not used here.

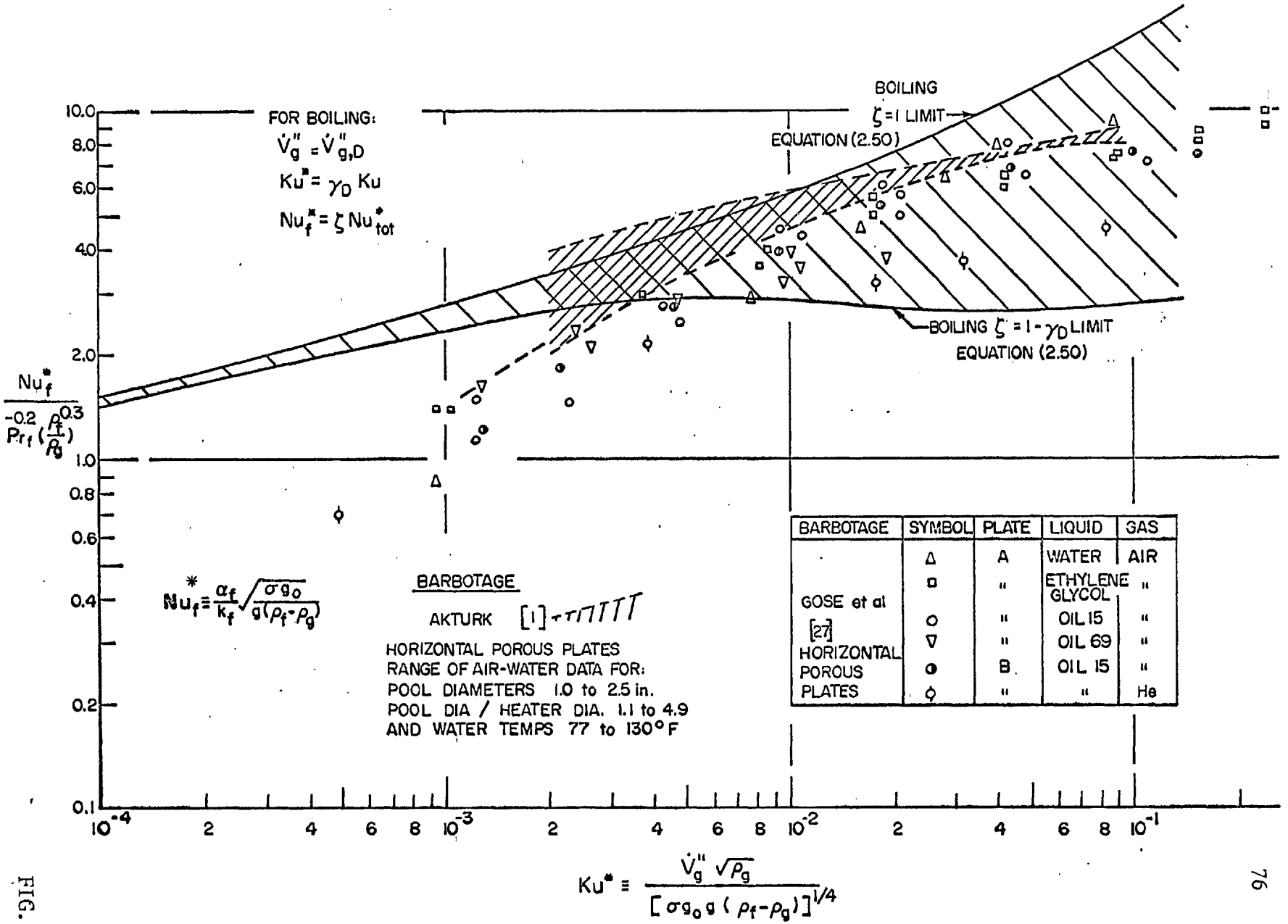

FIG. 2.7 COMPARISON OF HEAT-TRANSFER-COEFFICIENTS-THROUGH-THE-LIQUID IN BOILING AND BARBOTAGE AT ATMOSPHERIC PRESSURE

Table 2.4 Experimental Details for the Horizontal Porous Plate Barbotage Data of Akturk [1] and Gose et al. [27]

	Akturk [1]	Gose et al. [27]		
Liquids	Water	Water Ethylene Glycol Shell Tellus Oil 15 Shell Tellus Oil 69		
Gases	Air	Air Helium		
Range of Pr_f at heating surface temperature	3.3 to 6.2	3.4 to 574		
Geometry	Circular plates, diameters 1.0 to 2.5 in. Ratio pool diameter to porous plate diameter, 1.1 to 4.9	Circular plates, diameter 2.75 in.		
Description of porous plates	"Porosint" sintered porous bronze, grade C. Average particle size 0.0045 in. Maximum particle size to pass through pores 12.5 μ (0.0005 in.) Volumetric porosity* 38%.	Sintered porous bronze.		
		Plate	A	B
		Surface porosity**, %	30	30
		Mean pore dia., in.	0.0015	0.015
		Mean particle dia., in.	0.0025	0.020
		Pores/in.^{2}	80,000	1140
		Particles /in.^{2}	86,000	1290

* Volumetric porosity $\equiv \frac{\text{volume of voids}}{\text{total volume}}$

** Surface porosity $= \frac{\text{area of pores}}{\text{total projected area}}$

The data of Akturk [1] and Gose et al. [27] for bubbling rates less than the critical (i.e. $\dot{V}''_g < \dot{V}''_{g,cr}$ where $\dot{V}''_{g,cr}$ is that obtained experimentally for each system of gas, liquid and porous plate) are plotted in Figs. 2.5 and 2.7. The fluid properties were evaluated at the heating surface temperature. In Fig. 2.5 equation (2.44) has been used for ω in barbotage as well as boiling.

Although the heat fluxes considered in the model (Section 2.2.2) can include effects due to natural convection, the main interest here is in conditions where bubbles determine the flow near the heating surface; for this reason eight data points of Gose et al., all at the lowest values of Ku^* where natural convection processes probably control the heat transfer, have been omitted from Figs. 2.5 and 2.7.

2.7.5 Comparison and Discussion

Case 1 - Most general case. Comparison of the boiling equation representing all liquids with existing barbotage data for horizontal porous plates.

Fig. 2.5 shows the comparison of the dimensionless heat-transfer-coefficient-through-the-liquid α_f in pool barbotage and saturated nucleate pool boiling for the most general case (see Table 2.3). The most important feature of the figure is that the majority of the barbotage results lie within the two limits of the boiling equation. The conclusion to be drawn is that, providing

suitably-defined heat-transfer coefficients and vapour velocities are used, there is indeed good correspondence between pool barbotage and pool boiling results, at least for $Ku^* > 0.005$. The width of the "band" between the two limits $\zeta = 1$ and $\zeta = 1 - \gamma_D$ is rather wide at large values of Ku^*; unfortunately, with the present state of knowledge it is very difficult, if not impossible, to assign a more precise value to ζ.

The barbotage data of Gose et al. [27] encompasses a wide range of fluid properties, at least as far as Pr_f is concerned ($3.4 \leq Pr_f \leq 574$). In Fig. 2.5 it is noted that their data are well correlated among themselves except for three of the five Oil 15 - helium data points which fall approximately 40% below a mean line (not drawn in) through the remainder of the Gose et al. data in which air was the injected gas (the other two Oil 15 - helium data points fall within the scatter of the rest of the Gose et al. data). For the present work, in which the object is to compare barbotage and boiling heat-transfer coefficients, the error is not of great concern.

Case 2 - Comparison of the equation representing boiling water and organic liquids at atmospheric pressure with atmospheric pressure barbotage data for horizontal porous plates.

Fig. 2.7 shows the comparison of the dimensionless α_f for this case (see Table 2.3). As with Fig. 2.5, the most important

feature of this figure is that the majority of the barbotage results lie within the two limits of the boiling equation. The comments above for Case 1 may be applied in the present case as there is no significant difference between the two cases as far as the degree of agreement between boiling and barbotage is concerned.

Case 3 - Comparison of water boiling at atmospheric pressure with atmospheric-pressure air-water barbotage data for horizontal porous plates.

This case (see Table 2.3) of comparisons is also depicted in Fig. 2.7. The boiling equation of Case 2 obviously applies to the present case as well. The barbotage data under consideration is only that of air-water systems, i.e. all the Akturk [1] data and the "upright triangles" of the Gose et al. [27] data. As with Cases 1 and 2 the agreement between boiling and barbotage is good.

General comments.

Case 1 is the most general case, but involves the most speculation with respect to the application of the latent heat fraction of the D-surface γ_D (Fig. 2.3) to all liquids regardless of fluid properties.

Case 2 still involves speculation with respect to the application of $\gamma_D \sim Ku$ to water and organic liquids boiling at atmospheric pressure. For this case though, the equation representing boiling has advantages over that for Case 1, namely, a dimensional constant

was eliminated and a very simple ordinate on the comparisons graph resulted. Case 3 involved virtually no speculation with respect to the application of the $\gamma_D \sim Ku$ function to boiling water at atmospheric pressures. Regardless of which case is considered, the comparisons graphs (Fig. 2.5 and 2.7) appear similar; in every case the agreement between barbotage and boiling is good.

In earlier quantitative comparisons [80,27,49] between barbotage and saturated nucleate pool boiling heat-transfer coefficients, the implicit assumptions were that $\zeta = 1$ and $\gamma_D = 1$ for boiling. The present treatment is the result of further consideration, particularily in the light of the Rallis and Jawurek [68] work which has since become available.

Greif [30] has recently state, "Gas volume injection and saturated nucleate boiling may be similar when the two systems have the same injection velocity and the same number of bubble sources. Matching the gas injection velocity alone will not result in similar systems". The justification for making comparisons between barbotage and boiling which do not take into account the number of bubble sources (as in all the previous and the present comparisons) is that many boiling correlations e.g. [22,51,55,70,74,83], do not take into account the number of bubble sources and yet are successful in correlating the boiling data, at least for water and organics on "smooth" surfaces. The barbotage data of Akturk [1] and Gose et al. [27] are for water and organics; in these papers the number of bubble sources was not reported.

It is hoped that the work contained in the present chapter will stimulate future thought about the connection between saturated nucleate pool boiling and pool barbotage (Link 2 in Fig. 1.1) and about the processes occurring in boiling; this might well lead to an improved correlation for boiling which includes two terms, one accounting for the heat transfer through the liquid, the second covering the latent heat transport. Barbotage experiments should assist in determining the first of these.

Conclusions and summary for the present chapter.

1. The processes of saturated nucleate pool boiling and pool barbotage were examined with the main differences emerging as: (i) the vapour velocity and (ii) the heat flux through the liquid in boiling are functions of the distance y from the heating surface while for barbotage these quantities are uniform with respect to y.

2. For the purpose of comparing heat-transfer coefficients a "heat-transfer-coefficient-through-the-liquid" α_f was defined which accounts for the same heat-transfer mechanisms in barbotage and boiling. Further, from data appearing in the literature an estimate was made of the vapour formation rate in boiling; this information in turn was used in the comparisons.

3. The dimensionless α_f in saturated nucleate pool boiling and pool barbotage are closely comparable in magnitude.

Table 2.5 Summary of Equations Used in Chapter 2

Boiling	Common	Barbotage	
Eq. no.			Eq. no.
2.2	$\dot{m}''_{f,in} = \dot{m}''_{f,out} + \dot{m}''_g$	$\dot{m}''_{f,in} = \dot{m}''_{f,out}$	
2.3	$h_g - h_{f,in} \simeq h_g$		
2.4	$\dot{q}''_{tot} = \dot{q}''_{diff} + \dot{m}''_{f,out} \times (h_{f,out} - h_{f,in}) + \dot{m}''_g h_{fg}$	$\dot{q}''_{tot} = \dot{q}''_{diff} + \dot{m}''_{f,out} \times (h_{f,out} - h_{f,in})$	2.8
2.5	$\dot{q}''_{LH} = \dot{m}''_g h_{fg}$		
2.6	$\dot{q}''_f \equiv \dot{q}''_{diff} + \dot{m}''_{f,out}(h_{f,out} - h_{f,in})$		
2.7	$\dot{q}''_{tot} = \dot{q}''_f + \dot{q}''_{LH}$	$\dot{q}''_{tot} = \dot{q}''_f$	2.9
2.10	$\alpha_f \equiv -\dfrac{1}{\int_{T_S}^{T_B} \frac{dT}{\dot{q}''_f}}$		
2.11	$\alpha_{tot} \equiv \dfrac{\dot{q}''_{tot}}{T_S - T_B}$		
2.12	$\zeta = \dfrac{\alpha_f}{\alpha_{tot}}$		
		$\alpha_f = \dfrac{\dot{q}''_f}{T_S - T_B} = \dfrac{\dot{q}''_{tot}}{T_S - T_B}$	2.15
2.16	$\dot{V}''_g = \dfrac{\dot{m}''_g}{\rho_g}$		

Table 2.5 (Cont'd)

Boiling	Common	Barbotage	
Eq. no.			Eq. no.
2.17 2.21	$\dot{V}''_g = \frac{\dot{q}''_{LH}}{\rho_g h_{fg}} = \gamma \frac{\dot{q}''_{tot}}{\rho_g h_{fg}}$		
2.18 2.20	$\gamma \equiv \frac{\dot{q}''_{LH}}{\dot{q}''_{tot}} = \frac{\dot{V}''_g}{\dot{V}''_{g,\infty}}$		
2.13 2.22	$\gamma_D \equiv \frac{\dot{q}''_{LH,D}}{\dot{q}''_{tot}} = \frac{\dot{V}''_{g,D}}{\dot{V}''_{g,\infty}}$		
2.19	$\dot{V}''_{g,\infty} = \frac{\dot{q}''_{tot}}{\rho_g h_{fg}}$		
2.26	$\dot{V}''_{g,b} = \frac{n}{A} \overline{fV_b}$		
2.27	$\dot{q}''_{LH,b} = \dot{V}''_{g,b} \rho_g h_{fg}$		
2.28	$\dot{V}''_{g,b} \simeq \dot{V}''_{g,D}$ $\dot{q}''_{LH,b} \simeq \dot{q}''_{LH,D}$ $\frac{\dot{q}''_{LH,b}}{\dot{q}''_{tot}} \simeq \frac{\dot{q}''_{LH,D}}{\dot{q}''_{tot}} \simeq \gamma_D$ $\frac{\dot{V}''_{g,b}}{\dot{V}''_{g,\infty}} \simeq \frac{\dot{V}''_{g,D}}{\dot{V}''_{g,\infty}} \simeq \gamma_D$			
	Tolubinskii-Sagan:		
2.42	$Nu^*_{tot} Pr_f^{0.2} = 41.3 \left(\frac{\dot{q}''_{tot}}{\rho_g h_{fg} D_b f}\right)$		

Table 2.5 (Cont'd)

Boiling	Common	Barbotage

Eq. no. 2.47

or

$$\frac{Nu^*_f \, Pr_f^{0.2}}{N_1^{0.6}} = 41.3 \, \frac{\zeta}{\gamma_D^{0.6}} \, (Ku^*)^{0.6}$$

Zuber:

$$D_b \, f = 0.59 \left[\frac{\sigma g_o \, g(\rho_f - \rho_g)}{\rho_f^2}\right]^{1/4}$$

Tolubinskii-Sagan with $D_b f$ of Zuber:

Eq. no. 2.49

$$Nu^*_{tot} \, Pr_f^{0.2} = 56.7 \, \left(Ku\sqrt{\frac{\rho_f}{\rho_g}}\right)^{0.6}$$

or

Eq. no. 2.50

$$\frac{Nu^*_f \, Pr_f^{0.2}}{\left(\frac{\rho_f}{\rho_g}\right)^{0.3}} = 56.7 \, \frac{\zeta}{\gamma_D^{0.6}} \, (Ku^*)^{0.6}$$

Dimensionless Groups

Eq. no. 2.24

$$Ku \equiv \frac{\dot{q}''_{tot}}{h_{fg} \, \rho_g^{1/2} [\sigma g_o \, g(\rho_f - \rho_g)]^{1/4}}$$

Eq. no. 2.25

$$Ku_{cr} \equiv \frac{\dot{q}''_{tot,cr}}{h_{fg} \, \rho_g^{1/2} [\sigma g_o \, g(\rho_f - \rho_g)]^{1/4}}$$

Eq. no. 2.34

$$Ku^* \equiv \frac{\dot{V}''_g \, \rho_g^{1/2}}{[\sigma g_o \, g(\rho_f - \rho_g)]^{1/4}}$$

Table 2.5 (Cont'd)

Boiling		Common		Barbotage	
Eq. no.					Eq. no.
	In Ku^*, $\dot{V}''_g = \dot{V}''_{g,D}$				
2.35	$Ku^* = \gamma_D Ku$				
2.36	$Ku^*_{cr} = \gamma_D Ku_{cr}$			$Ku^*_{cr} = \dfrac{\dot{V}''_{g,cr}\,\rho_g^{1/2}}{[\sigma g_o\, g(\rho_f - \rho_g)]^{1/4}}$	2.37
2.43	$Nu^*_{tot} \equiv \dfrac{\alpha_{tot}}{k_f}\sqrt{\dfrac{\sigma g_o}{g(\rho_f - \rho_g)}}$				
2.41		$Nu^*_f \equiv \dfrac{\alpha_f}{k_f}\sqrt{\dfrac{\sigma g_o}{g(\rho_f - \rho_g)}}$			
	$Nu^*_f = \zeta\, Nu^*_{tot}$				
2.46		$N_l \equiv \dfrac{[\sigma g_o\, g(\rho_f - \rho_g)]^{1/4}}{\omega\, \rho_g^{1/2}}$			
2.44		$\omega = D_b f = 918\,(\dfrac{\rho_g'}{\rho_g})$ ft/h			

CHAPTER 3 APPARATUS

3.1 General

The most important component of the apparatus was the test section in which the heat-transfer coefficient was measured while bubbling air through a heated porous wall into a stream of water or air-water mixture. A device, called here an "upstream air-injector" or just "upstream injector", introduced air into the water upstream of the heated test section. The circuits of the apparatus were:

(i) the water circuit,

(ii) the air-to-test-section circuit,

(iii) the-air-to-upstream-injector circuit,

(iv) the power supply to the test section,

(v) the thermocouple emf-measuring circuit.

These are described briefly in this chapter while the details of the equipment (model number, range, manufacturer, etc.) are given in Table F.2 of Appendix F. The numbers appearing beside the equipment in Figs. 3.2, 3.4 and 3.5 correspond to item numbers in Table F.2.

As an aid in determining flow patterns in the channel, high speed still photographs were taken with a 5 x 4 M.P.P. camera and a microflash light-source of 5 microseconds duration and 12 joules energy. The light source was mounted behind the test section with a diffusing screen placed between the light source and the test section. Stroboscopic flow-observations were also made. Details

of the photographic and stroboscopic equipment are in Table F.2.

The apparatus was situated in the Heat Transfer Laboratory of the Mechanical Engineering Department of Imperial College.

The accuracy and calibration of each measuring instrument is discussed in Appendix E, wherein a full error analysis is performed.

3.2 Test Section

3.2.1 General

The test section is shown in Fig. 3.1. It consisted of a horizontal rectangular channel of internal cross-sectional dimensions 0.52 x 0.257 in. (equivalent diameter 0.344 in.) with the 0.52-in. side vertical. In the bottom of the channel for a length of 5.91 in. was a heated porous element 0.0365-in. thick and 0.257-in. wide through which air was bubbled. The method of sealing between the porous element and the sides of the channel is shown in Fig. 3.1. The heated porous section was preceded by a 6-in. length and followed by an observation section of 12-in. length of the same cross-section. The sides of the channel were of transparent plastic allowing flow observations to be made along the channel length. The location of the upstream air-injector relative to the test section is shown in Fig. 3.3C.

3.2.2 Porous Heating Element

The porous element was used as an electrical resistance to

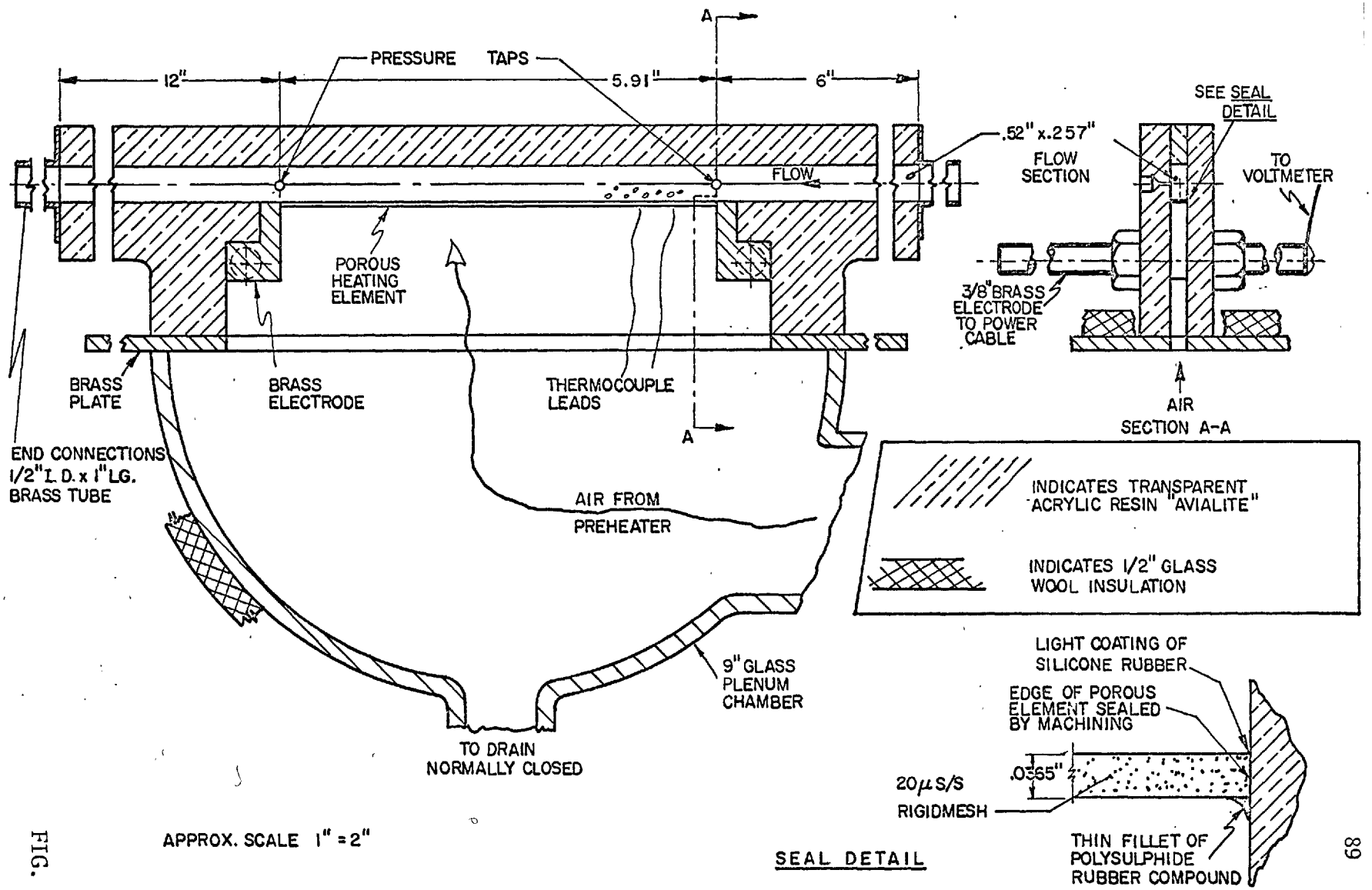

FIG. 3.1 DIAGRAM OF TEST SECTION

generate ac Joulean heating; with the present geometry this method of heating offered the advantage of simplicity, minimum heat flux losses to the ambient and minimum time to reach thermal equilibrium. The material used, stainless steel "Rigid Mesh" of 20μ nominal pore size, was chosen mainly because of its suitability as a resistance heater; it had high electrical resistivity, was available in thin sections, had good strength and was readily machinable; the combination of these properties was difficult to find in other porous materials such as porous carbon or sintered powdered bronze. Details of the Rigid Mesh material are given in Table 3.1 which includes a picture of the porous surface magnified 6.7 times.

3.2.3 Temperature Measurement

Two types of thermocouple were electrically resistance-welded along the bottom centre-line of the porous element; one type was iron-constantan (Honeywell Controls Ltd., 30 B. & S. gauge; type J) while the other was copper-constantan (Honeywell Controls Ltd., 30 B. & S. gauge, type T). The position of each thermocouple is listed in Table 3.2. A thermocouple from each reel of wire was calibrated in a bath over the temperature range used in the present experiments. As it was difficult to calibrate the thermocouples in situ once they had been welded to the test section, the presence of the two types of thermocouples allowed a check on whether welding affected the output emf of the thermocouples. There appeared to be no effect except in one thermocouple which has been omitted from Table 3.2.

Table 3.1 Details of Rigid Mesh Porous Material

Trade name	Porosint Rigid Mesh
Manufacturer	Sintered Products Limited, England.
Material	Stainless steel, American I.S.I. type 316, (British Spec. BS: En. 58J), Wire was Firth-Vickers' "Staybrite" F.M.B. Steel [96].
Nominal pore size	20 microns (0.0008 in.)
Construction	Three layers of screen calendered (rolled) and furnace welded. Each screen: warp, 0.125 in. dia., 24 wires/in.; weft, 0.010 in. dia., 110 wires/in. Adjacent layers have warp wires at right angles to each other. Hollander Weave.
Thickness	0.0365 in.
Volumetric porosity ($\equiv \frac{\text{vol. void}}{\text{total vol.}}$)	18.9%
Thermal conductivity k_{eff}	6.6_5 Btu/ft h degF (See Appendix B.)
Maximum possible pores/in.^{2}	5300
Approximate rms roughness	0.0006 in. in direction along channel

Table 3.1 (Cont.)

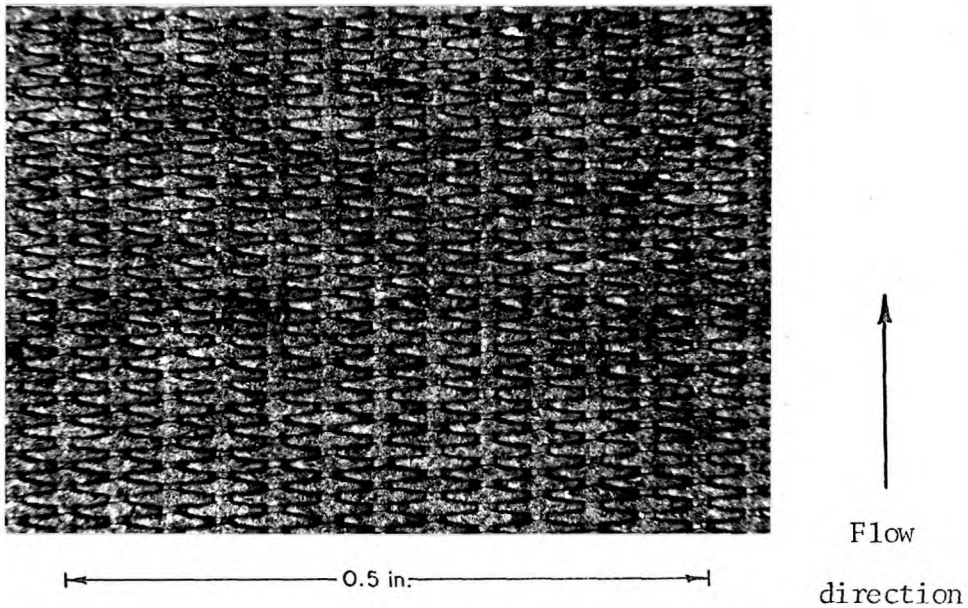

PICTURE OF POROUS SURFACE MAGNIFIED 6.7 TIMES

Table 3.2 Thermocouple Location Along the Bottom Centre-Line of the Porous Element

Distance from beginning of heated section x in.	x/L (L = total length of heated section)	Type of thermocouple
0.65	0.110	Fe Con
0.95	0.161	Cu Con
1.49	0.252	Fe Con
2.46	0.417	Fe Con
3.39	0.575	Fe Con
4.34	0.735	Fe Con
4.85	0.821	Cu Con

In the experiments, the air temperature approaching the bottom face of the porous element (to which the thermocouples were welded) was made approximately equal to the temperature of that face (by the use of an air-preheater, Item 17, Fig. 3.2). For equal temperatures there would be no thermal conduction error in the thermocouple readings as the thermocouple leads would be in a zone of zero temperature gradient. When temperature gradients did exist a small correction (generally ½ to 3% in the heat-transfer coefficient) was necessary; the method of correction is given in Appendix D.

The present thermocouple arrangement, had the advantage that the upper surface of the porous element, at which bubbling occurred, was left completely intact. Also, thermocouples resistance-welded to the bottom surface of the porous element were in intimate thermal contact with that surface. However, the arrangement had the disadvantage that the thermal conductivity of the porous material had to be known in order to obtain the temperature T_S of the upper surface of the porous material; T_S was necessary for the calculation of the heat-transfer coefficient. The method of obtaining the thermal conductivity k_{eff} of the Rigid Mesh material is given in Appendix B.

Although the electrical heating current passed through the porous element was ac, there was some small dc component (about ¼% at 50 amps ac) which affected the thermocouple emf readings. For accurate determination of the heat-transfer coefficient α when α is large, it is necessary to correct for this dc component - see example in

Appendix C wherein the method of correction is given. Generally this correction was less than 2% in the heat-transfer coefficient for the present data. It is believed that this is the first time this correction has been applied; the method therefore appears to be novel.

3.3 Water Circuit

The water circuit is shown in Fig. 3.2. Tap water (analysis in Appendix F) from the city mains supply was used; the items in the flow path were:

(i) a heater (or cooler) which controlled the water temperature,

(ii) one of two calibrated* Rotameters in parallel for the measurement of water flow rates,

(iii) one of two needle control valves in parallel,

(iv) a calibrated thermocouple probe measuring water temperature at entry to the upstream air-injector,

(v) the upstream injector where air was introduced into the water,

(vi) the test section,

(vii) a calibrated thermocouple probe measuring the outlet water temperature,

(viii) an open tank, thence to drain.

The static pressure in the channel at the inlet-end of the porous section was measured on a vertical U-tube mercury manometer.

* The term "calibrated" in this chapter indicates that a calibration of the measuring device was performed by the author, as opposed to a "manufacturer's calibration".

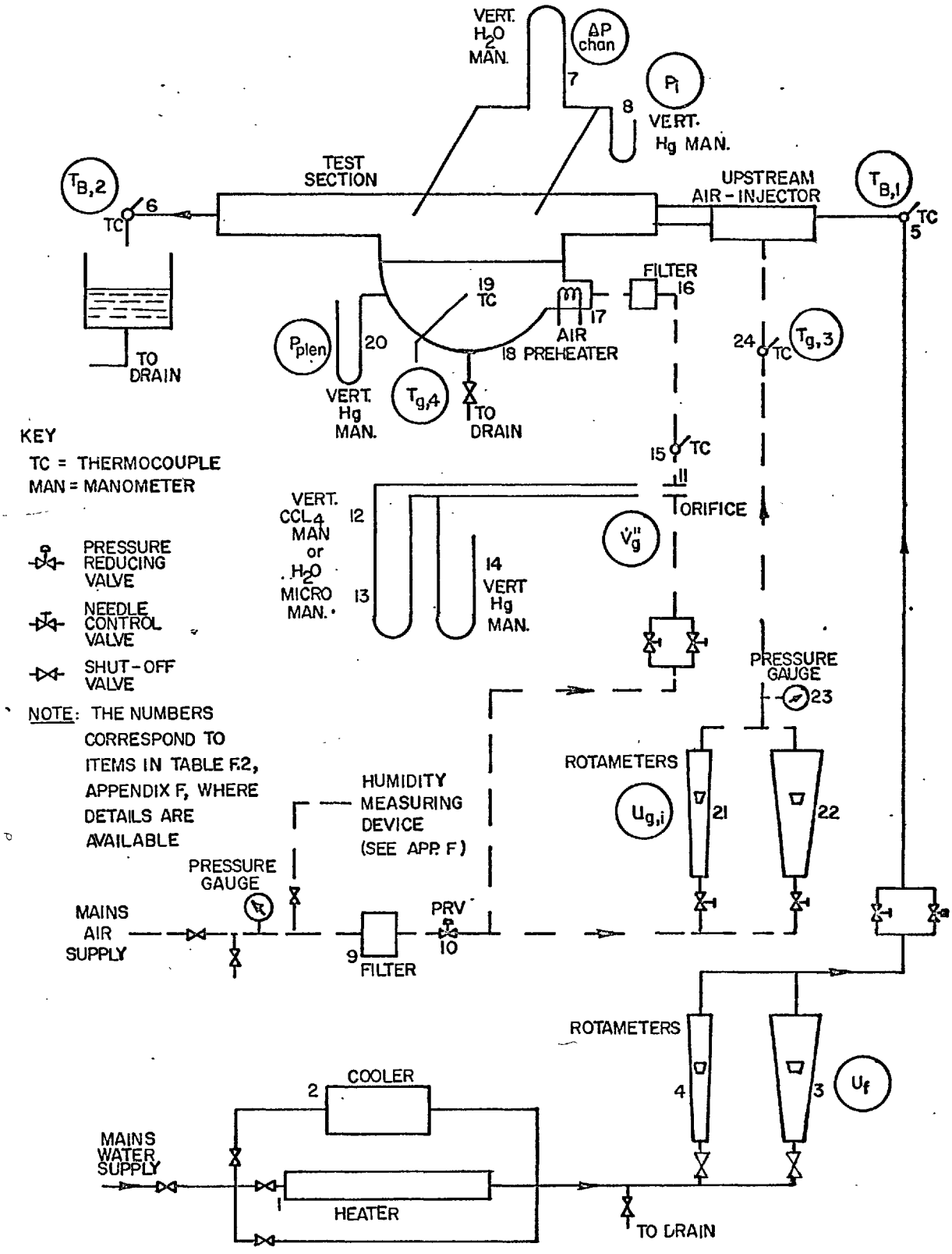

FIG. 3.2 FLOW DIAGRAM

FIG. 3.2

As a precaution, the thermocouples measuring the water temperature were isolated from any electrical contact with the water.

By far the majority of data were taken with the water heater in operation. The heating was electrical and controlled by means of variable autotransformers, which were fed by constant-voltage transformers. Over a ten-minute period, the water temperature at the outlet from the heater seldom changed by more than 0.2 deg F.

3.4 Air-to-Test-Section Circuit

The flow path is shown in Fig. 3.2. The usual source of air was the department compressed air supply at 56 psig; no pressure fluctuations could be detected in this supply so giving steady air flow rates. The flow path included the following items:

(i) a coarse air filter,

(ii) a pressure reducing valve,

(iii) one of two needle control valves in parallel,

(iv) a calibrated orifice measuring air flow rates,

(v) a calibrated thermocouple probe measuring the air temperature leaving the orifice,

(vi) a fine air filter,

(vii) an air-preheater controlled by a variable autotransformer,

(viii) the plenum chamber in which was located a calibrated thermocouple for air temperature measurement.

From the plenum chamber, which was directly beneath the test section,

the air passed through the porous heater into the water or air-water mixture in the flow channel.

The pressure drop across the orifice was measured on either a vertical U-tube carbon tetrachloride manometer or a water micro-manometer depending on the air flow rate; the static pressure at the orifice high pressure tap was measured on a vertical U-tube mercury manometer.

3.5 Air-to-Upstream-Injector Circuit

The flow circuit is shown in Fig. 3.2. After the pressure reducing valve the flow path included the following items:

(i) a needle control valve,

(ii) one of two calibrated Rotameters in parallel for measuring air flow rates,

(iii) a calibrated pressure gauge,

(iv) a calibrated thermocouple probe for measuring air temperature,

(v) the upstream air-injector.

A diagram of the upstream air-injector is shown in Fig. 3.3a. The air and water were introduced in one of two arrangements depicted in Fig. 3.3b:

(i) Injector Arrangement 1.

The air was introduced into the water through the porous material on the bottom of the injector (connection E) while the water entered the horizontal connection D, the mixture leaving through the horizontal outlet connection B.

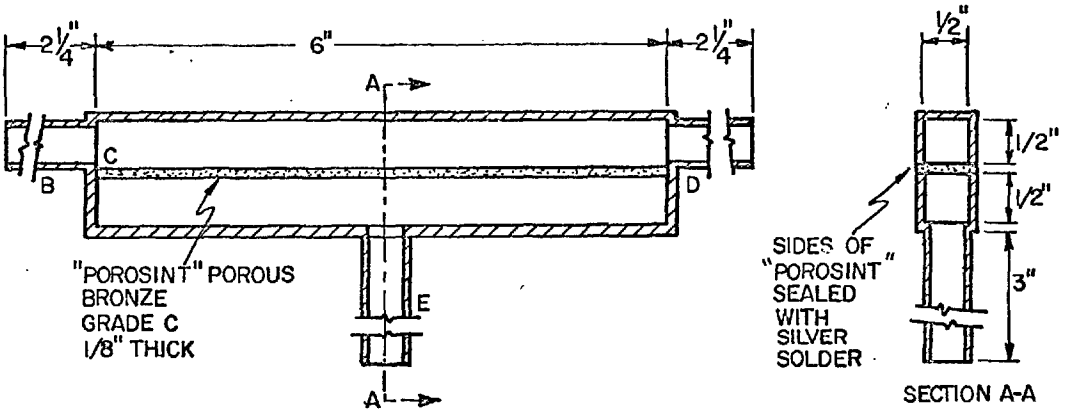

FIG. 3.3a DIAGRAM OF UPSTREAM AIR-INJECTOR

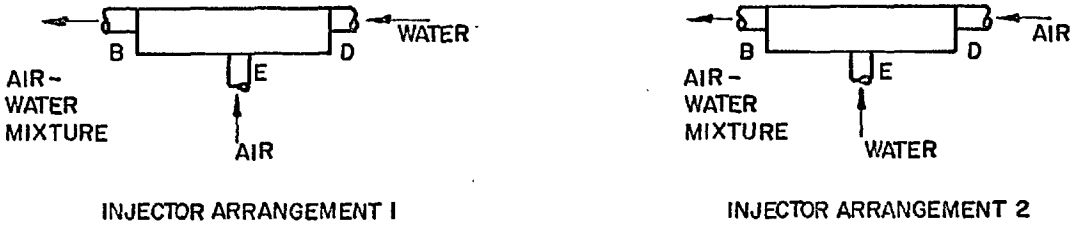

FIG. 3.3b AIR AND WATER CONNECTIONS TO INJECTOR

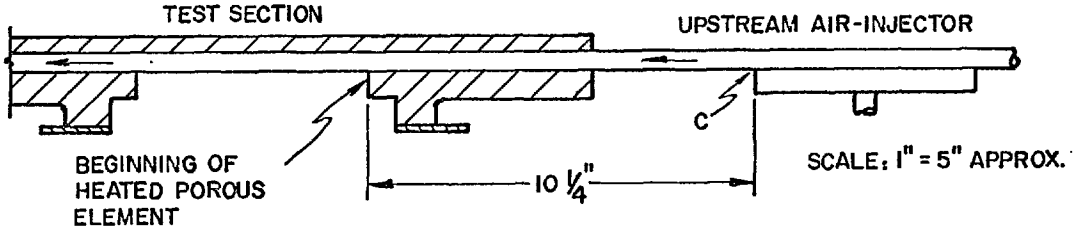

FIG. 3.3c LOCATION OF UPSTREAM AIR-INJECTOR

FIG. 3.3 UPSTREAM AIR-INJECTOR

(ii) Injector Arrangement 2.

The inlet water and air connections were reversed compared with Arrangement 1.

For both of these arrangements the position of the injector with respect to the test section was not changed (Fig. 3.3c).

These arrangements represented two extremely different methods of introducing upstream-air into the water; the object was to learn whether or not the heat-transfer coefficient was affected by the method of upstream air-introduction.

With the injector located as shown (Fig. 3.3c) it was sufficiently far from the heated porous section that thermal equilibrium* prevailed at the beginning of the heated element and sufficiently close to the heated element that differences in flow regimes generated by the two different injector arrangements were not obliterated.

3.6 Power Supply to the Test Section

The circuit is shown in Fig. 3.4. The electrical source was the 240 volt ac laboratory supply. The circuit included the following items:

(i) constant-voltage transformer to give a steady power supply (output 240 V ± 1%),

(ii) a variable autotransformer for control of the electrical power to the test section,

---

*"Thermal equilibrium" here means that the temperature of both phases were equal and the air was saturated with water vapour at the prevailing temperature.

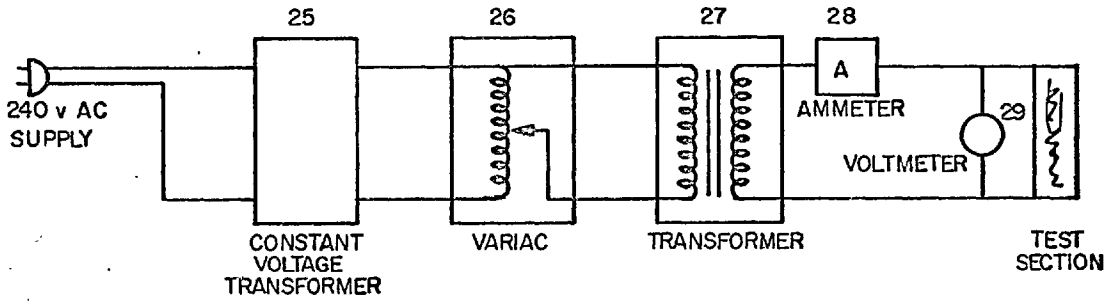

FIG. 3.4 POWER CIRCUIT

NOTE: THE NUMBERS CORRESPOND TO ITEMS IN TABLE F.2, APPENDIX F WHERE DETAILS ARE AVAILABLE

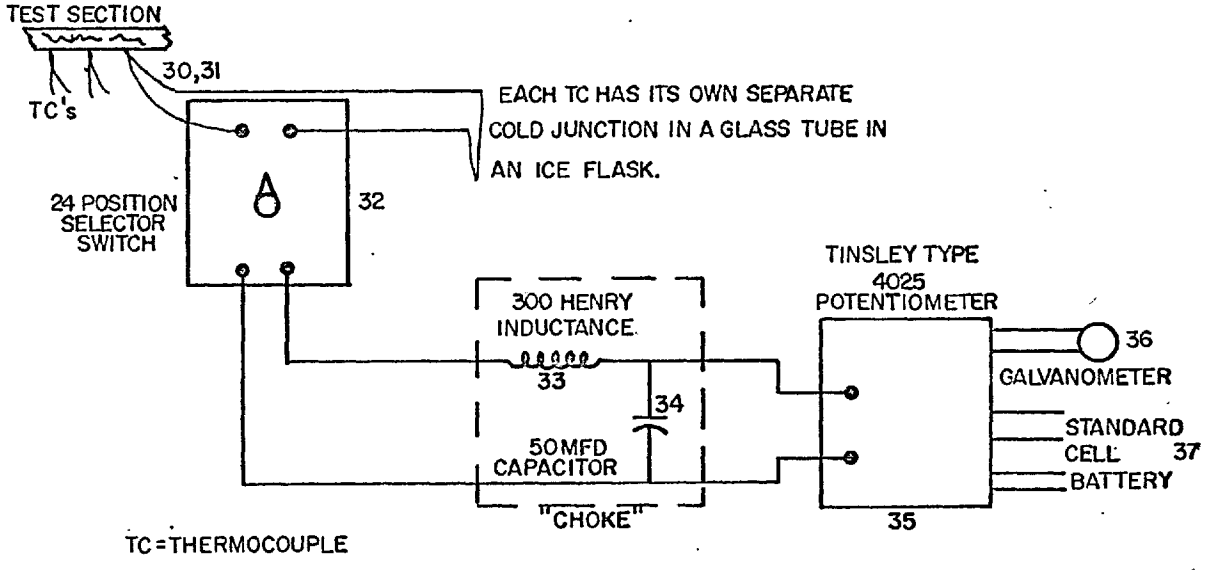

FIG. 3.5 THERMOCOUPLE CIRCUIT

(iii) a transformer,

(iv) a calibrated ammeter and voltmeter,

(v) the test section.

The electrical resistance through the water in the test section was approximately 10^6 times the electrical resistance through the porous heater. Virtually all of the electrical current was therefore passing through the porous heater.

3.7 Thermocouple Circuit

The thermocouple circuit is shown in Fig. 3.5. Each thermocouple had its own separate cold junction which was a thin glass tube in a Thermos filled with crushed ice and water. The thermocouples were connected through a selector switch and a "choking circuit" to a potentiometer. The choking circuit, which attenuated the ac emf in the thermocouple circuit to $\frac{1}{1500}$ its original value, was found necessary in order to obtain no electrical vibration of the galvanometer indicator. It was shown by calculation and demonstrated by experiment that the inclusion of this particular choking circuit did not affect the accuracy of the true thermocouple dc emf reading. The sensitivity of the galvanometer was approximately 11μv per mm of deflection.

CHAPTER 4 PROCEDURE

4.1 Introductory Remarks

This chapter describes the procedure used in the experiments. As mentioned in the Introduction, the main independent variables in this investigation were: $\dot{V}''_g$ the barbotage-rate, u_f the water velocity and $u_{g,i}$ the air velocity at entrance to the heated porous section. Fig. 4.1 illustrates the definition of these quantities. A minor independent variable was the upstream-injector arrangement. The main dependent variables were the heat-transfer coefficient and the flow pattern. Section 4.5 gives details of the range of independent variables and the conditions during the tests.

In this chapter various measured quantities are mentioned; in Fig. 3.2, the quantities in the circles are measured by the instrument beside which the circle appears. The procedure for calculating the heat-transfer coefficients and hydrodynamic quantities is given in Appendix D. The calculations were performed on the University of London Atlas Computer; the programming language was Extended Mercury Autocode.

4.2 Start-up Procedure

Before the rig was run on any one day, the test section was completely dry. Prior to operating any of the flow circuits the following checks were made: the air circuits and plenum chamber were tested for leaks; the leads from the orifice to the manometer were

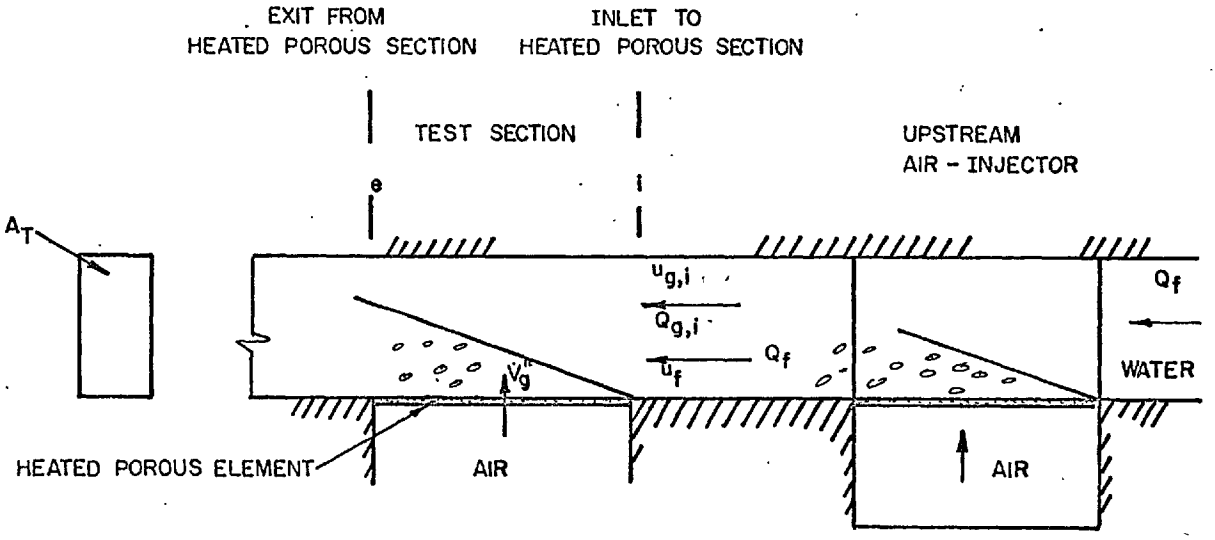

$$u_{g,i} \equiv \frac{Q_{g,i}}{A_T}$$

$$u_f \equiv \frac{Q_f}{A_T}$$

$u_{g,i}$ and $Q_{g,i}$ ARE THE AIR VELOCITY AND VOLUMETRIC AIR FLOW RATE RESPECTIVELY, IN THE CHANNEL AT INLET TO THE HEATED POROUS SECTION,

u_f and Q_f ARE THE WATER VELOCITY AND VOLUMETRIC WATER FLOW RATE RESPECTIVELY, IN THE CHANNEL,

A_T IS THE TOTAL CROSS-SECTIONAL AREA OF THE TEST SECTION FLOW CHANNEL,

$\dot{V}_g''$ IS THE BARBOTAGE-RATE OR GAS VOLUME INJECTED THROUGH THE POROUS HEATER PER UNIT TIME AND UNIT HEATER AREA.

MORE DETAILS ARE GIVEN IN APPENDIX D.

RELATIONS FOR "INLET QUALITY" β_i

$$\text{INLET VOLUMETRIC QUALITY} = \beta_i \equiv \frac{Q_{g,i}}{Q_f + Q_{g,i}} = \frac{u_{g,i}}{u_f + u_{g,i}} = \frac{\frac{u_{g,i}}{u_f}}{1 + \frac{u_{g,i}}{u_f}}$$

FIG. 4.1 DEFINITIONS OF HYDRODYNAMIC QUANTITIES

FIG. 4.1

tested to be clear by allowing air to pass through them; all manometer leads containing liquid were checked for the presence of air and if necessary, purged.

Air was first supplied to the test section, and then the water supply was turned on; this ensured that there was no seepage of water into the porous material. The other circuits then were put into operation, the last always being the power supply to the test section.

The following quantities were controlled:

(i) the water flow rate (this was set to give one of the predetermined values of u_f listed in Table 4.1);

(ii) the water temperature $T_{B,i}$ at inlet to the heated porous section* (at approximately $68^{o}F$);

(iii) the air flow rate to the test section (to give values of $\dot{V}''_g$ as shown in Table 4.2);

(iv) the air flow rate to the upstream injector (to give values of $u_{g,i}$ as shown in Table 4.2);

(v) the air temperature $T_{g,4}$ in the plenum chamber (this temperature was made approximately equal to the temperature of the bottom face of the porous element, for reasons discussed in Section 3.2.3);

(vi) the electrical heat-input to the porous heating element to give a wall-temperature minus bulk-temperature of approximately 10 deg F.

---

*The difference in temperature between $T_{B,i}$ and $T_{B,1}$ the temperature at inlet to the upstream air-injector is discussed in Appendix D.

To hasten the start-up procedure a heater was included in the plenum chamber. This was used only during start-up and not during data-taking. The controls were adjusted to give the desired conditions and the rig was allowed to come to equilibrium. The criterion for equilibrium before the first data were taken was that readings did not change over a period of ten minutes.

As with other two-phase forced convection studies, (see Ref. 9 for discussion), it was found necessary to have a large pressure drop across the upstream control valve in order to prevent oscillations in the water flow rate.

4.3 Taking of Data

After equilibrium conditions had been established, instrument readings were taken to allow the calculation of items (i) to (vi) above as well as the following:

(vii) the water temperature $T_{B,e}$ at outlet from the heated porous section (the difference in temperature between $T_{B,e}$ and $T_{B,2}$ the temperature at the outlet from the test section is negligible - see Appendix D);

(viii) the temperatures at the thermocouple stations along the porous element;

(ix) the static pressure P_i in the channel at inlet to the heated porous section;

(x) the drop in channel static pressure ΔP_{chan} over the length of the porous element;

(xi) the pressure in P_{plen} the plenum chamber;

(xii) the water vapour content of the air supply (for the use of this measurement see Appendix D);

(xiii) air temperature $T_{g,3}$ at entry to the upstream air-injector.

Flow conditions as observed by unaided eye were noted.

If during the recording of all the thermocouple readings, the water temperature varied by more than 0.2 deg F the data were rejected.

Tests with zero inlet-quality.

A series of tests was conducted with zero air-flow to the upstream injector, i.e. water only was present at inlet to the heated porous section ($u_{g,i} = 0$). This condition is termed "zero inlet-quality"*; the analogous condition in a boiling experiment is when water at its saturation temperature is supplied to a heated test section.

For a given "run", the water velocity u_f was held constant; only the barbotage-rate $\dot{V}''_g$ was varied beginning at the largest values and reducing in steps to zero (single-phase liquid flow). Early in the investigation it was found that,providing the water was never allowed to seep through the porous material (i.e. air flow rates to the test section always finite), hysteresis effects were indiscernible, any effect being smaller than the scatter in the experimental data.

*It is understood that neither $u_{g,i}$ nor $u_{g,i}/u_f$ are synonymous with "inlet quality". The relation is shown in Fig. 4.1.

Tests with finite inlet-quality.

Tests in which some air was supplied to the upstream injector, so giving an air-water mixture at entry to the heated porous section ($u_{g,i}$ finite), are called "finite inlet-quality" tests.

For a given "run", the normal procedure was to hold water velocity u_f and barbotage-rate $\dot{V}''_g$ constant while the air velocity $u_{g,i}$ at inlet to the heated porous section was varied in steps beginning at zero and increasing to the maximum used. Besides this normal procedure, some data were taken by first increasing the air flow rate to the upstream injector, then decreasing the air flow rate; it was found that any hysteresis effects were less than the scatter in the experimental data.

4.4 Shut-down Procedure

The electrical power supply to all the circuits was turned off; the water flow was stopped and the test section drained; the air supply to the test section was left on at least 20 minutes in order to dry out the test section.

4.5 Range of Variables and Conditions during Tests

The conditions obtaining for the tests were as follows:

Liquid: water.

Gas: air.

Temperature difference between heating surface and bulk water: approximately 10 deg F.

Water temperature at inlet to the heated porous section $T_{B,i}$,

zero inlet-quality tests: $68 \pm \frac{1}{2}^{o}F$,

finite inlet-quality tests: $68 \begin{smallmatrix} + 2 \\ - 4 \end{smallmatrix}^{o}F$.

Water temperature at outlet from the heated porous section $T_{B,e}$,

zero inlet-quality,

liquid velocity 0.084 ft/s: 69.3 to $76.0^{o}F$,

liquid velocity 0.29 ft/s: 68.3 to $70.7^{o}F$,

other liquid velocities: $68 \begin{smallmatrix} + 1 \\ - \frac{1}{4} \end{smallmatrix}^{o}F$,

finite inlet quality: $68 \pm 3\frac{1}{2}^{o}F$.

Pressure at inlet to the heated porous section: nominally atmospheric, in detail,

zero inlet-quality: 14.8 to 16.7 psia,

finite inlet-quality: 14.8 to 21.6 psia.

Table 4.1 lists the values of u_f used in the present investigation together with the corresponding value of the mass velocity G_f, the Reynolds number Re_f and a modified Froude number Fr^* which is used later in this work.

Table 4.2 gives details of the runs performed. Repeatability checks were made throughout the program; these are discussed in Appendix E where the accuracy of the experimental work is treated in detail.

The limitation on the barbotage-rate $\dot{V}''_g$ was the pressure drop through the porous material. (The plenum chamber, a 9-in. "Quickfit" glass column adaptor, had a safe working pressure of

Table 4.1 Dimensional and Dimensionless Water Velocities Used in the Present Experiments

Velocity u_f ft/s		Mass velocity G_f at 68°F 10^4 lb/ft^{2}h	Reynolds number † Re_f at 68°F	Modified Froude number †† Fr^* at 68°F
Values used in labelling diagrams, etc.	Values used in calculations			
0.084	0.084	1.88	222	0.156
0.29	0.292	6.54	774	0.544
0.72	0.718	16.1	1900	1.335
1.55	1.555	34.8	4120	2.89
3.1	3.08	69.0	8150	5.73
5.1	5.08	114	13,500	9.45

† Defined in equation (6.4)

†† Defined in equation (6.42)

Table 4.2 Experimental Runs

Water velocity u_f ft/s	Barbotage-rate $\dot{V}''_g$ ft/s	Air velocity in channel at entrance to porous section $u_{g,i}$ ft/s
Zero Inlet-Quality		
0.084	Zero to approximately 0.67 ft/s	Zero
0.29	↓	↓
0.72		
1.55		
3.1		
5.1		
Finite Inlet-Quality		
Injector Arrangement 1		
	Nominal	
0.29	0	Zero to approximately 75 ft/s
	0.05	↓
	0.1	
	0.2	
	0.4	
	0.6	
1.55	0	Zero to approximately 72 ft/s
	0.05	↓
	0.1	
	0.2	
	0.4	
	0.6	
5.1	0	Zero to approximately 58 ft/s
	0.05	↓
	0.1	
	0.2	
	0.4	
Injector Arrangement 2		
1.55	0	Zero to approximately 72 ft/s
	0.05	↓
	0.6	

1 atm gauge). The limitation on $\dot{V}''_g$ was not serious as the critical barbotage-rate $\dot{V}''_{g,cr}$ was exceeded in all but one condition (highest water velocity, zero inlet-quality). The limitations on the water flow rate was the source in the laboratory. The maximum upstream air flow rate was chosen to give conditions well into the annular flow regime (air flow rates 3 to 4 times that at the slug-to-annular flow regime boundary); the capacity of measuring Rotameters was selected accordingly.

4.6 Flow Observations

High speed still photographs were taken of flow conditions in the porous and outlet sections for zero inlet-quality to the porous section. They were taken with no heating of the porous section and covered the range of water velocities and barbotage rates used in the heat-transfer experiments.

Stroboscopic observations were also made in the absence of heat transfer from the porous surface. All conditions for both zero inlet-quality and finite inlet-quality were covered as for the heat-transfer experiments. Two portable stroboscopic light sources were positioned to give back-lighting and to allow simultaneous observations of the inlet, porous and outlet sections.

CHAPTER 5 FLOW PATTERN OBSERVATIONS

5.1 Introductory Remarks

When gas and liquid flow together in a channel, the two phases arrange themselves in various configurations called "flow patterns". The discussion of flow patterns is a desirable prelude to the discussion of heat-transfer coefficients as the former can affect the latter. Further, flow patterns for precisely the same geometry as used in the present experiment have not been reported elsewhere. The method of observation of the flow patterns was described in Chapter 4 while the results are presented here.

The order of presentation is as follows.

(i) The flow patterns are described.

(ii) For tests with zero inlet-quality and finite barbotage ($u_{g,i} = 0$, finite $\dot{V}''_g$) "flow maps" are given for the flow regimes in the porous section and in the outlet section.

(iii) For zero barbotage and finite inlet-quality ($\dot{V}''_g = 0$, finite $u_{g,i}$), the patterns are listed in Table 5.1 together with the approximate flow pattern "boundaries".

(iv) The flow patterns encountered when both the barbotage-rate and inlet-quality are finite are discussed (finite $\dot{V}''_g$, finite $u_{g,i}$).

The main results of this chapter are the flow map Fig. 5.3, the tabulated flow pattern boundaries Table 5.1 and the discussion in Section 5.5.

An excellent review of the flow pattern literature is given by Vohr [85]. The literature of interest here will be treated in the appropriate section. Throughout this chapter it must be borne in mind that the "boundaries" between the flow patterns are not sharply defined; there is a gradual transition from one pattern to another.

5.2 Description of Flow Patterns

Although there is as yet no completely standard nomenclature in describing flow patterns in horizontal two-phase flow, the terminology of Alves [2] has been used by a number of investigators [3, 7, 65]; wherever possible, in this work Alves' terminology will be used. Alves' flow patterns refer to flow in a channel where there is no gas injection through the walls of the channel. In the present experiment Alves' flow descriptions require modification to describe patterns when gas is injected through one of the channel walls in the section under observation. Further, even without gas injection through the channel walls, two patterns not specifically described by Alves will be used here (froth and stratified froth flow).

In connection with zero inlet-quality tests, the term "two-phase boundary layer" will be used; it is the layer within which the gas and liquid mixture is contained; this is illustrated in the sketch below.

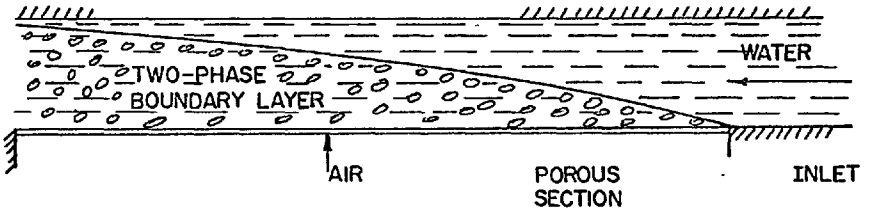

SKETCH ILLUSTRATING "TWO-PHASE BOUNDARY LAYER"

Below, the main feature of each flow pattern is described. Patterns (a) to (f) were distinguished in the present experiments; Fig. 5.1 shows sketches of these patterns. For a given pattern, e.g. bubble flow, more than one sketch may appear depicting the different conditions encountered within that pattern; each sketch is referred to either on a flow-map or in a table later in this section.

(a) Bubble flow - The main characteristic is the existence of spherical or nearly spherical discrete bubbles.

(b) Plug flow - Long bubbles of a bullet shape, occupying 2/3 of the channel height, travel along the top of the channel separated by plugs of liquid.

POROUS SECTION
ZERO INLET-QUALITY, FINITE AIR INJECTION THROUGH THE POROUS WALL.

ALL SECTIONS WITH NO AIR INJECTION THROUGH THE WALL

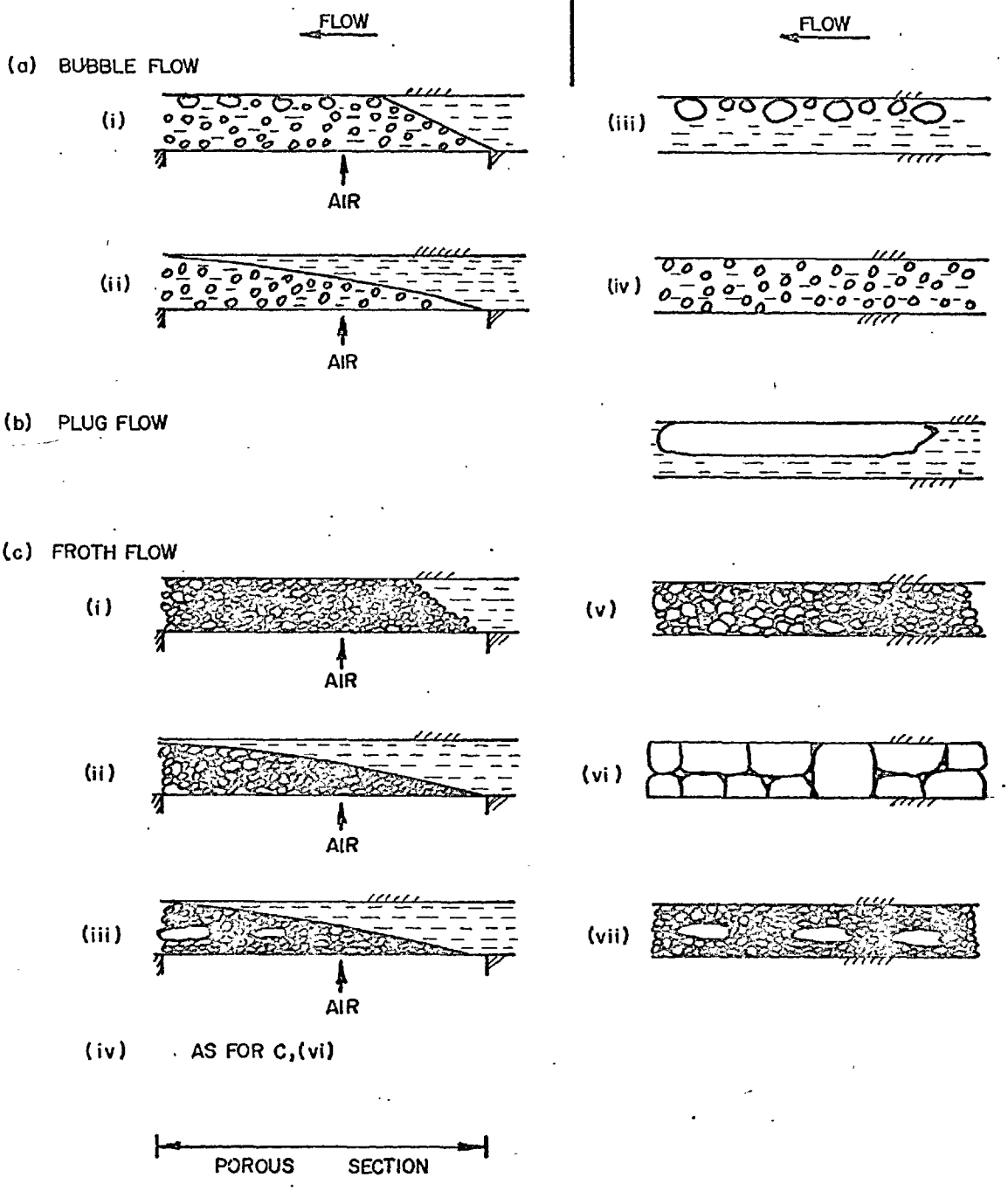

FIG. 5.1 FLOW PATTERNS DISTINGUISHED IN PRESENT WORK

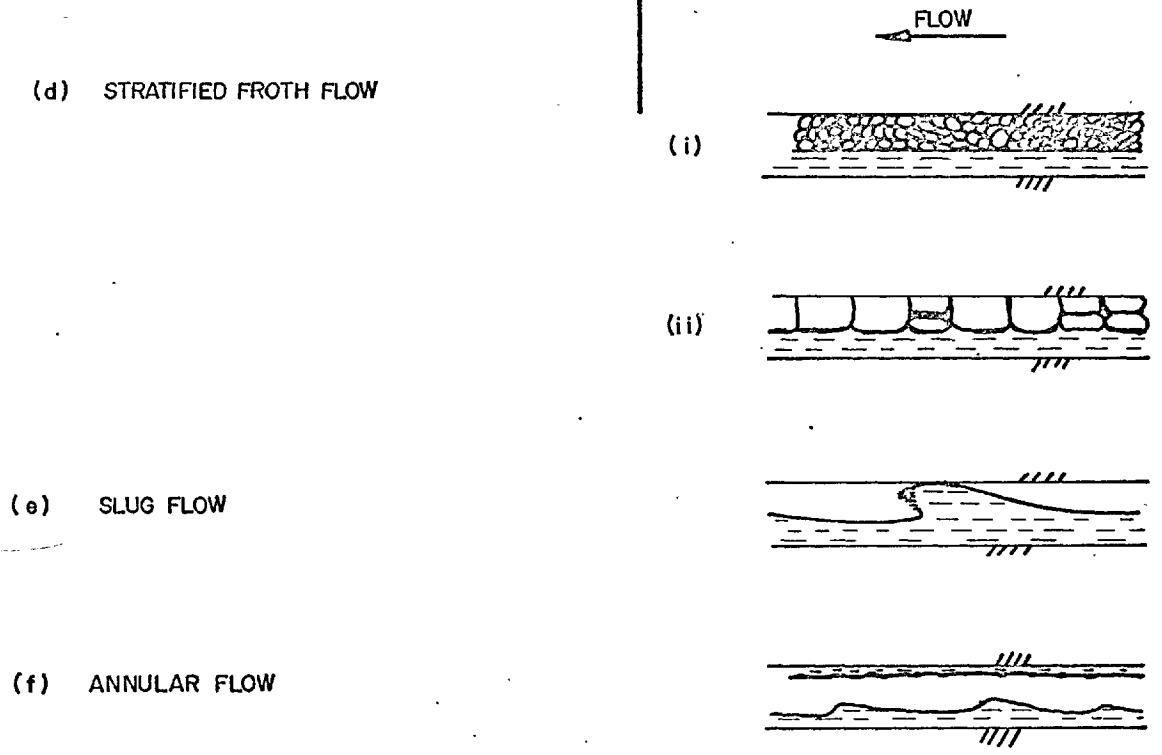

FIG. 5.1 (CONT.) FLOW PATTERNS DISTINGUISHED IN PRESENT WORK

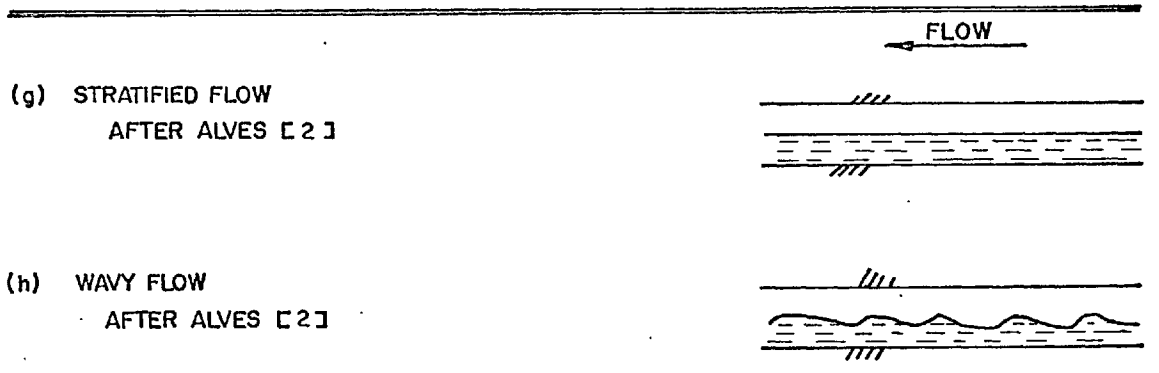

FIG. 5.2 FLOW PATTERNS NOT DISTINGUISHED IN PRESENT WORK, BUT NEEDED FOR DISCUSSION (NO GAS INJECTION THROUGH WALLS)

FIGS. 5.1 AND 5.2

(c) Froth flow - The main feature of this flow is coalescence; bubbles touch each other and coalesce, resulting in a "frothy" mixture which is either contained within the "two-phase boundary layer" or fills the channel. In the "froth" the liquid is the continuous phase, but is transported mainly in the form of the film between the bubbles or air cells. Included within this flow pattern is the condition where coalescence results in a bullet-shaped bubble approximately 3/4-in. long which travels down the centre-line of the channel.

(d) Stratified froth flow - A layer of liquid flows along the bottom of the channel covered by a frothy-layer extending to the top of the channel.

(e) Slug flow - A wave of water periodically seals the top of the channel and passes along the channel.

(f) Annular flow - The liquid flows in a film around the inside wall of the channel and the air flows as a central core; large amplitude waves may still form on the bottom film of water, but the crest of the wave does not appear to seal the channel.

In order to compare the present observations for zero barbotage with those of other investigators it is necessary to describe the following patterns (g) and (h) which were not distinguished in the present experiments. These two patterns are sketched in Fig. 5.2.

(g) Stratified flow - Described by Alves[2] as, "Flow in which liquid flows along the bottom of the pipe and gas flows above it over a smooth liquid-gas interface".

(h) Wavy flow - According to Alves [2], "Flow which is similar to stratified flow except that the gas moves at a higher velocity and the interface is disturbed by waves travelling in the direction of flow".

In order to aid in the discussion of observations for finite barbotage-rate $\dot{V}''_g$, is is necessary to give below the descriptions used by Wallis and Griffith [90] in their photographic study of flow patterns.

(i) Bubbly flow - (Wallis and Griffith) - Air bubbles of all sizes exist with the interstices filled with water. The distribution of the two phases looks fairly uniform across the channel.

(j) Transition flow - (Wallis and Griffith) - This pattern is a hybrid of bubbly and annular flow.

(k) Annular flow - (Wallis and Griffith) - This pattern consists essentially of a core of air surrounded by bubbly layers on the porous walls. The pattern is not steady and in places there are bridges of bubbles which appear to span the channel, although these may be only one or two layers thick on the walls. The bubbly layer on the porous walls forms surface waves some of which develop into crests and appear to be torn off to form droplets in the gas core.

5.3 Flow Patterns for Zero-Inlet-Quality Tests

5.3.1 Flow Patterns in the Porous Section

For zero inlet-quality and finite barbotage ($u_{g,i} = 0$, finite $\dot{V}''_g$) two main flow patterns were observed in the porous section; these were bubble flow and froth flow. Fig. 5.3 shows the boundary between these two regions and indicates the relevant flow pattern sketch. For the two highest liquid velocities tested (u_f = 3.1 and 5.1 ft/s) the two-phase boundary layer did not touch the top of the channel within the porous section (e.g. Fig. 5.1c (ii)) while for the other liquids velocities tested ($u_f \leq$ 1.55 ft/s), it did (e.g. Fig. 5.1c (i)).

There are only three other investigations where flow patterns have been observed or inferred in a channel with gas addition through the walls of the section of interest; these are Wallis and Griffith [90]*, Wallis [89] and Kudirka [48]. In none of these works was the channel geometry the same as in the present experiment.

For comparisons with the present observations the most important work is that Wallis and Griffith [90] who have classified flow patterns within a vertical rectangular channel having two porous walls 10-in. long by ½-in. wide placed ¼-in. apart; the other two walls were of a transparent plastic material; air was blown through the porous walls into a stream of water flowing

*It is understood here that the Wallis and Griffith [90] investigation supersedes an earlier investigation by Di Menza [18] on a similar apparatus in the same laboratory.

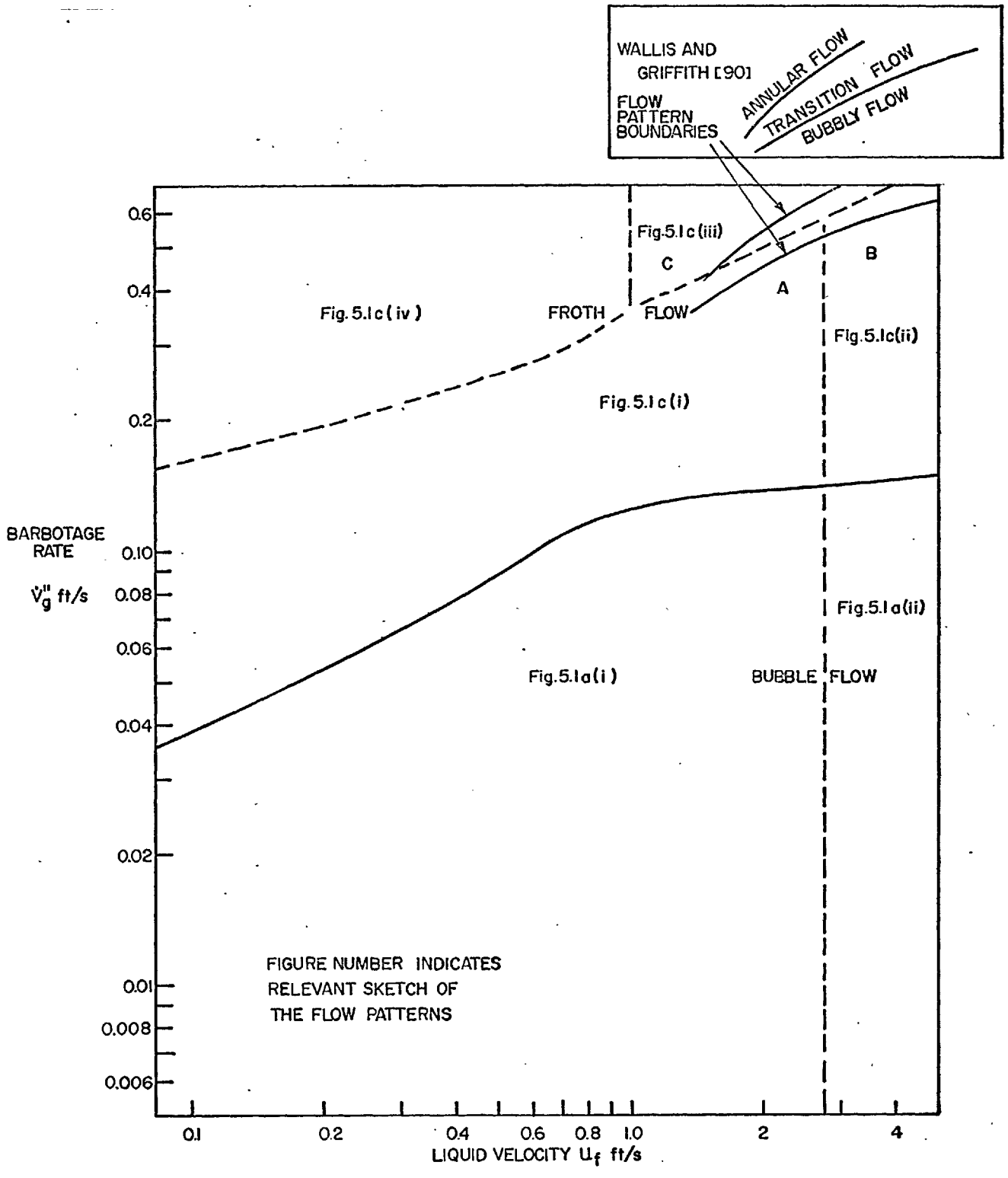

FIG. 5.3 FLOW PATTERNS IN THE POROUS SECTION FOR ZERO-INLET-QUALITY TESTS

downwards. The importance of this work is that observations were made of flow conditions along the porous section itself. The boundaries among their bubbly, transition and annular flow were plotted on a flow map* for zero inlet-quality at the entrance to the porous section; the boundaries are shown here on Fig. 5.3. From the Wallis and Griffith flow pattern descriptions their bubbly flow appears to include the present bubble flow and also froth flow of the type shown in Fig. 5.1c (i) and (ii) (A and B in Fig. 5.3) while their transition flow could probably include froth flow of the type depicted in Fig. 5.1c (iii) (C in Fig. 5.3). It is interesting then that there is agreement between Wallis and Griffith's bubbly-to-transition flow boundary and the present observations. However in the present porous section, for zero inlet-quality no annular flow pattern was observed.

As with the Wallis and Griffith [90] experiment there was no significant change in flow pattern along the length of the porous section.

---

*Strictly speaking the boundaries on the Wallis and Griffith [90] flow map referred to above were obtained using a flow pattern classification based on mass-flow profiles measured at the channel exit: in bubbly flow the liquid flow showed an approximately parabolic distribution being more concentrated at the channel centre; in annular flow the liquid became more concentrated at the walls; between bubbly and annular flow was transition flow. The authors commented that the study of high speed still photographs in conjunction with the visual flow pattern definitions (given here in Section 5.2) would yield flow pattern boundaries at higher air rates than the boundaries obtained using the measurements of mass-flow profiles..

Wallis [89] inferred flow patterns within horizontal porous tubes of 3/8, 5/8 and 7/8-in. diameter by observing the jet of air-water mixture issuing freely into the atmosphere at the exit from the tube being tested; no quantitative data on the pattern boundaries were given.

Kudirka [48] observed flow patterns with air-water and air-ethylene glycol mixtures in a transparent outlet pipe following a vertical porous tube; patterns within the porous tube were inferred from these observations. Since the observations were in a vertical system and in the outlet, the observations will not be considered here.

5.3.2 Flow Patterns in the Outlet Section

For the present geometry it was of considerable interest to learn whether the flow patterns in the outlet section were similar to or different from the patterns in the porous section. A flow pattern map is presented in Fig. 5.4 for conditions at approximately 10 in. (about 30 equivalent diameters) downstream from the end of the porous section. This map is drawn to the same scale as the one for the porous section and may be compared with it directly. The regions where differences in flow pattern occur are cross-hatched; the most significant difference is that there is a region on the maps which is slug flow in the outlet section while being froth flow in the porous section. Wallis [89] has made a similar observation with horizontal tubes. It is seen that

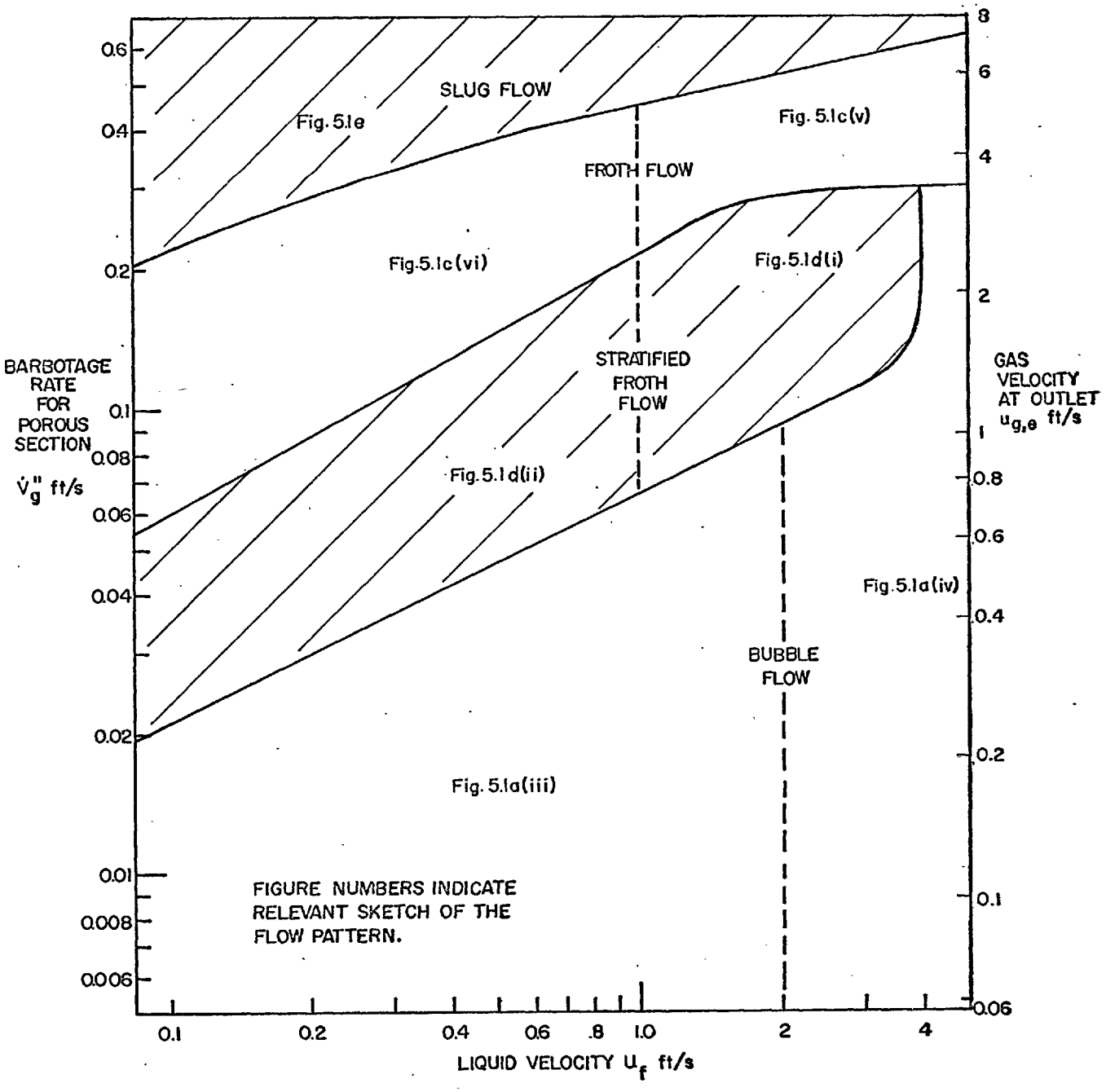

FIG. 5.4 FLOW PATTERNS IN OUTLET SECTION AT 10 INCHES FROM THE END OF THE POROUS SECTION, FOR ZERO INLET-QUALITY TO POROUS SECTION.

one must exercise some caution when inferring flow patterns in a bubbling section from observations made downstream of the bubbling section.

5.4 Flow Patterns for Zero Barbotage and Finite Inlet-Quality ($\dot{V}''_g = 0$, Finite $u_{g,i}$)

The flow patterns observed for conditions of zero barbotage and finite inlet-quality ($\dot{V}''_g = 0$, finite $u_{g,i}$) are listed in Table 5.1 together with the approximate gas velocity $u_{g,i}$ at the pattern boundaries and the figure number of the relevant flow pattern sketch.

In the present experiments, at a water velocity u_f of 1.55 ft/s the two arrangements of the upstream injector were used in order to determine whether the method of mixing of the phases upstream would affect the heat-transfer coefficient in the test section; it was observed that at low values of $u_{g,i}$ there was a marked difference in flow pattern with the two injector arrangements used. With Injector Arrangement 1, in order of increasing $u_{g,i}$, the patterns observed were bubble, stratified froth, slug and annular flow while with Injector Arrangement 2 plug flow was observed in place of bubble and stratified froth flow. (This last difference markedly affected the heat-transfer coefficient.) The transition to slug flow was only mildly affected by the injector arrangement (transitions at $u_{g,i} \simeq 3.7$ and 4.5 ft/s for

Table 5.1 Flow Patterns and Boundaries for Zero-Barbotage, Finite Inlet-Quality Tests

Liquid Velocity u_f, ft/s	Injector Arrangement	Flow Pattern	Sketch in Figure 5.1	Approximate Boundary Upstream Injection Rate $u_{g,i}$ ft/s
0.29	1	Stratified froth	d(ii)	1.9
		Slug	e	28
		Annular	f	
1.55	1	Bubble	a(iii)	1.2
		Stratified froth	d(i)	3.7
		Slug	e	20
		Annular	f	
	2	Plug	b	4.5
		Slug	e	19
		Annular	f	
5.1	1	Bubble	a(iv)	4.3
		Froth	c(vii)	6.1
		Slug	e	14
		Annular	f	

Injector Arrangements 1 and 2 respectively) while there was virtually no effect on the slug-to-annular flow boundary ($u_{g,i} \simeq 20$ ft/s).

A comparison of the flow patterns observed in the present zero-barbotage experiments and those observed in some well-known horizontal flow investigations [2,3,7,47] is presented in Fig. 5.5*; this form of comparison has been used by Vohr [85]. The flow patterns and boundaries have been obtained from flow maps; these maps were based on air-water [7,47] or air-water and air-SAE 10 oil [2,3] flowing at 1-2 atm abs pressure in horizontal circular pipes of 1-in. [2,7,47] or 1-in. to 4-in. diameter [3].

In Fig. 5.5 the important points to note are as follows.

(i) There is, in detail, disagreement among the various investigators as regards the flow patterns which are occurring and the position of the boundaries. The worst discrepancies occur at low values of the upstream injection-rate $u_{g,i}$, where, at least in the present experiment, the flow pattern was affected by the method of mixing the two phases.

(ii) There is however, broadly speaking, general agreement among the present and other investigations in the occurrence of the slug and annular flow patterns.

---

*Krasiakov's [47] results appear on Fig. 5.5; the terminology of this investigator is different from that used so far in this discussion. The relation between Krasiakova's terminology and that being used here is presented on Page 23 of Vohr's [85] report.

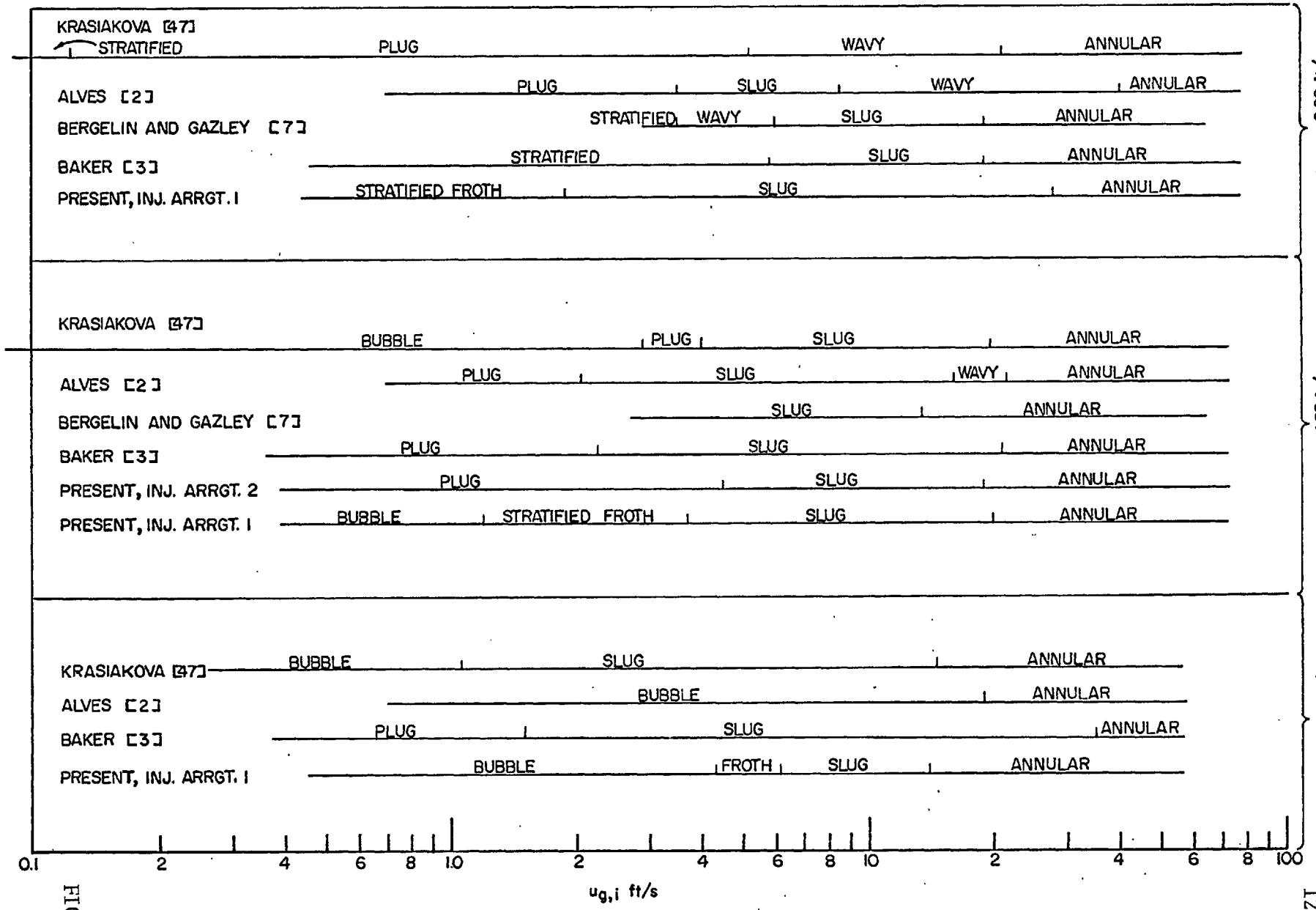

FIG. 5.5 COMPARISON OF FLOW PATTERNS IN THE PRESENT ZERO-BARBOTAGE EXPERIMENTS AND IN OTHER INVESTIGATIONS

In the present zero-barbotage experiments, from approximately 3 in. from the inlet connection (9 equivalent diameters) to the outlet connection (a further 21 in. or 60 equivalent diameters downstream), there was no significant change in flow pattern.

5.5 Flow Pattern Observations with Finite Barbotage and Finite Inlet-Quality

The following remarks are concerned principally with flow pattern observations in the porous section when there is finite barbotage and finite inlet-quality. First, the pattern observed in the inlet section before the porous section would be that as described in Section 5.4. The pattern observed in the inlet section tended in general to persist throughout the porous section* with the following modifications or exceptions.

(i) When the flow pattern at the inlet to the porous section was stratified froth or bubble flow, the pattern becomes froth flow in the porous section for $\dot{V}''_g$ greater than approximately 0.1 ft/s.

(ii) When the pattern at the inlet to the porous section is plug, slug or annular flow, in the porous section the liquid on the bottom of the channel becomes either interspersed with bubbles or frothy. The sketch below illustrates this for slug flow.

---

*Wallis [89] has made a similar observation with regard to horizontal porous tubes.

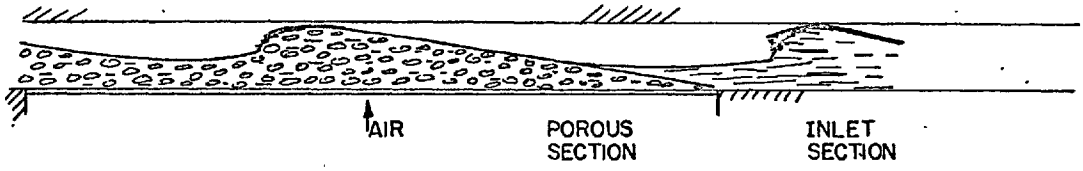

SKETCH OF SLUG FLOW IN POROUS SECTION WHEN $\dot{V}''_g$ AND $u_{g,i}$ ARE BOTH FINITE

The upstream injection-rates $u_{g,i}$ at which slug and annular flow occur in the porous section are not significantly affected by having finite barbotage.

Remark on Hysteresis

In the present experiment it was found that any hysteresis in the flow pattern boundary was less than the accuracy with which the boundary could be fixed.

CHAPTER 6 PRESENTATION AND DISCUSSION OF HEAT-TRANSFER RESULTS

6.1 Introductory Remarks

This chapter deals with the heat-transfer results of the experiments. First the mean heat-transfer coefficient, on which the discussion and analysis are based, is defined and present single-phase results are compared with the most relevant literature correlation. Then the raw data are presented and discussed. The results are then correlated and compared with other investigations. A crude correlation is given for the critical barbotage-rate observed in the present experiments. Finally there is a short discussion on possible future work.

The data from the present investigation are tabulated in Appendix G.

6.2 Definition of the Mean Heat-Transfer Coefficient

In the present work, the analysis of the heat-transfer results is based on the mean heat-transfer coefficient $\bar{\alpha}$, defined as:

$$\bar{\alpha} \equiv \frac{1}{L} \int_0^L \alpha \, dx \qquad (6.1)$$

where:

L is the total length of the heated porous test section,

α is the local heat-transfer coefficient,

x is position along the heater.

The $\alpha \sim x$ relation is obtained by connecting linearly the local (α, x) points; the lines connecting the two (α, x) points closest to each end of the heater are extrapolated to the ends of the heater. Details of the calculation of $\bar{\alpha}$ are given in Appendix D.

Throughout the rest of this work, mean heat-transfer coefficients are discussed unless otherwise specified; the "bar" above α is omitted while α still retains the significance of a mean.

6.3 Single-Phase Heat-Transfer Coefficients

A check on the reliability of the results obtained from the present apparatus is effected by comparing the present turbulent-flow single-phase ($\dot{V}_g'' = 0$, $u_{g,i} = 0$) results with the correlation of James, Martin and Martin [43]; these authors obtained an accurate (±10%) correlation of their own measured mean heat-transfer coefficients in rectangular ducts heated on one side, i.e. in the same geometry as for the present experiment. The comparison is shown in Fig. 6.1. Before discussing the comparison the symbols appearing on the figure are introduced.

The ordinate, the single-phase Nusselt number Nu_{SP}, is that conventionally used and is defined below in order to distinguish it from the special forms of Nusselt number employed earlier in Chapter 2:

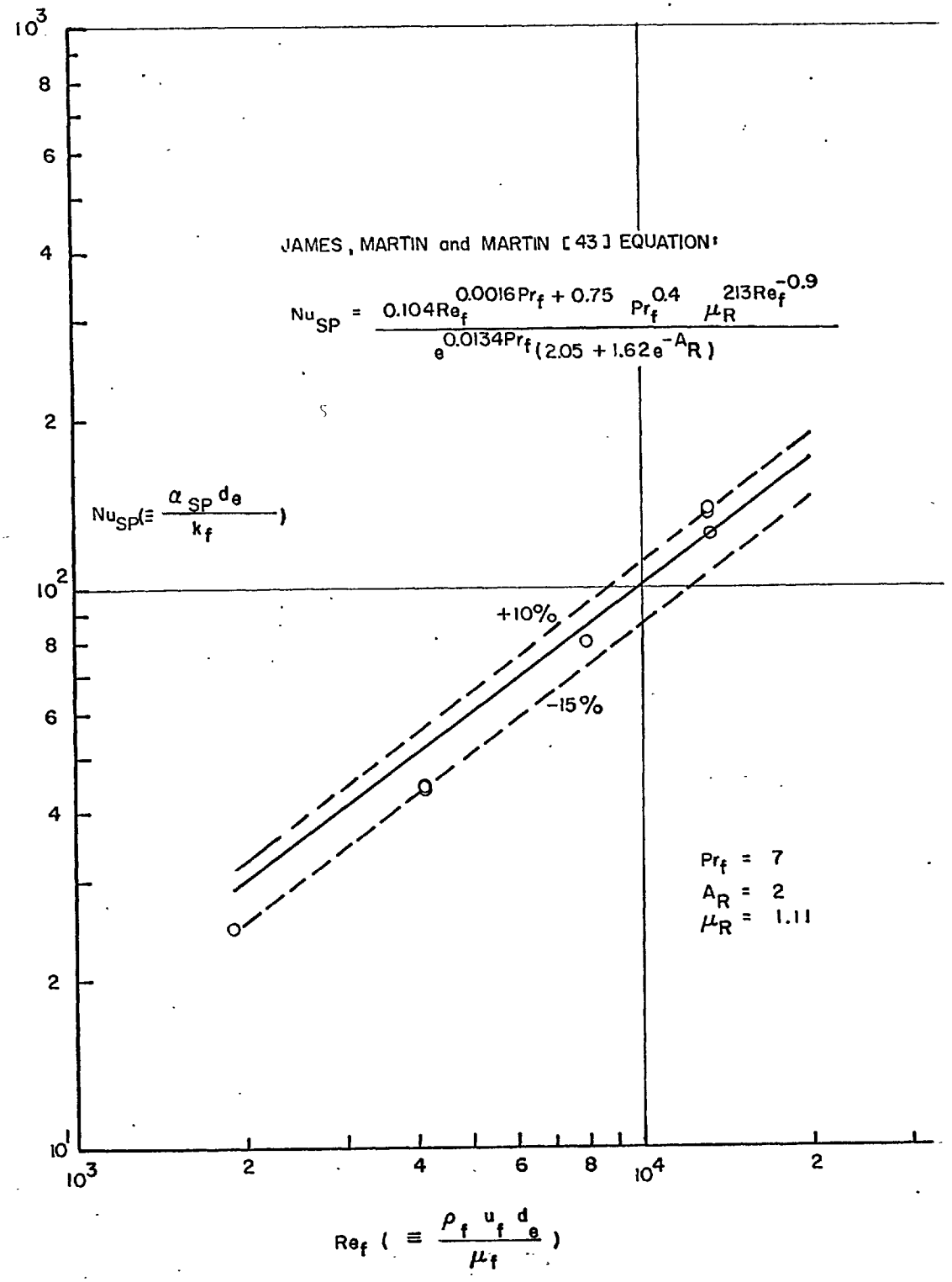

FIG. 6.1 COMPARISON OF PRESENT TURBULENT SINGLE-PHASE RESULTS WITH THE JAMES ET AL. [43] EQUATION

$$Nu_{SP} \equiv \frac{\alpha_{SP}\, d_e}{k_f} \tag{6.2}$$

where:

α_{SP} is the single-phase heat-transfer coefficient,

d_e is the equivalent diameter of the channel defined as

$$d_e \equiv \frac{4(\text{cross-sectional area})}{\text{wetted perimeter}}, \tag{6.3}$$

k_f is the liquid thermal conductivity evaluated here at the bulk temperature.

The Reynolds number Re_f used here and throughout this work is:

$$Re_f \equiv \frac{\rho_f u_f d_e}{\mu_f} \tag{6.4}$$

where the symbols have been defined previously; Re_f is evaluated at the bulk temperature. The symbol μ_R is the ratio of the liquid viscosity evaluated at bulk temperature to that evaluated at the wall temperature. The liquid Prandtl number Pr_f has been introduced previously and is evaluated here at the bulk temperature. The aspect ratio A_R is defined as:

$$A_R \equiv \frac{a}{b}$$

where a is the height of the channel normal to the heated surface and b is the width of the heated surface (and of the channel).

The present aspect ratio (2) and bulk-temperature Prandtl number (7) are within the range tested by James, Martin and Martin [43]. The minimum Re_f tested by these authors was 3000; their correlating equation has been extrapolated back to approximately 2000 in Fig. 6.1. The present data lie within +10% and -15% of the James et al. correlation. This is considered a satisfactory agreement.

6.4 Tests with Zero Inlet-Quality

The results for the zero-inlet-quality tests are shown in Figs. 6.2 to 6.4; the data points are plotted in Figs. 6.2 and 6.3 while Fig. 6.4 displays the lines drawn through the data for all the liquid velocities. The symbol α_o is used for the heat-transfer coefficient under conditions of zero inlet-quality.

The significant features of the results are discussed below.

(i) The liquid velocity u_f appears as a parameter in Fig. 6.4. In general, for a fixed barbotage-rate $\dot{V}''_g$ the heat-transfer coefficient α_o increases with increasing u_f. Gose et al. [27,28] have also observed this same trend in their experiments with vertical porous tubes.

(ii) For a given u_f, the $\alpha_o \sim \dot{V}''_g$ curve at first rises steeply with increasing $\dot{V}''_g$; the curves then pass through a "knee" beyond

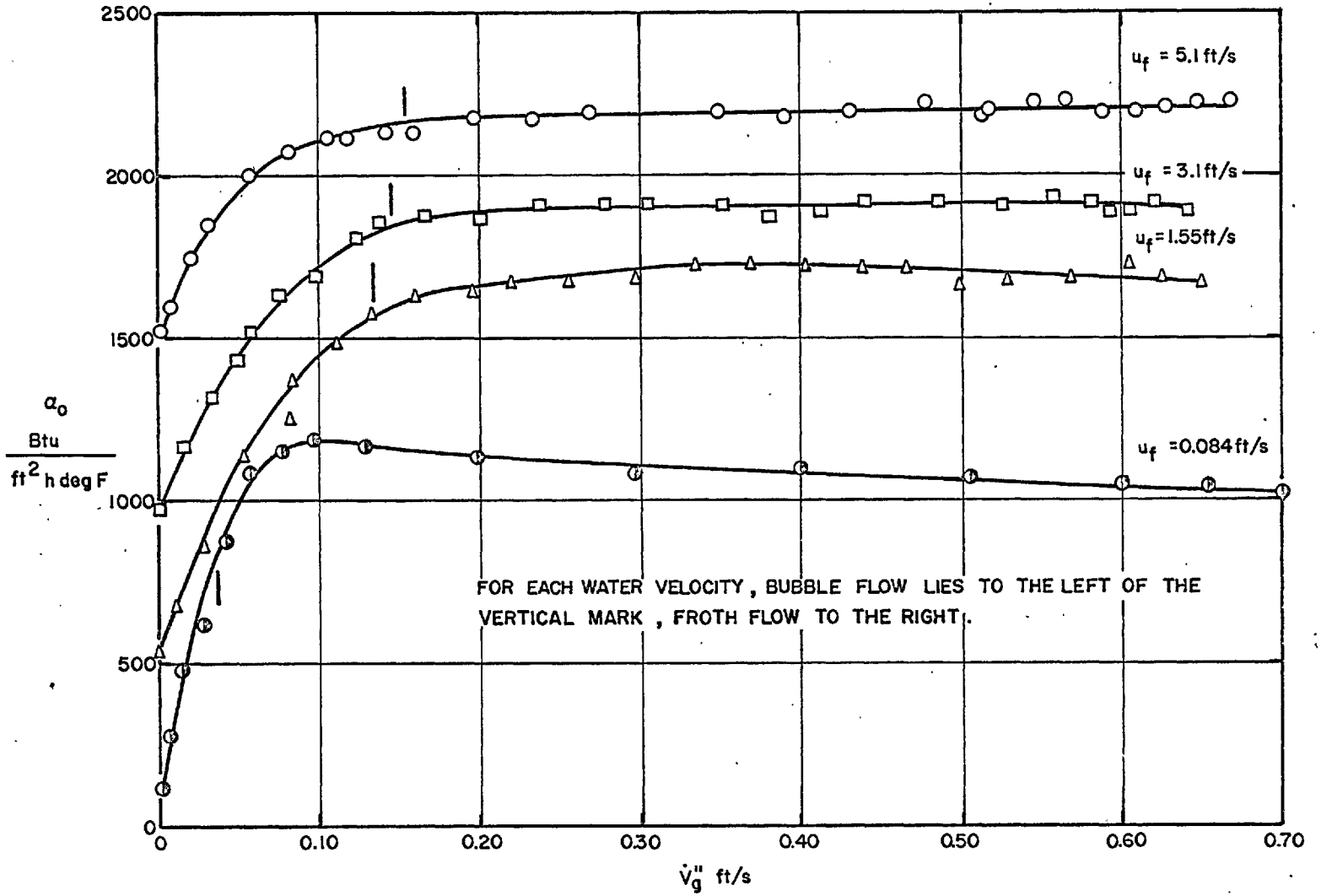

FIG. 6.2 HEAT-TRANSFER COEFFICIENTS FOR TESTS WITH ZERO INLET-QUALITY

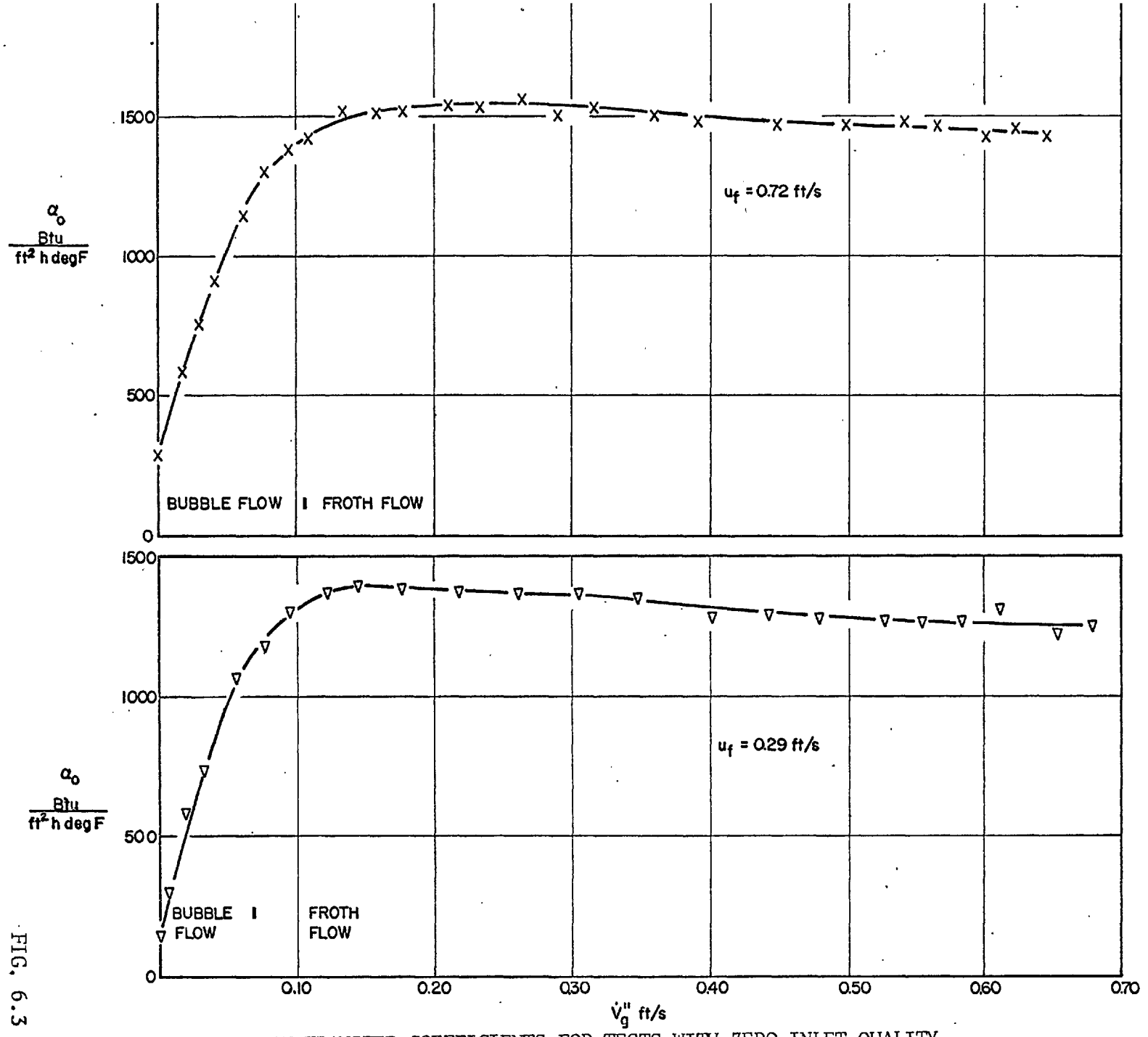

FIG. 6.3 HEAT-TRANSFER COEFFICIENTS FOR TESTS WITH ZERO INLET-QUALITY

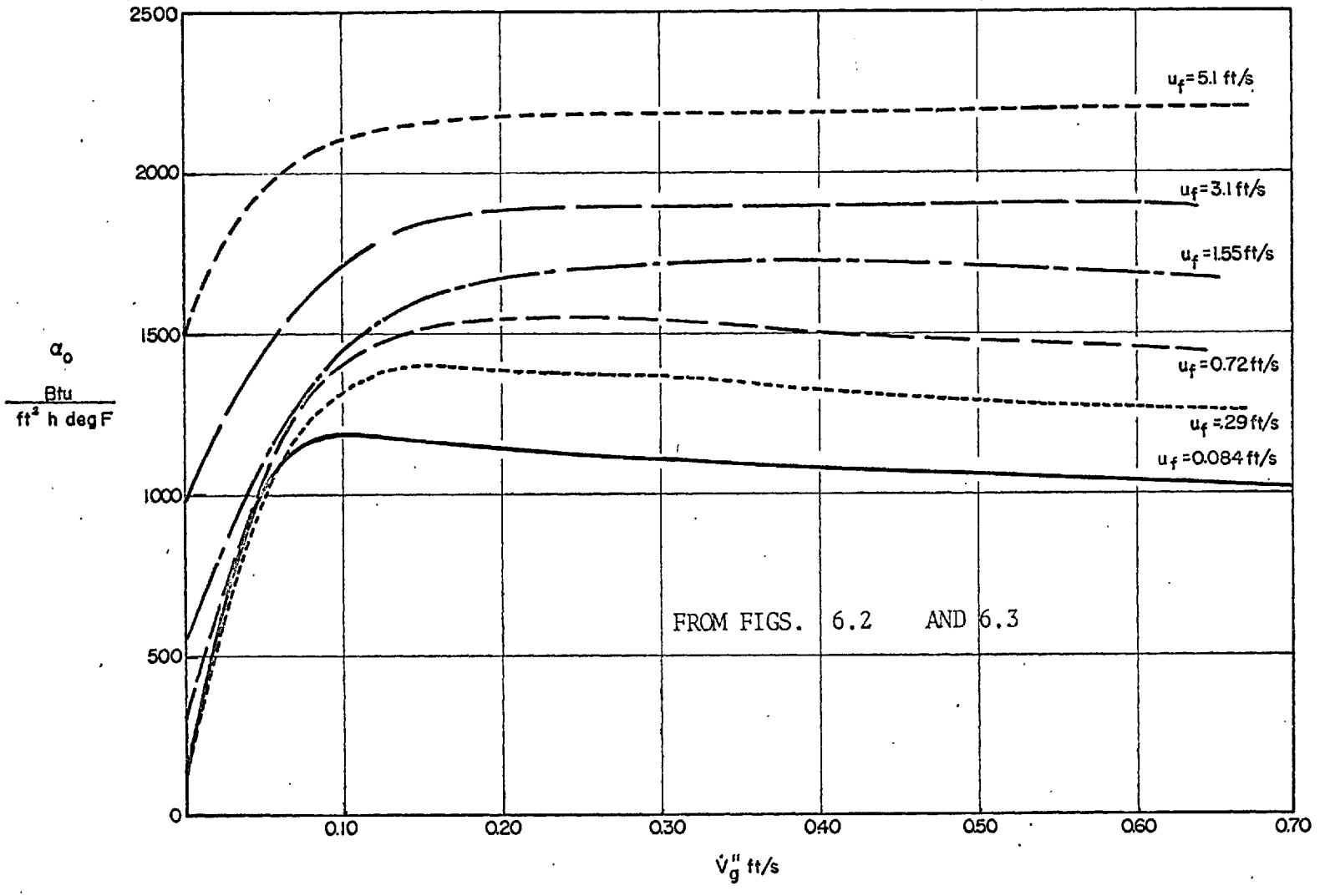

FIG. 6.4 HEAT-TRANSFER COEFFICIENTS FOR TESTS WITH ZERO INLET-QUALITY

which the increase in α_o with $\dot{V}''_g$ is markedly reduced; the curves (except for the highest u_f) then exhibit a maximum beyond which α_o decreases with an increase in $\dot{V}''_g$. The boundary between bubble flow and froth flow is marked (short vertical lines) on Fig. 6.2 and 6.3. It can be seen that the region of steeply rising α_o corresponds approximately with bubble flow.

(iii) In a manner similar to that in free convection [1,80], the value of $\dot{V}''_g$ at which a maximum occurs in a plot of $\alpha \sim \dot{V}''_g$ for a constant inlet-quality, or in this case $\alpha_o \sim \dot{V}''_g$, is called the "critical" barbotage-rate $\dot{V}''_{g,cr}$. For $u_f \leqslant 1.55$ ft/s the maximum in $\alpha_o \sim \dot{V}''_g$ curve is easily seen while for $u_f = 3.1$ ft/s the maximum is vague and the way in which the smoothed curve has been drawn may not be fully justified. For $u_f = 5.1$ ft/s, the highest liquid velocity used in the present experiments, no maximum in α_o occurred within the range of $\dot{V}''_g$ tested.

6.5 Tests with Finite Inlet-Quality

6.5.1 Tests with Zero Barbotage

The results for tests with zero barbotage and finite inlet-quality are shown in Fig. 6.5; the symbol α_{TP} is used for the heat-transfer coefficient under these conditions ($\dot{V}''_g = 0$, finite $u_{g,i}$). In the figure the observed flow patterns are indicated.

It is first noted that the liquid flow rate appears systematically as a parameter, α_{TP} increasing with u_f for fixed $u_{g,i}$.

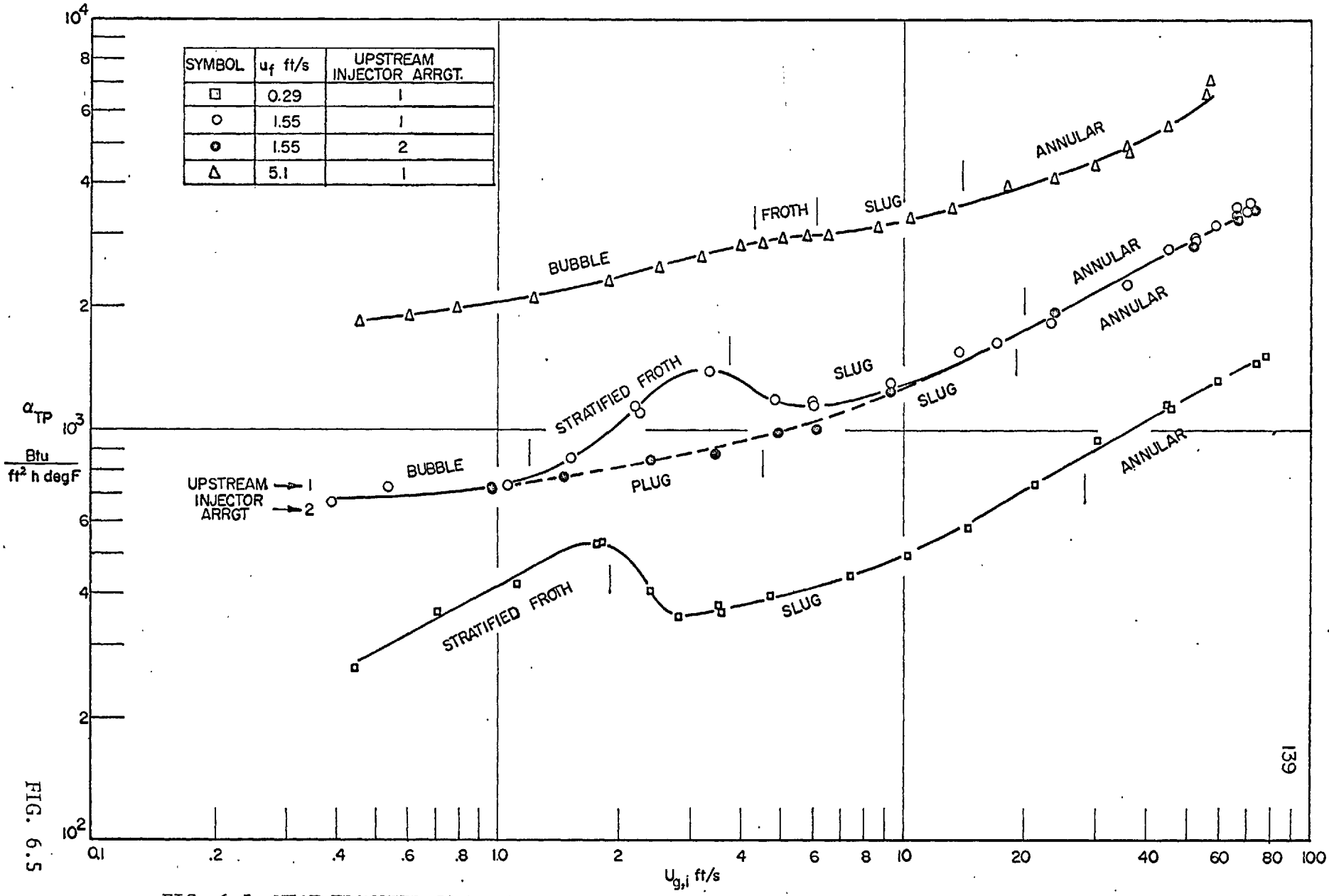

FIG. 6.5 HEAT-TRANSFER COEFFICIENTS FOR TESTS WITH ZERO BARBOTAGE AND FINITE INLET-QUALITY

The trend is consistent with observations by Johnson and Abou-Sabe [45] of air-water flows in an impermeable horizontal tube (more detailed comparisons appear later in this chapter).

The most striking feature of the results shown in Fig. 6.5 is that with Injector Arrangement 1, α_{TP} does not increase monotonically with $u_{g,i}$ and appears to be connected with flow regime. For liquid velocities u_f of 1.55 and 0.29 ft/s and for increasing $u_{g,i}$: α_{TP} shows a steep increase in stratified froth flow; with the onset of slug flow α_{TP} begins to decrease; the curve exhibits a minimum and then increases as slug flow fully develops and progresses into annular flow. At the highest liquid velocity of 5.1 ft/s there is no stratified froth flow; froth flow occurs where stratified froth flow would otherwise be expected to occur; slug flow occurs over a small range of $u_{g,i}$. For this velocity there is no region of steeply increasing, nor of decreasing α_{TP}, with increasing $u_{g,i}$. It would appear then that the existence of the steeply increasing α_{TP} followed by a decreasing α_{TP} is characteristic of stratified froth flow followed by slug flow.

Tests performed at a water velocity of 1.55 ft/s with Injector Arrangement 2 are also shown in Fig. 6.5; with this arrangement there is a monotonic increase in α_{TP} with increasing $u_{g,i}$. Of particular note is that, where with Injector Arrangement 1 stratified froth flow occurs and gives steeply rising α_{TP} and

then decreasing α_{TP} as the transition to slug flow occurs, Injector Arrangement 2 gives plug flow, lower values of α_{TP} and a smoothly increasing α_{TP} with increasing $u_{g,i}$. In well-developed slug flow and annular flow, both injector arrangements give the same heat-transfer coefficients.

From the above discussion it may be concluded that the heat-transfer coefficient depends on the flow pattern. Where more than one flow pattern can exist, not only gas and liquid flow rates need to be specified, the flow pattern must in general be specified as well. The previous statement was qualified with the words "in general" because, at the left-hand end of the curves for u_f = 1.55 ft/s, it appears that the values of α_{TP} obtained in bubble flow with Injector Arrangement 1 and in plug flow with Injector Arrangement 2 are the same for given values of $u_{g,i}$.

6.5.2 Tests with Finite Barbotage and Finite Inlet-Quality

The results of the tests with finite barbotage-rate and finite inlet-quality (finite $\dot{V}''_g$, finite $u_{g,i}$) are shown in Figs. 6.6 to 6.12. Figs. 6.6 to 6.10 show the data points while Fig. 6.11 shows the range of heat-transfer coefficients encountered for the three values of u_f. Fig. 6.12 shows a cross-plot of the smoothed data contained in Figs. 6.6 to 6.10. All the data in these figures are for Injector Arrangement 1. The flow patterns for zero-barbotage tests are marked in Figs. 6.6 to 6.10. Any changes in flow pattern

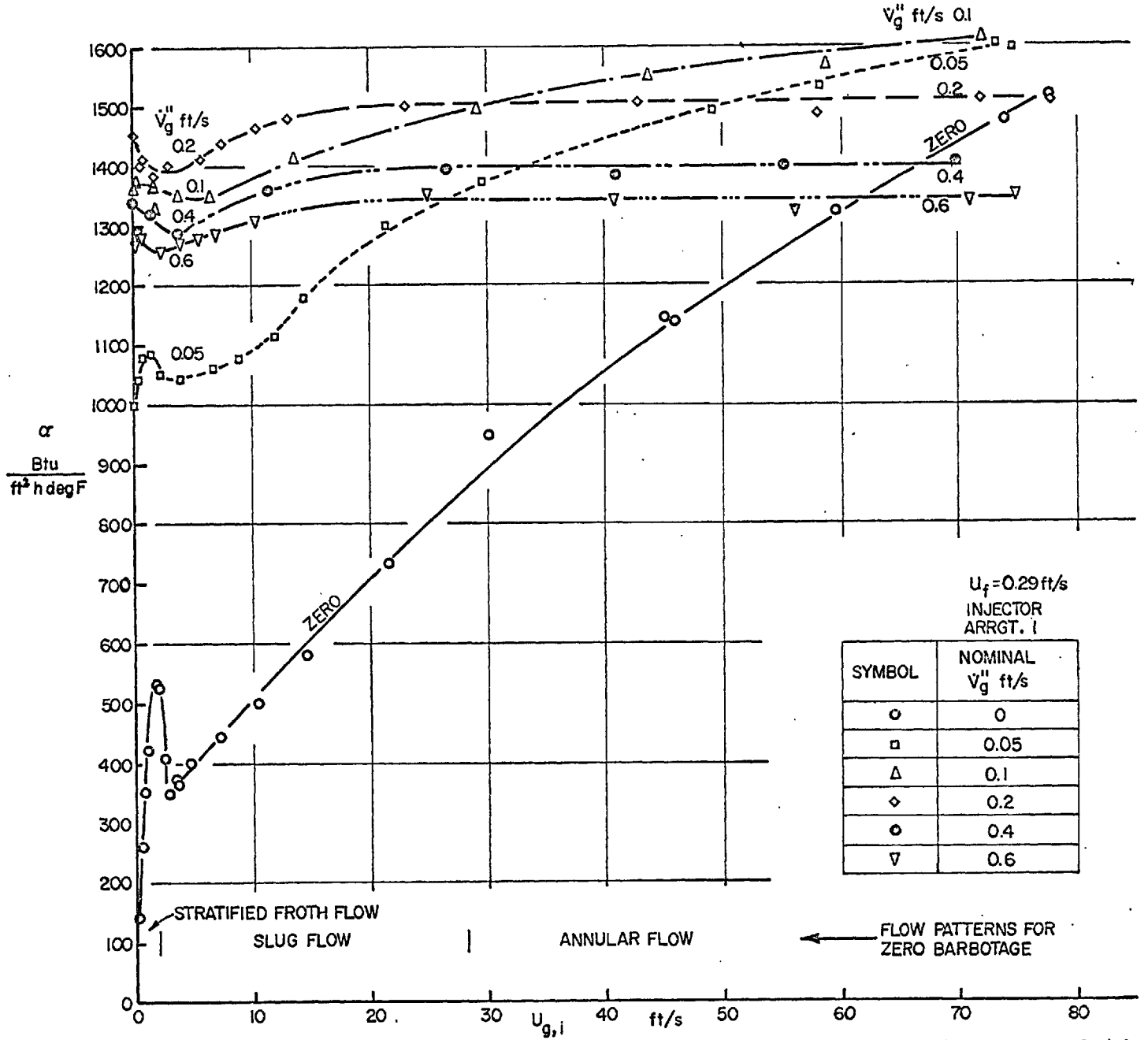

FIG. 6.6 HEAT-TRANSFER COEFFICIENTS FOR TESTS WITH FINITE INLET-QUALITY (u_f = 0.29 ft/s)

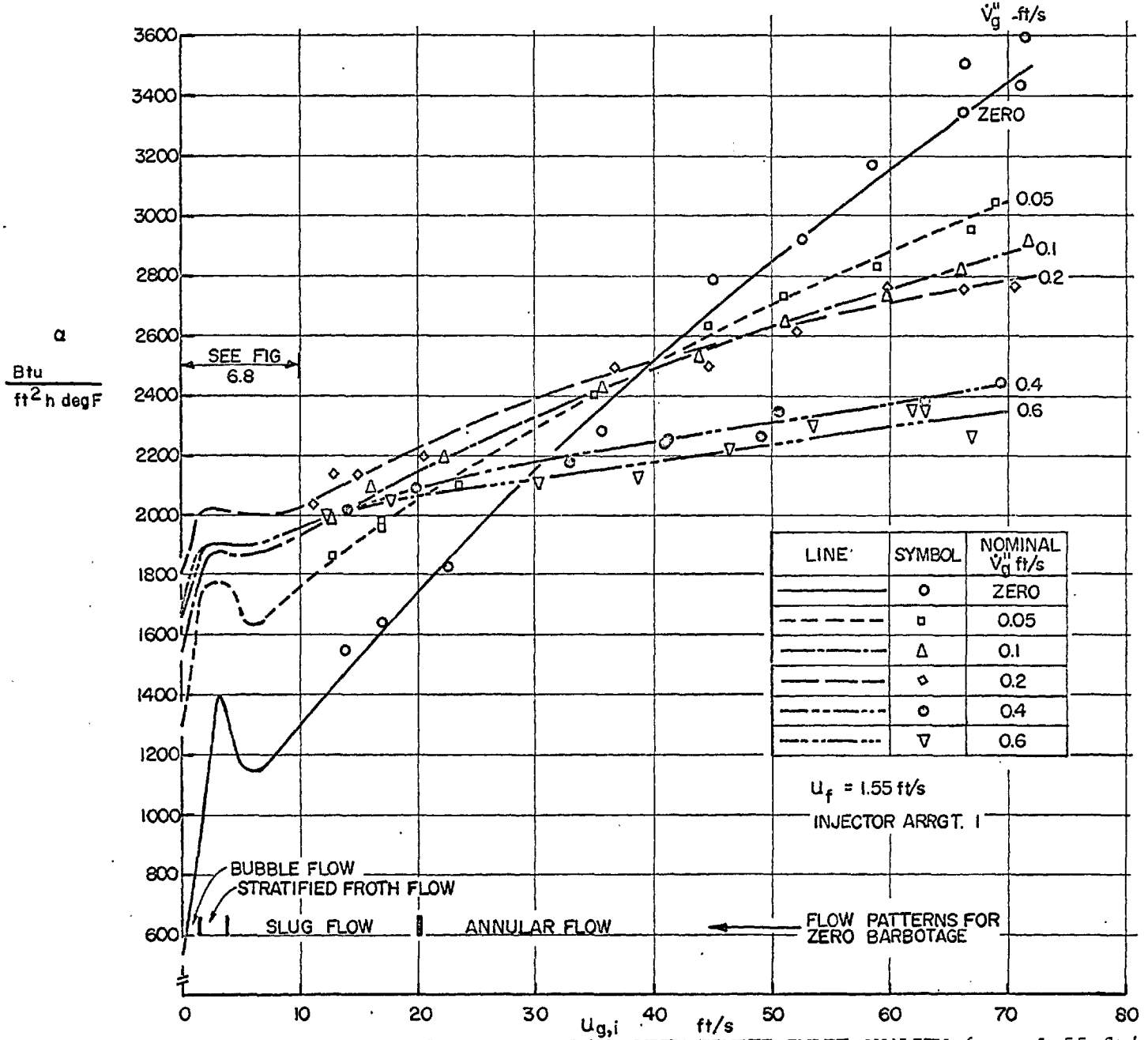

FIG. 6.7 HEAT-TRANSFER COEFFICIENTS FOR TESTS WITH FINITE INLET-QUALITY (u_f = 1.55 ft/s)

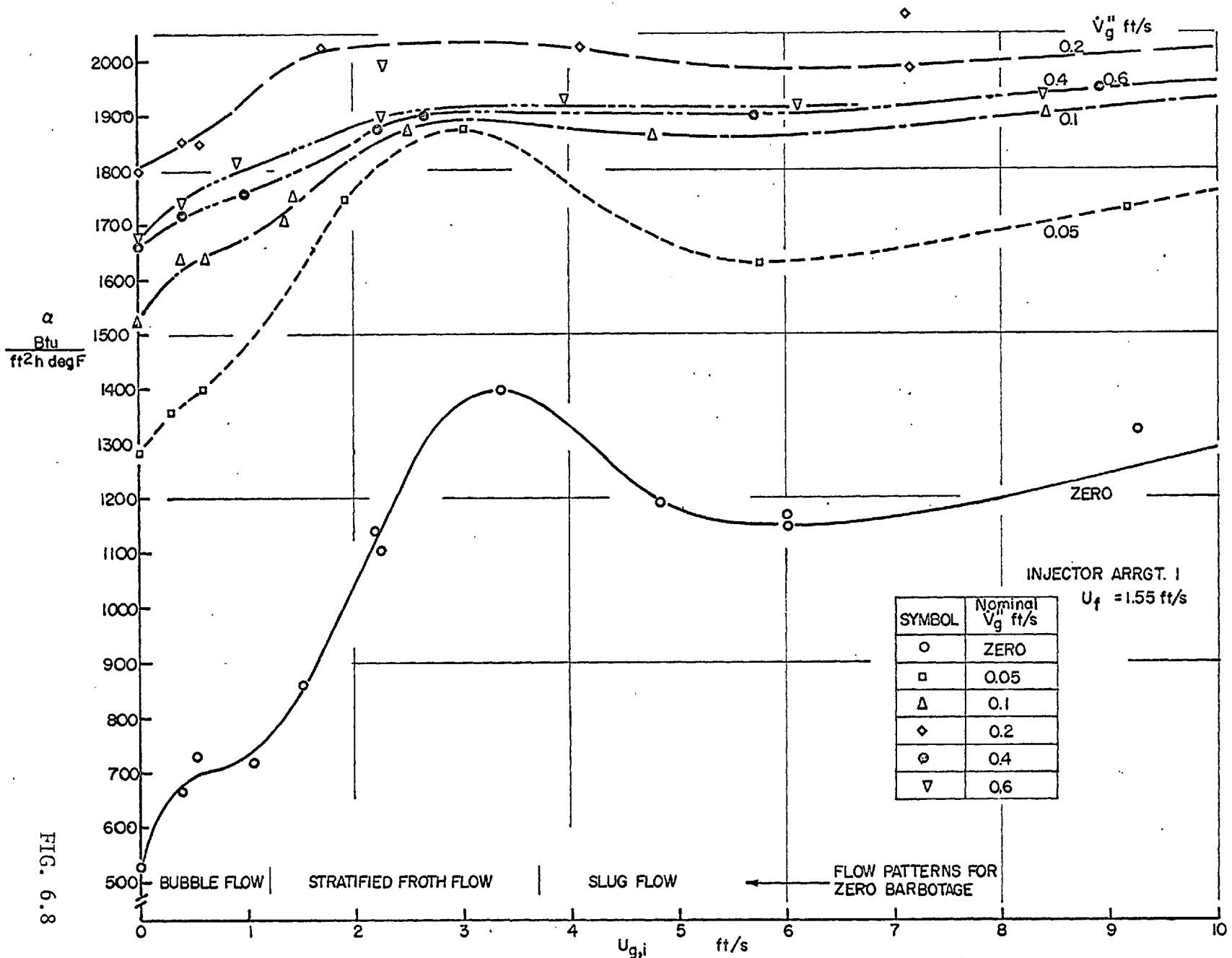

FIG. 6.8 HEAT-TRANSFER COEFFICIENTS FOR TESTS WITH FINITE INLET-QUALITY (u_f = 1.55 ft/s)

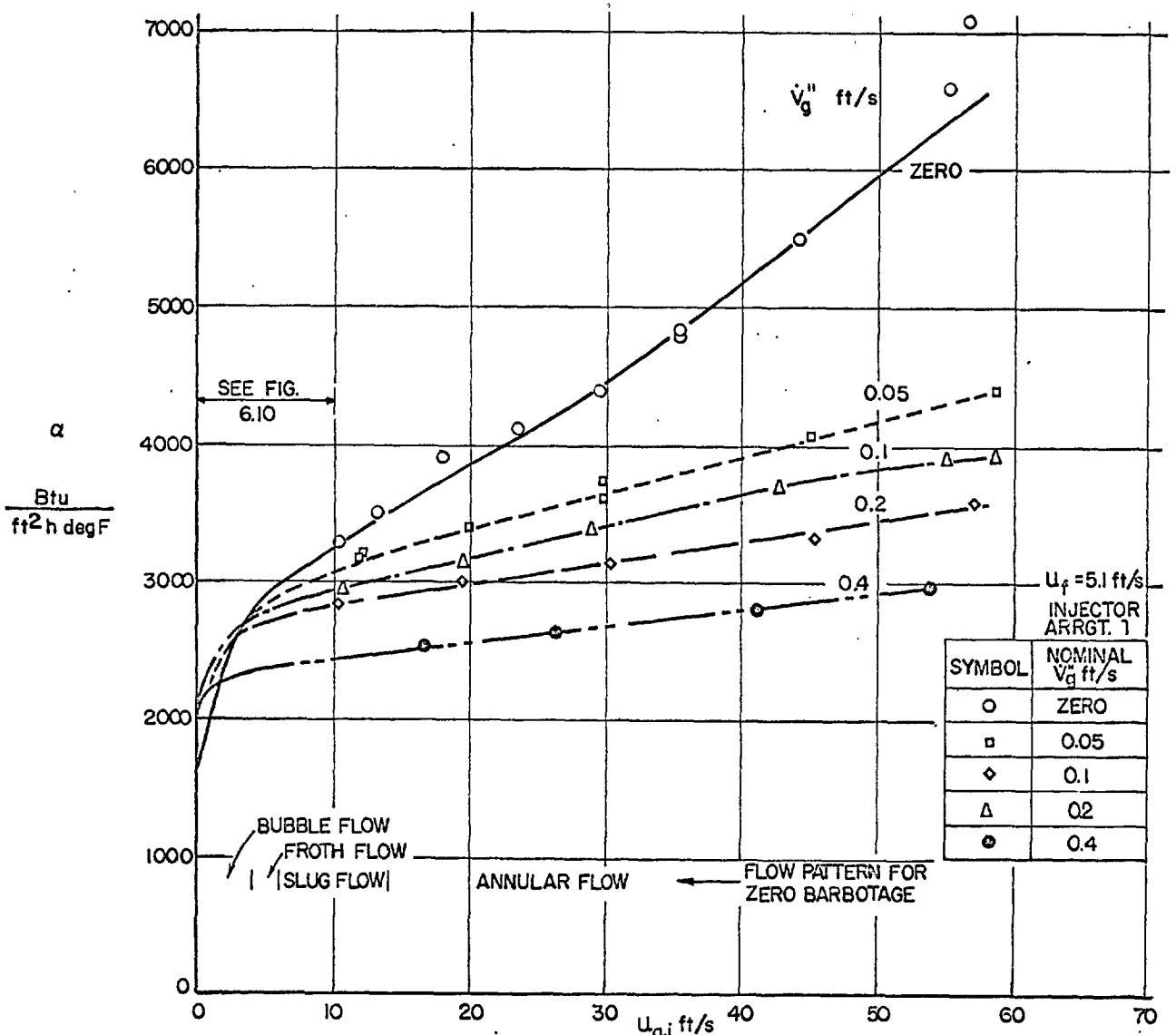

FIG. 6.9 HEAT-TRANSFER COEFFICIENTS FOR TESTS WITH FINITE INLET-QUALITY (u_f = 5.1 ft/s)

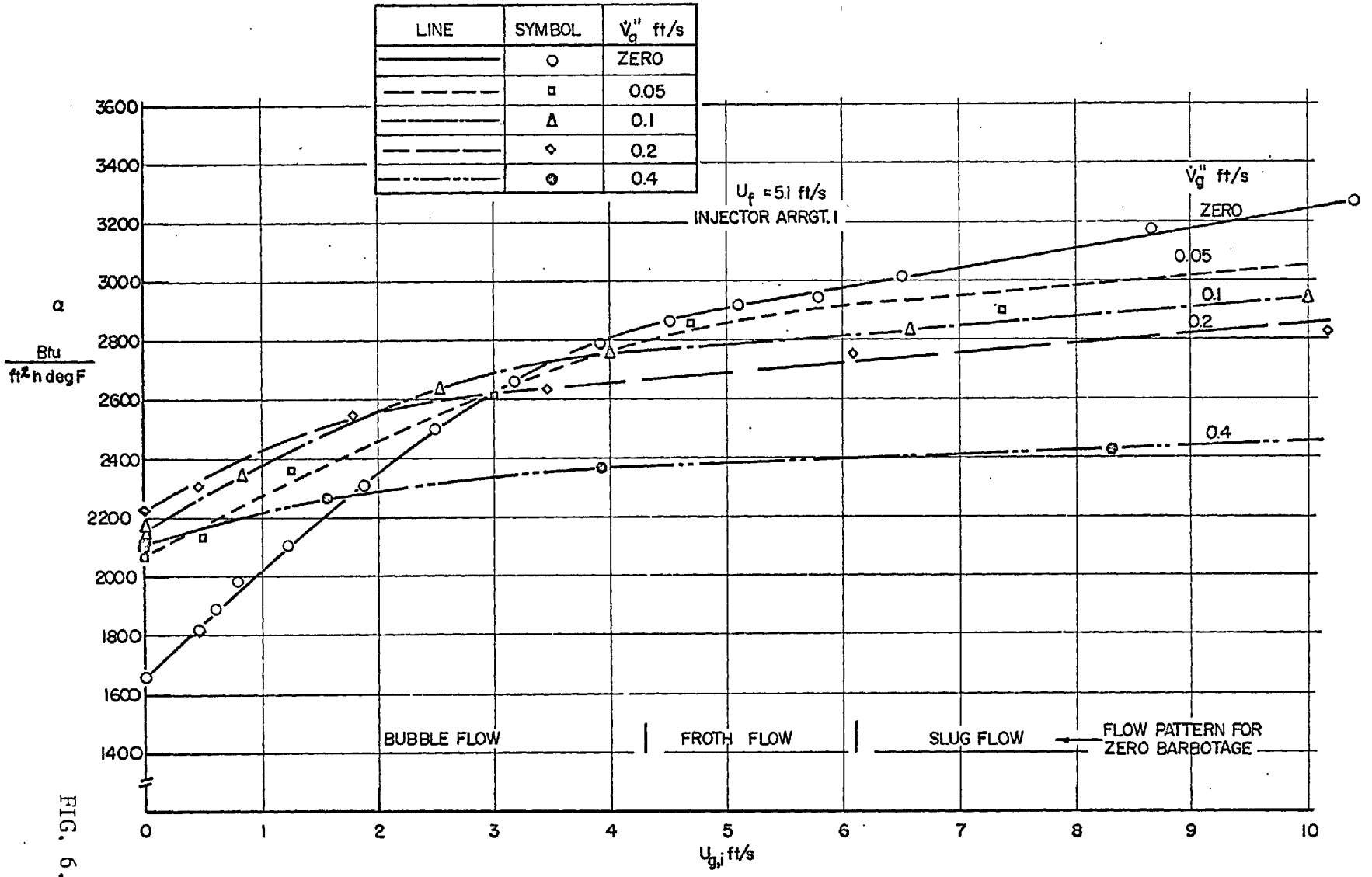

FIG. 6.10 HEAT-TRANSFER COEFFICIENTS FOR TESTS WITH FINITE INLET-QUALITY (u_f = 5.1 ft/s)

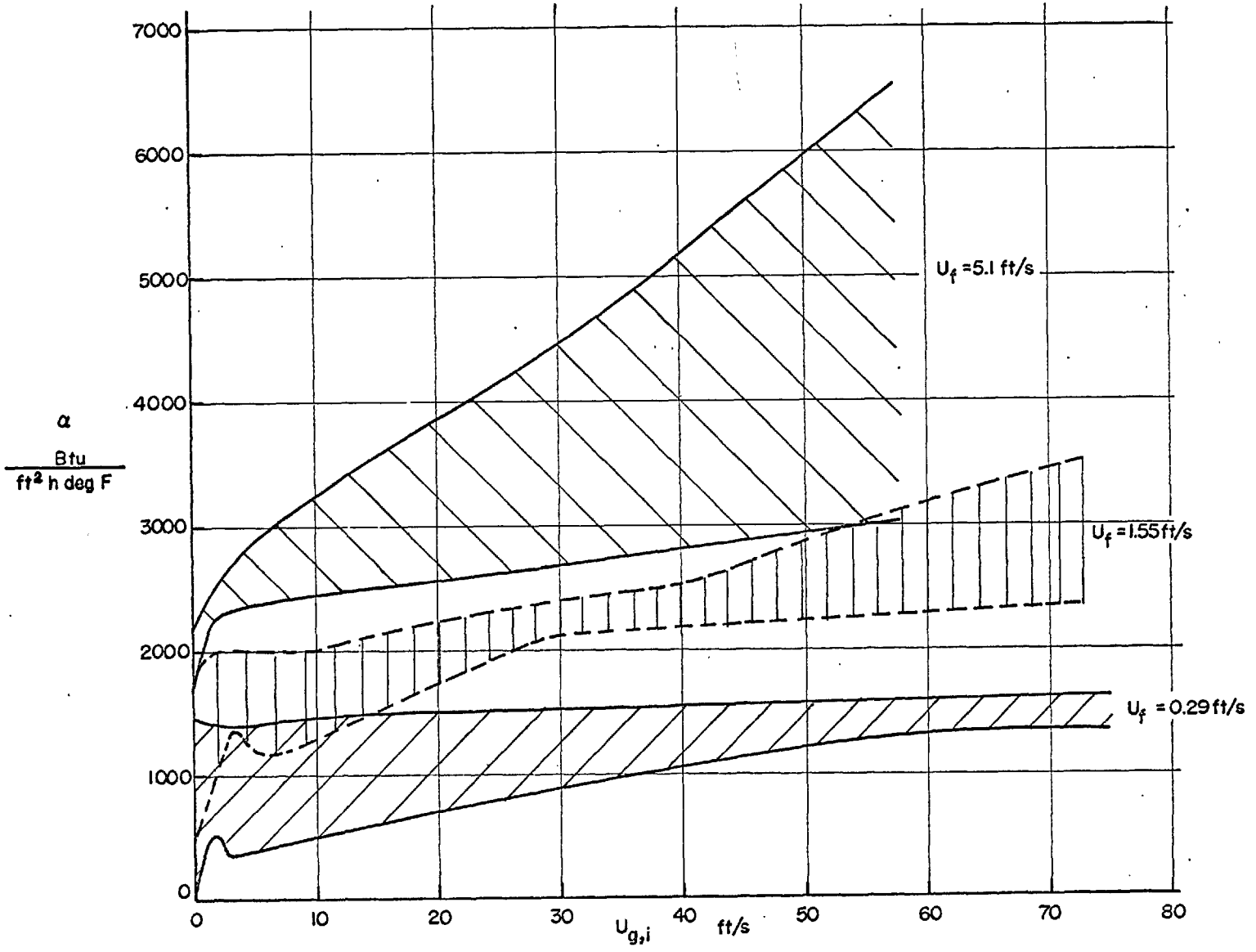

FIG. 6.11 RANGE OF HEAT-TRANSFER COEFFICIENTS ENCOUNTERED IN TESTS WITH FINITE INLET-QUALITY

FIG. 6.11

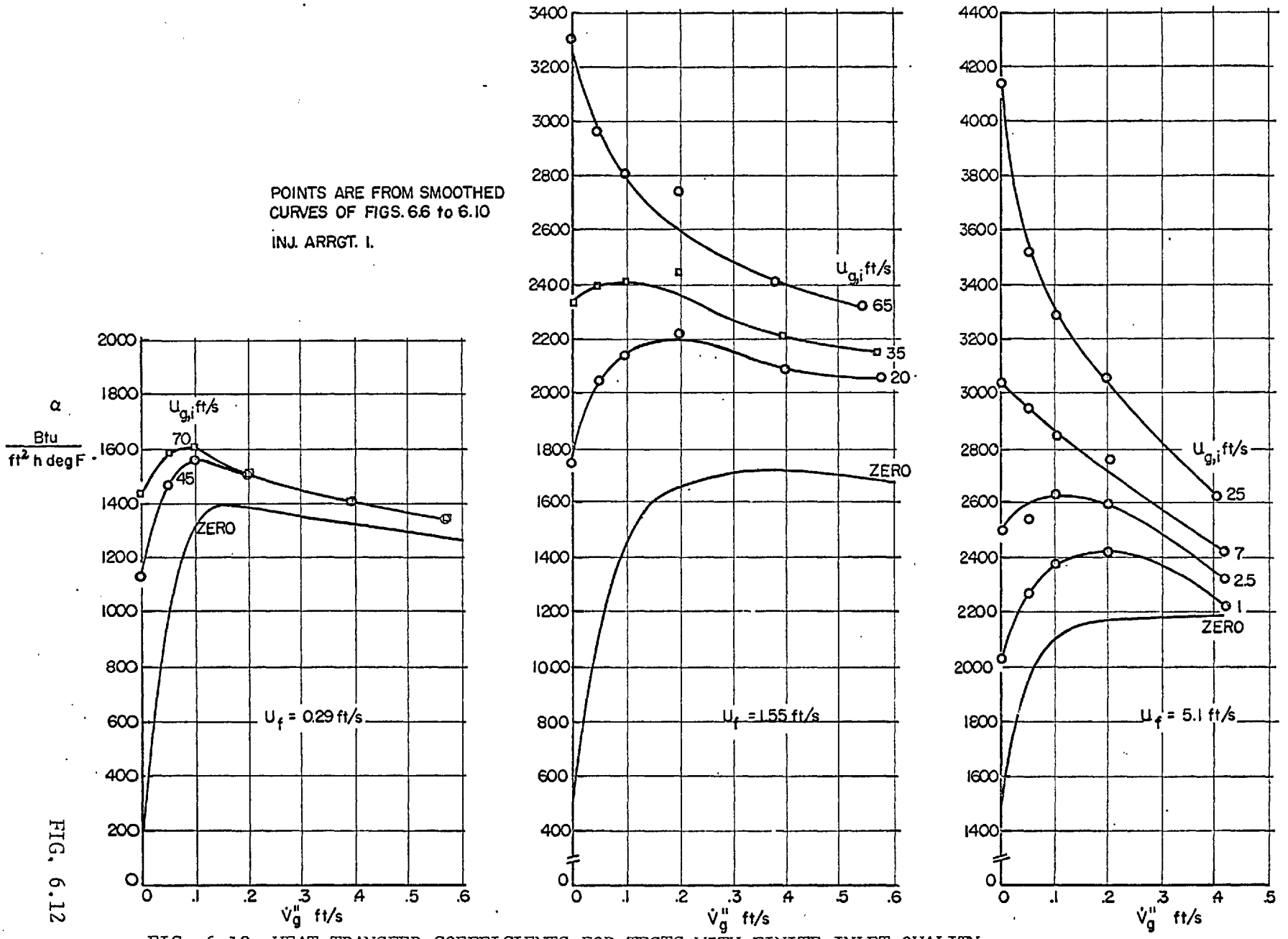

FIG. 6.12 HEAT-TRANSFER COEFFICIENTS FOR TESTS WITH FINITE INLET-QUALITY

in the porous section which result because of finite barbotage are given in Section 5.5. The results for each liquid velocity will be treated in turn.

Water velocity of u_f = 0.29 ft/s (Fig. 6.6).

As the barbotage-rate $\dot{V}''_g$ increases, the heat-transfer coefficient α becomes very insensitive to the upstream air velocity $u_{g,i}$. This is illustrated by noting that as $u_{g,i}$ is varied from zero to 75 ft/s: for $\dot{V}''_g = 0$, α increases about 10 times while for $\dot{V}''_g \geq 0.2$, the increase in α is only a few percent. Also the "dip" which occurs with the zero-barbotage experiments at $u_{g,i} \simeq$ 2 ft/s is considerably reduced as $\dot{V}''_g$ is increased.

Water velocity of u_f = 1.55 ft/s (Figs. 6.7 and 6.8).

The results for u_f = 1.55 ft/s are presented in two graphs; Fig. 6.7 shows the complete range of $u_{g,i}$ covered while Fig. 6.8 shows in greater detail the range for $u_{g,i} < 10$ ft/s. The most important features of the figures are discussed below.

(i) As with the water velocity of 0.29 ft/s, α becomes very insensitive to $u_{g,i}$ as the barbotage-rate is increased from zero to 0.6 ft/s. This is clearly illustrated by considering the two extremes shown in $\dot{V}''_g$. For $\dot{V}''_g = 0$, on increasing $u_{g,i}$ from zero to 72 ft/s, the heat-transfer coefficient increases by 5 1/2 times while for $\dot{V}''_g = 0.6$ ft/s, the increase in α is only 40% over the

same range of $u_{g,i}$. The "dip" in α which is very apparent for the zero-barbotage test at $u_{g,i} \simeq 4$ ft/s is all but eliminated as $\dot{V}''_g$ is increased to 0.6 ft/s.

(ii) For $u_{g,i} > 40$ ft/s there is a monotonic decrease in α with increasing $\dot{V}''_g$ for fixed $u_{g,i}$. This is clearly shown in Fig. 6.12 which presents a cross-plot of the smoothed data from Fig. 6.7. Kudirka et al. [49] have reported a few data for air-water flow in a vertical tube ($u_f = 4.5$ ft/s) where this same trend is apparent.

Water velocity of $u_f = 5.1$ ft/s (Figs. 6.9 and 6.10).

The results for $u_f = 5.1$ ft/s are shown in Fig. 6.9, which shows the complete range of $u_{g,i}$ covered, and in Fig. 6.10 which shows in greater detail the region of $u_{g,i} < 10$ ft/s. The features to note are as follows.

(i) As with the other two liquid velocities tested, α becomes more and more insensitive to $u_{g,i}$ as $\dot{V}''_g$ is increased.

(ii) For values of $u_{g,i}$ greater than 4 ft/s, there is a monotonic decrease in α with increasing $\dot{V}''_g$ for fixed $u_{g,i}$. This is best illustrated in Fig. 6.12.

Fig. 6.11 shows the range of heat-transfer coefficients encountered with the finite-inlet-quality tests. It is seen that the greater the liquid velocity, the greater are the heat-transfer coefficients.

An examination of Fig. 6.12 shows that for each water velocity u_f, the critical barbotage-rate $\dot{V}''_{g,cr}$ decreases with increasing gas velocity $u_{g,i}$ at inlet to the porous section. Further, an examination would show that $\dot{V}''_{g,cr}$ is not restricted to appearing in any particular flow pattern or at the transition from one pattern to another as $\dot{V}''_g$ is increased; this is illustrated in the table below.

u_f ft/s	$u_{g,i}$ ft/s	Flow pattern in which $\dot{V}''_{g,cr}$ occurs
0.29	0	Froth flow
	45	Annular flow
	70	Annular flow
1.55	0	Froth flow
	15	Slug flow
	35	Annular flow
5.1	1	Froth flow
	2.5	Boundary bubble flow to froth flow

Effect of injector arrangement.

The results of tests run with Injector Arrangement 2 are shown in Fig. 6.13 together with those for Injector Arrangement 1. Remarks specifically concerning the zero-barbotage experiments were made previously. For fixed values of $u_{g,i}$, the trend of results is the same for both injector arrangements: for $u_{g,i} < 10$ ft/s, α increases with increasing $\dot{V}''_g$ for the three $\dot{V}''_g$ values shown; for $u_{g,i} > 40$ ft/s, α decreases with increasing $\dot{V}''_g$; in the region $10 < u_{g,i} < 40$, the behavior of α undergoes a transition. At fixed values of $u_{g,i}$, comparing the heat-transfer coefficients obtained with the two different injector arrangements, it is seen that the

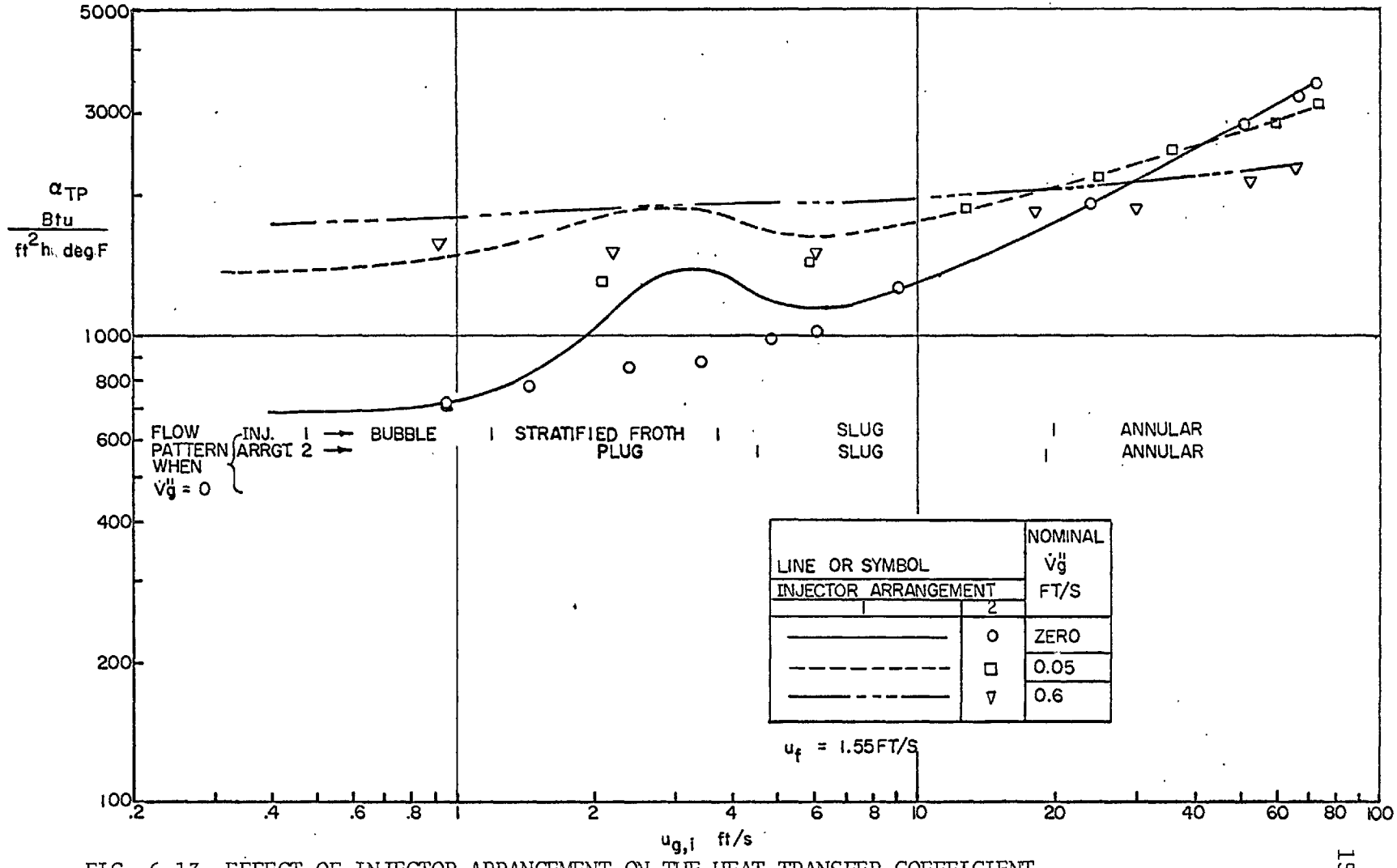

FIG. 6.13 EFFECT OF INJECTOR ARRANGEMENT ON THE HEAT-TRANSFER COEFFICIENT

agreement is generally good where both injector arrangements give the same flow pattern (annular and well-developed slug flow) while the agreement is worst where differences in flow patterns exist ($u_{g,i} < 5$ ft/s).

6.6 A Method of Correlating the Present Forced Convection Heat-Transfer Data For Barbotage Rates Less than the Critical

6.6.1 General Remarks and Summary of Equations

A method of correlating the heat-transfer coefficients obtained in the present experiments is now presented. Attention is restricted to barbotage rates less than the critical ($\dot{V}''_g < \dot{V}''_{g,cr}$), i. e. to the region in which the heat-transfer coefficient increases with increasing barbotage-rate $\dot{V}''_g$. This region is analogous in saturated boiling to the "nucleate" region in which the heat-transfer coefficient increase with increasing vapour formation rate, i.e. with heat flux.

The method of correlating the heat-transfer coefficient is similar to that of Chen [10] for the boiling of saturated liquids in two-phase forced convective flow. Chen postulated that two basic mechanisms take part in this process. These are (i) the ordinary "macroconvective" mechanism of heat transfer which normally operates with flowing fluids and (ii) the "microconvective" mechanism associated with bubble nucleation and growth. He further postulated that the two mechanisms are additive in their contributions to total heat transfer, i.e.,

$$\alpha_{tot} = \alpha_{mac} + \alpha_{mic} \tag{6.5}$$

where:

$$\alpha_{mac} = \alpha_{SP} F_C \tag{6.6}$$

$$\alpha_{mic} = \alpha_{tot,PB} S \tag{6.7}$$

α_{mac} is the heat-transfer coefficient due to macroconvection;

α_{mic} is the heat-transfer coefficient due to microconvection;

$\alpha_{tot,PB}$ is the heat-transfer coefficient which would obtain in pool boiling for the same liquid, pressure and wall superheat based on the Forster and Zuber [22] correlation;

F_C is the "Reynolds number factor", this is purely hydrodynamic and depends only on the Martinelli flow parameter X_{tt}(*); F_C was determined empirically;

---

*The Martinelli parameter X_{tt} is defined by

$$\frac{1}{X_{tt}} \equiv \left(\frac{W_g}{W_f}\right)^{0.9} \left(\frac{\rho_f}{\rho_g}\right)^{0.5} \left(\frac{\mu_g}{\mu_f}\right)^{0.1} \tag{6.8}$$

where:

W_g and W_f are the mass flow rates of the gas phase and liquid phase respectively, μ_g is the dynamic viscosity of the gas phase and the other symbols have been defined previously.

S is the "suppression factor"; it accounts for reduced bubble activity due to a reduced "effective superheat" for the bubbles due to the presence of the forced convective field; it is a function of the hydrodynamic parameters F_C and Re_f the liquid phase Reynolds number; S has the limits of unity at zero flow rate and zero at infinite flow rate and was determined empirically.

For barbotage, the analogous concept of two contributions is also used, one for the forced convection flow (α_{mac}) and one for bubbling (α_{mic}):

$$\alpha = \alpha_{mac} + \alpha_{mic}$$

where

$$\alpha_{mac} = \alpha_{SP} F$$

and

$$\alpha_{mic} = \Psi \alpha_{bub}$$

i.e.

$$\alpha = \alpha_{SP} F + \Psi \alpha_{bub} \qquad (6.9)$$

where:

F is a factor accounting for the increased velocity and turbulence in the forced convective flow due to air having been introduced upstream of the test section; for identification F is called here the "upstream turbulence factor";

α_{bub} is the maximum heat-transfer coefficient that can be achieved, for a given barbotage rate and fluid properties, due to agitation by the barbotage bubbles; α_{bub} is called here the "bubbling function";

Ψ is a factor which accounts for the reduced effectiveness of the barbotage-bubble agitation process as the turbulence in the forced convective flow increases; it is called here the "bubble effectiveness factor".

The three functions F, α_{bub} and Ψ are determined empirically as

$$\left.\begin{aligned} F &= \phi(u_{g,i}/u_f) \\ \Psi &= \phi(u_{g,i}/u_f,\ Re_f) \\ \alpha_{bub} &= \phi(\dot{V}''_g,\ \text{fluid properties}) \end{aligned}\right\} \qquad (6.10)$$

The expressions for the three functions of equation (6.10), obtained in the next section of this chapter, are listed below. (The symbol Ψ_o is the value of Ψ for zero-inlet-quality tests while Ψ^+ is the ratio Ψ/Ψ_o)

$$F = 1 + 0.64\sqrt{\frac{u_{g,i}}{u_f}} \qquad (6.11)$$

(Except for zero-barbotage data in stratified froth flow).

$$\Psi = \Psi^+ \Psi_o \qquad (6.19)$$

$$\left.\begin{aligned} \Psi_o &= 1 \qquad \text{for } Re_f \leqslant 2000 \\ \Psi_o &= 9.78\, Re_f^{-0.3} \qquad \text{for } Re_f \geqslant 2000 \end{aligned}\right\} \quad (6.16)$$

$$\Psi^+ = e^{-\left\{\frac{0.68}{10^6}\,(Re_f^{1.4})\,\frac{u_{g,i}}{u_f}\right\}} \quad (6.25)$$

α_{bub} is from Fig. 6.17 or

$$\left.\begin{aligned} Nu^*_{bub}\, Pr_f^{0.2} &= 167(K_T^*)^{0.75} \qquad \text{for } 0.009 \leqslant K_T^* \leqslant 0.15 \\ Nu^*_{bub}\, Pr_f^{0.2} &= 48.7(K_T^*)^{0.1} \qquad \text{for } 0.15 \leqslant K_T^* \leqslant 1.27 \end{aligned}\right\} \quad (6.34)$$

where:

$$Nu^*_{bub} \equiv \frac{\alpha_{bub}}{k_f}\sqrt{\frac{\sigma g_o}{g(\rho_f - \rho_g)}}$$

$$K_T^* \equiv \frac{\dot{V}''_g \sqrt{\rho_f}}{[\sigma g_o\, g(\rho_f - \rho_g)]^{1/4}}$$

Under certain conditions, the functions F, Ψ and α_{bub} and equation (6.9) have special forms. The information is shown in Table 6.1.

Table 6.1 Special Forms of Equation (6.9) and of the Functions F, Ψ and α_{bub}

Conditions	Special values of F, Ψ and α_{bub}	Equation (6.9) for α
$u_{g,i} = 0$ $\dot{V}''_g = 0$	$F = 1$ $\alpha_{bub} = 0$	$\alpha = \alpha_{SP}$
$u_{g,i} = 0$ Finite $\dot{V}''_g$	$F = 1$ $\Psi = \Psi_o$	$\alpha = \alpha_{SP} + \Psi_o \alpha_{bub}$
Finite $u_{g,i}$ $\dot{V}''_g = 0$	$\alpha_{bub} = 0$	$\alpha = \alpha_{SP} F$

6.6.2 Upstream Turbulence Factor F

The F-function is found from experiments with zero barbotage, in which case $\alpha_{bub} = 0$ and equation (6.9) becomes

$$\alpha_{TP} = \alpha_{SP} F$$

or

$$F = \frac{\alpha_{TP}}{\alpha_{SP}}$$

(α_{TP} is the designation for α under zero-barbotage conditions). A graph of α_{TP}/α_{SP} vs. $u_{g,i}/u_f$ is shown in Fig. 6.14*; values of α_{SP} are those measured. It is noted that α_{TP}/α_{SP} is practically independent of liquid velocity. A simple equation representing the data is

$$F = 1 + 0.64\sqrt{\frac{u_{g,i}}{u_f}} \qquad (6.11)$$

In Fig. 6.14, data in stratified froth flow (five and four data points for water velocities of 0.29 ft/s and 1.55 ft/s respectively) have been omitted; equation (6.11) represents data in all the other flow patterns to the accuracy shown in Fig. 6.14.

The form of equation (6.11) was chosen such that when $u_{g,i}/u_f = 0$, $F = 1$ or $\alpha_{TP} = \alpha_{SP}$.

Comparisons with existing zero-barbotage air-water experiments [23,45,65] in horizontal channels (all round tubes) are now made. The effect of fluid properties on F cannot be determined because of lack of experimental evidence; the three existing [44,65,

---

*The Martinelli flow parameter X_{tt} is often used, e.g. [10,13,23,45], in the correlation of two-phase heat-transfer data. The use of X_{tt} implies that both liquid-and gas-phase Reynolds numbers Re_f and Re_g are greater than 2000. In the present experiment both Re_f and Re_g straddle the value of 2000. It would therefore be inconsistent in the present case, when all the data are presented on a single graph, to use a parameter derived specifically for Re_f and Re_g greater than 2000.

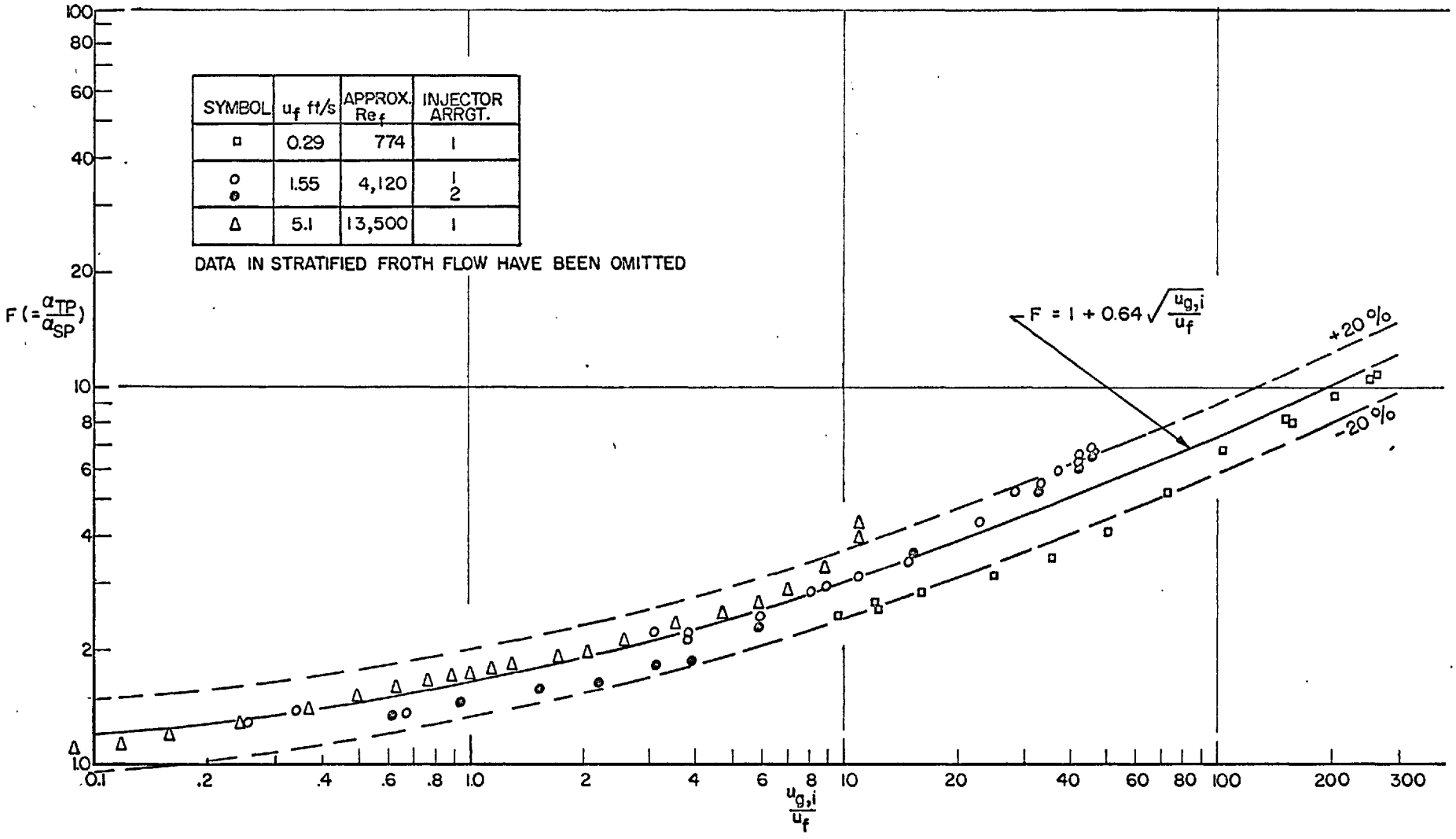

FIG. 6.14 CORRELATION OF PRESENT ZERO-BARBOTAGE DATA

FIG. 6.14

67] investigations for other than air-water flows in horizontal tubes are commented on where the Newson [65] data is presented.

Results of Johnson and Abou-Sabe.

Johnson and Abou-Sabe [45] measured heat-transfer coefficients to air-water mixtures flowing in a steam-heated horizontal tube 0.870-in. ID and 15.5-ft long; the tube wall was impermeable. The results show that for a fixed liquid flow rate, the heat-transfer coefficient α_{TP} at first increases with increasing air flow rate and then tends to pass through a maximum beyond which there is a monotonic decrease in α_{TP}. In the discussion which follows only heat-transfer coefficients less than these maxima are treated. This is because comparison is being made against the present F-function which increases monotonically with $u_{g,i}/u_f$. In the present experiments no condition was reached beyond which, for a given u_f, α_{TP} decreased monotonically with $u_{g,i}$. The reasons for the existence of these maxima appears to be not very well understood. The Johnson and Abou-Sabe smoothed results, plotted in terms of α_{TP}/α_{SP} vs. $(u_g/u_f)_{mean}$ are shown in Fig. 6.15. The subscript "mean" indicates that u_g/u_f was evaluated at the mean bulk temperature and pressure in the test section.

It should be noted that α_{TP}/α_{SP} is practically independent of the liquid velocity, as with the present experiments. The results lie within ±20% of the equation

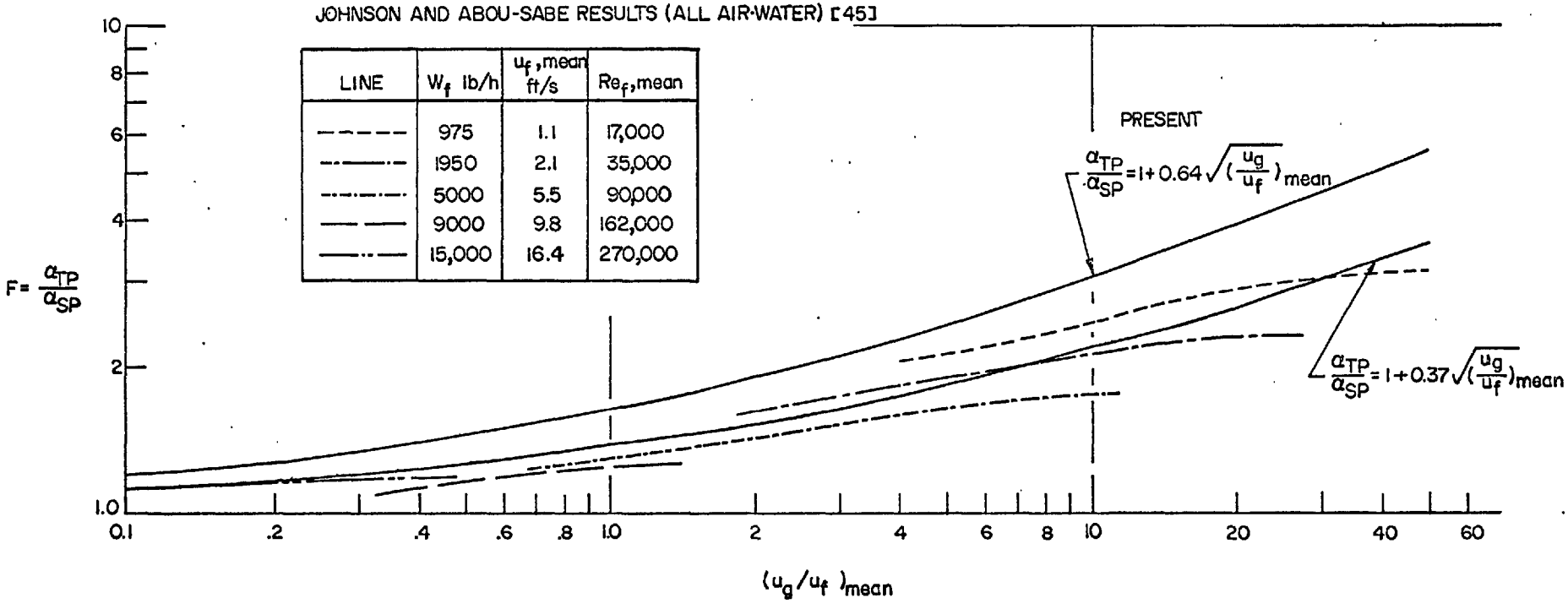

FIG. 6.15 COMPARISON OF RESULTS OF JOHNSON AND ABOU-SABE WITH PRESENT F-FUNCTION

$$\frac{\alpha_{TP}}{\alpha_{SP}} = 1 + \text{Const.} \sqrt{\left(\frac{u_g}{u_f}\right)_{mean}} \qquad (6.12)$$

with Const. = 0.37. The equation which correlates the present data, i.e. (6.12) with Const. = 0.64 is also shown for comparison. (For the present zero-barbotage experiments, the difference between $u_{g,i}/u_f$ (as in equation 6.11) and $(u_g/u_f)_{mean}$ (as in equation 6.12) does not exceed 1 3/4%). It is noted that the Johnson and Abou-Sabe data lie below the equation representing the present data. The worst deviation of equation (6.12) with Const. = 0.37 from (6.12) with Const. = 0.64 is 34% at $(u_g/u_f)_{mean} = 50$.

Possible reasons for the discrepancy between the present results and those of Johnson and Abou-Sabe are given below.

(i) The heat-transfer surface, a drawn-brass tube (expected rms roughness 10-200 μ in. [74a]), was very likely smoother than the porous heating surface (approximate rms roughness 600 μ in.) in the present apparatus. This could affect the ratio α_{TP}/α_{SP}, probably making it larger for the rougher (present) surface.

(ii) The geometry in the two investigations is different. The heat-transfer coefficients reported by Johnson and Abou-Sabe represent some circumferential mean in a tube while those reported here are for the bottom surface of a rectangular channel. In horizontal two phase flow, it is expected that conditions around the periphery of the channel will vary due to the influence of

gravity on the distribution of the two phases. Further, the heat transfer tube in the Johnson and Abou-Sabe experiments was very long (15.5 ft) compared with the present heated section (6 in.). In the former experiments, under extreme conditions the gas velocity doubled from inlet to outlet of the test section, so making the reported heat-transfer coefficients difficult to interpret [82]. In the present zero- barbotage experiments these gas velocity changes did not exceed 3 1/2%.

Results of Fried.

In a continuation of the Johnson and Abou-Sabe [45]work, Fried [23] measured heat-transfer coefficients between air-water mixtures and a steam-heated, impermeable, horizontal tube 0.737-in. ID and 15-ft long. Fried's results show the same trends as those of Johnson and Abou-Sabe; when plotted on coordinates of α_{TP}/α_{SP} vs. $(u_g/u_f)_{mean}$ (Fig. 3 of Ref. 46), the results are practically independent of water flow rate; the maximum deviations of the smoothed Fried results from those of Johnson and Abou-Sabe occur at $(u_g/u_f)_{mean} > 20$ with the former being 35% below the latter. The discussion relevant to the Johnson and Abou-Sabe results is also relevant to the Fried results.

Results of Newson.

Newson [65] measured heat-transfer coefficients between

air-water mixtures and a steam-heated, horizontal tube of 0.495-in. ID and 3-ft length; the tube wall was impermeable. He also used air with a 50% glycerol and water mixture as the gas-liquid combination. His air-water results, for heat-transfer coefficients less than the maximum for each liquid flow rate, are shown in Fig. 6.16 on coordinates of α_{TP}/α_{SP} vs. $(u_g/u_f)_{mean}$. The equation correlating the results of the present investigation is shown for comparison.

In Fig. 6.16 it is noted that the Newson data lie below the equation for the present results. It is further noted that the ratio α_{TP}/α_{SP} is largely independent of liquid velocity for fixed values of $(u_g/u_f)_{mean}$. Equation (6.12) with Const. = 0.43 is drawn on the figure and correlates the smoothed Newson data to ±20%. The discussion relating to the discrepancy between the present and the Johnson and Abou-Sabe results applies to the Newson results as well except for the comment concerning the large changes in gas velocity from inlet to outlet of the test section.

If the air-50% glycerol results of Newson had been plotted on Fig. 6.16 it would have been seen that, for fixed $(u_g/u_f)_{mean}$, the ratio α_{TP}/α_{SP} is largely independent of viscosity (the ratio of the viscosity of the 50% glycerol mixture to that of water was 3.7) as well as velocity. Equation (6.12) with Const. = 0.45 correlates both the air-water and air-50% glycerol smoothed data to ±22%. The results of Oliver and Wright [67], for air and an 88% glycerol and

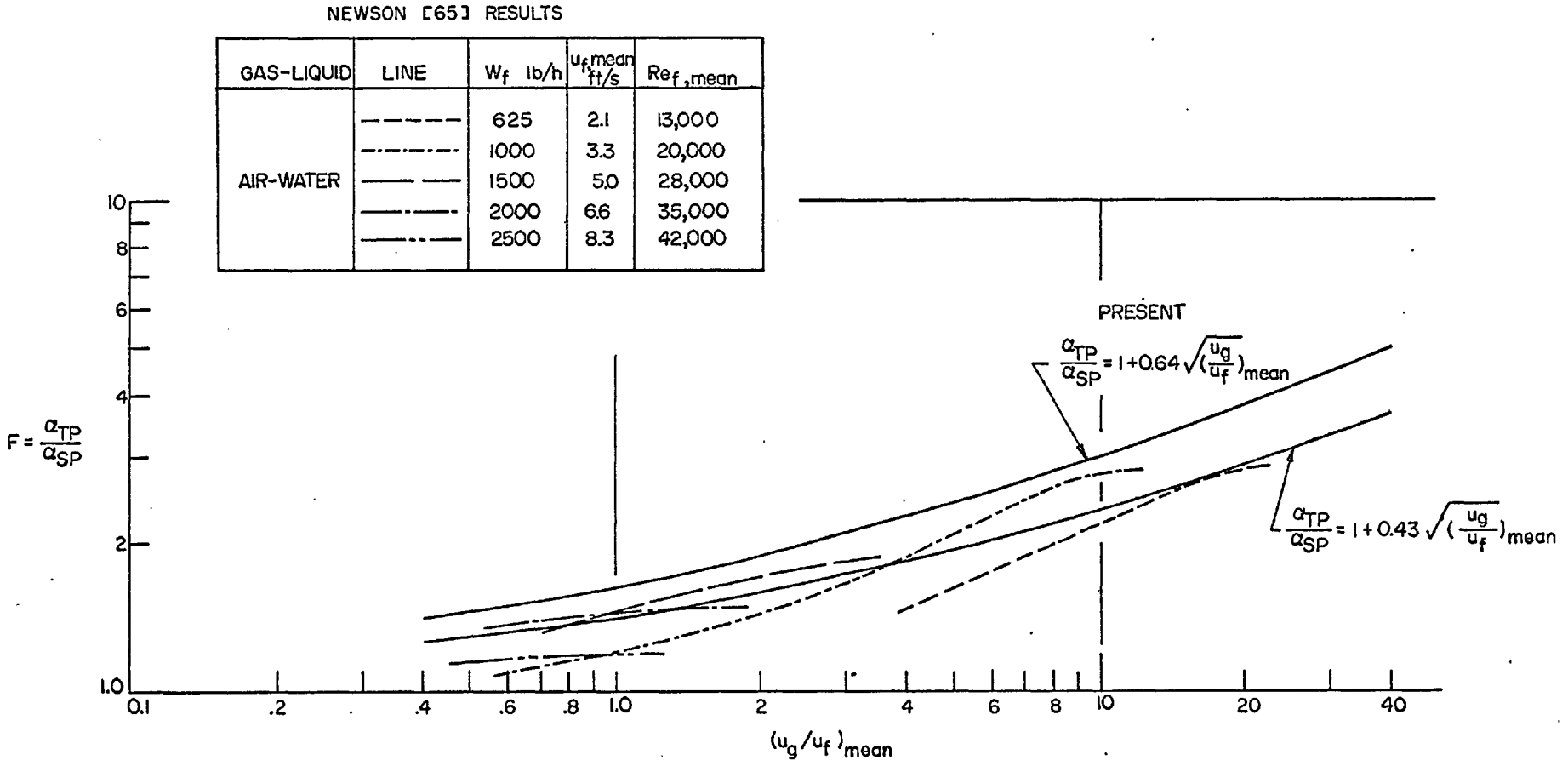

FIG. 6.16 COMPARISON OF NEWSON AIR-WATER RESULTS WITH PRESENT F-FUNCTION

FIG. 6.16

water mixture flowing in a 1/4-in. ID 3-ft long heat-transfer tube, would be scattered around the Newson data on Fig. 6.16. On the information available it is not claimed that F can be correlated only as a function of the ratio of the gas velocity to liquid velocity. The data of Johnson [44], for air-oil flow in the same apparatus as that of Fried [23], lie some 200 or 300% above Fried's air-water results on a graph such as Fig. 6.16 (Fig. 3 of Ref. 46). Considerably more evidence is necessary on the effect of fluid properties on F.

6.6.3 Bubble Effectiveness Factor Ψ and Bubbling Function α_{bub} for the Present Data

The bubble effectiveness factor Ψ accounts for the reduced effectiveness of the barbotage-bubble agitation process as the turbulence in the forced convective flow increases. It is therefore expected that

$$\Psi = \phi(Re_f, F) \tag{6.13}$$

As

$$F = \phi(u_{g,i}/u_f) \tag{6.14}$$

equation (6.13) becomes

$$\Psi = \phi(Re_f, u_{g,i}/u_f) \tag{6.15}$$

The analysis proceeds by treating Ψ in two stages, first for zero inlet-quality and then for finite inlet-quality. The bubbling

function α_{bub} will be obtained from the analysis of the zero-inlet-quality results.

Zero inlet-quality.

When $u_{g,i}/u_f = 0$, $\Psi = \Psi_o$ the bubble effectiveness factor for zero inlet-quality; Ψ_o is expected to be a function of Re_f only. Further, when the turbulence in the main stream is low, for instance in pools or laminar forced convection, it is expected that $\Psi_o \simeq 1$. The simplest form of the Ψ_o function is found to be

$$\left.\begin{aligned} \Psi_o &= 1 && \text{for } Re_f \leqslant 2000 \\ \Psi_o &= 9.78\, Re_f^{-0.3} && \text{for } Re_f \geqslant 2000 \end{aligned}\right\} \qquad (6.16)$$

and is sketched below.

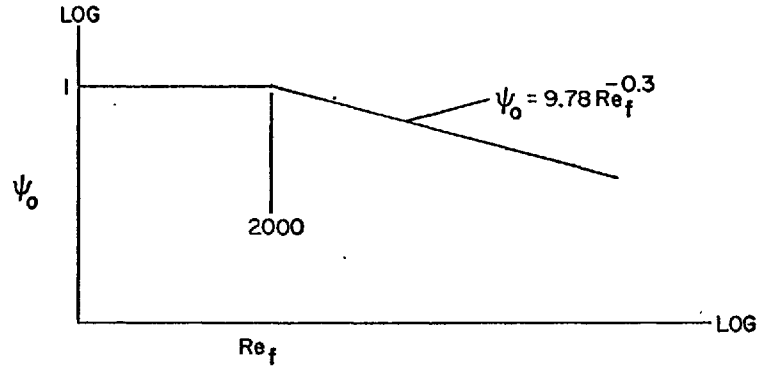

SKETCH OF Ψ_o VS. Re_f FOR PRESENT EXPERIMENTS

As might be expected, Ψ_o decreases in the turbulent flow region with increasing Re_f and hence turbulence.

The test of the Ψ_o function is its ability to collapse the

zero inlet-quality data. For $u_{g,i}/u_f = 0$, F = 1 and equation (6.9) becomes

$$\alpha_o = \alpha_{SP} + \Psi_o \alpha_{bub} \tag{6.17}$$

or

$$\alpha_{bub} = \frac{\alpha_o - \alpha_{SP}}{\Psi_o} \tag{6.18}$$

When values of $(\alpha_o - \alpha_{SP})/\Psi_o$ are plotted against $\dot{V}_g''$, they should fall approximately on a single curve. This curve would represent the α_{bub}-function for the given fluid properties and porous surface. This plot is shown in Fig. 6.17 where α_o and α_{SP} are measured values and Ψ_o is from equation (6.16). For simplicity, two straight lines have been drawn to represent the data. The ±15% limits are shown; three points fall outside these limits. The error in α_o (as opposed to $(\alpha_o - \alpha_{SP})/\Psi_o$) in these three points is 8%, 12% and 7 1/2% for points 1, 2 and 3 respectively. It is concluded that the collapse of the data is satisfactory.

Finite inlet-quality.

The function Ψ for finite inlet-quality is obtained by first defining a function Ψ^+ according to

$$\Psi = \Psi^+ \Psi_o \tag{6.19}$$

Then Ψ^+ is correlated in terms of Re_f and $u_{g,i}/u_f$ and is of the form such that, when $u_{g,i}/u_f = 0$

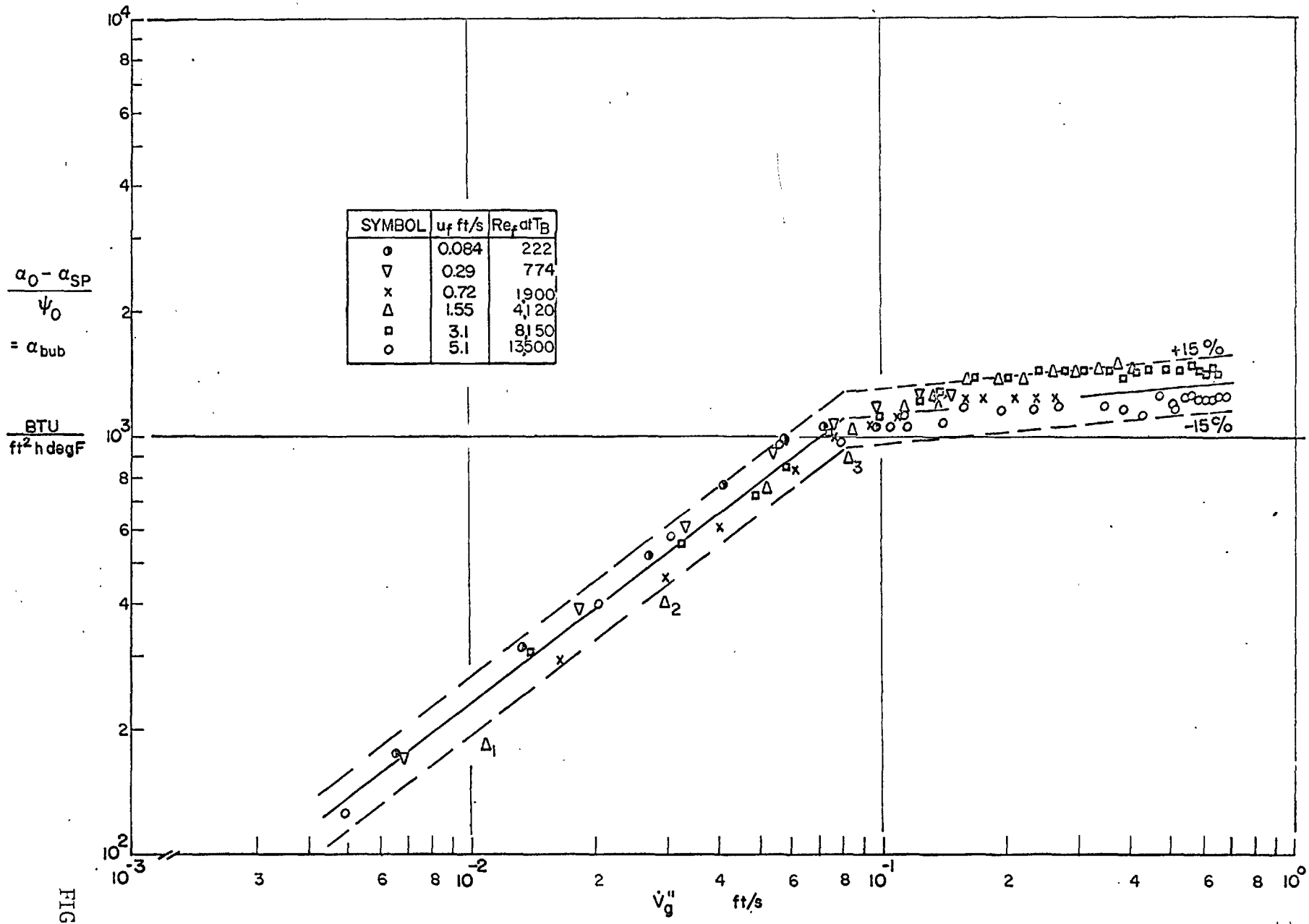

FIG. 6.17 COLLAPSED PRESENT ZERO-INLET-QUALITY DATA FOR $\dot{V}_g'' < \dot{V}_{g,\,cr}''$

$$\left.\begin{aligned} \Psi^+ &= 1 \\ \Psi &= \Psi_o \end{aligned}\right\} \qquad (6.20)$$

It was seen in Section 6.6.2 that $\alpha_{SP}\ F = \alpha_{TP}$; substitution of this relation and (6.19) into (6.9) yields

$$\alpha = \alpha_{TP} + \Psi^+ \Psi_o \alpha_{bub} \qquad (6.21)$$

Substitution of equation (6.18) into (6.21) and rearrangement results in

$$\Psi^+ = \frac{\alpha - \alpha_{TP}}{\alpha_o - \alpha_{SP}} \qquad (6.22)$$

A "measured" value of Ψ^+ may therefore be obtained from equation (6.22) for a given combination of u_f, $\dot{V}''_g$ and $u_{g,i}$ using:

α as measured for the given u_f, $\dot{V}''_g$ and $u_{g,i}$;

α_{TP} for the same u_f, $u_{g,i}$ and zero-barbotage results from the smoothed curves of Fig. 6.5;

α_o for the same $\dot{V}''_g$, u_f and zero-inlet quality (in each run in which $u_{g,i}$ was varied, the first datum point taken was for $u_{g,i} = 0$; this value was used here in equation (6.22));

α_{SP} as measured for the given u_f.

It is found that when the data are plotted in terms of Ψ^+ vs. $u_{g,i}/u_f$ on "semi-logarithmic" coordinates, there results essentially a straight line for each Re_f independent of barbotage-rate,

as sketched below.

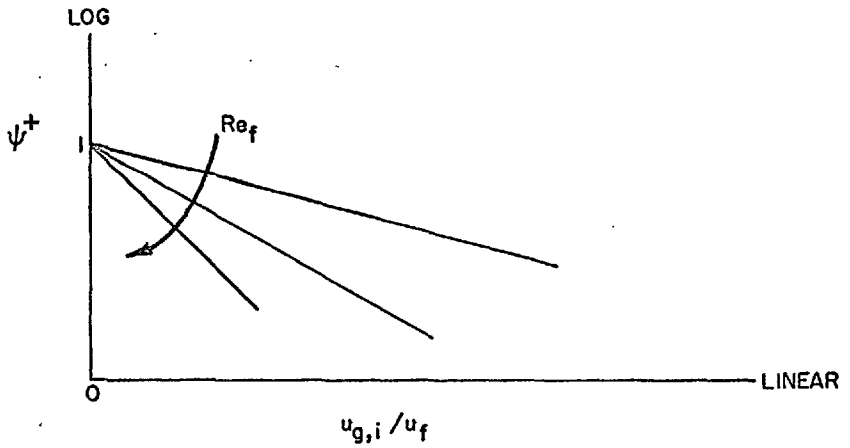

SKETCH OF Ψ^+ VS. $u_{g,i}/u_f$

Each line is described by

$$\psi^+ = e^{-j\, u_{g,i}/u_f} \tag{6.23}$$

A cross-plot of j vs. Re_f on logarithmic coordinates yields

$$j = \frac{0.68}{10^6}\, Re_f^{1.4} \tag{6.24}$$

The final relation for Ψ is therefore

$$\left.\begin{aligned} \Psi &= \psi^+ \Psi_o \\ \Psi_o &= 1 \qquad \text{for } Re_f \leqslant 2000 \\ \Psi_o &= 9.78\, Re_f^{-0.3} \qquad \text{for } Re_f \geqslant 2000 \\ \psi^+ &= e^{-\{\frac{0.68}{10^6}\, Re_f^{1.4}\, \frac{u_{g,i}}{u_f}\}} \end{aligned}\right\} \tag{6.25}$$

The function Ψ as described by equation (6.25) is always $\leqslant 1$ and decreases with increasing Re_f and $u_{g,i}/u_f$ (except $\Psi_o = 1$ for $Re_f \leqslant 2000$ and $u_{g,i}/u_f = 0$); Ψ has a lower limit of zero as either, or both, of Re_f and $u_{g,i}/u_f$ become very large. Physically this means that the bubble effectivenss factor Ψ decreases as Re_f and $u_{g,i}/u_f$ increase since increases in Re_f and $u_{g,i}/u_f$ should result in increased turbulence in the forced convective flow and hence a resulting decrease in the effectiveness of the bubble agitation process.

6.6.4 A Test of the F-, Ψ- and α_{bub}-Functions for Finite Barbotage and Finite Upstream-Quality Data

If equation (6.9) is used to predict heat-transfer coefficients α_{pred} it may be written

$$\alpha_{pred.} = \alpha_{SP} F + \Psi \alpha_{bub} \qquad (6.26)$$

For conditions of finite barbotage and finite inlet-quality, α_{pred} here is obtained using:

F from equation (6.11),

Ψ from equation (6.25),

α_{bub} from the solid lines in Fig. 6.17,

α_{SP} as measured.

The measured values of the heat-transfer coefficient α_{meas} are compared in Fig. 6.18 with α_{pred}. It is seen that the agreement

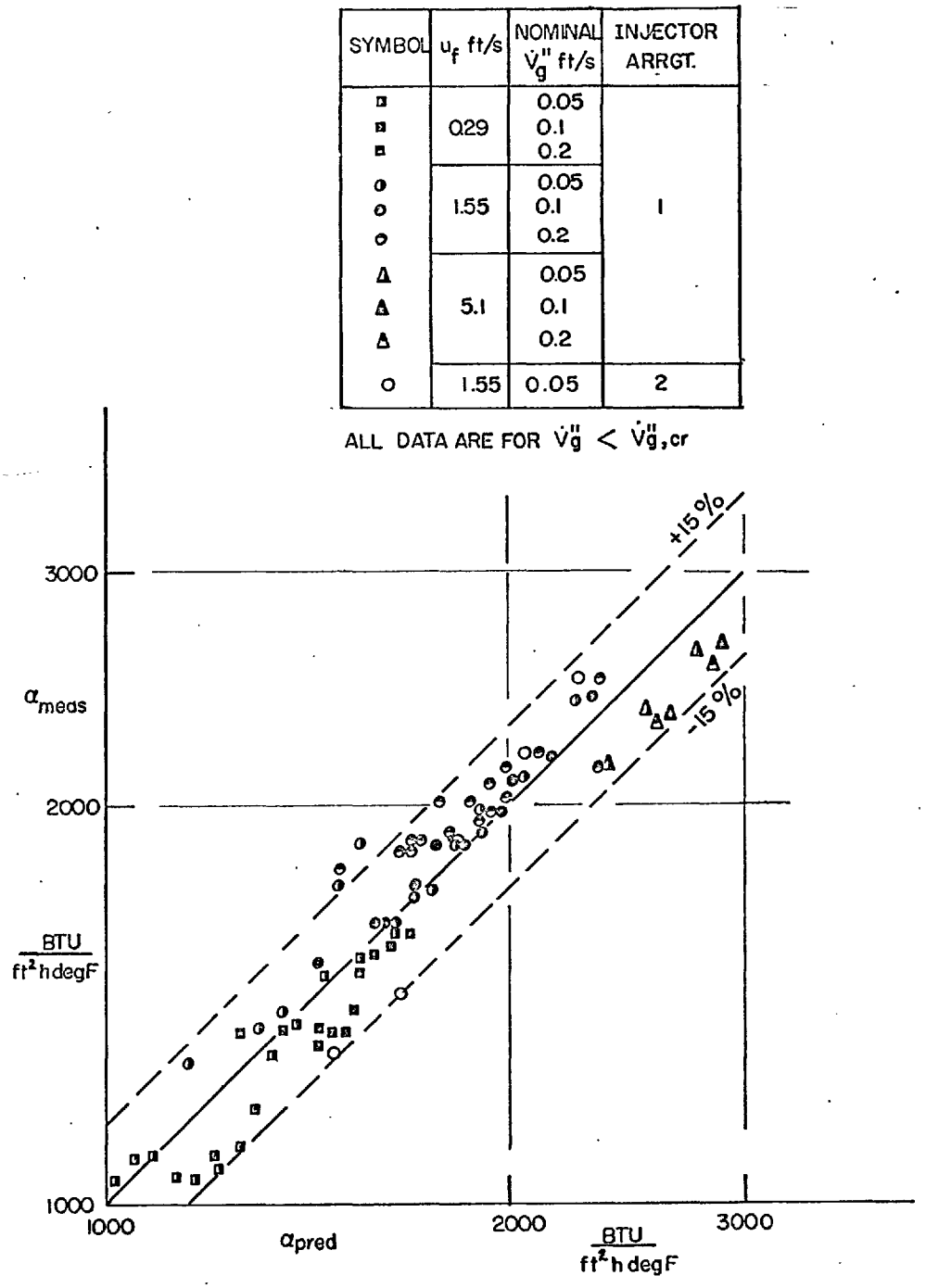

FIG. 6.18 TEST OF PRESENT CORRELATION FOR FINITE-INLET-QUALITY AND FINITE-BARBOTAGE RESULTS

is most satisfactory with only three data points lying outside the ±15% limits. It is understood that all the data shown are for $\dot{V}''_g < \dot{V}''_{g,cr}$.

6.7 A Comparison of Akturk's Pool Barbotage Results with the Present Forced Convection Results

The connection between pool barbotage and forced convection barbotage, Link 3 in Fig. 1.1, is now being discussed. Akturk [1], for pool barbotage, has taken a considerable number of data with air and water at the same wall and bulk temperatures as in the present forced convection investigation. Comparison between Akturk's and the present results are therefore of special interest in that there can be no question of fluid property differences in the two investigations. The comparison demonstrates the application of equation (6.9) to pool barbotage.

In pool barbotage, there is, of course, no "upstream air-injection", so making F = 1 in equation (6.9). Further, it is expected that the bubble effectiveness factor Ψ is approximately equal to 1 because the low levels of turbulence in a natural convection pool would not reduce the effectiveness of the barbotage-bubble agitation process. Equation (6.9) therefore becomes

$$\alpha = \alpha_{SP} + \alpha_{bub} \tag{6.27}$$

Experimental values of α_{bub} may be obtained from equation (6.27) using measured values of α and the appropriate free convection relation [60] for α_{SP}. The "band" of Akturk's results, representing the range of smoothed data for various geometrical arrangements, is shown in Fig. 6.19 together with the lines representing the present data. There is generally close agreement between Akturk's and the present results for $\dot{V}''_g > 0.04$ ft/s. The comparison does, however, involve somewhat different porous surfaces (details in Tables 2.4 and 3.1). Therefore, although not conclusive, the evidence suggests that pool barbotage may be treated as a special case of the more general situation embracing both pool and forced convection barbotage.

6.8 Dimensionless Form of the Bubbling Function α_{bub}

The α_{bub}-function is now presented in dimensionless form. The dimensionless groups involved are obtained by analogy with boiling experience.

In Chapter 2 the following equation was seen to satisfactorily correlate data for saturated nucleate pool boiling of water and organics at atmospheric pressure:

$$Nu^*_{tot} = \text{Const.}\ K_T^{0.6}\ Pr_f^{-0.2} \qquad (6.28)$$

formerly (2.49)

where:

$$K_T \equiv \frac{\dot{q}''_{tot}}{\rho_g h_{fg}} \quad \frac{\rho_f^{1/2}}{[\sigma g_o\ g(\rho_f - \rho_g)]^{1/4}} = Ku\sqrt{\frac{\rho_f}{\rho_g}} \qquad (6.29)$$

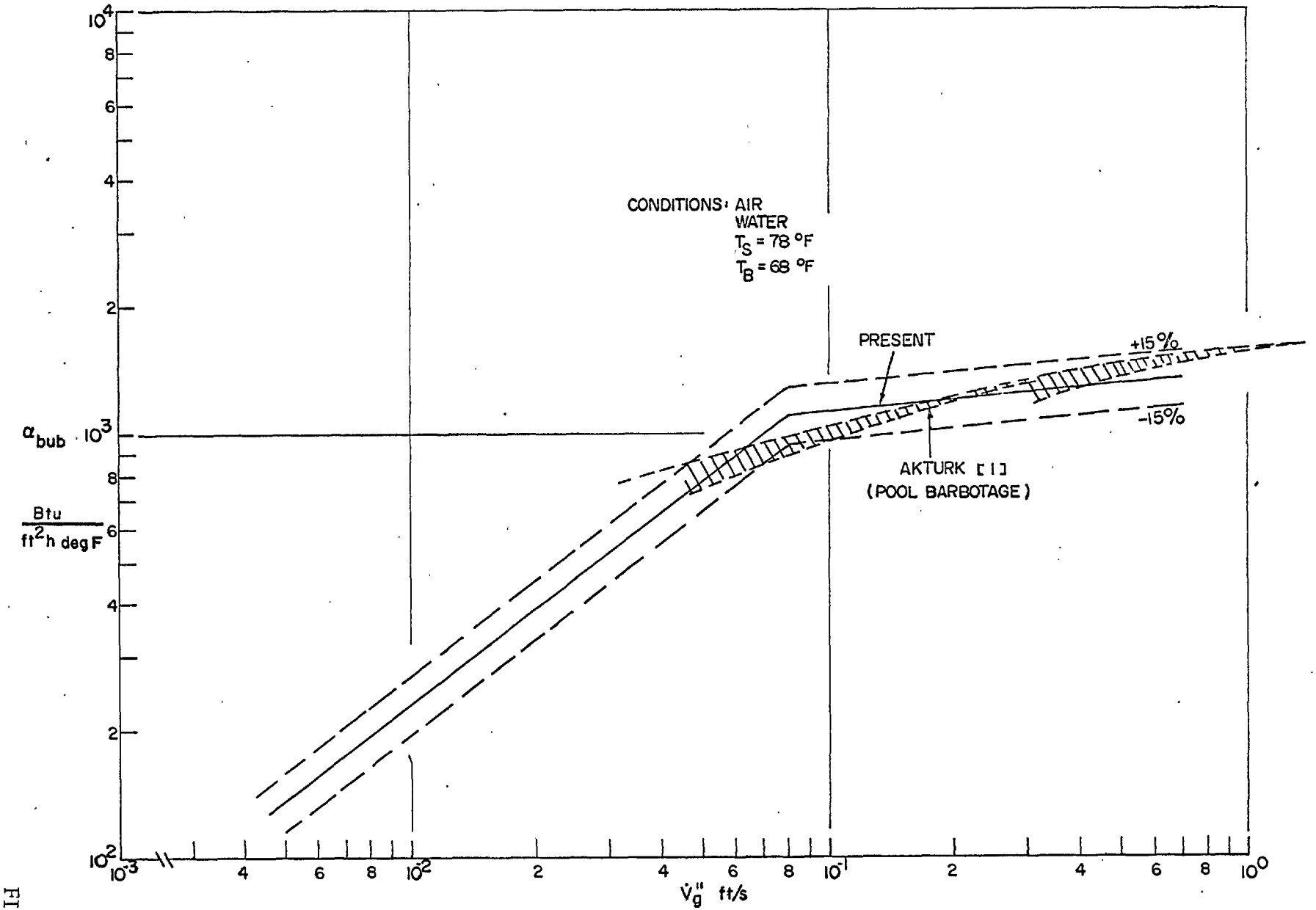

FIG. 6.19 COMPARISON OF AKTURK'S POOL BARBOTAGE DATA WITH THE PRESENT FORCED CONVECTION RESULTS

FIG. 6.19

Nu^*_{tot} was defined in equation (2.43).

Therefore, for boiling under the specified conditions

$$Nu^*_{tot} = \phi(K_T, Pr_f) \tag{6.30}$$

By analogy it might be expected that α_{bub} in barbotage, at least for the existing information which is all at atmospheric pressure, will be correlated by

$$Nu^*_{bub} = \phi(K_T^*, Pr_f) \tag{6.31}$$

where:

$$Nu^*_{bub} \equiv \frac{\alpha_{bub}}{k_f} \sqrt{\frac{\sigma g_o}{g(\rho_f - \rho_g)}} \tag{6.32}$$

$$K_T^* \equiv \frac{\dot{V}''_g \, \rho_f^{1/2}}{[\sigma g_o \, g(\rho_f - \rho_g)]^{1/4}} \tag{6.33}$$

This is indeed shown to be the case.

The pool-barbotage investigation of Gose, Acrivos and Petersen [27] provides the information necessary to determine the Prandtl number dependence in equation (6.31). It is assumed that

$$Nu^*_{bub} = Pr_f^n \, \phi(K_T^*)$$

The α_{bub} for use in Nu^*_{bub} is obtained from equation (6.27). A satisfactory value of n is found to be approximately -0.2, i.e. the

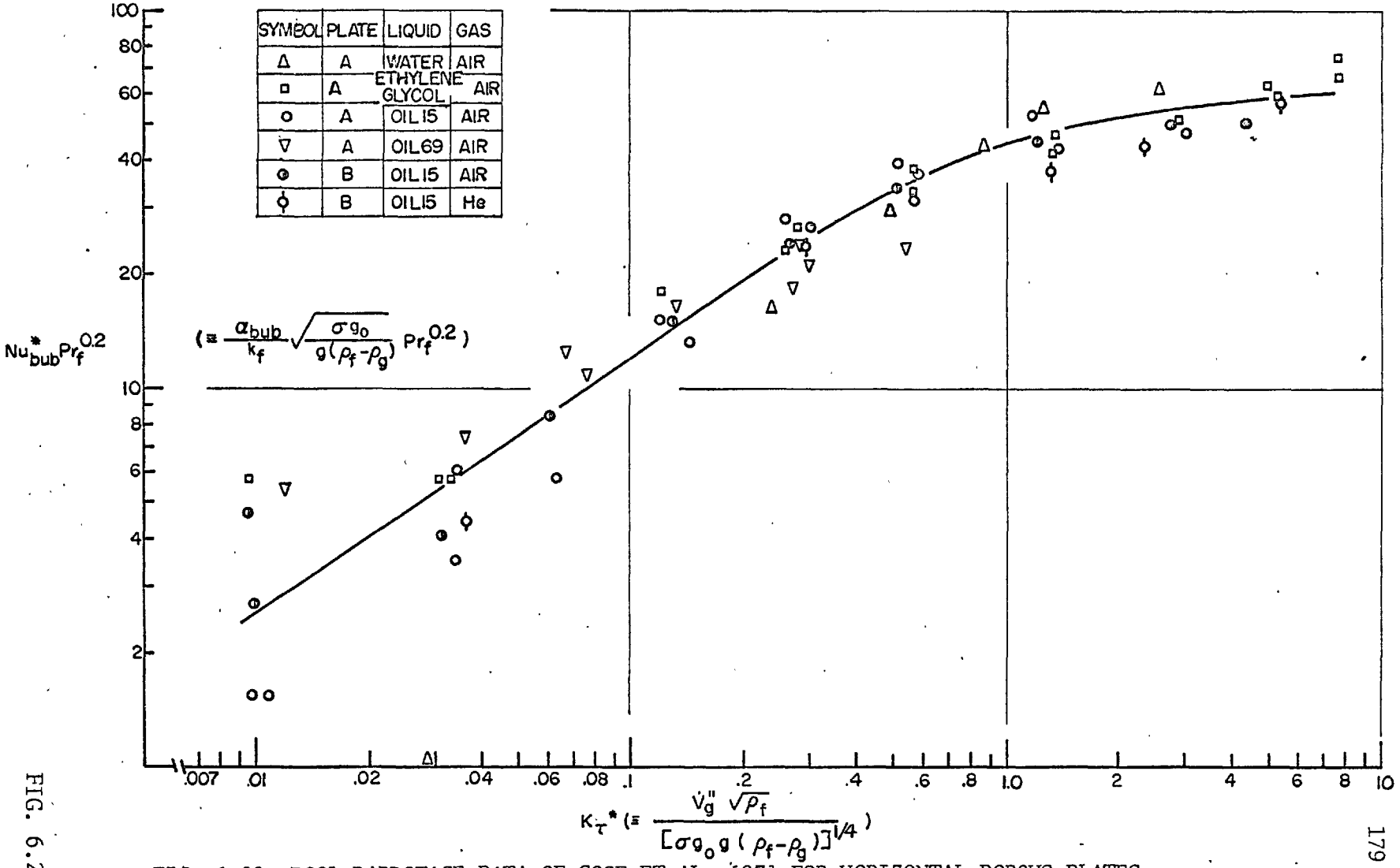

FIG. 6.20 POOL BARBOTAGE DATA OF GOSE ET AL. [27] FOR HORIZONTAL POROUS PLATES

Prandtl number dependence is the same as in boiling. The collapsed data of Gose et al. [27] are presented in Fig. 6.20 on coordinates of $Nu^*_{bub}\ Pr_f^{0.2}$ vs. K_T^*. Fluid properties were evaluated at the wall temperature. The scatter at $K_T^* < 0.08$ is due mainly to the error which results in α_{bub} when α and α_{SP} are of nearly equal magnitude ($\alpha_{bub} = \alpha - \alpha_{SP}$).

The solid lines drawn through the data in Fig. 6.17 represent α_{bub} for the present investigation; in dimensionless terms the equations of these lines are (with fluid properties evaluated at the wall temperature):

$$\left.\begin{aligned} Nu^*_{bub}\ Pr_f^{0.2} &= 167\ K_T^{*\,0.75} \quad \text{for } 0.009 \leqslant K_T^* \leqslant 0.15 \\ Nu^*_{bub}\ Pr_f^{0.2} &= 48.7\ K_T^{*\,0.1} \quad \text{for } 0.15 \leqslant K_T^* \leqslant 1.27 \end{aligned}\right\} \quad (6.34)$$

6.9 Application of the Present Correlating Procedure to Other Forced Convection Barbotage Investigations

The data of Gose, Petersen and Acrivos [28] and of Gose, Acrivos and Petersen [27] are amenable to analysis in the same manner as for the present results. In both investigations, vertical porous tubes (details in Table 1.1) were used with zero-inlet-quality conditions. Nitrogen-water in the earlier [28] and air-water and air-ethylene glycol in the later [27] investigations were used.

Results of Gose, Petersen and Acrivos [28] (identified below as Gose et al., 1957).

Analysis shows that the Ψ_o function found for the present results fits the results of Gose et al., 1957 very well indeed. The data are shown in dimensionless form in Fig. 6.21 where the α_{bub} used in Nu^*_{bub} was obtained from equation (6.18) with Ψ_o from equation (6.16). It is seen that the collapse of the data is satisfactory.

Results of Gose, Acrivos and Petersen [27] (identified below as Gose et al., 1960).

The Ψ_o function for the Gose et al., 1960 results is found to be

$$\left.\begin{aligned} \Psi_o &= 1 \qquad \text{for } Re_f \leqslant 2000 \\ \Psi_o &= 2.14\, Re_f^{-0.1} \qquad \text{for } Re_f \geqslant 2000 \end{aligned}\right\} \tag{6.35}$$

and is sketched in the corner of Fig. 6.22.

The trends are the same as for the present Ψ_o function, but for $Re_f > 2000$, the dependence of Ψ_o on Re_f is considerably weaker ($Re_f^{-0.1}$ for Gose et al., 1960, compared with $Re_f^{-0.3}$ for the present investigation). Indeed, on the basis of their measurements, Gose et al., 1960 concluded that the effect of barbotage on the heat transfer is "linearly additive" to the effect of forced convection.

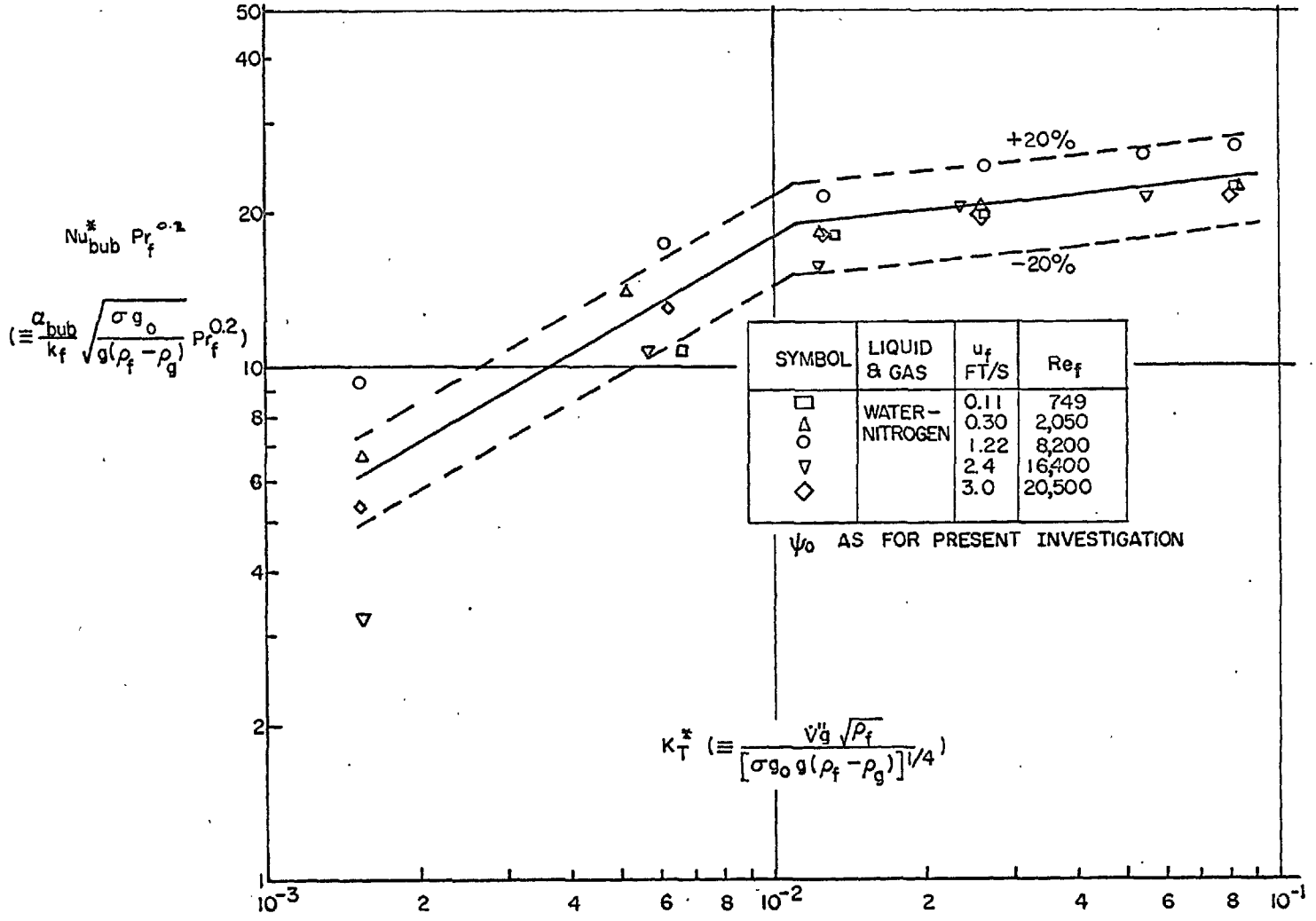

FIG. 6.21 FORCED CONVECTION BARBOTAGE RESULTS OF GOSE, PETERSEN AND ACRIVOS [28]

FIG. 6.21

This is the equivalent of having $\Psi_o = 1$ in equation (6.17). For the largest values of Re_f ($\simeq$50,000) used by these authors, from equation (6.35) $\Psi_o \simeq 0.73$, which to a first approximation does not differ markedly from 1 (so justifying their conclusion based on their own data). However, the results of the present investigation support the observation of Kudirka et al. [49] that the effect of barbotage on the heat transfer is "algebraically additive" to the effect of forced convection, that is Ψ_o, and more generally, Ψ are not necessarily equal to 1.

Values of α_{bub} were obtained from equation (6.18) with Ψ_o from equation (6.35); the results are plotted in dimensionless form in Fig. 6.22 where the correlation is seen to be satisfactory. It is pointed out that the ordinate of $Nu^*_{bub}\ Pr_f^{0.2}$, which correlates fluid property effects in pool-barbotage experiments, also correlates the fluid property effects in forced convection barbotage, at least as far as the existing data are concerned.

Comparison of Gose et al., 1957 and Gose et al., 1960 with the present results.

The results of the Gose et al., 1957, Gose et al., 1960 and present investigation are shown in Fig. 6.23. All investigations show the same trends, but discrepancies among them can be large. It was indicated [27] that the Gose et al., 1957, work was more in the nature of a preliminary investigation. The maximum discrepancy

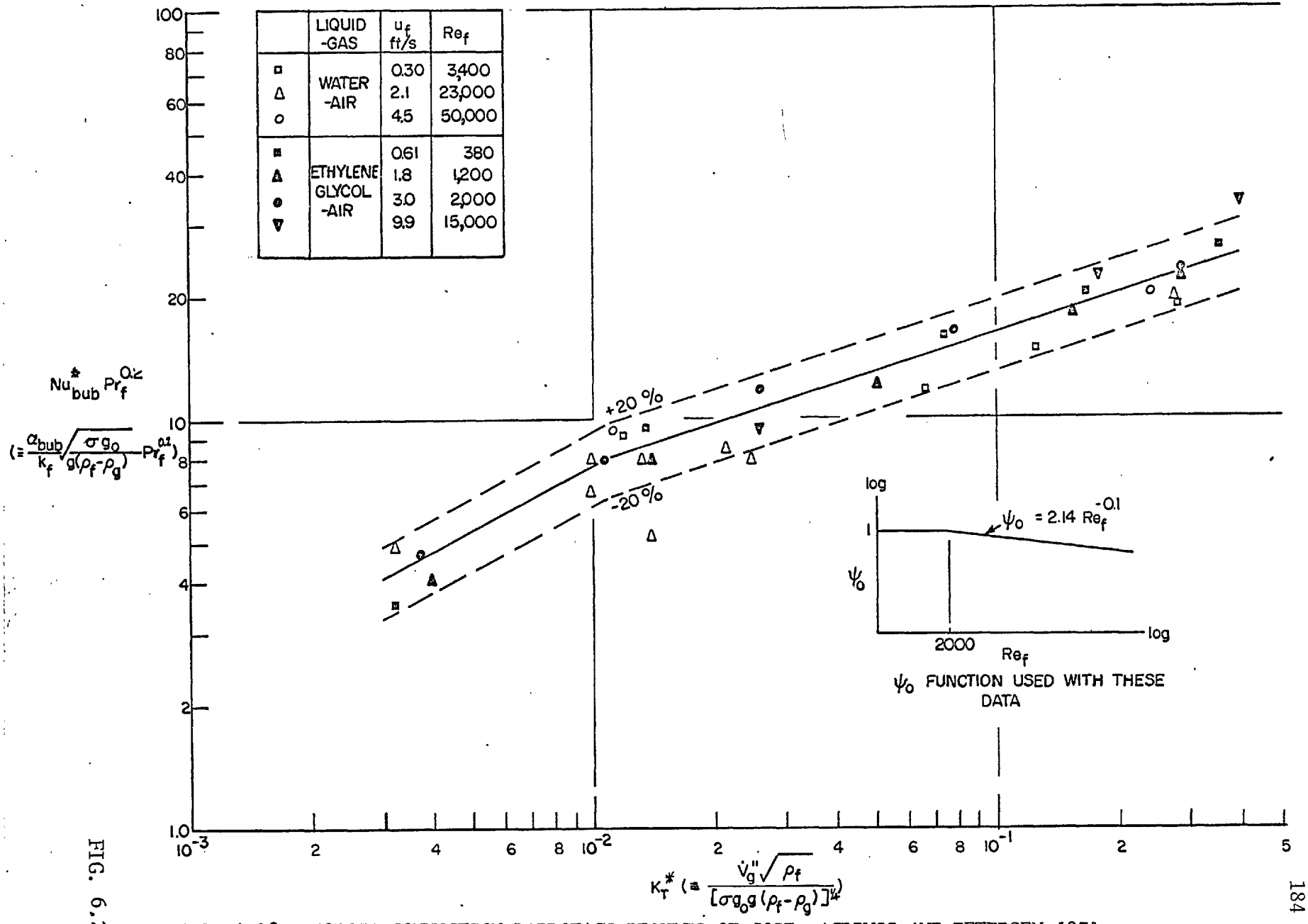

FIG. 6.22 FORCED CONVECTION BARBOTAGE RESULTS OF GOSE, ACRIVOS AND PETERSEN [27]

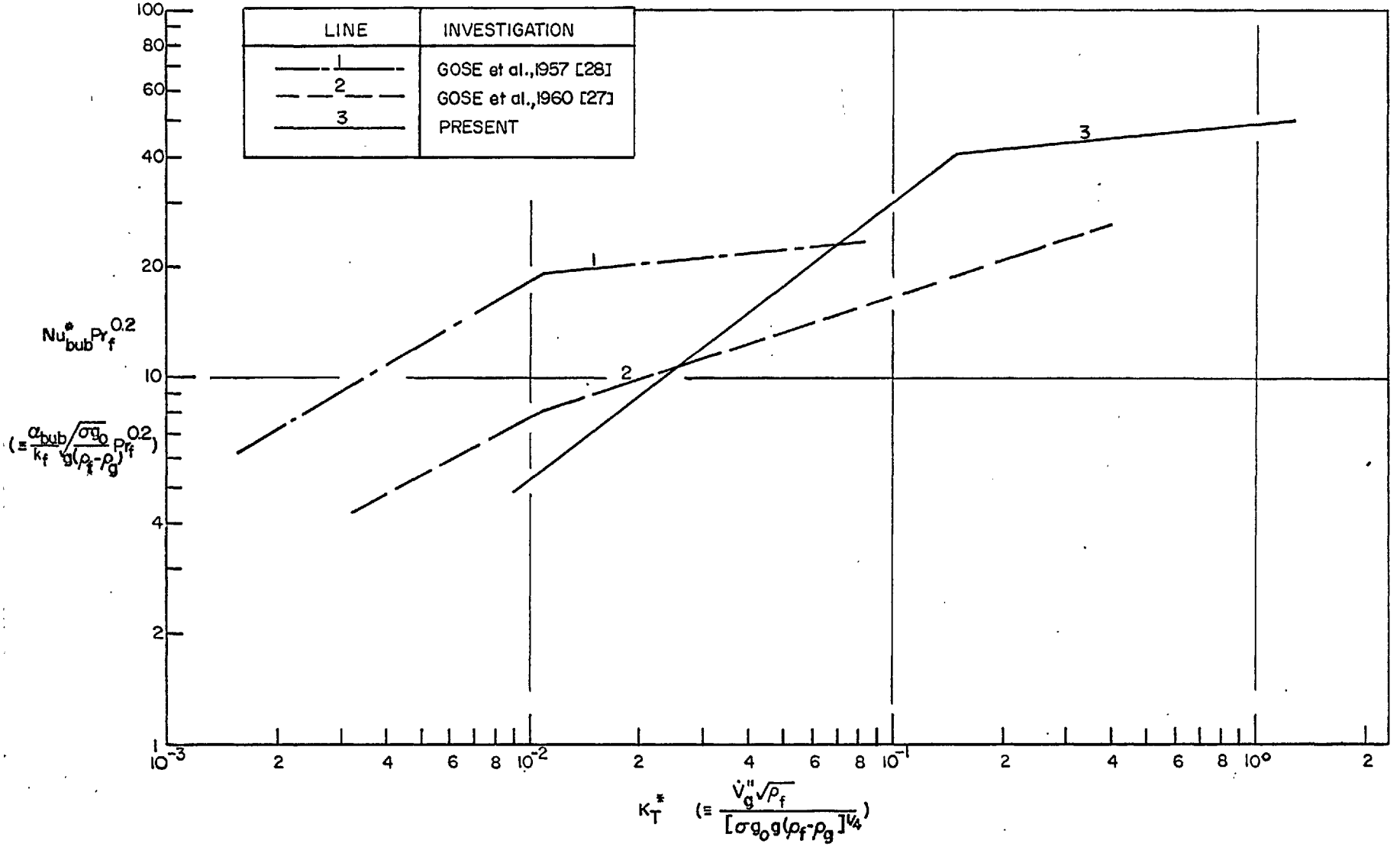

FIG. 6.23 COMPARISON OF EXPERIMENTAL DIMENSIONLESS α_{bub}-FUNCTION FOR FORCED CONVECTION BARBOTAGE INVESTIGATIONS

FIG. 6.23

between the present and the Gose et al., 1960, investigation occurs at $K_T^* \simeq 0.15$ with the latter lying some 50% below the former. (However, it should be borne in mind that α here is obtained from

$$\alpha = \alpha_{SP} + \Psi_o \alpha_{bub};$$

errors in α_{bub}, when multiplied by Ψ_o ($\ll 1$) and added to α_{SP}, produce smaller errors in α.) No doubt some of the discrepancies among the investigations are attributable to the use of different porous surfaces [27]; details as reported by the investigators are given in Table 1.1 and 3.1.

Results of Kudirka, Grosh and McFadden.

Kudirka, Grosh and McFadden [49] have reported local values of the heat-transfer coefficient at one position ($x/d \simeq 14$) in a vertical porous tube (details in Table 1.1); air-water and air-ethylene glycol were the gas-liquid combinations. The data of Kudirka et al. cannot be analyzed to give Ψ- and α_{bub}-functions. However the present functions may be used to predict the heat-transfer coefficient α_{pred} under their experimental conditions.

Equation (6.9), with $\alpha_{SP} F = \alpha_{TP}$, may be written as

$$\alpha_{pred} = \alpha_{TP} + \Psi \alpha_{bub} \qquad (6.36)$$

In equation (6.36), Ψ from equation (6.25) is used, except that

local values of the velocity ratio $u_{g,x}/u_f$ at x/d ≈ 14 are used in place of the inlet values $u_{g,i}/u_f$ (the local gas velocity $u_{g,x}$ along the tube varies with distance x). Values of α_{bub} are obtained from Line 3 in Fig. 6.23 (i.e. as for the present experiment). Values of α_{TP} are those measured by Kudirka et al. The ratio $\alpha_{meas}/\alpha_{pred}$, where α_{meas} is the measured value of the heat-transfer coefficient, is plotted in Fig. 6.24* for $\dot{V}''_g < \dot{V}''_{g,cr}$ ($\dot{V}''_{g,cr}$ here is the value of $\dot{V}''_g$ at which a maximum occurs in a plot of α vs. $\dot{V}''_g$ for constant local gas velocity $u_{g,x}$ in the tube at x/d ≈ 14). It is seen that the ratio $\alpha_{meas}/\alpha_{pred}$ lies within +15% and -35% of the value of 1.0, which is surprisingly good. The existing discrepancies between the measured and predicted values of the heat-transfer coefficient may be attributed to the use of different porous surfaces, different geometries and the fact that the predicting equations were based on average heat-transfer coefficients while the measured heat-transfer coefficients of Kudirka et al. [49] were local values at one x/d position.

6.10 Comparison of the Bubbling Function in Forced Convection Barbotage and Pool Boiling

In Chapter 2, comparisons were made between heat-transfer coefficients in pool barbotage and saturated nucleate pool boiling.

---

*Additional data were taken from Fig. 28 of the original document [48].

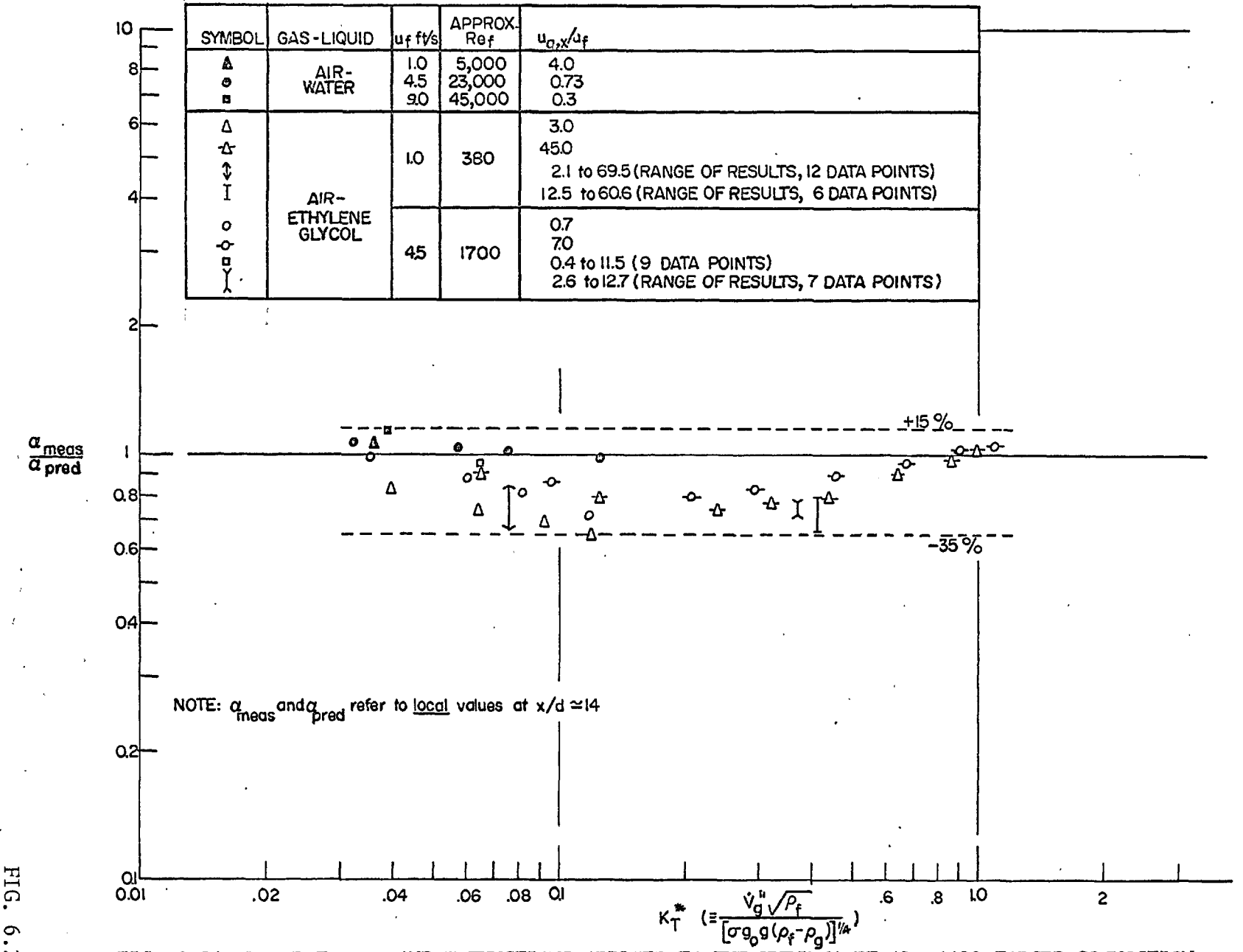

FIG. 6.24 PRESENT α_{bub}-AND Ψ-FUNCTIONS APPLIED TO THE KUDIRKA ET AL. [49] FORCED CONVECTION BARBOTAGE DATA

In performing this comparison it was necessary to know the latent heat fraction γ_D. For the case of forced convection saturated nucleate boiling there is at present no information from which to deduce γ_D. This means that neither the vapour formation rate of bubbles on the heating surface nor the heat-transfer-coefficient-through-the-liquid α_f (see Sections 2.3.1 and 2.3.2) are known. It is therefore impossible to compare directly the heat-transfer coefficients in forced convection barbotage and forced convection saturated nucleate boiling.

However, there is a possible comparison between forced convection barbotage and pool boiling (Link 5 in Fig. 1.1). The basis of the comparison is $\alpha_{bub,f}$ the maximum heat-transfer-coefficient-through-the-liquid due to agitation of the bubbles forming at the heating surface for fixed $\dot{V}''_g$ ($\dot{V}''_{g,D}$ in boiling) and fluid properties. The comparison is between the dimensionless $\alpha_{bub,f}$ in saturated nucleate pool boiling and that obtained in the two Gose et al. [27,28] and the present forced convection barbotage investigations.

Equation (6.9), with $F = 1$ and $\Psi = 1$ (for reasons analogous to those given in Section 6.7 for pool barbotage), may be applied to heat-transfer-coefficients-through-the-liquid α_f in pool boiling with the following result:

$$\alpha_f = \alpha_{SP} + \alpha_{bub,f} \tag{6.37}$$

where α_{SP} is the heat-transfer coefficient due to natural convection. Now, at least at all but the smallest bubbling rates, natural convection heat transfer should be small compared with heat transfer through the liquid due to bubble agitation. Therefore

$$\alpha_f \simeq \alpha_{bub,f} \tag{6.38}$$

In barbotage, the symbol α_{bub} used so far, has the same meaning as $\alpha_{bub,f}$, i.e.

$$\alpha_{bub} = \alpha_{bub,f} \tag{6.39}$$

A dimensionless group, analogous to Nu^*_f of Chapter 2, is defined as

$$Nu^*_{bub,f} \equiv \frac{\alpha_{bub,f}}{k_f} \sqrt{\frac{\sigma g_o}{g(\rho_f - \rho_g)}} \tag{6.40}$$

Proceeding in a manner analogous to that of Case 2 Chapter 2, there results Fig. 6.25 in which the dimensionless $\alpha_{bub,f}$ for pool boiling and the forced convection barbotage experiments is presented. It is noted that there is reasonable agreement between the boiling and barbotage results particularily with Gose et al., 1957, for $Ku^* > 3 \times 10^{-4}$ and with the present data for $Ku^* > 2 \times 10^{-3}$.

The comparison was based on the assumption that equation (6.9) could be applied to pool boiling heat-transfer-coefficients-

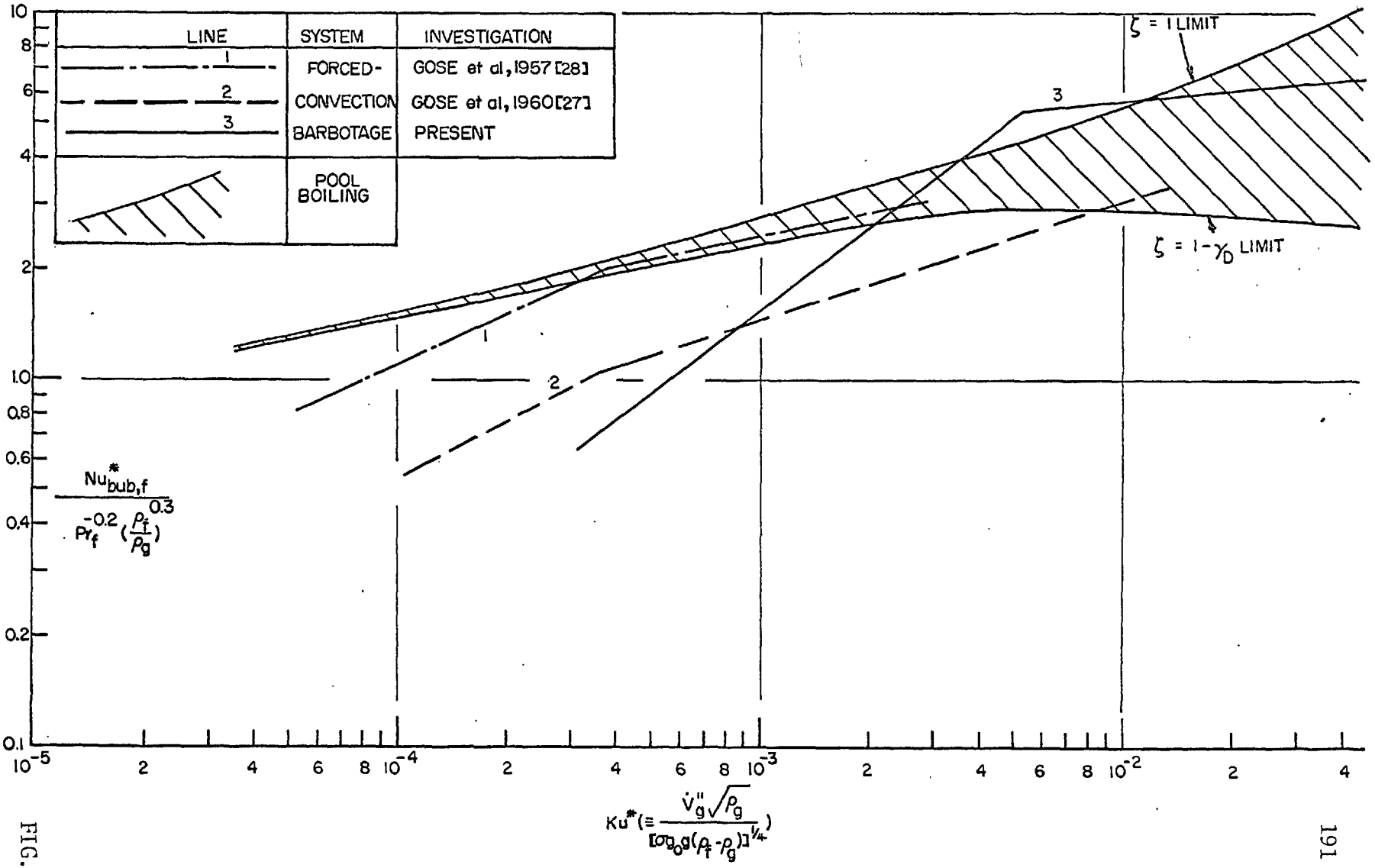

FIG. 6.25 COMPARISON OF DIMENSIONLESS $\alpha_{bub,f}$ IN BOILING AND BARBOTAGE

through-the-liquid; this equation has already been applied to pool barbotage (Sections 6.7 and 6.8). The favorable comparisons which result (Section 6.7 and the present section) suggest that equation (6.9), together with the necessary latent heat information, may serve as a basis for tying together results for boiling and barbotage, pools and forced convection systems.

6.11 A Tentative Expression for the Critical Barbotage-Rate $\dot{V}''_{g,cr}$

A crude correlation of the critical barbotage-rate observed in the present experiments is given in this section. It is stressed that the relation obtained and the ideas presented here are tentative since there are few data on $\dot{V}''_{g,cr}$ with which to work. The correlating expression has been found empirically and kept as simple as possible, the main object being to illustrate the trends.

It was shown in Section 6.5.2 that the occurrence of the critical barbotage rate $\dot{V}''_{g,cr}$ is not restricted to appearing in any particular flow pattern, nor at any particular flow pattern boundary. Therefore $\dot{V}''_{g,cr}$ is analyzed without regard to flow pattern. The postulate implied [1,80] in pool barbotage heat transfer, that the occurrence of $\dot{V}''_{g,cr}$ is caused by some hydrodynamic crisis similar to that occurring in boiling at the critical heat flux, is tentatively extended here to forced convection barbotage. Therefore the dimensionless groups used by Kutateladze [53] to correlate the critical heat flux

in forced convection boiling are used here; the relevant groups are:

$$Ku^*_{cr} = \phi(Fr^*, u_{g,i}/u_f) \tag{6.41}$$

where:

Fr^* is a special form of Froude number defined by

$$Fr^* \equiv u_f \left[\frac{\rho_f - \rho_g}{\sigma g_o\, g}\right]^{1/4} \tag{6.42}$$

Ku^*_{cr} is, as before, a modified form of the critical Kutateladze number defined by

$$Ku^*_{cr} \equiv \frac{\dot{V}''_{g,cr}(\rho_g)^{1/2}}{[\sigma g_o\, g(\rho_f - \rho_g)]^{1/4}} \quad \text{formerly (2.37)} \tag{6.43}$$

Because it is difficult to ascribe a precise value to $\dot{V}''_{g,cr}$ (Figs. 6.2 and 6.3 for $u_{g,i}/u_f = 0$ and Fig. 6.12 for finite $u_{g,i}/u_f$), and hence to Ku^*_{cr}, each datum point for Ku^*_{cr} is shown as a closed symbol with a vertical line extending from it; the closed symbol represents the "most likely" value while the vertical line covers the approximate range over which Ku^*_{cr} could be chosen.

Zero inlet-quality tests.

The symbol $(Ku^*_{cr})_o$ represents the value of Ku^*_{cr} when $u_{g,i}/u_f = 0$; the values of $(Ku^*_{cr})_o$ for the zero inlet-quality tests

are shown in Fig. 6.26. A line of slope 1/2 is drawn through the data, the equation of the line being

$$(Ku^*_{cr})_o = 0.0145\ Fr^{*\,1/2} \tag{6.44}$$

The value of $(Ku^*_{cr})_o$ for $Fr^* = 5.73$ ($u_f = 3.1$ ft/s) is vague and a broken vertical line only is shown in Fig. 6.26 to indicate this. At the highest liquid velocity $Fr^* = 9.45$ ($u_f = 5.1$ ft/s) and $u_{g,i}/u_f = 0$, sufficiently high values of $\dot{V}''_g$ were not possible to achieve $\dot{V}''_{g,cr}$.

Finite-inlet-quality tests.

For finite $u_{g,i}/u_f$, $\dot{V}''_{g,cr}$ was obtained from Fig. 6.12. The following simple relation was fitted to the data:

$$\frac{Ku^*_{cr}}{(Ku^*_{cr})_o} = 1 - B\,\frac{u_{g,i}}{u_f} \tag{6.45}$$

$$B = 0.003\ Fr^* + 0.0015\ Fr^{*\,3} \tag{6.46}$$

A plot of $Ku^*_{cr}/(Ku^*_{cr})_o$ vs. $u_{g,i}/u_f$ is shown in Fig. 6.27; in this plot $(Ku^*_{cr})_o$ was calculated from equation (6.44). Equation (6.45) is of course only valid for $Ku^*_{cr}/(Ku^*_{cr})_o > 0$.

In Fig. 6.27, for each of the two higher values of Fr^*, there is a datum point at $Ku^*_{cr}/(Ku^*_{cr})_o = 0$, i.e. at $Ku^*_{cr} = 0$;

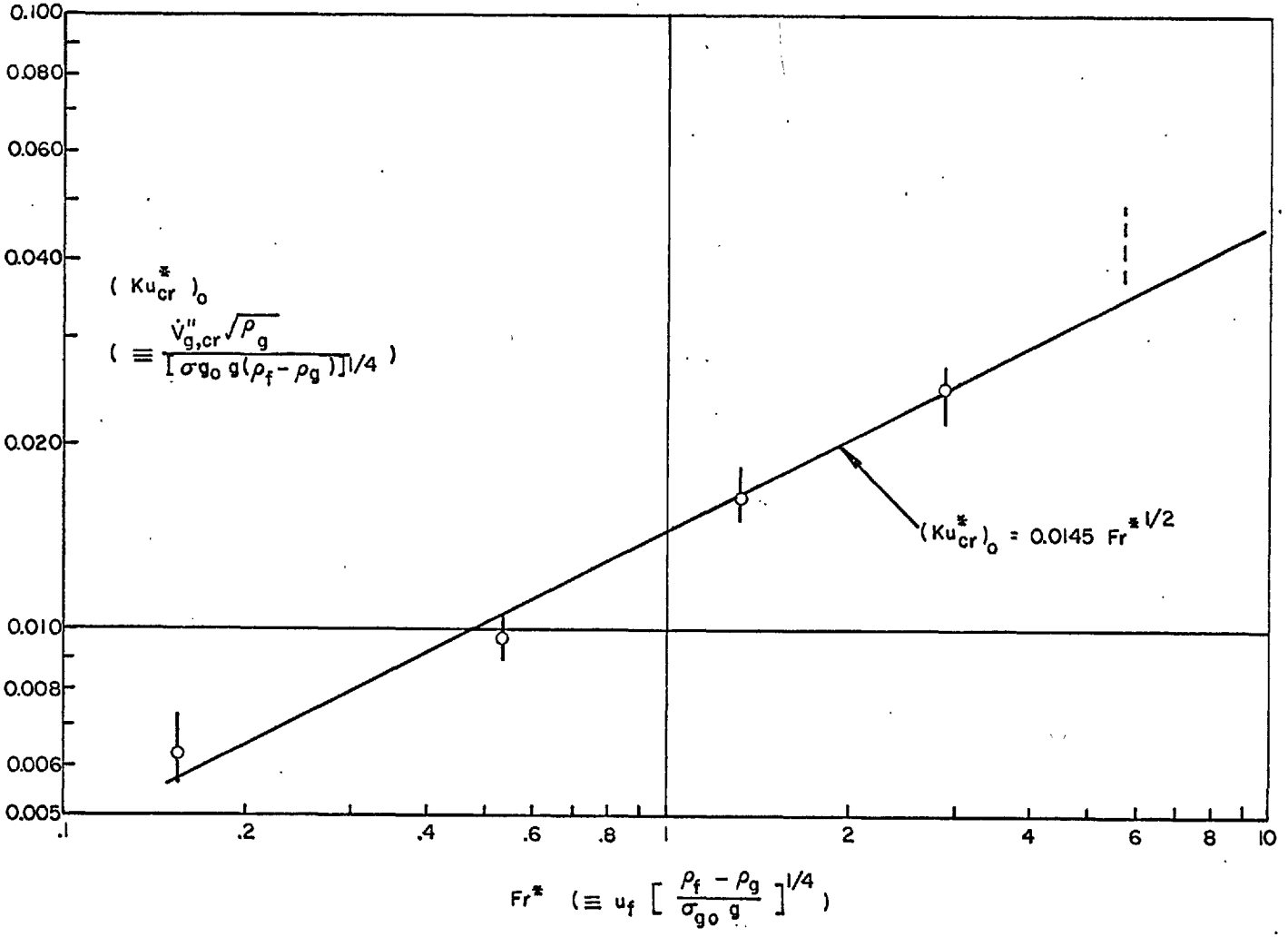

FIG. 6.26 CRITICAL KUTATELADZE NUMBER FOR ZERO-INLET-QUALITY TESTS

FIG. 6.26

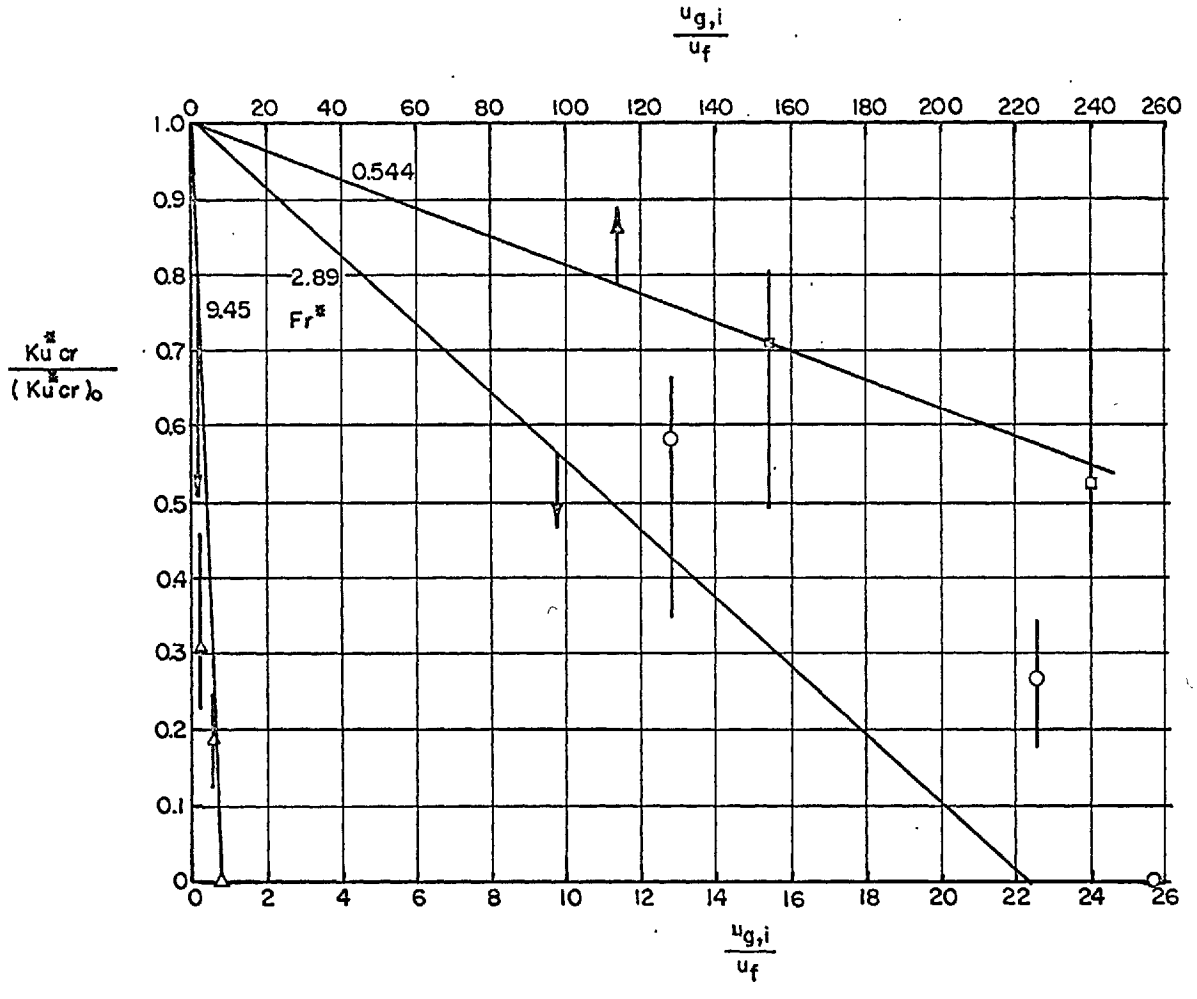

NOTES

1. $(Ku^*_{cr})_o$ IS THE VALUE OF Ku^*_{cr} when $u_{g,i}/u_f = 0$ & IS CALCULATED FROM EQN. (6.44)
2. SOLID LINES ARE EQN. (6.45)
3. $Ku^*_{cr} \equiv \dfrac{\dot{v}''_{g,cr}\sqrt{\rho_g}}{[\sigma g_o g(\rho_f - \rho_g)]^{1/4}}$

$$Fr^* \equiv u_f \left[\frac{\rho_f - \rho_g}{\sigma g_o g}\right]^{1/4}$$

FIG. 6.27 CRITICAL KUTATELADZE NUMBER FOR FINITE-INLET-QUALITY TESTS

FIG. 6.27

this point corresponds to a "transition inlet gas velocity" $(u_{g,i})_{tr}$ and a "transition inlet gas velocity ratio" $(u_{g,i}/u_f)_{tr}$ beyond which any finite barbotage-rate $\dot{V}_g''$ causes a reduction in the heat-transfer coefficient. Obviously, for a fixed Fr^*, there can be no Ku^*_{cr} for $u_{g,i}/u_f > (u_{g,i}/u_f)_{tr}$. The values of $(u_{g,i})_{tr}$ as obtained from Figs. 6.7 and 6.10 and $(u_{g,i}/u_f)_{tr}$ are listed below.

u_f ft/s	Fr^*	Possible Minimum		Most Likely		Possible Maximum	
		$(u_{g,i})_{tr}$ ft/s	$(\frac{u_{g,i}}{u_f})_{tr}$	$(u_{g,i})_{tr}$ ft/s	$(\frac{u_{g,i}}{u_f})_{tr}$	$(u_{g,i})_{tr}$ ft/s	$(\frac{u_{g,i}}{u_f})_{tr}$
1.55	2.89	38	24.4	40	25.7	42	27.0
5.1	9.45	3.6	0.71	4.0	0.79	4.2	0.83

Remarks.

It is interesting to compare the trends in the present Ku^*_{cr} with those obtained in forced convection boiling. Two conditions of similar trends are noted. (The present discussion of course concerns only the critical heat flux due to hydrodynamic crisis and not the "dry out" heat flux.)

(i) In boiling, Kutateladze [53] obtained

$$(Ku_{cr})_o = \text{Const. } Fr^{*\,1/2} \qquad (6.47)$$

where:

$$\left.\begin{aligned} \text{Const.} &= 0.023 \text{ for tubes,} \\ \text{Const.} &= 0.085 \text{ for wide annuli,} \end{aligned}\right\} \quad (6.48)$$

as before,

$$Ku_{cr} \equiv \frac{\dot{q}''_{tot,cr}}{h_{fg}\,\rho_g} \frac{\rho_g^{1/2}}{[\sigma g_o\, g(\rho_f - \rho_g)]^{1/4}} \quad (6.49)$$

formerly (2.25)

and the bracket with the subscript "o" around Ku_{cr} for boiling indicates that the local quality is zero.

If all of the heat flux is converted to vapour near the heating surface ($\dot{q}''_{tot,cr}/h_{fg}\,\rho_g = \dot{V}''_{g,cr}$)†, then Ku_{cr} (equation 6.49) becomes synonymous with Ku^*_{cr} (equation 6.43) in which case $(Ku_{cr})_o$ in equation (6.47) may be replaced by $(Ku^*_{cr})_o$. From equations (6.44) and (6.47) it is therefore seen that in both the present barbotage experiment and in boiling $(Ku^*_{cr})_o$ is proportional to $Fr^{*\,1/2}$. The value of the proportionality constant in the present barbotage experiment is approximately 2/3 of that for boiling in tubes.

It is noted that the effect of geometry on the critical heat flux in boiling is dramatic; this is illustrated by the

---

†It would be futile to attempt a discussion on the vapour formation rate in saturated forced convection boiling as there is no information available.

different values of the constant for tubes and annuli in equation (6.47); by analogy it is expected that $\dot{V}''_{g,cr}$ in barbotage would be markedly affected by geometry.

(ii) In boiling, for a fixed mass flow rate, Ku_{cr} decreases with increasing vapour content of the stream; similarily for barbotage Ku^{*}_{cr} decreases with increasing gas content $u_{g,i}/u_f$.

The only other forced convection barbotage investigation to provide any data on $\dot{V}''_{g,cr}$ is that of Kudirka et al. [49] with a vertical porous tube (see Fig. 5 of Ref. 49). Because of the few data (two points) and the differences expected in $\dot{V}''_{g,cr}$ due to the different geometry, no comparisons with the present data are made here.

6.12 Future Work

There are a number of areas connected with the present investigation where profitable future work could be pursued. These are discussed briefly below.

In Chapter 2 a "heat-transfer-coefficient through-the-liquid" α_f was defined according to equation (2.10) and used as the basis of heat-transfer comparisons in pool barbotage and saturated nucleate pool boiling. It was necessary to work with two limiting values of α_f in boiling because of the absence of information on the function $\dot{q}''_f \sim T$ where $\dot{q}''_f$ is the heat transfer through the liquid defined in equation (2.6) and T is the temperature.

Considerable thought should be given to devising a method of measuring $\dot{q}''_f \sim T$ in order that more precise values of α_f in boiling may be obtained.

Further, in connection with these comparisons, it was seen that the information available on vapour formation rate and latent heat transport in saturated nucleate pool boiling is very limited. More information is necessary particularly on the effect of fluid properties. Also of considerable interest, though, are the effects of surface roughness and geometry.

In forced convection saturated nucleate boiling no information on vapour formation rates and latent heat transport is known to the author. This information is necessary if it is desired to make heat-transfer comparisons between this type of boiling and forced convection barbotage.

For the upstream turbulence factor F, appearing in the barbotage correlating equation (6.9), there was insufficient evidence to determine the effect of fluid properties. The function F was determined from tests with zero barbotage and finite inlet-quality. In this connection, future investigators could use impermeable-walled ducts and find the effect on the heat-transfer coefficient, not only of fluid properties, but also of geometry, surface roughness, orientation of the heating surface and the method of mixing the two phases (such an investigation would be rather formidable). For

this type of heat transfer (zero barbotage, finite inlet-quality) each flow pattern should be analyzed individually with the object of reducing the empiricism involved in correlating the heat transfer.

For the fluids tested so far in barbotage, the effect of fluid properties on the bubbling function α_{bub} appears to be adequately accounted for (Fig. 6.20 and 6.22). However, particularly in forced convection barbotage, it would be advantageous to perform further tests with other fluids. These tests would give additional information on the bubble effectiveness factor Ψ as well. Further, the effect of the properties of the porous surface in forced convection barbotage should be investigated; Gose et al.[27] have made an admirable beginning with pool barbotage.

Also, precisely the same porous surface should be used in pool and forced convection barbotage experiments (analogous to the tests of Bergles and Rohsenow [8,9] in boiling) in order to verify conclusively, or disprove, the acceptability of equation (6.9), in the form of equation (6.27), for pool barbotage.

The phenomenon of the critical barbotage-rate has barely been touched upon. An extensive investigation of this phenomenon, finding the effects of fluid properties, liquid and gas velocities in the channel and geometry, would be in order. Studies in this area should assist in the understanding of the critical heat flux (that due to a hydrodynamic crisis) in forced convection boiling.

CHAPTER 7 SUMMARY AND CONCLUSIONS

The work reported here and the conclusions drawn may be summarized as follows.

1. A method was presented for quantitatively comparing the heat-transfer coefficients in saturated nucleate pool boiling and pool barbotage.

(a) These two phenomena were examined with the main differences emerging as: (i) the vapour velocity and (ii) the heat flux through the liquid in boiling are functions of the distance y from the heating surface while for barbotage these quantities are uniform with respect to y.

(b) For the purpose of comparison a "heat-transfer-coefficient-through-the-liquid" α_f was defined which accounts for the same heat-transfer mechanisms in barbotage and boiling. Further, from data appearing in the literature an estimate was made of the vapour formation rate in boiling; this information in turn was used in the comparisons.

(c) The dimensionless α_f in saturated nucleate pool boiling and pool barbotage are closely comparable in magnitude.

2. Heat-transfer coefficients and flow patterns were reported for a wide range of conditions in the forced convective flow of water and air-water mixtures in a horizontal rectangular duct with air injection through one porous heated wall.

3. In curves of heat-transfer coefficient α vs. the barbotage-rate $\dot{V}''_g$ there are two types (with a smooth transition between them) of behaviour of α depending on the inlet-quality and the water velocity. In one type, α decreases monotonically with $\dot{V}''_g$ for all finite barbotage-rates while in the other type α increases with $\dot{V}''_g$, passes through a maximum at the "critical" barbotage-rate $\dot{V}''_{g,cr}$ and then decreases with increasing $\dot{V}''_g$ (see Fig. 6.12).

The conditions for which the heat-transfer coefficients increased with $\dot{V}''_g$ were of greatest interest here (analogous in boiling to the increase in the heat-transfer coefficient with increasing vapour formation rate, i.e. with heat flux). For these conditions, the heat-transfer coefficients were correlated using the concept (analogous to Chen's proposal for forced convection saturated boiling) that the heat-transfer coefficient was comprised of two contributions, one associated with the forced convective flow and one associated with the barbotage-bubbling. The correlating equation is (6.9). The "upstream turbulence factor" F, the "bubbling function" α_{bub} and the "bubble effectiveness factor" Ψ appearing in (6.9) were found empirically; the equations describing these are summarized in Section 6.6.1.

4. For the case of zero barbotage and increasing inlet-quality, the behaviour of the heat-transfer coefficient depends on the flow pattern. Of particular note was that with increasing inlet-quality

stratified froth flow gave steeply rising heat-transfer coefficients α_{TP}; with the onset of slug flow from stratified froth flow α_{TP} began to decrease, exhibited a minimum and then increased again as slug flow fully developed and progressed into annular flow. Further, where at the same gas and liquid flow rates, different flow patterns can exist due to different upstream air-injector arrangements, it is in general necessary to specify the flow pattern in order to determine the heat-transfer coefficient (see Fig. 6.5, water velocity u_f of 1.55 ft/s, $u_{g,i} < 5$ ft/s).

5. It was not possible to compare the heat-transfer coefficients in forced convection barbotage and forced convection saturated nucleate boiling in the same manner as that performed in Chapter 2 for pool systems. This is because information on the bubble formation rate and latent heat transport in forced convection nucleate boiling does not exist. However, a comparison between the dimensionless $\alpha_{bub,f}$, the maximum heat-transfer-coefficient through-the-liquid due to bubble agitation, in saturated nucleate pool boiling and forced convection barbotage showed these to be comparable in magnitude.

REFERENCES

1. N.U. Akturk, Heat transfer from a heated porous surface to a pool of liquid with gas injection at the interface, Proceedings of the Symposium on Two Phase Flow, Vol. II, Exeter, pp. D 501-520 (1965).

2. G.E. Alves, Co-current liquid-gas flow in a pipe-line contactor, Chem. Eng. Prog., 50, 449-456 (1954).

3. O. Baker, Simultaneous flow of oil and gas, The Oil and Gas Journal, 185-195, July 26 (1954).

4. M. Behar and R. Semeria, Sur la mise en évidence par strioscopie de certains mécanismes d' échanges thermiques dans le dégazage et l'ébullition de l'eau, C.R. Acad. Sc. Paris, 257, 2801-2803 (1963).

5. J.A.R. Bennett, J.G. Collier, H.R.C. Pratt and J.D. Thornton, Heat transfer to two-phase gas-liquid systems; Part I: Steam-water mixtures in the liquid-dispersed region in an annulus, Trans. Instn. Chem. Engrs., 39, 113-126 (1961).

6. P.J. Berenson, Experiments on pool-boiling heat transfer, Int. J. Heat Mass Transfer, 5, 985-999 (1962).

7. O.P. Bergelin and C. Gazley, Jr., Co-current gas-liquid flow, I: Flow in horizontal tubes, Heat Transfer and Fluid Mechanics Institute, Berkeley, California, 5-18 (1949).

8. A.E. Bergles and W.M. Rohsenow, The determination of forced-convection surface-boiling heat transfer, J. of Heat Transfer, Trans. ASME, Series C, 86, 365-372 (1964).

9. A.E. Bergles and W.M. Rohsenow, Forced-convection surface-boiling heat transfer and burnout in tubes of small diameter, Engineering Projects Laboratory Report No. 8767-21, Massachusetts Institute of Technology (1962).

10. J.C. Chen, A correlation for boiling heat transfer to saturated liquids in convective flow, ASME Paper No. 63-HT-34 (1963).

11. M.T. Cichelli and C.F. Bonilla, Heat transfer to liquids boiling under pressure, Trans. A.I. Ch.E., 41, 755-787 (1945).

12. R. Cole, A photographic study of pool boiling in the region of the critical heat flux, A.I. Ch.E. J., 6, 533-538 (1960).

13. J.G. Collier and D.J. Pulling, Heat transfer to two-phase gas-liquid systems, Part II: Further data on steam/water mixtures in the liquid dispersed region in an annulus. Atomic Energy Authorities report AERE - R 3809 (1962).

14. D.S. Cryder and A.C. Finalborgo, Heat transmission from metal surfaces to boiling liquids: Effect of temperature of the liquid on the liquid film coefficient, Trans. A.I.Ch.E., 33, 346-362 (1937).

15. D.S. Cryder and E.R. Gilliland, Heat transmission from metal surfaces to boiling liquids, I: Effect of physical properties of boiling liquid on liquid film coefficient, Industrial and Engineering Chemistry, 24, 1382-1387 (1932).

16. V.I. Deev, V.V. Gusev and G.P. Dubrovskii, An investigation into the mechanism of boiling with water at reduced pressures, Teploenergetika, 12, 73-76 (1965); translation in Thermal Engineering, 12, 90-92 (1965).

17. C.E. Dengler and J.N. Addoms, Heat transfer mechanism for vaporization of water in a vertical tube, Chem. Eng. Prog. Symp. Series, 52, 95-103 (1956).

18. R.G. Di Menza, Flow regimes in a two-phase boiling analogy, S.M. Thesis, Dept. Nuclear Engineering, Massachusetts Institute of Technology (1958).

19. P.L. Duffield, Diffusion-controlled electrolysis at a porous electrode with gas injection, Ph.D. Thesis, Dept. of Mechanical Engineering, Imperial College of Science and Technology, University of London (1966).

20. P.L. Duffield, Personal Communication.

21. H.K. Forster and R. Greif, Heat transfer to boiling liquid-Mechanism and correlations, J. of Heat Transfer, Trans. ASME, Series C, 81, 43-53 (1959).

22. H.K. Forster and N. Zuber, Dynamics of vapor bubbles and boiling heat transfer, A.I.Ch.E. Journal, 1, 531-535 (1955).

23. L. Fried, Pressure drop and heat transfer for two-phase, two-component flow, Chem. Eng. Prog. Symp. Series, 50, 47-51 (1954).

24. R.F. Gaertner, Photographic study of nucleate boiling on a horizontal surface, J. of Heat Transfer, Trans. ASME, Series C, 87, 17-29 (1965).

25. R.F. Gaertner and J.W. Westwater, Novel method for determining nucleate boiling sites, Chem. Eng. Prog., 55, 58-61 (1959).

26. W.R. Gambill and R.D. Bundy, High-flux heat-transfer characteristics of pure ethylene glycol in axial and swirl flow, A.I.Ch. E. Journal, 9, 55-59 (1963).

27. E.E. Gose, A. Acrivos and E.E. Petersen, Heat transfer to liquids with gas evolution at the interface, presented at the Mexico City meeting of the A.I.Ch.E. (1960).

28. E.E. Gose, E.E. Petersen and A. Acrivos, On the rate of heat transfer in liquids with gas injection through the boundary layer, J. of Applied Physics, 28, 1509 (1957).

29. I.D.R. Grant and T.D. Patten, Thickness of the thermal layer at the initiation of nucleate pool boiling, Paper 16, Symposium on Boiling Heat Transfer in Steam-Generating Units and Heat Exchangers, Manchester, September (1965).

30. R. Greif, Heat transfer with gas injection at the surface, Int. J. Heat Mass Transfer, 8, 1253-1254 (1965).

31. H. Groothuis and W.P. Hendal, Heat transfer in two-phase flow, Chemical Engineering Science, 11, 212-220 (1959).

32. S.A. Guerrieri and R.D. Talty, A study of heat transfer to organic liquids in single-tube, natural-convection, vertical-tube boilers, Chem. Eng. Prog. Symp. Series, 52, 69-77 (1956).

33. F.C. Gunther and F. Kreith, Photographic study of bubble formation in heat transfer to subcooled water, Report JPL 4-120, California Institute of Technology (1950).

34. G.F. Hewitt, H.A. Kearsey, P.M.C. Lacey and D.J. Pulling, Burnout and film flow in the evaporation of water in tubes, Symposium on Boiling Heat Transfer in Steam-Generating Units and Heat Exchangers, Manchester, September (1965).

35. M. Hirata, Diameters and slip velocities of air bubbles injected from a hole into water flow in a horizontal channel, Report HTL TR No. 53, Heat Transfer Laboratory, Mechanical Engineering Dept., University of Minnesota, August (1963).

36. M. Hirata and N. Nishiwaki, Skin friction and heat transfer for liquid flow over a porous wall with gas injection, Int. J. Heat Mass Transfer, 6, 941-949 (1963).

37. D.A. Huber and J.C. Hoehne, Pool boiling of benzene, diphenyl and benzene-diphenyl mixtures under pressure, J. of Heat Transfer, Trans. ASME, Series C, 85, 215-220 (1963).

38. T.H. Insinger, Jr. and H. Bliss, Transmission of heat to boiling liquids, Trans. A.I.Ch.E.,36,491-516 (1940).

39. A.A. Ivashkevich, Critical heat fluxes and heat-transfer coefficients for boiling of a liquid in channels under conditions of forced movement, Teploenergetika, 10, 74-78 (1961); translated by Atomic Energy Authority, Risley.

40. M. Jakob and W. Fritz, Versuche uber den Verdampfungsvorgang, Forschung a.d.Geb.d. Ingenieurwes, 2, 435-447 (1931).

41. M. Jakob and W. Linke, Der Warmeubergang beim Verdampfen von Flussigkeiten an senkrechten und waagerechten Flachen, Physik. Zeitschr., 36, 267-280 (1935).

42. D.D. James, C.J. Bardoliwalla and D.G. Martin, An apparatus for the study of heat transfer to a fluid flowing in a rectangular duct, Paper No. 11, I. Mech. E. Symposium on Two-Phase Fluid Flow, London (1962).

43. D.D. James, B.W. Martin and D.G. Martin, Forced convection heat transfer in asymmetrically heated ducts of rectangular cross-section, Proceedings of the Third International Heat Transfer Conference, Chicago, Vol. 1, pp. 85-98 (1966).

44. H.A. Johnson, Heat transfer and pressure drop for viscous-turbulent flow of oil-air mixtures in a horizontal pipe, Trans. ASME, 77, 1257-1264 (1955).

45. H.A. Johnson and A.H. Abou-Sabe, Heat transfer and pressure drop for turbulent flow of air-water mixtures in a horizontal pipe, Trans. ASME, 74, 977-987 (1952).

46. R.F. Knott, R.N. Anderson, A. Acrivos and E.E. Petersen, An experimental study of heat transfer to nitrogen-oil mixtures, Industrial and Engineering Chemistry, 51, 1369-1372 (1959).

47. L.I. Krasiakova, Some characteristics of the flow of a two-phase mixture in a horizontal pipe, Zh. Tekh. Fiz., 22, 654-669; translated by Atomic Energy Authority, report AERE Lib./ Trans. 695 (1957).

48. A.A. Kudirka, Two-phase heat transfer with gas injection through a porous boundary surface, U.S. Atomic Energy Commission report ANL-6862 (1964).

49. A.A. Kudirka, R.J. Grosh and P.W. McFadden, Two-phase heat transfer in a tube with gas injection from the walls, ASME Paper No. 65-HT-47 (1965).

50. S.S. Kutateladze, Heat Transfer in Condensation and Boiling, Second Edition (1952); translated as U.S. Atomic Energy Commission report AEC-tr-3770 (1959), p. 99.

51. Ibid. p. 129.

52. S.S. Kutateladze, Heat Transfer, p. 366, Arnold, London (1963).

53. Ibid. p. 391.

54. S.S. Kutateladze and V.N. Moskvicheva, Hydrodynamics of a two-component layer as related to the theory of crises in the process of boiling, Zh. Tek. Fiz., 29, 1135-1139 (1959).

55. D.A. Labountsov, Generalized correlation for nucleate boiling, Teploenergetika, 7, 76-80 (1960).

56. S. Levy, Generalized correlation of boiling heat transfer, Journal of Heat Transfer, Trans. ASME, Series C, 81, 37-42 (1959).

57. N. Madsen, Temperature fluctuations at a heated surface supporting pool boiling of water, Paper 14, Symposium on Boiling Heat Transfer in Steam-Generating Units and Heat Exchangers, Manchester, September (1965).

58. R.G. Malenkov, Critical phenomena in bubbling and boiling processes, Zh. Prik. Mek. Tek. Fiz., 6, 166-169 (1963); translated by National Lending Library for Science and Technology as RTS 2835.

59. B.D. Marcus and D. Dropkin, Measured temperature profiles within the superheated boundary layer above a horizontal surface in saturated nucleate pool boiling of water, ASME Paper No. 64-WA/HT-4 (1964).

60. W.H. McAdams, Heat Transmission, Third Edition, p. 180, McGraw-Hill, New York (1954).

61. B. Metais, Effect of gas separation on heat transfer during heating of liquids, Chemie-Ing. Techn., 33, 182-184 (1961); translated as Central Electricity Generating Board report C.E. Trans. 2711.

62. P.E. Meyer and G.B. Wallis, Bubbly flow in straight pipes, U.S. Atomic Energy Commission report NYO-3114-12 (1965).

63. F.O. Mixon, Jr., W.Y. Chon and K.O. Beatty, Jr., The effect of electrolytic gas evolution on heat transfer, Chem. Eng. Prog. Symp. Series, 56, 75-81 (1960).

64. F.D. Moore and R.B. Mesler, The measurement of rapid surface temperature fluctuations during nucleate boiling of water, A.I.Ch.E. Journal, 7, 620-624 (1961).

65. I.H. Newson, Heat transfer and pressure drop during pipe flow of two-phase two-component mixtures, Ph.D. Thesis, Dept. of Chem. Eng., University College, Univ. of London (1964).

66. K. Nishikawa and K. Yamagata, On the correlation of nucleate boiling heat transfer, Int. J. Heat Mass Transfer, 1, 219-235 (1960).

67. D.R. Oliver and S.J. Wright, Pressure drop and heat-transfer in gas-liquid slug flow in horizontal tubes, Brit. Chem. Eng., 9, 590-596 (1964).

68. C.J. Rallis and H.H. Jawurek, Latent heat transport in saturated nucleate boiling, Int. J. Heat Mass Transfer, 7, 1051-1068 (1964).

69. T.F. Rogers and R.B. Mesler, An experimental study of surface cooling by bubbles during nucleate boiling of water, A.I.Ch.E. Journal, 10, 656-660 (1964).

70. W.M. Rohsenow, A method of correlating heat-transfer data for surface boiling of liquids, Trans. ASME, 74, 969-976 (1952).

71. W.M. Rohsenow and J.A. Clark, A study of the mechanism of boiling heat transfer, Trans. ASME, 73, 609-620 (1951).

72. J.B. Roll and J.E. Myers, The effect of surface tension on factors in boiling heat transfer, A.I.Ch.E. Journal, 10, 530-534 (1964).

73. J.B. Roll and J.E. Myers, Measurement of dynamic surface tension in bubbling systems, Journal of Chemical and Engineering Data, 9, 256-258 (1964).

74. I.I. Sagan, Analysis of criterion relationships for liquids boiling in tubes, Izv. Vyssh. Uchebn. Zavedenii, Energetika, 108-114 (1959); translated as U.K. Ministry of Aviation Technical Information and Library Services report TIL/T. 5338 (1963).

74a. G.S. Schaller, Engineering Manufacturing Methods, Second Edition, p. 493, McGraw-Hill, New York (1959).

75. R. Semeria, An experimental study of the characteristics of vapour bubbles, Paper 7, I. Mech. E. Symposium on Two Phase Flow, London (1962).

76. R. Semeria, Caractéristiques des bulles de vapeur sur une paroi chauffante dans l'eau en ebullition à haute pression, C.R.Acad. Sc., 256, 1227-1230 (1963).

77. R. Semeria, Les échanges thermiques en ébullition nucléée, Extrait des Actes de la Semaine d'Information sur la Transmission de la Chaleur (Poitiers, 1963), Publications Scientifique et Techniques du Minisitère de l'Air, No. 417 (1963).

78. R.R. Sharp, The nature of liquid film evaporation during nucleate boiling, NASA TN D-1997 (1964).

79. E.N. Sieder and G.E. Tate, Heat transfer and pressure drop of liquids in tubes, Ind. and Eng. Chem, 28, 1429-1436 (1936).

80. G.E. Sims, U. Akturk and K.O. Evans-Lutterodt, Simulation of pool boiling heat transfer by gas injection at the interface, Int. J. Heat Mass Transfer, 6, 531-535 (1963).

81. D.B. Spalding, Heat transfer in rocket motors, Inaugural Lecture, Imperial College of Science and Technology, December (1958).

82. C.V. Sternling and C.E. Sanborn, Discussion to Ref. 45.

83. V.I. Tolubinskii, Theory of heat exchange in boiling, Izv. Vyssh. Uchebn. Zavedenii, Energetika, 15-22 (1959); translated as U.K. Ministry of Aviation Technical Information and Library Services report TIL/T. 5387 (1963).

84. W.R. Van Wijk and S.J.D. Van Stralen, Growth rate of vapour bubbles in water and in a binary mixture boiling at atmospheric pressure, Physica, 28, 150-171 (1962).

85. J.H. Vohr, Flow patterns of two-phase flow, a survey of the literature, U.S. Atomic Energy Commission report TID-11514 (1960).

86. G.B. Wallis, The analogy between the bubbling of air into water and nucleate boiling at saturation temperature, U.K. Atomic Energy Authority report AEEW-R 28 (1960).

87. G.B. Wallis, Two-phase flow aspects of pool boiling from a horizontal surface, U.K. Atomic Energy Authority report AEEW-R 103 (1961).

88. G.B. Wallis, A gas-liquid analogue of nucleate boiling, Nuclear Power, 5, 99-101 (1960).

89. G.B. Wallis, Some hydrodynamic aspects of two-phase flow and boiling, Proceedings of the 1961 International Heat Transfer Conference, Boulder, Colorado, Part II, pp. 319-340 (1961).

90. G.B. Wallis and P. Griffith, Liquid and gas distributions in a two-phase boiling analogy, Technical Report No. 13, DSR 7-7673, Massachusetts Institute of Technology (1958).

91. K. Yamagata, F. Hirano, K. Nishikawa and H. Matsuoka, Nucleate boiling of water on the horizontal heating surface, Mem. Fac. Engng. Kyushu, 15, No. 1, 97-163 (1955).

92. N. Zuber, Hydrodynamic aspects of boiling heat transfer (Thesis), U.S. Atomic Energy Commission report AECU-4439 (1959).

93. N. Zuber, The dynamics of vapour bubbles in non-uniform temperature fields, Int. J. Heat Mass Transfer, 2, 83-105 (1961).

94. N. Zuber and E. Fried, Two-phase flow and boiling heat transfer to cryogenic liquids, ARS Journal, 32, 1332-1341 (1962).

95. L.M. Zysina-Molozhen and S.S. Kutateladze, The influence of pressure on the mechanism of steam formation in boiling liquids, Zh. Tek. Fiz., 20, 110-116 (1950); translation available from Science Museum Library.

96. Anon., Mechanical and physical properties of Firth-Vickers "Staybrite" and stainless steels, Firth-Vickers Stainless Steels Ltd., Publication No. 108/15 (1963).

APPENDIX A TEMPERATURE DROP THROUGH THE POROUS MATERIAL

This appendix presents the method of calculating the temperature T_S at the upper surface of the porous material, i.e., that surface in contact with water or air-water mixture. It will be seen that for the conditions of the present experiment, it is justified in using a simplified form (equation (A.5)) to which the general equation (A.4) reduces. The treatment closely follows that of Green [A.1], the main difference here being in the boundary conditions.

Fig. A.1 depicts the problem under consideration. A gas at temperature $T_{g,4}$ approaches a semi-infinite porous wall which is generating heat. At $z = 0$, the temperature of the porous material is T_0. In this case $T_{g,4} = T_0$. The following assumptions are made, after Green:

(i) In the porous wall, the gas and solid temperature are equal at any given position.

(ii) Gas flow and heat flow are steady and one-dimensional.

(iii) All the heat conduction in the wall takes place in the solid.

(iv) The thermal conductivity of the solid and the specific heat of the gas are constant.

From a heat balance on an element of volume in the wall (see Fig. A.2), Green obtained the differential equation for the distribution of temperature in the porous wall:

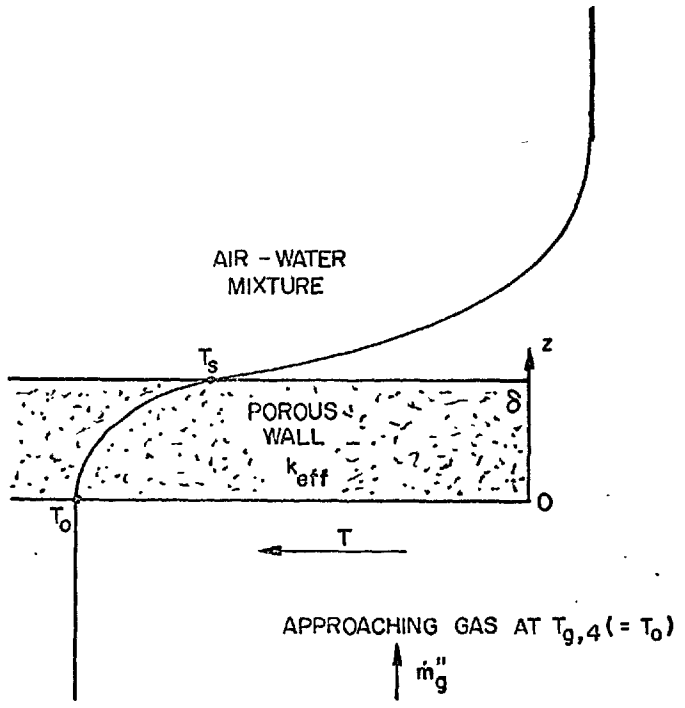

FIG. A.1 TEMPERATURE DISTRIBUTION FOR ONE-DIMENSIONAL POROUS GENERATING WALL

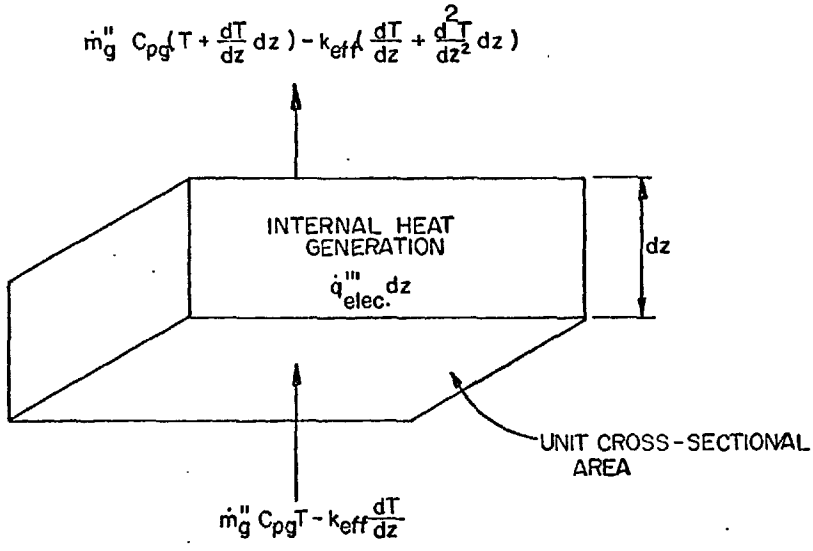

FIG. A.2 HEAT BALANCE ON A VOLUME ELEMENT IN A WALL

FIGS. A.1 AND A.2

$$\frac{d^2T}{dz^2} - \frac{\dot{m}_g'' C_{pg}}{k_{eff}} \frac{dT}{dz} + \frac{\dot{q}'''_{elec}}{k_{eff}} = 0 \qquad (A.1)$$

where:

$\dot{m}_g''$ is the superficial mass flow rate of gas through the porous wall,

C_{pg} is the specific heat of the gas at constant pressure,

k_{eff} is the "effective" or "apparent" (based on bulk volume) thermal conductivity of the wall,

$\dot{q}'''_{elec}$ is the "effective" or "apparent" (based on bulk volume) rate of electrical heat generation in the wall.

The present boundary conditions are:

$$\left.\begin{aligned} z = 0,\ \frac{dT}{dz} = 0 \\ z = 0,\ T = T_0 \end{aligned}\right\} \qquad (A.2)$$

The solution to equation (A.1) is therefore

$$T - T_0 = \frac{\dot{q}'''_{elec}}{\dot{m}_g'' C_{pg} \xi} \left[1 + \xi z - e^{\xi z} \right] \qquad (A.3)$$

where: $$\xi \equiv \frac{\dot{m}_g'' C_{pg}}{k_{eff}}$$

and has the dimension of $\frac{1}{(\text{length})}$.

At $z = \delta$ (δ is the thickness of the porous material), $T = T_S$ in which case equation (A.3) becomes

$$T_0 - T_S = \frac{\dot{q}'''_{elec}}{\dot{m}''_g C_{pg} \xi} \left[e^{\xi\delta} - \xi\delta - 1 \right] \qquad (A.4)$$

For a given set of experimental conditions, all the quantities in equation (A.4) are known excepting T_S; therefore T_S may be calculated.

When $\xi\delta \ll 1$, then equation (A.4) may be simplified by expanding the exponential term in the square bracket and neglecting terms higher than the second order; the result is

$$T_0 - T_S = \frac{\dot{q}'''_{elec}\, \delta^2}{2k_{eff}} \qquad (A.5)$$

This is, of course, the equation for the temperature drop through an impermeable wall insulated on one side. In the present experiments, the maximum value of $\xi\delta$ was approximately 0.02. The error in the heat-transfer coefficient due to using equation (A.5) instead of (A.4) for the calculation of T_S was:

generally < 0.4%,

worst case ever 3/4%.

When the approach gas temperature $T_{g,4}$ is not precisely equal to T_0, it is necessary to apply a correction to the heat-transfer coefficient as obtained using T_S from the above relations. For a quantitative discussion, see Appendix D.

Reference for Appendix A

A.1 L. Green, Jr., Gas cooling of a porous heat source, Trans. ASME, J. Applied Mechanics, 19, 173-178 (1952).

APPENDIX B THERMAL CONDUCTIVITY OF THE RIGID MESH POROUS MATERIAL

This appendix presents the method of obtaining the thermal conductivity k_{eff} of the "Rigid Mesh" porous material used as the heated wall in the test section. The material is anisotropic; it is therefore necessary to distinguish the direction in which k_{eff} is required. Fig. B.1 shows a sketch of the material; the transverse direction, as indicated on the figure, is the relevant direction here.

Measurements of k_{eff} by conventional methods such as the "divided disk" [B.1] would be unsatisfactory because the surface roughness of this thin material would present a large proportion of the total thermal resistance [B.2]. The method of the "thermal comparator" [B.3] would not give usable values as this method too, is very sensitive to the surface roughness of the specimen. Tewfik [B.4] has presented a method of measuring k_{eff} in various directions in the plane perpendicular to the transverse direction; this method, however, cannot be used for the determination of k_{eff} in the transverse direction. As measurements by existing methods were not applicable, three calculation methods as outlined below were used to obtain k_{eff}. For identification purposes, these methods are entitled as follows:

Method 1 - Grootenhuis et al., spheres.

Method 2 - Extension of Grootenhuis et al., true geometry.

Method 3 - Upper limit.

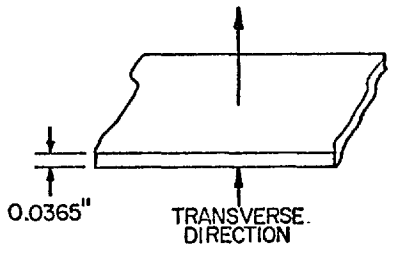

FIG. B.1 SKETCH SHOWING RELEVANT DIRECTION FOR k_{eff}

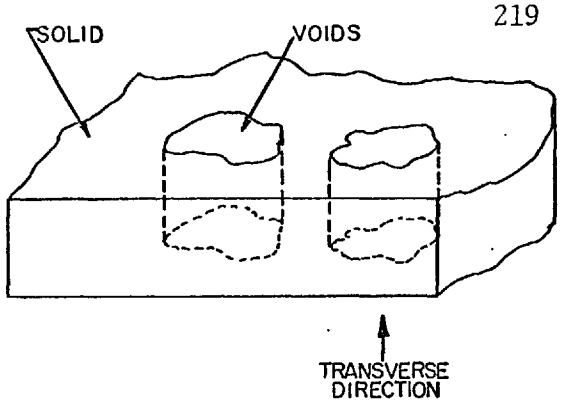

FIG. B.3 SKETCH OF POSSIBLE VOID GEOMETRY FOR UPPER LIMIT OF k_{eff}

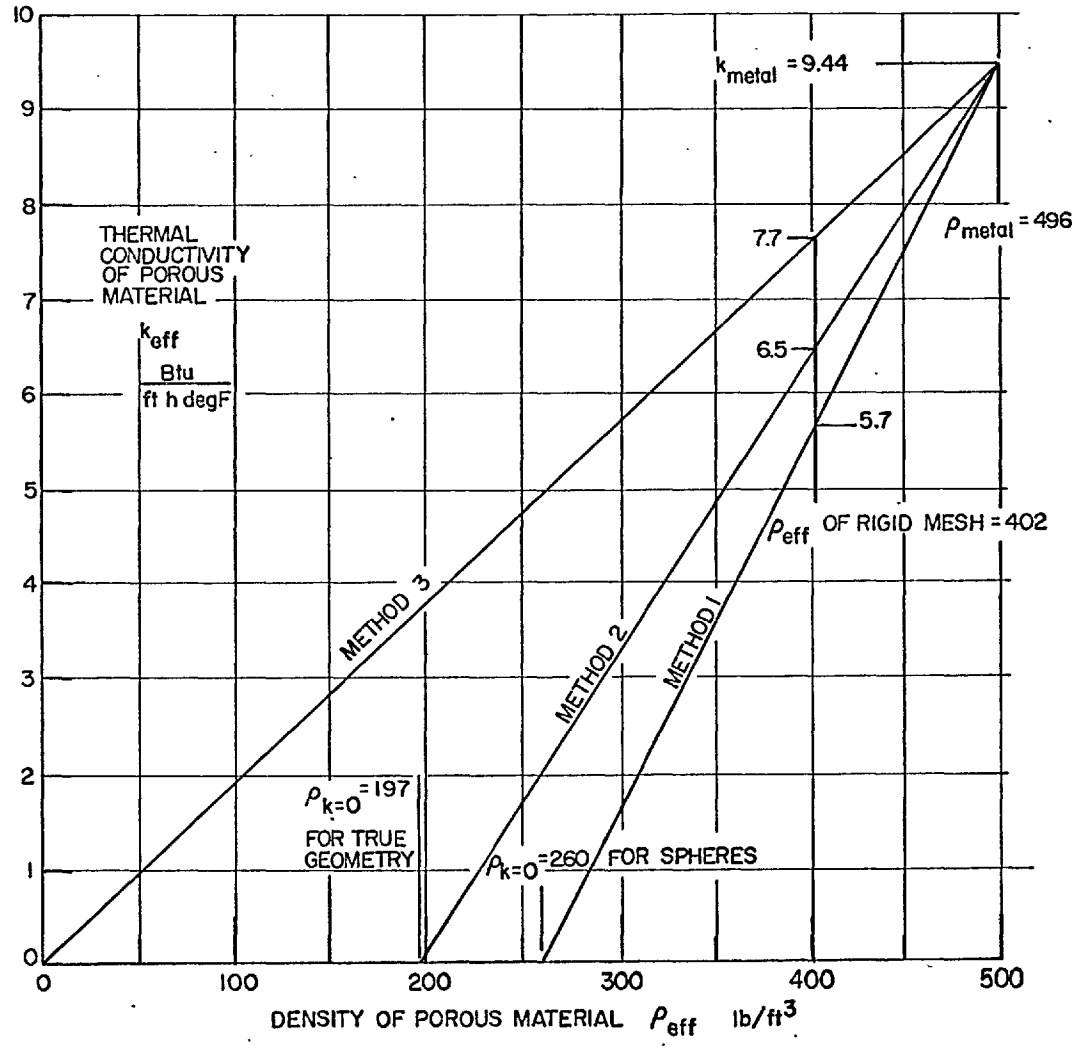

FIG. B.2 METHODS OF ORTAINING k_{eff} FOR POROUS MATERIAL

FIGS. B.1, B.2 and B.3

The calculations below are based on a temperature of 68°F. The working temperature of the hottest surface of the Rigid Mesh seldom exceeded 83°F; any temperature correction would therefore be negligible compared with other uncertainties.

Method 1 - Grootenhuis et al., spheres.

Grootenhuis et al. [B.5] have presented a method for obtaining the thermal conductivities of sintered porous metals, the constituent powder particles of which were spherical in shape. The method is described briefly below; it is based on the correlation of their own experimental results.

The essence of the method is that the thermal conductivity k_{eff} is linear with respect to the density of the porous material ρ_{eff}, having a value of zero at a density corresponding to 47.64% porosity* and a value equal to that of the solid metal when the porosity p equals zero (i.e., no voids). The porosity value of 47.64% corresponds to the maximum porosity that can be attained by packing equal sized spheres. Any increase in porosity would cause the spheres to no longer touch each other; as the air in the voids has negligible thermal conductivity, this condition would give $k_{eff} = 0$.

The method is now applied to the Rigid Mesh as if the

---

* The porosity p is defined as

$$p \equiv \frac{\text{volume of voids}}{\text{total volume}}$$

Rigid Mesh were comprised of compacted sintered spheres. The following information is used below.

ρ_{eff} of the Rigid Mesh = 402 lb/ft^3 (measured),

ρ_{Metal} = 496 lb/ft^3 [B.6],

k_{Metal} = 9.44 Btu/ft h degF at 68°F [B.6]

where:

ρ_{eff} is the density of the porous material,

ρ_{Metal} and k_{Metal} are the density and thermal conductivity, respecitvely, of the solid metal of which the Rigid Mesh is comprised.

The density $\rho_{k=0}$ of the porous material when $k_{eff} = 0$ is

$$\rho_{k=0} = (1 - .4764)\ 496 = 260 \text{ lb/ft}^3$$

The method is illustrated in Fig. B.2 whence a value of

$$k_{eff} = 5.7$$

is obtained for the Rigid Mesh.

Method 2* - Extension of Grootenhuis et al., true geometry.

In this method, instead of assuming the Rigid Mesh to be comprised of spheres, the true geometry is taken into account. The first step is to obtain the density $\rho_{k=0}$ the porous material would have for $k_{eff} = 0$. It is then assumed that a linear relationship exists (as it does with sintered spheres) between ($\rho_{k=0}$, 0) and (ρ_{Metal}, k_{Metal}) as shown in Fig. B.2. The thermal

* This method was suggested by Dr. P. Grootenhuis, Department of Mechanical Engineering, Imperial College.

conductivity of the Rigid Mesh may then be obtained at the appropriate ρ_{eff}.

The value of $\rho_{k=0}$ is obtained as follows. Table 3.1 in the body of the thesis presents details of the construction of the Rigid Mesh. Three layers of woven screen are calendered (rolled) and furnace welded together. An enlarged drawing was made showing the physical arrangement of the screens before they are calendered and welded with the adjacent layers of screen just not quite touching, so giving $k_{eff} = 0$. From the drawing it was possible to obtain (i) the total volume occupied by the screens and (ii) the volume occupied by the metal wires of the screens; items (i) and (ii) plus the knowledge that $\rho_{Metal} = 496$ lb/ft^3 gave

$$\rho_{k=0} = 197 \text{ lb/ft}^3$$

with a corresponding porosity of 60.2%. From Fig. B.2 for $\rho_{eff} = 402$ lb/ft^3 (the actual density of the Rigid Mesh), it follows that

$$k_{eff} = 6.5 \text{ Btu/ft h degF}.$$

Method 3 - Upper limit.

The upper limit of the thermal conductivity of the porous material is given by

$$k_{eff} = k_{Metal} \frac{\rho_{eff}}{\rho_{Metal}} = k_{Metal} (1 - p)$$

This line is shown on Fig. B.2, from which at

ρ_{eff} = 402 lb/ft^3,

k_{eff} = 7.7 Btu/ft h degF.

The pore geometry of voids of any uniform cross-sectional area would give this upper limit in k_{eff}.

Selection of k_{eff}.

There are two ways of selecting k_{eff} with the above information:

(i) is to take an average of the three methods,

(ii) is to choose k_{eff} of Method 2 as this method attempted to accommodate the real geometry.

The first way gives $k_{eff} = 6.6_5$ Btu/ft h degF, the second gives k_{eff} = 6.5 Btu/ft h degF, a difference of only 2.3%, so that it matters little which is chosen (the allowable error will be much greater than the 2.3%). So the value of 6.6_5 is used here with an allowable error of ±12%. If an error of ±15% were allowed, this would encompass both Method 1 and Method 3; it would seem, however, that it is unnecessary to allow quite such a large error.

References for Appendix B

B.1 E. H. Ratcliffe, Thermal conductivities of fused and crystalline quartz, British Journal of Applied Physics, 10, 22 - 25 (1959).

B.2 R. W. Powell, R. P. Tye and M. J. Hickman, Personal communication.

B.3 R. W. Powell, Thermal conductivity measurements by the thermal-comparator method, Invited Paper III, presented at Black Hills Summer Conference on Transport Phenomena at Rapid City, South Dakota, U.S.A. on 22nd August, 1962.

B.4 O. E. Tewfik, Measurements of thermal conductivity of porous anisotropic materials, A.I.A.A. Journal, 1, 919 - 921 (1963).

B.5 P. Grootenhuis, R. W. Powell and R. P. Tye, Thermal and electrical conductivity of porous metals made by powder metallurgy methods, Proc. Roy. Soc., B, 65, 502 - 511 (1952).

B.6 Mechanical and physical properties of Firth-Vickers 'Staybrite' and stainless steels, Firth-Vickers Stainless Steel Ltd., Publication No. 108/15 (1963).

APPENDIX C CORRECTION IN THERMOCOUPLE EMF READINGS TO ACCOUNT FOR THE PRESENCE OF A DC COMPONENT ALONG WITH THE MAIN AC HEATING CURRENT

C.1 Introductory Remarks

In the test section of the present apparatus, thermocouples were resistance-welded to the porous heater. Although the electrical heating current passing through the porous heater was essentially ac, there was some small dc component along with the ac (about ¼% at 50 amps (rms) ac). This dc component produced a dc ohmic potential drop along the heater. Since the two wires of any given thermocouple were not at precisely the same electrical potential on the heater, an ohmic dc emf was impressed across the two wires of the thermocouple. This dc emf was algebraically additive to the thermal dc emf produced by the thermocouple. Ignoring the presence of the ohmic dc emf in the thermocouple signal would result in errors in temperature measurement, which in turn would produce errors in the heat-transfer coefficient α; an example of the magnitude of the error in α is given below for the following conditions in the present test section:

- ac heating current of 50 amps (rms),
- dc component ¼% of the ac current,
- FeCon thermocouple wire (28.8 μV/degF in the temperature range 70 - 80°F) with the leads 0.010-in. apart in the direction of current flow,
- a heat-transfer coefficient of 5000 Btu/ft^2 h degF.

For these conditions, the error in α due to ignoring the presence

of the ohmic dc emf in the signal from such a thermocouple would be 4.5%. It can be shown that the error in α due to this source is proportional to α. It is therefore at the higher values of α (the example above is for α = 5000 Btu/ft^2 h degF) that the error becomes appreciable. A correction was applied, however, for all values of α. This appendix describes the method of correction for the ohmic dc emf in the thermocouple signal.

The method utilizes two reference wires of the same material in which no thermal emf was generated and a simple "calibration" procedure involving the reversal of a dc current. It is believed that this is the first time that a correction has been applied for the dc ohmic emf when the main heating current was ac. (Methods of correction for the ohmic dc emf have been proposed [C.1, C.2, C.3, C.4], some [C.1, C.2, C.4] involving dc current reversal, for situations in which the main heating current was dc. Where applicable to the present problem [C.1, C.2] they would have proved more complicated than the present solution.)

Two possible sources of the dc current in the heating circuit were as follows. One was the presence of an oxide film on the brass and copper connections causing some rectification of the ac current. (Every effort was made to minimize this source by periodically polishing the faces of the connections with emery cloth and coating the polished faces with silicone oil.) A second possible source was the generation of thermoelectric currents due to junctions of dissimilar metals at different temperatures in the electric circuit.

C.2 Correction Method

The system under consideration is shown in Fig. C.1 where "normal running conditions" using ac heating current (along with some dc component) are depicted. The signal from any thermocouple was fed through a selector switch and "choking circuit" (see Fig. 3.5) which attenuated the ac emf E_{ac} to 1/1500 its original value without changing the dc emf E_{dc} before being fed to the dc potentiometer. (The attenuation of E_{ac} was found necessary in order to eliminate electrical vibration of the galvanometer indicator in the dc potentiometer circuit.) The dc potentiometer, of course, only measured the dc component of the signal. Only the dc emf is of interest here. One thermocouple is treated below, but the method applies to all the thermocouples on the heater.

The dc emf E_{dc} at A-A was comprised of two parts, the thermal emf E_{th} due to the difference in temperature between the "hot junction" and the "cold junction" and the ohmic dc potential drop $I_{dc}R_{TC}$ which occurred in the heater between the points of attachment of the two wires of the thermocouple, i.e.,

$$E_{dc} = E_{th} + I_{dc}R_{TC} \qquad (C.1)$$

where I_{dc} is the dc current in the heater and R_{TC} is the resistance of the heater between the points of electrical contact of the two wires of the thermocouple. For any thermocouple the points of electrical contact were fixed, the magnitude varying between zero and approximately 0.015 in. It was desired to obtain E_{th} during normal running conditions.

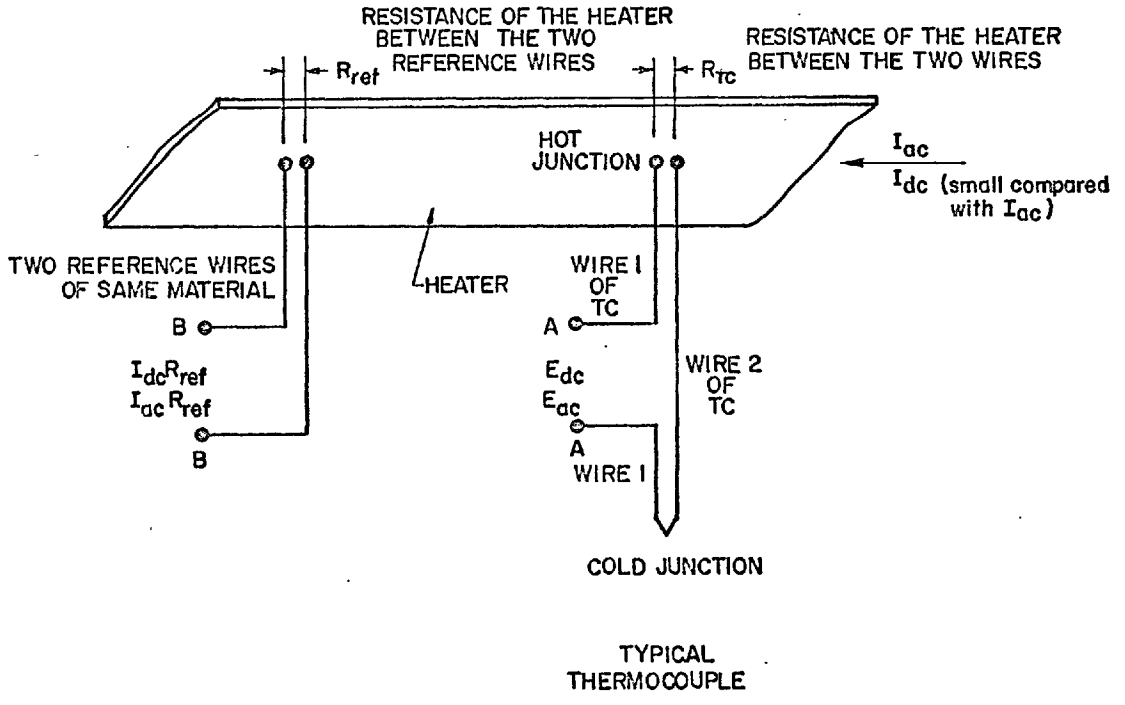

FIG. C.1 NORMAL RUNNING CONDITIONS USING AC HEATING CURRENT WITH SOME SMALL DC COMPONENT

The discussion is divided into two parts, one dealing with what is called the "calibration" procedure and the other dealing with the "normal running conditions".

Calibration Procedure

The object of this procedure was to obtain the ratio R_{TC}/R_{ref} where R_{ref} is the resistance of the heater between the two reference wires. The distance between the wires in the direction of current flow was approximately 0.02 in. The reference wires used here were constantan, mainly because of its excellent resistance-welding properties. These wires were connected to the selector switch (see Fig. 3.5) in the same manner as were the thermocouples. Where the reference wires were connected to the selector switch, care was taken to ensure that the two connections were at the same temperature by enclosing the connections in a thick brass insulated cup. During the calibration no ac current was used.

Step 1

The porous heater was cooled by allowing water to flow in the channel, and by having some finite air flow (barbotage-rate) through the porous heater. The temperature difference between the hot and cold junctions of the thermocouple was kept as small as conveniently possible (the cold junction was kept at room temperature) in order to give a large $I_{dc}\ R_{TC}$ emf compared with the thermal emf. A dc current (4 amps in the present case) $I_{dc,1}$ was initiated and maintained in the heater. The resulting dc emf from the thermo-

couple E_1 was read on the potentiometer and was

$$E_1 = E_{th,1} + I_{dc,1} R_{TC} \qquad (C.2)$$

where $E_{th,1}$ is the thermal emf generated by thermocouple for the given conditions.

Step 2

The hydrodynamic conditions were kept the same (water and air flow rates) as in Step 1 and the current leads to the test section were reversed so giving a dc current $I_{dc,2}$ equal and opposite to $I_{dc,1}$ (i.e., $I_{dc,2} = -I_{dc,1}$). The resulting dc emf from the thermocouple E_2 was read on the potentiometer and was

$$E_2 = E_{th,2} - I_{dc,1} R_{TC} \qquad (C.3)$$

where $E_{th,2}$ is the thermal emf generated in Step 2; it was equal in magnitude to, and was in the same sense as, $E_{th,1}$. Subtracting equation (C.3) from (C.2) yields

$$R_{TC} = \frac{E_1 - E_2}{2I_{dc,1}} \qquad (C.4)$$

The quantity R_{ref} may be determined from either Step 1 or Step 2 as

$$R_{ref} = \frac{E_{ref,1}}{I_{dc,1}} = \frac{E_{ref,2}}{I_{dc,2}} \qquad (C.5)$$

where $E_{ref,1}$ and $E_{ref,2}$ are the dc emf signals at the terminals of the two reference wires in Steps 1 and 2 respectively. These two emf's should be equal in magnitude and opposite in sign when $I_{dc,1}$ and $I_{dc,2}$ are equal and opposite as there should be no thermal emf

generated by the two reference wires. Indeed, this was a check that there was no thermal emf generated by the two reference wires (within, of course, the accuracy of the instrumentation).

The ratio R_{TC}/R_{ref} was then obtained for each thermocouple.

Normal Running Conditions

During the normal running of the apparatus the main heating current was ac. The dc component in the ac current caused a dc ohmic potential drop across the two reference wires of $I_{dc}R_{ref}$ and across the thermocouple of

$$I_{dc}\ R_{TC} = \frac{R_{TC}}{R_{ref}}\ (I_{dc}\ R_{ref}) \qquad (C.6)$$

For any set of running conditions, the thermal emf E_{th} generated by the thermocouple could be obtained from equation (C.1) by measuring E_{dc} and obtaining $I_{dc}\ R_{TC}$ from equation (C.6) wherein $I_{dc}\ R_{ref}$ was measured and R_{TC}/R_{ref} obtained from the calibration procedure.

Throughout both the calibration procedure and normal running conditions, a consistent sign convention must be observed in the measurement and recording of dc emf's.

References for Appendix C

C.1 R. Dutton and E. C. Lee, Surface-temperature measurement of current-carrying objects, Instrument Society of America Journal, 6, 49 - 51 (1959)

C.2 H. Buchberg, V. N. Tramontini, W. L. Martin, F. E. Romie, et al., Final report on studies in boiling heat transfer, pp. I-C-2 to 9, U. S. Atomic Energy Commission report COO-24 (1951).

C.3 M. E. Davenport, P. M. Magee and G. Leppert, Thermocouple attachment to a direct-current heater, Journal of Heat Transfer, Trans. ASME, Series C, 84, 187 - 188 (1962).

C.4 I. D. R. Grant and T. D. Patten, Thickness of the thermal layer at the initiation of nucleate pool boiling, Paper 16, Symposium on Boiling Heat Transfer in Steam-Generating Units and Heat Exchangers, Manchester, September (1965).

APPENDIX D CALCULATION PROCEDURE

This appendix gives the procedure for calculating the heat-transfer coefficients and the hydrodynamic quantities in the present experiments.

Because of the length of this appendix, the section headings are listed below in order to facilitate access to any desired material. Attention is drawn particularly to Section D.7 which summarizes the calculation procedure for the heat-transfer coefficient.

Heat losses from the heater to the ambient

D.5 The Ratio F_E of the Local to the Overall Heat Generation Rate

D.6 The $[\alpha/\alpha_{app}]$ Correction

D.7 Summary of the Calculation Procedure for the Heat-Transfer Coefficient

D.8 Calculation of the Barbotage-Rate $\dot{V}''_g$

D.9 Calculation of the Liquid Velocity u_f

D.10 Calculation of the Gas Velocity at Inlet to the Porous Section $u_{g,i}$

References for Appendix D

D.1 Definition of the Heat-Transfer Coefficients

In the body of the thesis the heat-transfer coefficient reported was the mean heat-transfer coefficient $\bar{\alpha}$ (a symbol α, without the "bar" was used, but had the significance of a mean) defined as

$$\bar{\alpha} \equiv \frac{1}{L} \int_0^L \alpha dx \qquad \text{(D.1) formerly (6.1)}$$

where, in this appendix:

α is the local heat-transfer coefficient,

L is the total length of the heated porous section,

x is the position along the heater.

The $\alpha \sim x$ relation was obtained by connecting linearly the local (α,x) points; the lines connecting the two (α,x) points closest to

each end of the heater were extrapolated to the ends of the heater; this is illustrated qualitatively below.

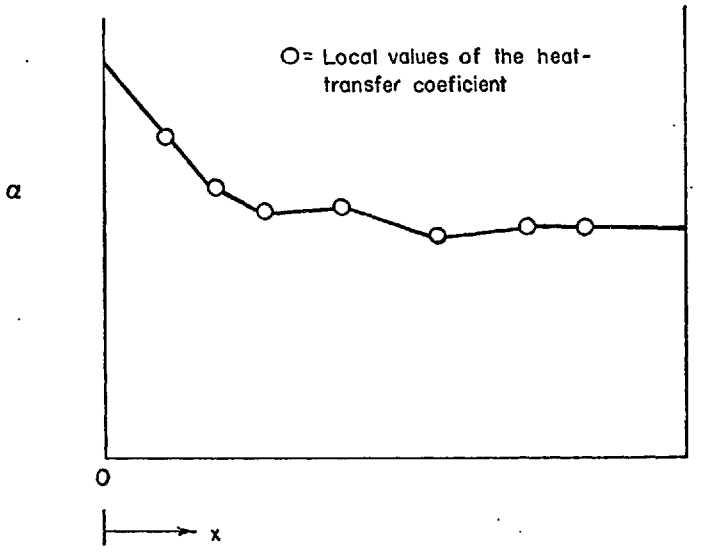

SKETCH OF $\alpha \sim x$ AS USED IN EQUATION (D.1)

The local heat-transfer coefficient is defined as

$$\alpha \equiv \frac{\mathring{q}''_{net}}{T_S - T_B} \qquad (D.2)$$

where:

$\mathring{q}''_{net}$ is the "net" heat flux (based on the projected area of the heater) through the thermal boundary layer and is considered in detail in Section D.4,

T_S is the local temperature at the solid-liquid interface (S - surface),

T_B is the local bulk water (or air and water mixture) temperature.

D.2 Calculation of T_S the Temperature at the Solid-Liquid Interface

Case 1: $T_{g,4} = T_0$ (symbols defined immediately below).

When the temperature $T_{g,4}$ of the air approaching the porous heater is precisely equal to the temperature T_0 of the lower face of the heater, the temperature at the solid-liquid interface T_S was calculated from equation (A.5) derived in Appendix A as

$$T_0 - T_S = \frac{\dot{q}'''_{elec}\,\delta^2}{2\,k_{eff}} \qquad (D.3)$$

where:

$\dot{q}'''_{elec}$ is the local value of electrical heat generation per unit volume (based on bulk volume),

δ is the thickness of the porous heater,

k_{eff} is the effective thermal conductivity (based on bulk volume) of the porous material.

The quantity $\dot{q}'''_{elec}$ is related to the local electrical heat flux $\dot{q}''_{elec}$ by

$$\dot{q}'''_{elec} = \frac{\dot{q}''_{elec}}{\delta} \qquad (D.4)$$

where $\dot{q}''_{elec}$ may be calculated from equation (D.33).

Case 2: $T_{g,4} \neq T_0$.

When $T_{g,4} \neq T_0$, then equation (A.5) is not strictly correct (one of the boundary conditions for its derivation no longer obtains). One can write, however

$$T_{0,app} - T_{S,app} = \frac{\dot{q}'''_{elec}\,\delta^2}{2\,k_{eff}} \qquad (D.5)$$

where:

$T_{0,app}$ is the "apparent" temperature indicated by the thermocouples in contact with the lower face of the porous heater (when $T_{g,4} \neq T_0$, then $T_{0,app} \neq T_0$ due to conduction along the thermocouple leads; when $T_{g,4} = T_0$, then $T_{0,app} = T_0$ as well);

$T_{S,app}$ is the "apparent" temperature of the porous heater at the solid-liquid interface as obtained from equation (D.5).

Further, an "apparent" local heat-transfer coefficient α_{app} may be defined as

$$\alpha_{app} \equiv \frac{\dot{q}''_{net}}{T_{S,app} - T_B} \qquad (D.6)$$

and α is given by

$$\alpha = \alpha_{app}\left[\frac{\alpha}{\alpha_{app}}\right] \qquad (D.7)$$

The ratio $[\alpha/\alpha_{app}]$ used in this last equation is treated in detail in Section D.6.

When performing the experiments, the approach gas temperature $T_{g,4}$ was made as close in magnitude as experimentally practical to T_O. Because of the time necessary to completely stabilize $T_{g,4}$, it was desirable to allow $T_{g,4}$ to differ a small amount from T_O. Besides, there were always some differences in the individual measurements of T_O along the porous element; since $T_{g,4}$ was the same for all thermocouple positions, then $T_{g,4}$ could not be equal to T_O for all thermocouple positions.

In the local heat-transfer coefficients, the magnitude of the $[\alpha/\alpha_{app}]$ correction was generally between 0.97 and 1.03. Further comments on $[\alpha/\alpha_{app}]$ appear in Section D.6.

D.3 Calculation of the Local Bulk Temperature T_B

The local bulk temperature of the water or air-water mixture was calculated from

$$T_B = T_{B,i} + \frac{x}{L}(T_{B,e} - T_{B,i}) \qquad (D.8)$$

where:

$T_{B,i}$ is the bulk temperature of water or air-water mixture at inlet to the heated porous section,

$T_{B,e}$ is the bulk temperature at exit from the heated porous section,

x is the distance from the beginning of the heated porous section,

L is the total heated length of the porous section.

It can be seen that a linear increase in the bulk temperature has been assumed. The effect on T_B of the local heat generation rate not being equal to the overall heat generation rate is negligibly small.

Calculation of $T_{B,i}$ from $T_{B,1}$ for conditions of finite upstream-quality.

The system under consideration is shown in Fig. D.1. The water temperature $T_{B,1}$ was measured at entrance to the upstream injector. When air was injected into the water upstream of the test section, this caused a reduction in temperature of the water due to evaporation of water into the injected air; thus making $T_{B,i} < T_{B,1}$. The main result of this subsection is equation (D.17).

The injector is supplied with water at the rate of $\dot{m}_{f,1}$ at temperature $T_{B,1}$. Previously (in the body of the thesis) $\dot{m}_{g,3}$ was called the "gas" or loosely, the "air" flow rate to the injector. In the present section a distinction is made between $\dot{m}_{g,3}$, called here the "gas" flow rate $\dot{m}_{g,3}$ (air and vapour) and the "air" flow rate $\dot{m}_{a,3}$ (air only). These are related by

$$\dot{m}_{g,3} = \dot{m}_{a,3} + \dot{m}_{v,3} \qquad (D.9)$$

where $\dot{m}_{v,3}$ is the mass flow rate of water vapour in the air at entrance to the upstream injector.

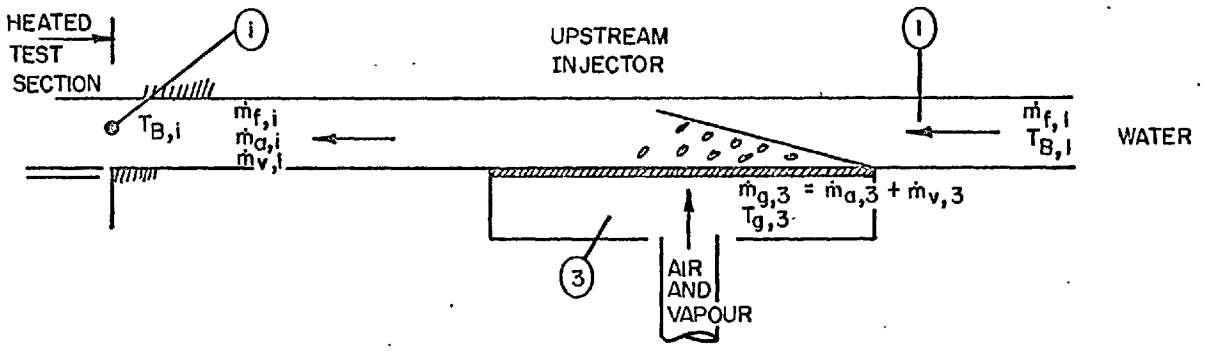

FIG. D.1 MASS FLOWS AND TEMPERATURES AT THE UPSTREAM AIR-INJECTOR

A heat balance for the injector yields

$$\dot{m}_{f,1}h_{f,1} + \dot{m}_{a,3}h_{a,3} + \dot{m}_{v,3}h_{v,3} = \dot{m}_{f,i}h_{f,i} + \dot{m}_{a,i}h_{a,i} + \dot{m}_{v,i}h_{v,i} \qquad (D.10)$$

where:

$\dot{m}_{f,1}$ is the mass flow rate of water at entrance to the injector,

$h_{f,1}$ is the enthalpy of the water at entrance to the injector, i.e. at temperature $T_{B,1}$,

$h_{a,3}$ and $h_{v,3}$ are the enthalpies of the air and vapour respectively at position 3, i.e. at $T_{g,3}$,

$\dot{m}_{f,i}$, $\dot{m}_{a,i}$ and $\dot{m}_{v,i}$ are the mass flow rates of the water, air and vapour respectively at entrance to the heated porous section,

$h_{f,i}$, $h_{a,i}$ and $h_{v,i}$ are the enthalpies of the water, air and vapour respectively at entrance to the heated porous section.

The equations for the conservation of mass are

$$\dot{m}_{f,i} = \dot{m}_{f,1} - (\dot{m}_{v,i} - \dot{m}_{v,3}) \qquad (D.11)$$

$$\dot{m}_{a,i} = \dot{m}_{a,3} \qquad (D.12)$$

Equations (D.11), (D.12) and the following relations may be substituted into (D.10):

$$
\left.
\begin{aligned}
h_{fg,i} &= h_{v,i} - h_{f,i} \\
\dot{m}_{v,i} &= F_{v,i}\,\dot{m}_{a,i} = F_{v,i}\,\dot{m}_{a,3} \\
\dot{m}_{v,3} &= F_{v,3}\,\dot{m}_{a,3} \\
h_{f,1} - h_{f,i} &= C_{pf}\,(T_{B,1} - T_{B,i}) \\
h_{a,3} - h_{a,i} &= C_{pa}\,(T_{a,3} - T_{a,i})
\end{aligned}
\right\} \quad (D.13)
$$

The result is

$$
T_{B,1} - T_{B,i} = \frac{\dot{m}_{a,3}}{\dot{m}_{f,1}\,C_{pf}} \left[(F_{v,i} - F_{v,3}) h_{fg,i} - C_{pa}(T_{a,3} - T_{a,i}) + F_{v,3}(h_{v,i} - h_{v,3}) \right] \qquad (D.14)
$$

where:

$h_{fg,i}$ is the latent heat of vaporisation at the inlet to the heated porous section,

$F_{v,i}$ and $F_{v,3}$ are the vapour contents (lb of vapour/lb of dry air) in the gas (air and vapour mixture) at positions i and 3 respectively,

C_{pf} and C_{pa} are the specific heats at constant pressure for the water and air respectively,

$T_{a,i}$ and $T_{a,3}$ are the air temperatures at entrance to the heated porous section, position i, and at entrance to the injector, position 3 respectively, ($T_{a,3} = T_{g,3}$).

The term $F_{v,3}\ (h_{v,i} - h_{v,3})$ is small compared with the other terms in the square bracket in equation (D.14) and has been neglected. The following assumptions are now made for conditions at the inlet to the heated porous section, i.e. at position i.

(i) The temperature of the water and air are equal, i.e.

$$T_{B,i} = T_{a,i} \tag{D.15}$$

(ii) The air is saturated with water vapour at the water (and air) temperature, i.e.

$$F_{v,i} = F_{v,sat\ i} \tag{D.16}$$

where $F_{v,sat\ i}$ is the saturation vapour content (lb vapour/lb dry air) of the air and vapour mixture at position i.

When conditions (i) and (ii) above prevail, the combination of these has been called the condition of "thermal equilibrium" elsewhere in the thesis. Substitution of these two conditions in (D.14) yields

$$T_{B,1} - T_{B,i} = \frac{\dot{m}_{a,3}}{\dot{m}_{f,1}\, C_{pf}} \left[(F_{v,sat\ i} - F_{v,3})h_{fg,i} - C_{pa}\,(T_{g,3} - T_{B,i})\right] \tag{D.17}$$

This equation represents the main result of this subsection. For conditions of finite inlet-quality, i.e. finite air supply to the upstream injector, the above equation was used to calculate $T_{B,i}$ when the following quantities were measured: $T_{B,1}$, $\dot{m}_{a,3}$, $\dot{m}_{f,1}$, $F_{v,3}$, $T_{g,3}$. It is seen that in the form above, equation (D.17) requires a trial and error solution since $F_{v,sat\ i}$ is a function of $T_{B,i}$. The necessary information on saturation vapour content was obtained from Ref. D.1.

Before accepting that equation (D.17) was suitable for the calculation of $T_{B,i}$ in the present experiments, a separate test was run to determine its suitability. This was done by disconnecting the injector from the test section, and then connecting the injector to a tube in which was situated a thermocouple probe with the measuring junction at the same distance from the injector as was the beginning of the heated porous section. The thermocouple junction was located approximately 0.040 in. above the bottom of the tube in order to be in the liquid annulus when the flow pattern was annular. The results of the test are shown in Fig. D.2 where values of $(T_{B,1} - T_{B,i})$ calculated from equation (D.17) are plotted against measured values of the same quantity. Lines of ±0.1 deg F are also shown. (An error of 0.1 deg F in the water temperature would give an error in the heat-transfer coefficient of approximately 1%). Of the 24 data points on the figure, 22 fall within the ±0.1 deg F

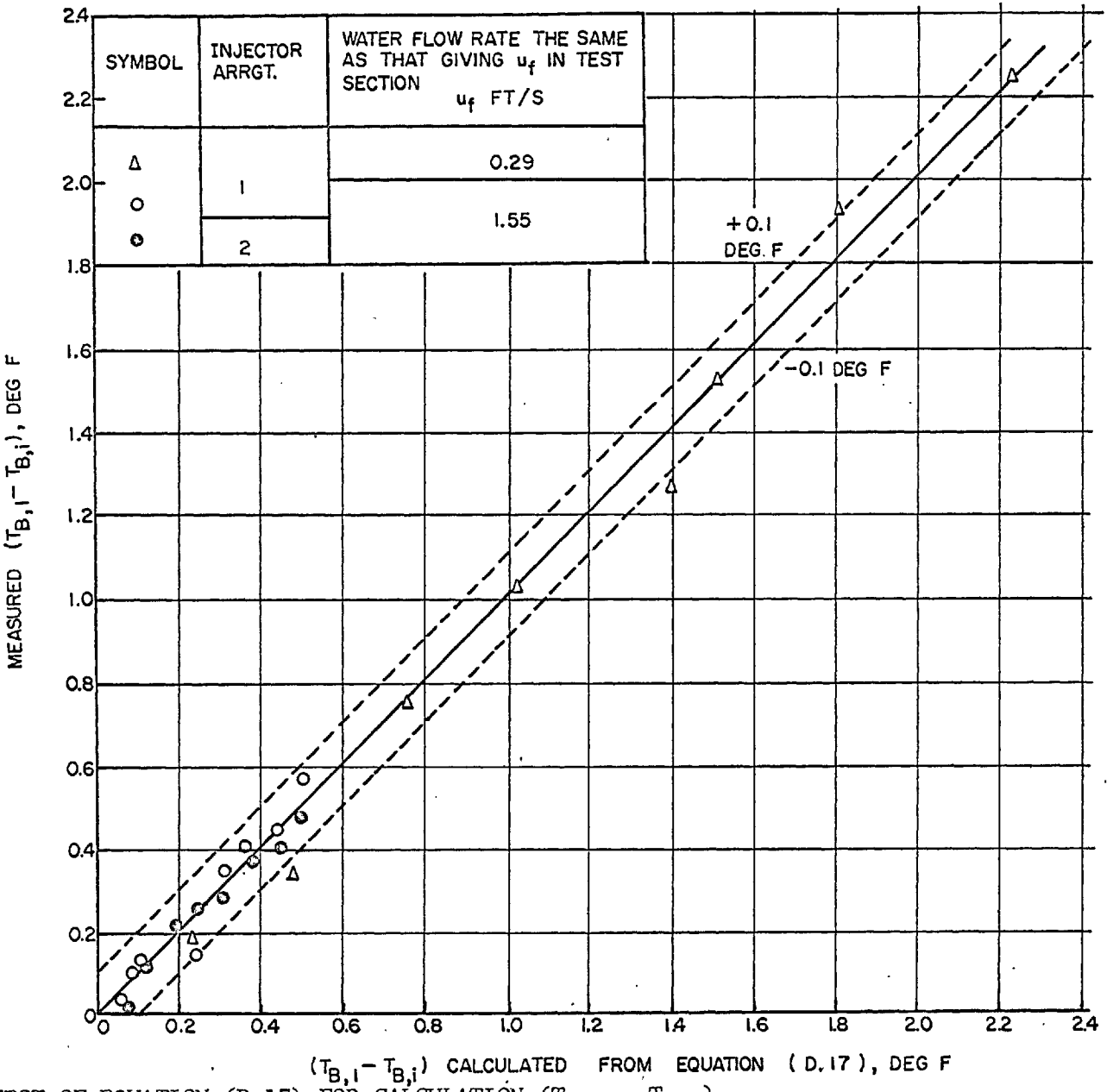

FIG. D.2 TEST OF EQUATION (D.17) FOR CALCULATION $(T_{B,1} - T_{B,i})$

FIG. D.2

lines and there are no systematic deviations from the 45° line. It was therefore concluded that equation (D.17) was suitable for the calculation of $T_{B,i}$ and that the assumption of "thermal equilibrium" used in obtaining equation (D.17) was valid, at least as far as the calculation of $T_{B,i}$ was concerned. No results for u_f = 5.1 ft/s appear on Fig. D.2. For this liquid velocity, the largest values of $(T_{B,1} - T_{B,i})$ were approximately 0.17 deg. F and hence any errors in calculating this quantity would produce entirely negligible errors in $T_{B,i}$.

The effect on the hydrodynamic quantities u_f and $u_{g,i}$ is generally negligibly small and is discussed quantitatively in Sections D.9 and D.10 for u_f and $u_{g,i}$ respectively.

Heat gains from the ambient to the water.

In the calculation of T_B the local bulk temperature in equation (D.8), $T_{B,i}$ was obtained from equation (D.17) and $T_{B,e}$ was assumed equal to $T_{B,2}$ the temperature of the thermocouple at the outlet from the test section (Fig. 3.2). If there were substantial heat gains from the ambient to the water as it traversed the test section, errors would result in $T_{B,i}$ and $T_{B,e}$ and hence in T_B and in the heat-transfer coefficients. An experiment was run to determine the magnitude of this effect; it was found that for the usual temperature difference between the ambient and the

water (approximately 10 deg F), the heat gain from the ambient to the water traversing the test section was negligibly small, the worst case being for the lowest liquid velocity, u_f = 0.084 ft/s. Even in this worst case the resulting error in the mean heat-transfer coefficient due to this effect was approximately 3/4% and so justified neglecting the effect.

D.4 Calculation of the Net Heat Flux $\dot{q}''_{net}$

Summary.

The net heat flux $\dot{q}''_{net}$ was calculated as follows:

$$\dot{q}''_{net} = \dot{q}''_S - Y\dot{m}''_{a,0}\,(F_{v,sat\ S} - F_{v,0})h_{fg} \qquad (D.32)$$

$$\dot{q}''_S = \dot{q}''_{elec} - \dot{m}''_{a,0}\,(h_{a,S} - h_{a,0}) \qquad (D.18)$$

$$Y = 0.65 \quad \text{in the present experiment.}$$

The symbols are defined above equation (D.18) and beneath equations (D.20), (D.29) in the text.

The heat flux through the S-surface $\dot{q}''_S$.

Figure D.3 shows the barbotage system under consideration. Here, the approaching air-vapour mixture is at the same temperature as the bottom face of the porous material (i.e. $T_{g,4} = T_0$; the $[\alpha/\alpha_{app}]$ correction mentioned earlier takes account of the situation

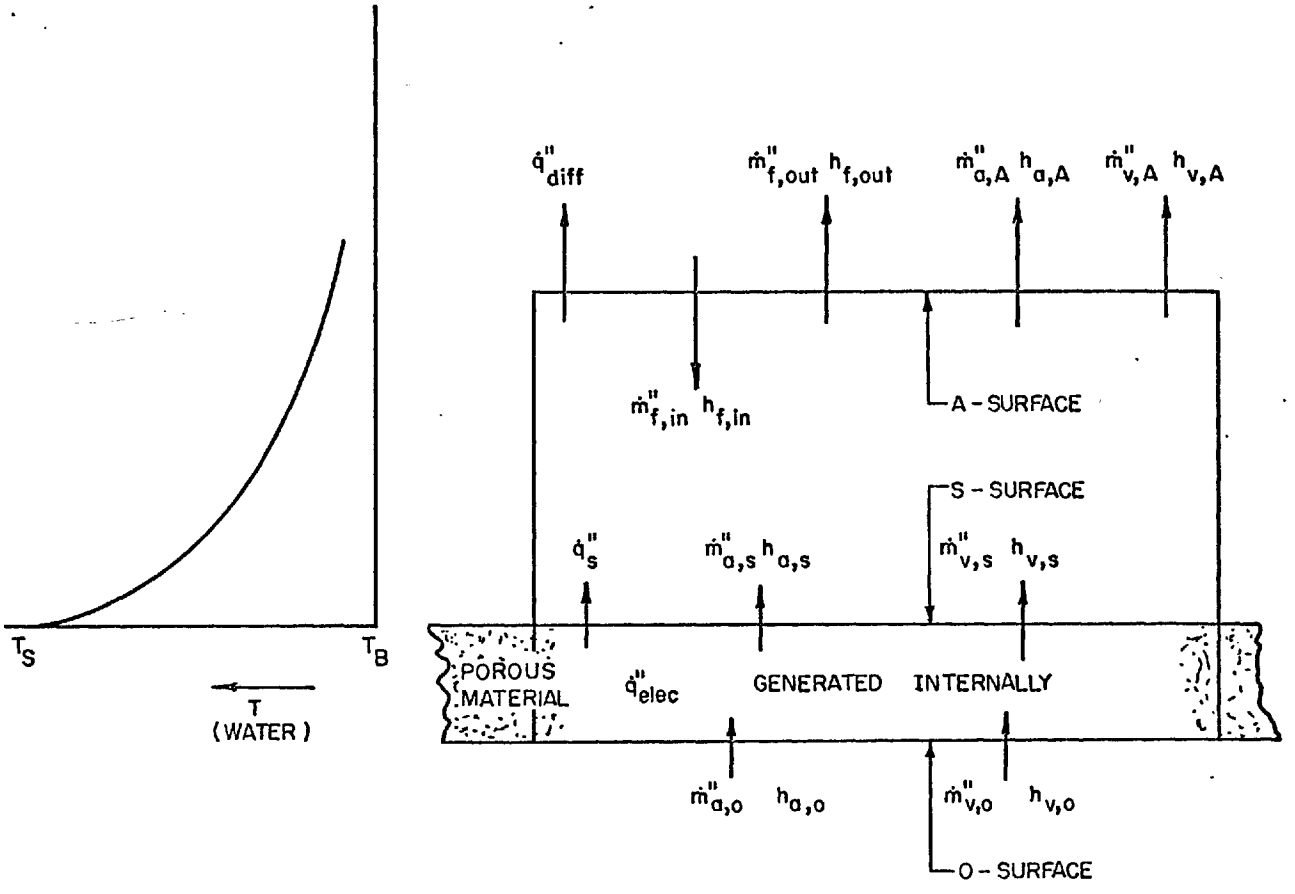

NOTE: APPROACH AIR – VAPOUR MIXTURE IS AT THE SAME TEMPERATURE $T_{9,4}$ AS THE BOTTOM FACE OF THE POROUS MATERIAL T_o ; THEREFORE NO CONDUCTIVE HEAT FLUX CROSSES THE O-SURFACE.

FIG. D.3 ONE-DIMENSIONAL SYSTEM OF ENERGY FLUXES IN BARBOTAGE

when $T_{g,4} \neq T_0$); therefore no conductive heat flux crosses the 0-surface. A heat balance written for the control volume bounded by the 0- and S-surfaces yields

$$\dot{q}''_S = \dot{q}''_{elec} - \dot{m}''_{a,0}(h_{a,S} - h_{a,0}) - \dot{m}''_{v,0}(h_{v,S} - h_{v,0})$$

where the "double dash" superscript indicates per unit projected area of porous element and

$\dot{q}''_S$ is the heat flux crossing the S-surface,

$\dot{q}''_{elec}$ is the heat flux produced internally in the porous element due to electrical resistive heating (see later in this section for more detail),

$\dot{m}''_{a,0}$ and $\dot{m}''_{v,0}$ are the mass fluxes of air and water vapour respectively approaching the porous element,

$h_{a,S}$ and $h_{a,0}$ are the enthalpies of the air at the S- and 0-surfaces respectively (the temperature of the air at the S-surface was assumed equal to the S-surface temperature of the porous wall),

$h_{v,S}$ and $h_{v,0}$ are the enthalpies of the water vapour at the S- and 0-surfaces respectively.

In the above equation the term $\dot{m}''_v(h_{v,S} - h_{v,0})$, representing the

change in enthalpy of the vapour, is extremely small compared with other terms and was neglected in the calculations. Indeed the largest values of the term representing the change in enthalpy of the air, $\dot{m}''_{a,0}(h_{a,S} - h_{a,0})$, is only approximately 2% of $\dot{q}''_{elec}$. The above equation, with the last term neglected, reads

$$\dot{q}''_S = \dot{q}''_{elec} - \dot{m}''_{a,0}(h_{a,S} - h_{a,0}) \qquad (D.18)$$

The net heat flux $\dot{q}''_{net}$ and the "evaporation correction".

This subsection concerns the calculation of the "net" heat flux $\dot{q}''_{net}$ which is used in the calculation of the heat-transfer coefficient, equations (D.2) or (D.6) and (D.7). This $\dot{q}''_{net}$ differs from $\dot{q}''_S$, treated above, by the inclusion of what is called here an "evaporation term" or "evaporation correction"; the main discussion here then is about this term. The main result is equation (D.32) with Y = 0.65. The development which follows is admittedly crude. However, as will be seen, the magnitude of the evaporation correction is not large enough to justify a more sophisticated approach.

In Chapter 2 of this thesis, a one-dimensional system of time and area means of heat-fluxes was used for barbotage (Fig. 2.1 b); no mention was made of evaporation of water into the air in the thermal boundary layer as the barbotage heat-transfer coefficients were already corrected for this effect. The method used by Gose [D.2]

differs somewhat from that given here (see page 71 of Ref. D.2); the end result of the method of Akturk [D.3] is the same as that given here [D.4].

The system under consideration is shown in Fig. D.3; it is one-dimensional and involves only time and area means (as in Chapter 2). The system can apply to either pool or forced convection barbotage (in the latter there is, of course, no net enthalpy flux between the downstream and upstream sides of the control volume). The bulk temperature T_B has a slightly different significance in pools and forced convection: in pool barbotage T_B is the temperature of the liquid at some large distance from the heating surface while for forced convection barbotage T_B is the "mixing cup temperature". With the excellent mixing obtained under barbotage conditions, the temperature profile in forced convection barbotage is expected to be very "flat" with the lowest temperature in the channel (at any x-position along the heater) being approximately equal to T_B.

A heat balance for the control volume bounded by the S-surface and the A-surface (any arbitrary surface within the thermal boundary layer) in the figure yields

$$q''_S = q''_{diff} + \dot{m}''_{f,out}(h_{f,out} - h_{f,in}) + \dot{m}''_{a,S}(h_{a,A} - h_{a,S})$$

$$+ \dot{m}''_{a,S} F_{v,S}(h_{v,A} - h_{v,S}) + \dot{m}''_{a,S}(F_{v,A} - F_{v,S})h_{fg} \qquad (D.19)$$

wherein the following relations obtain

$$\left.\begin{aligned} \dot{m}''_{f,out} &= \dot{m}''_{f,in} - (\dot{m}''_{v,A} - \dot{m}''_{v,S}) \\ F_{v,A}\,\dot{m}''_{a,A} &= \dot{m}''_{v,A} \\ F_{v,S}\,\dot{m}''_{a,S} &= \dot{m}''_{v,S} \\ \dot{m}''_{a,A} &= \dot{m}''_{a,S} = \dot{m}''_{a,0} \\ h_{fg} &\simeq h_{v,A} - h_{f,in} \end{aligned}\right\} \quad (D.20)$$

and where:

$\dot{q}''_{diff}$ is the heat flux through the A-surface due to the presence of the temperature gradient; it includes both molecular and eddy diffusion;

$\dot{m}''_{f,in}$ and $\dot{m}''_{f,out}$ are the mass fluxes of the liquid entering and leaving the control volume respectively;

$\dot{m}''_{a,S}$, $\dot{m}''_{a,A}$ and $\dot{m}''_{a,0}$ are the mass fluxes of air at the S-, A- and O-surfaces repectively;

$\dot{m}''_{v,S}$ and $\dot{m}''_{v,A}$ are the mass fluxes of the vapour at the S- and A-surfaces respectively;

$h_{f,in}$ and $h_{f,out}$ are the mean enthalpies of the liquid entering and leaving the control volume respectively;

$h_{a,S}$ and $h_{a,A}$ are the mean enthalpies of the air at the S- and A-surfaces respectively;

$h_{v,S}$ and $h_{v,A}$ are the mean enthalpies of the vapour at the S- and A-surfaces respectively;

h_{fg} is the latent heat of vaporization;

$F_{v,S}$, $F_{v,A}$ and $F_{v,O}$ (used immediately below) are the vapour contents (lb vapour/lb dry air) of the air and vapour mixture at the S-, A- and O-surfaces respectively.

It is assumed that

$$F_{v,S} = F_{v,O} \tag{D.21}$$

i.e., that there has been no change in the vapour content of the air and vapour mixture in passing through the porous element. In the present investigation $F_{v,O}$ was measured* (see Appendix F). The term, $\dot{m}''_{a,S} F_{v,S}(h_{v,A} - h_{v,S})$, in equation (D.19) is small compared with the other terms and is neglected below.

For the current presentation, the air temperature at the

---

*The extremes of values of $F_{v,O}$ in the present investigation were 0.0027 - 0.0080 lb vapour/lb dry air with by far the majority of conditions being around 0.0040.

A-surface need not be at the temperature of the water at that surface (except at the S-surface). Similarily the value of $F_{v,A}$ need not correspond to the saturation vapour content at the liquid temperature at the A-surface.

As in Chapter 2, the heat transport through the liquid is given the symbol $\dot{q}''_f$ defined as

$$\dot{q}''_f \equiv \dot{q}''_{diff} + \dot{m}''_{f,out} (h_{f,out} - h_{f,in}) \qquad (D.22)$$

Substituting equations (D.21) and (D.22) in (D.19), dropping the subscript A, noting that $\dot{m}''_{a,S} = \dot{m}''_{a,0}$ and neglecting $\dot{m}''_{a,S} F_{v,S} \times (h_{v,A} - h_{v,S})$ yields

$$\dot{q}''_f = \dot{q}''_S - \dot{m}''_{a,0} [(h_a - h_{a,S}) + (F_v - F_{v,0})h_{fg}] \qquad (D.23)$$

The heat-transfer coefficient desired in the present experiment is the heat-transfer-coefficient-through-the-liquid α (in Chapter 2, α_f was used as the symbol); it is the reciprocal of the total resistance to the flow of heat through the thermal boundary layer in the liquid (see Section 2.3.1), i.e.

$$\alpha \equiv \frac{1}{-\int_{T_S}^{T_B} \frac{dT}{\dot{q}''_f}} = \frac{1}{\int_{T_B}^{T_S} \frac{dT}{\dot{q}''_f}} \qquad (D.24) \text{ formerly } (2.10)$$

where $\dot{q}''_f$ is given by equation (D.22). If the function $h_a \sim T$ and $F_v \sim T$ were known, then α could be evaluated from equation (D.24). These two functions are however, not known and the following approach is adopted in order to evaluate α.

For convenience a symbol M is introduced and defined as

$$M \equiv \frac{\dot{m}''_{a,0}}{\dot{q}''_S} \left[(h_a - h_{a,S}) + (F_v - F_{v,0})\, h_{fg}\right] \qquad (D.25)$$

Substitution of equation (D.25) in (D.23) and the resulting equation in (D.24) yields

$$\alpha = \frac{1}{\frac{1}{\dot{q}''_S}\int_{T_B}^{T_S} \frac{dT}{1 - M}} \qquad (D.26)$$

The value of M is small compared with 1 (largest possible value of M was 0.25 and generally much smaller).

In this case, equation (D.26) may be approximated by

$$\alpha = \frac{1}{\frac{1}{\dot{q}''_S}\int_{T_B}^{T_S} (1 + M)\, dT} \qquad (D.27)$$

Equation (D.27) may be manipulated to yield

$$\alpha = \frac{1}{\frac{T_S - T_B}{\dot{q}''_S}\left[1 + \frac{1}{T_S - T_B}\int_{T_B}^{T_S} M\, dT\right]} \qquad (D.28)$$

It may be shown that the second term in the square bracket above is small compared with 1, in which case (D.28) may be approximated by

$$\alpha = \frac{1}{T_S - T_B}\left[\dot{q}''_S - \frac{\dot{q}''_S}{T_S - T_B}\int_{T_B}^{T_S} M\, dT\right] \qquad (D.29)$$

It can be shown that the maximum value of the second term in the square bracket of equation (D.29) is (the definition of M is given in equation (D.25); $(h_a - h_{a,S})$ therein is negative),

$$\dot{m}''_{a,0}(F_{v,\text{sat } S} - F_{v,0})h_{fg}$$

where $F_{v,\text{sat } S}$ is the "saturation" vapour content of the air and vapour mixture at the S-surface. This suggests that equation (D.29) be written as

$$\left.\begin{aligned} \alpha &= \frac{\dot{q}''_S - Y\,\dot{m}''_{a,0}\,(F_{v,\text{sat } S} - F_{v,0})h_{fg}}{T_S - T_B} \\ \text{or} \\ \alpha &= \frac{\dot{q}''_S}{T_S - T_B}\left[1 - \frac{Y\,\dot{m}''_{a,0}(F_{v,\text{sat } S} - F_{v,0})h_{fg}}{\dot{q}''_S}\right] \end{aligned}\right\} \qquad (D.30)$$

where

$$Y \equiv \frac{1}{(F_{v,sat\ S}-F_{v,0})(h_{fg})(T_S-T_B)} \int_{T_B}^{T_S} [(h_a - h_{a,S}) + (F_v - F_{v,0})h_{fg}]dT \qquad (D.31)$$

A symbol $\dot{q}''_{net}$ to be called the "net heat flux" is defined as

$$\dot{q}''_{net} \equiv \dot{q}''_S - Y\,\dot{m}''_{a,0}\,(F_{v,sat\ S} - F_{v,0})h_{fg} \qquad (D.32)$$

in which case (D.30) becomes

$$\alpha = \frac{\dot{q}''_{net}}{T_S-T_B}$$

which is the equation quoted earlier as (D.2).

The symbol Y has the significance of a proportionality constant with a maximum value of 1. The second term in the square bracket of equation (D.31) is likely to dominate the integral [the maximum value of the second term (that due to evaporation into the air in the thermal boundary layer) is approximately 7 times the maximum value of the first term (that due to changes in enthalpy of the air as it traverses the thermal boundary layer); for this reason $Y\,\dot{m}''_{a,0}\,(F_{v,sat\ S} - F_{v,0})h_{fg}$ and

$$\frac{Y\,\dot{m}''_{a,0}\,(F_{v,sat\ S} - F_{v,0})h_{fg}}{\dot{q}''_S}$$

are called

the "evaporation correction" to the heat flux and heat-transfer coefficient, respectively. The net heat flux $\dot{q}''_{net}$ therefore has the significance of some "heat flux through the thermal boundary layer corrected for evaporation effects". The value of Y was determined empirically as follows.

It was assumed that, for the conditions of the present experiment (air and water with T_S and T_B approximately constant), Y was a function only of $\dot{m}''_{a,0}$. Further, it was reasoned that the resistance to the flow of heat through the liquid (and hence α) should be unaffected by the vapour content $F_{v,0}$ of the air and vapour mixture supplied to the test section at the 0-surface. At various fixed values of $\dot{m}''_{a,0}$, the values of $\dot{q}''_S$ and T_B were fixed (as near as experimentally possible) while measurements of T_S were taken with two different $F_{v,0}$ conditions: the smaller value of $F_{v,0}$ was obtained using the laboratory air supply while the larger value of $F_{v,0}$ was obtained by bubbling the air through a tank of water before feeding the air to the test section. The raw data are shown in Fig. D.4. For lines of constant $\dot{m}''_{a,0}$, the value of $\dot{q}''_{elec}$ varies slightly so giving the variation of $T_S - T_B$ with $\dot{m}''_{a,0}$ shown. For each fixed value of $\dot{m}''_{a,0}$, equation (D.30) may be written for the condition obtaining with the smaller and the larger values of $F_{v,0}$; this then gives two simultaneous equations in α and Y, the only two unknowns, in the equations. Thus Y may be evaluated. The

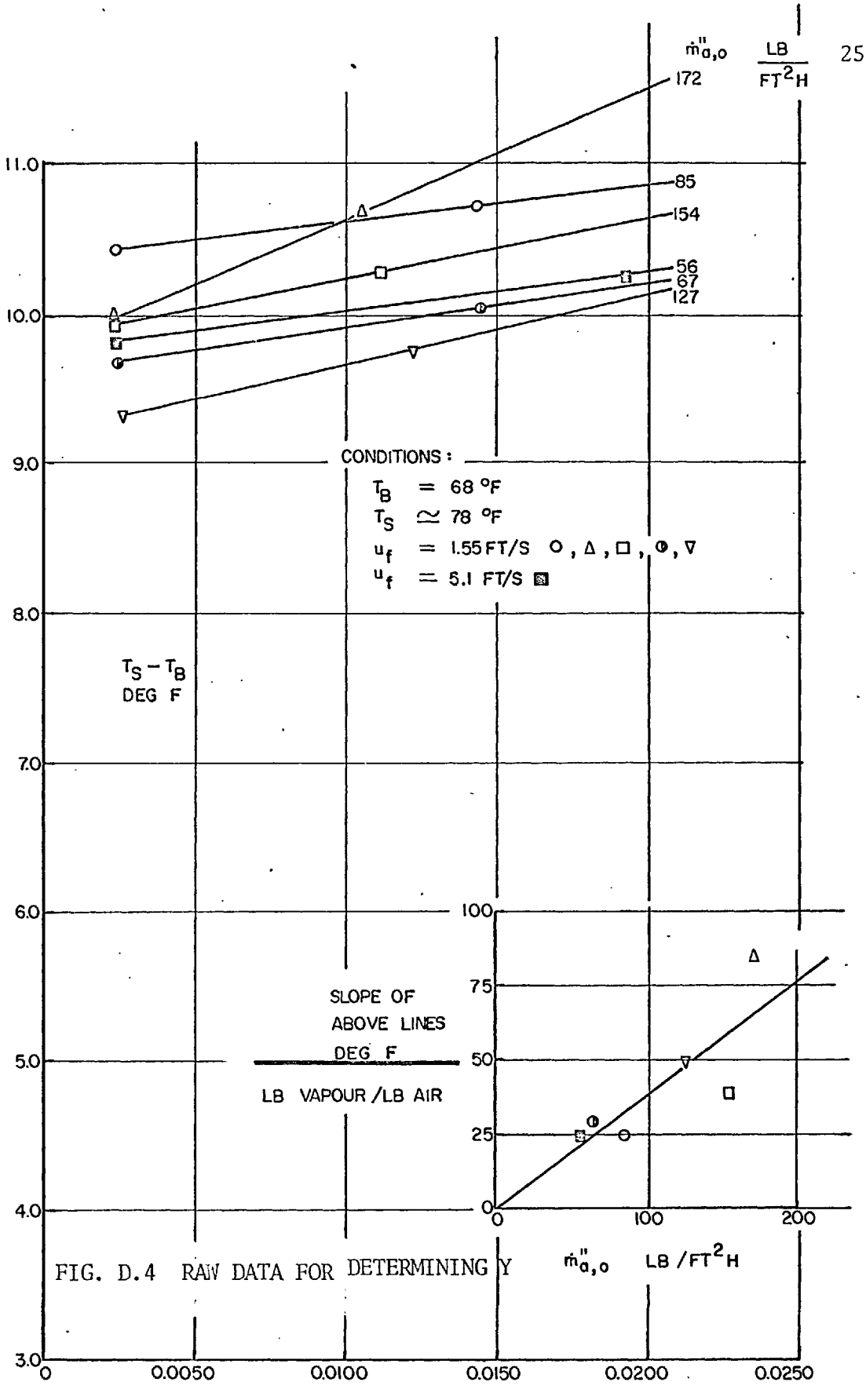

FIG. D.4 RAW DATA FOR DETERMINING Y

FIG. D.4 .

results of evaluating Y in this fashion are shown in Fig. D.5. (The results were evaluated for the thermocouple located at x/L = 0.417.) Data taken by the present investigator in forced convection and the pool data of Akturk [D.4] for water and air at approximately the same surface and bulk conditions as in the present experiment are shown in the figure. A value of Y = 0.65 has been used for the calculations in the present work.

The resulting error in α for errors in Y depends on the value of the parameter $Y \dot{m}''_{a,0} (F_{v,sat\ S} - F_{v,0}) h_{fg}/\dot{q}''_S$. For Y = 0.65 the maximum value of this parameter obtaining in the present experiments was approximately 0.16 and was generally much less than this. Even if the error in Y were as much as 30%, i.e. $0.45 \leqslant Y \leqslant 0.85$ (see Fig. D.5), then the resulting error in α is < 6% for the maximum value of the parameter quoted. For by far the majority of the data, even if the 30% error in Y were allowed, then the value of the parameter was such as to cause from zero to 3% error in α. (When $\dot{m}''_{a,0} = 0$, equations (D.30) and (D.18) reduce to

$$\alpha = \frac{\dot{q}''_{elec}}{T_S - T_B}$$

as indeed they should.)

In making an "evaporation correction" in the heat-transfer coefficient, Kudirka [D.5] used essentially equation (D.30) with Y = 0.60 and $F_{v,0} = 0$.

SYMBOL	AUTHOR	u_f FT/S
o	PRESENT	1.55
□	"	5.1
Δ	AKTURK [D.4]	POOL

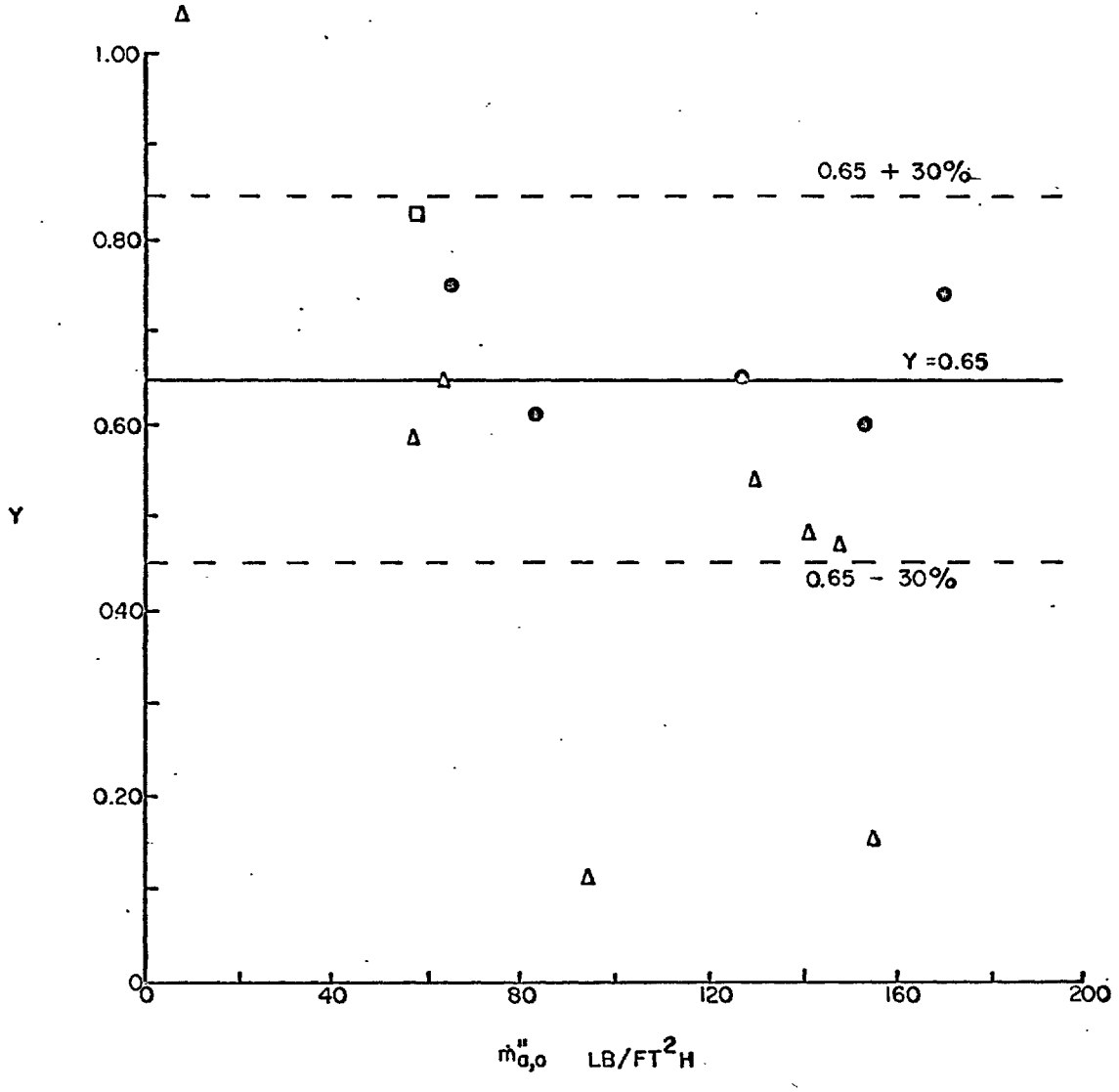

FIG. D.5 EVIDENCE ON Y

The electrical heat flux $\dot{q}''_{elec}$.

The local electrical heat flux $\dot{q}''_{elec}$ (in Btu/ft^{2}h) was calculated from

$$\dot{q}''_{elec} = \frac{3.4128\ F_E\ \Delta E_{overall}\ I}{Lb} \qquad (D.33)$$

where:

F_E is the ratio of the local to the overall heat flux and is discussed in Section D.5,

$\Delta E_{overall}$ is the voltage drop across the porous heater between the two brass electrodes (volts),

I is the current in the porous heater (amps),

L is the length of the porous heater (ft),

b is the width of the porous heater (ft).

Heat losses from the heater to the ambient.

The heat losses from the heater to the ambient were negligible. This was because: the heater temperature was generally within 3 or 4 deg F of the ambient temperature, the contact area of the heater with the sidewalls was small compared with the heat-transfer surface (see Fig. 3.1) and the heater sides were insulated from the ambient through a 1/2-in. thick low-thermal-conductivity material (k of the order of 0.1 Btu/ft h deg F).

D.5 The Ratio F_E of the Local to the Overall Heat Generation Rate

It was expected that the physical construction of the porous material may not be entirely uniform along its length. If there were small changes in the density of the porous material, then this could affect the local heat generation rate.

A quantity was defined

$$F_E \equiv \frac{\Delta E/\Delta x}{\Delta E_{overall}/L} \tag{D.34}$$

where:

ΔE is the electrical potential drop in the porous heater between two points Δx apart in distance,

$\Delta E_{overall}$ is the overall potential drop between the two ends of the heater,

L is the total length of the heater.

It can easily be shown that F_E is also the ratio of the local to the overall heat flux and also the ratio of the local to the overall volumetric heat generation rate. An experiment was performed as follows to find the value of F_E along the length of the porous heater.

A steel rod ending in a sharp point was connected to a sliding vernier gauge. A dc current of 3 - 3 1/2 amperes was passed through the porous heater and the pointed end of the rod was made

to touch the heater at predetermined positions along the heater. The rod was connected electrically to a digital voltmeter (Solartron, type LM 1010.2, resolution $\pm 2 \times 10^{-5}$ volts) which measured the electrical potential along the heater and the overall potential drop $\Delta E_{overall}$ between the brass electrodes at the ends of the heater. The potential-measuring circuit is shown in the inset in Fig. D.6. The test was conducted in situ with the test section assembled.

The results are plotted in Fig. D.6. It was assumed that the gradient $\Delta E/\Delta x$ existed at the mid-point between the measuring points. It is estimated that the accuracy of the measurement of F_E was approximately ±1%. The value of F_E used in the calculation of the local heat-transfer coefficients [F_E appears in equations (D.4) and (D.33)] is shown as the solid line in the figure.

D.6 The $[\alpha/\alpha_{app}]$ Correction

In Section D.2 the reasons for, and the use of, the $[\alpha/\alpha_{app}]$ correction were discussed. It is used for conditions where the gas temperature $T_{g,4}$ approaching the bottom side of the porous element did not equal the temperature T_0 of the lower face of the porous element. This section describes the method of obtaining this correction. The end result is equations (D.35) and (D.37).

During the tests with zero inlet-quality, for each liquid

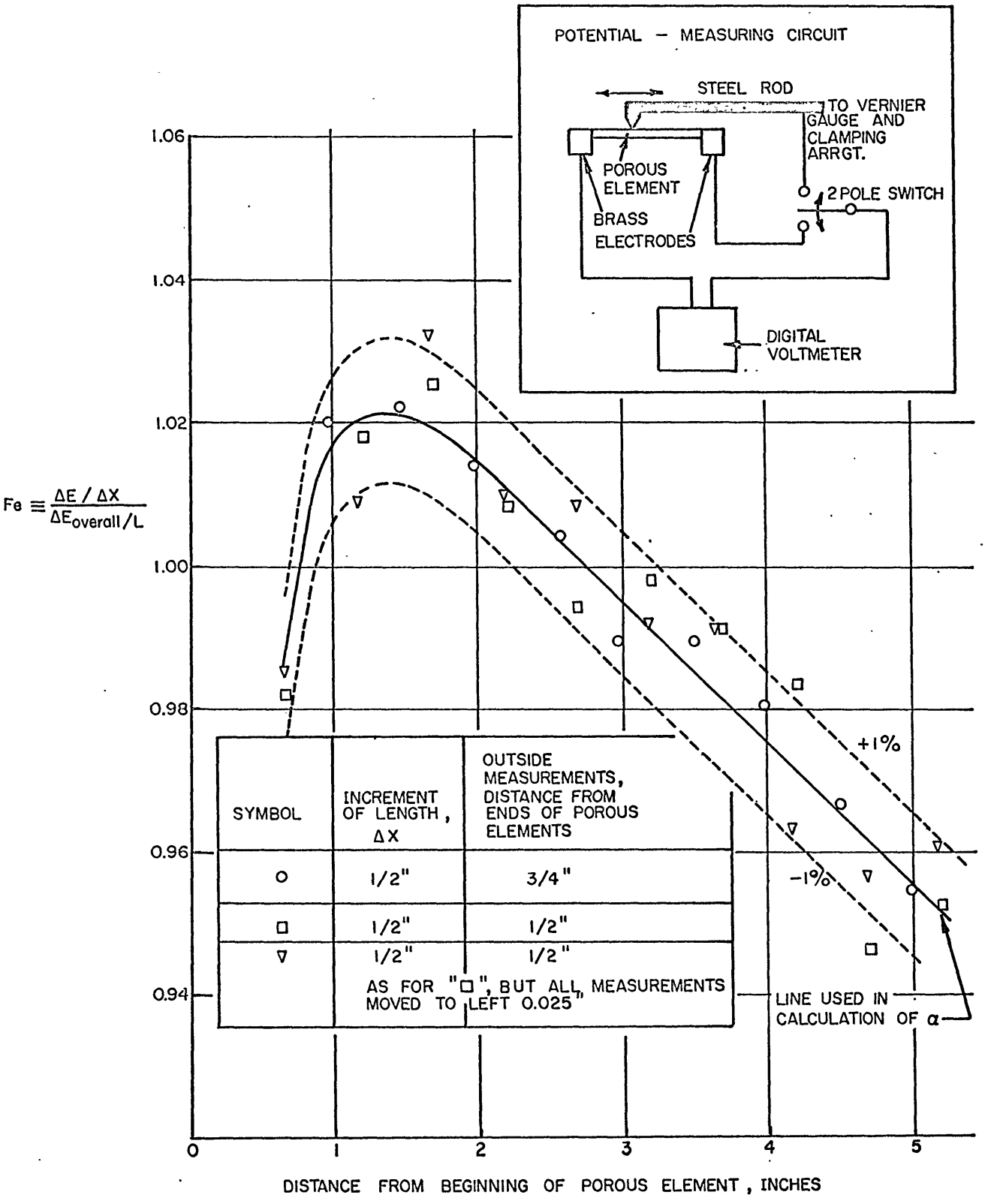

FIG. D.6 LOCAL ELECTRICAL POTENTIAL GRADIENT VS. POSITION ALONG HEATER

FIG. D.6

velocity u_f, the effect of the inequality of $T_{g,4}$ and T_0 was investigated at barbotage-rates $\dot{V}''_g$ of zero and approximately 0.11 and 0.6 ft/s. At each fixed combination of u_f and $\dot{V}''_g$, three sets of data were taken: one for $T_{g,4}$ nearly equal to T_0; one for $T_{g,4} > T_0$ and one for $T_{g,4} < T_0$; in the last two cases the difference between $T_{g,4}$ and T_0 was of the order of 4 to 11 deg F (the difference was obtained by varying the electrical heat flux and hence T_0). For each of these sets of data a value of the "apparent" heat-transfer coefficient was calculated using equation (D.6). The data from one thermocouple position ($x/L = 0.575$) were analyzed; the final relations obtained, namely equations (D.35) and (D.37), were assumed to apply to all the thermocouple positions. For each condition of $\dot{V}''_g$ and u_f the three values of α_{app} were used to obtain a "true" value of α, i.e. that which would obtain when $T_{g,4} = T_0$ (= $T_{0,app}$ in this case). This was done by plotting α_{app} against $(T_{0,app} - T_{g,4})$ and $(T_{0,app} - T_{g,4})/(T_{0,app} - T_{S,app})$ as shown in the sketches in Fig. D.7. The "true" value of α was obtained as the average of α_1, α_2, α_3 and α_4. The rms deviation of α(the "true" α) from α_1, α_2, α_3 and α_4 was only 1.2% for all the conditions covered. The three values of α_{app} for each combination of $\dot{V}''_g$ and u_f then had three corresponding values of α/α_{app}.

It was assumed that the effect of the inequality of $T_{g,4}$ and T_0 could be correlated by an equation of the form

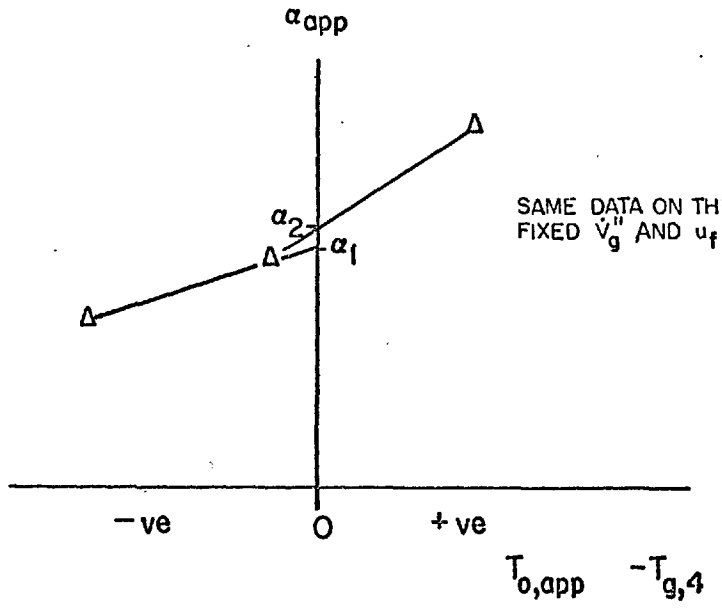

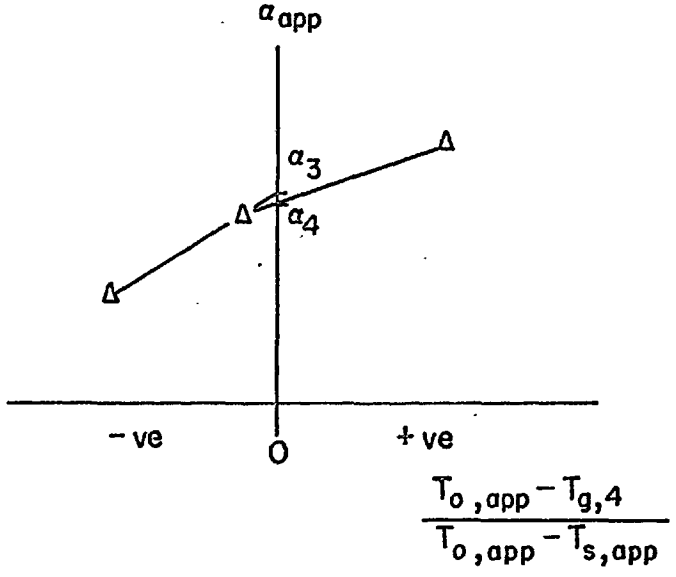

$$\alpha = \frac{\alpha_1 + \alpha_2 + \alpha_3 + \alpha_4}{4}$$

FIG. D.7 METHOD OF OBTAINING TRUE VALUE OF α FROM α_{app} DATA

$$\frac{\alpha}{\alpha_{app}} = 1 - S_\alpha \underbrace{(T_{O,app} - T_{g,4})}_{\text{in deg F}} \qquad (D.35)$$

and that

$$S_\alpha = \phi(\dot{V}''_g,\ T_{O,app} - T_{S,app}) \qquad (D.36)$$

where ϕ indicates "some function of".

In the equation immediately above, $\dot{q}''_{elec}$ could be used instead of $(T_{O,app} - T_{S,app})$ as the latter was directly proportional to the former. The function S_α was found empirically as:

$$\left.\begin{aligned} S_\alpha &= a'(T_{O,app} - T_{S,app})^{b'} \\ \text{where} \\ a' &= 0.009 + 0.16\ \dot{V}''^{0.84}_g \\ b' &= -0.72 - 1.22\ \dot{V}''_g \end{aligned}\right\} \qquad (D.37)$$

$\dot{V}''_g$ is in ft/s,

$(T_{O,app} - T_{S,app})$ is in deg F.

The experimental results are shown in Fig. D.8 together with the correlating equations (D.35) and (D.37). Within the ±2% deviation lines are contained 80% of the data, which is considered satisfactory for the present purposes.

The above analysis was performed using data obtained from

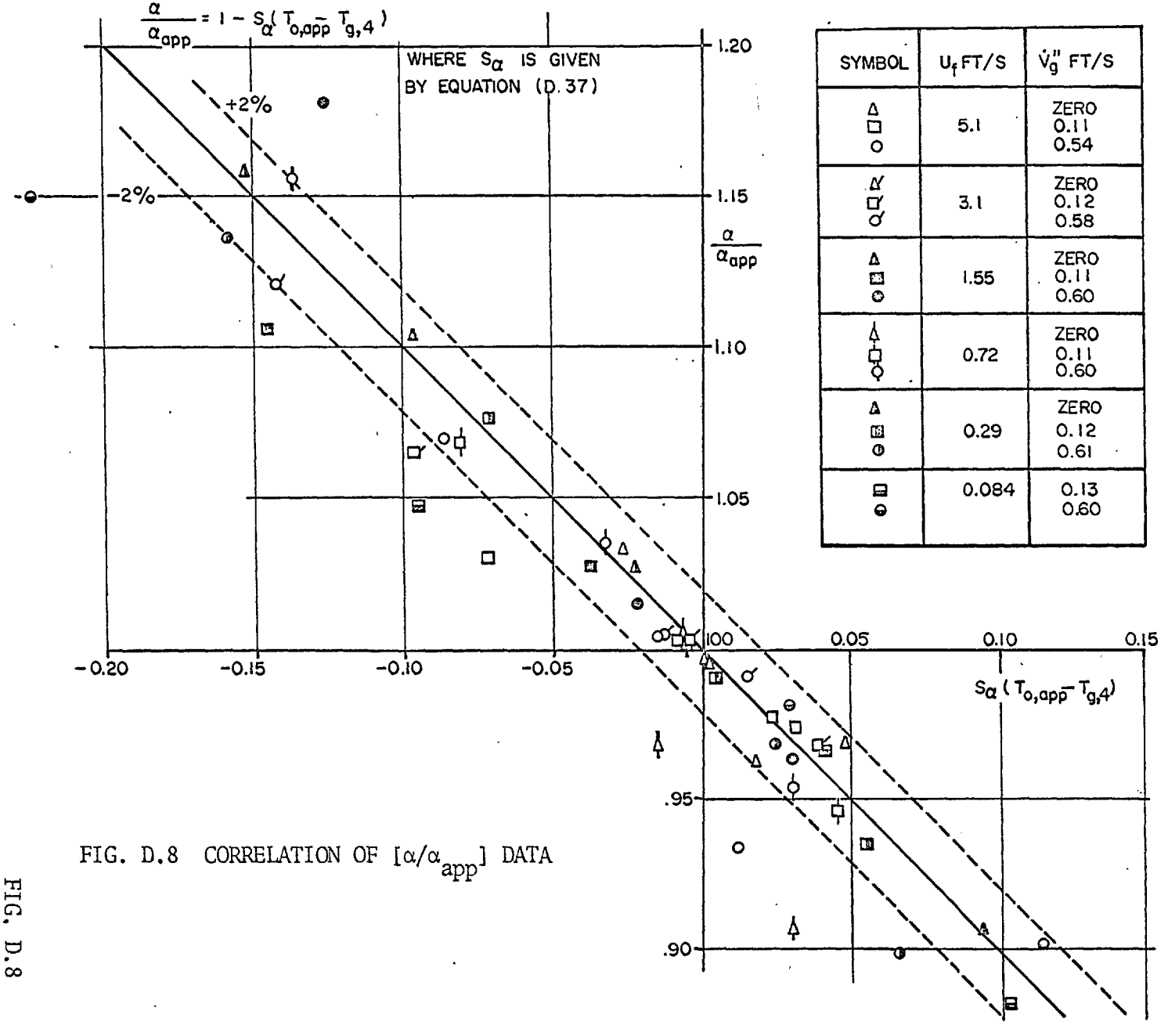

FIG. D.8 CORRELATION OF $[\alpha/\alpha_{app}]$ DATA

FIG. D.8

zero-inlet-quality tests. The correlating equations (D.35) and (D.37) were applied to the finite-inlet-quality tests as well. The implied assumption is, of course, that conditions in the flow channel per se do not affect the $[\alpha/\alpha_{app}]$ correction.

The present method of obtaining α/α_{app} is admittedly crude. However, for the data reported in this thesis the magnitude of this correction is small and does not warrant a more sophisticated approach. As mentioned in Section D.2, the magnitude of the $[\alpha/\alpha_{app}]$ correction in the local heat-transfer coefficients was generally between 0.97 and 1.03. Generally too, for any setting of the liquid velocity, barbotage-rate and the inlet-quality, the values of α/α_{app} for the various thermocouple locations along the porous element were both greater than, and less than, 1, so making the net correction in the mean heat-transfer coefficient negligibly small.

D.7 Summary of the Calculation Procedure for the Heat-Transfer Coefficient

The important equations used in the calculation of the heat-transfer coefficients are listed in Table D.1 together with an indication of where in the text the definitions of the symbols may be found.

The following quantities were measured: $T_{O,app}$, $\Delta E_{overall}$, I, $\dot{m}''_{a,O}$, $F_{v,O}$, L, b, δ, $T_{B,e}$ and $T_{B,i}$ (for more rigour, see Section D.3). The quantity k_{eff} was known (see Appendix B).

Table D.1 Summary of the Important Equations Used in the Calculation of the Heat-Transfer Coefficient

Equation no.	Equation	Symbols defined in text below equation no.
D.7	For local heat-transfer coefficient $\alpha = \alpha_{app} \left[\frac{\alpha}{\alpha_{app}}\right]$	D.5
	$\left[\frac{\alpha}{\alpha_{app}}\right]$ from equations (D.35) and (D.37)	
D.6	$\alpha_{app} = \frac{\dot{q}''_{net}}{T_{S,app} - T_B}$	D.2, D.5
D.32	$\dot{q}''_{net} = \dot{q}''_S - Y \dot{m}''_{a,0}(F_{v,sat\ S} - F_{v,0})h_{fg}$	D.20, D.29
	$Y = 0.65$	
D.18	$\dot{q}''_S = \dot{q}''_{elec} - \dot{m}''_{a,0}(h_{a,S} - h_{a,0})$	above D.18
D.33	$\dot{q}''_{elec} = \frac{3.4128\ F_E\ \Delta E_{overall}\ I}{Lb}$	D.33
	F_E from Fig. D.6	
D.5	$T_{S,app} = T_{0,app} - \frac{\dot{q}'''_{elec}\delta^2}{2k_{eff}}$	D.5, D.3

Table D.1 Continued

D.4	$\dot{q}'''_{elec} = \frac{\dot{q}''_{elec}}{\delta}$	D.3
D.8	$T_B = T_{B,i} + \frac{x}{L}(T_{B,e} - T_{B,i})$ Further details in Section D.3.	D.8
	For mean heat-transfer coefficient	
D.1	$\bar{\alpha} = \frac{1}{L}\int_0^L \alpha \, dx$ See Section D.1.	D.1

From equation (D.33) and (D.4) $\dot{q}''_{elec}$ and $\dot{q}'''_{elec}$, respectively, were calculated. Then $T_{S,app}$ was calculated from equation (D.5). Next $\dot{q}''_S$ and $\dot{q}''_{net}$ were calculated from equations (D.18) and (D.32) respectively; $F_{v,sat\ S}$ and $h_{a,S}$ were obtained knowing approximately T_S ($T_{S,app}$ was used for T_S for these last two mentioned quantities and the air temperature at the S-surface was assumed equal to the S-surface-temperature of the porous element); $h_{a,O}$ was obtained using $T_{O,app}$ as the air temperature at O-surface. The quantity T_B was calculated from equation (D.8). Then α_{app} and α were calculated from equations (D.6) and (D.7) respectively. The preceding calculations were performed for α for the various thermocouple positions along the porous heater. Finally $\bar{\alpha}$ was calculated using equation (D.1); see Section D.1 for more detail.

D.8 Calculation of the Barbotage-Rate $\dot{V}''_g$

The barbotage-rate reported in this thesis is a mean $\dot{V}''_g$ obtained in the following manner (for fixed conditions of u_f, $u_{g,i}$ and $\dot{V}''_g$). First, for each thermocouple position, a $\dot{V}''_g$ was calculated from

$$\dot{V}''_g = \frac{\dot{m}_{g,O}}{A_p \rho_g} \tag{D.38}$$

where:

A_p is the projected area of the porous surface;

$\dot{m}_{g,O}$ is the gas flow rate (air and vapour mixture) to the porous section; the gas flow rate per unit area of

porous surface is, of course, $\dot{m}''_{g,0} \equiv \frac{\dot{m}_{g,0}}{A_p}$

and is related to the previously-used air and vapour flow rates per unit area of porous surface $\dot{m}''_{a,0}$ and $\dot{m}''_{v,0}$ respectively, according to $\dot{m}''_{g,0} = \dot{m}''_{a,0} + \dot{m}''_{v,0}$;

ρ_g is the density of the gas based on the local pressure in the channel (assuming a linear pressure drop in the channel between the inlet to, and the exit from, the porous section) and the local wall temperature T_S; ρ_g was evaluated from relations for dry air.

Then the mean of these values of $\dot{V}''_g$ was taken and this is the value reported in this thesis. The largest deviation of any value of $\dot{V}''_g$, as obtained using equation (D.38), from the mean $\dot{V}''_g$ was 2 1/2% and occurred for the combination of largest u_f, largest $u_{g,i}$ and largest $\dot{V}''_g$.

The effect of evaporation into the air at the S-surface was neglected (evaporation would affect both the gas flow rate and ρ_g) as the amount of evaporation was unknown. However, the worst possible error in $\dot{V}''_g$ due to this effect would have been approximately 3%.

For fixed conditions of u_f, $u_{g,i}$ and $\dot{V}''_g$ the pressure in the plenum chamber P_{plen} (beneath the porous element) was constant while there was a drop in pressure ΔP_{chan} along channel from the entrance to, to the exit from, the porous section. It would therefore

be expected [D.5] that the local barbotage rate along the channel would change somewhat because the pressure drop across the porous element (between the plenum chamber and the flow channel) would vary with position along the channel (see sketch below).

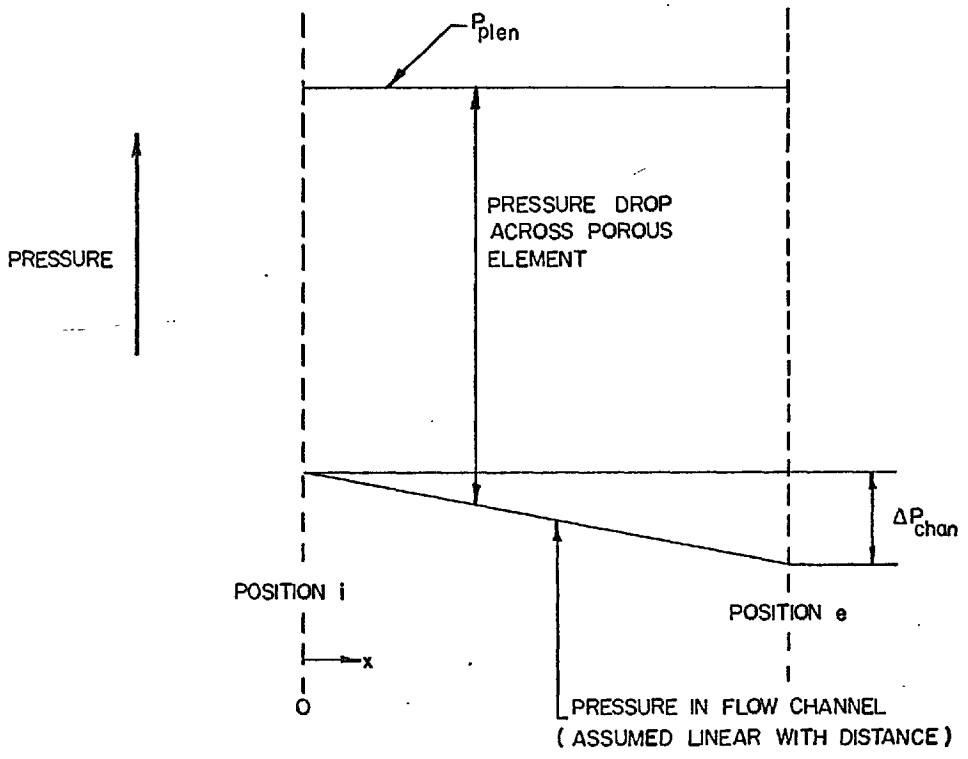

SKETCH OF PRESSURES FOR POROUS ELEMENT

The maximum deviation of the local barbotage rates at positions i (inlet) and e (exit) from the mean was approximately 20% (assuming the local $\dot{V}''_g$ was proportional to the pressure drop across the porous element [D.5]) and occurred for the combination of largest u_f, largest $u_{g,i}$ and smallest finite $\dot{V}''_g$.

D.9 Calculation of the Liquid Velocity u_f

The liquid velocity u_f was calculated from

$$u_f = \frac{Q_f}{A_T} \tag{D.39}$$

where:

Q_f is the volumetric flow rate of water to the test section,

A_T is the total cross-sectional area of the flow channel.

Any changes in u_f due to evaporation of water into the air in the flow channel were extremely small (worst case, 0.3% change) and hence were neglected.

D.10 Calculation of the Gas Velocity at Inlet to the Porous Section $u_{g,i}$

The gas velocity at inlet to the porous section $u_{g,i}$ was calculated from

$$u_{g,i} = \frac{\dot{m}_{g,3}}{A_T \rho_{g,i}} \tag{D.40}$$

where:

$\dot{m}_{g,3}$ is the mass flow rate of gas (air and vapour) to the upstream air injector (see Fig. D.1);

A_T is the total cross-sectional area of the flow channel;

$\rho_{g,i}$ is the density of the gas at the inlet to the heated porous section; $\rho_{g,i}$ was calculated using relations for

dry air at the bulk temperature $T_{B,i}$ and at the pressure ρ_i at entrance to the porous section.

The effect on $u_{g,i}$ of evaporation of water into the air between the inlet to the upstream injector and the inlet to the heated porous section (see Fig. D.1) was neglected [evaporation would affect both the gas (air and vapour) mass flow rate and the gas density]. The maximum error due to neglecting this effect was 2%.

References for Appendix D

D.1 D.B. Spalding, Graphical method of calculating heat transfer, condensation and vaporization rates in processes involving water-steam-air mixtures, Proc. I. Mech. E., 172, 839-864 (1958).

D.2 E.E. Gose, Heat transfer to liquids with gas evolution at the interface, Ph.D. Dissertation, University of California, Berkeley (1960).

D.3 N.U. Akturk, Heat transfer from a heated porous surface to a pool of liquid with gas injection at the interface, Proceedings of the Symposim on Two Phase Flow, Vol. II, pp. D501-520 (1965).

D.4 N.U. Akturk, Personal communication.

D.5 A. A. Kudirka, Two-phase heat transfer with gas injection through a porous boundary surface, U.S. Atomic Energy Commission report ANL-6862 (1964).

APPENDIX E ERROR ANALYSIS AND REPEATABILITY

This appendix deals with two main topics, namely error analysis and repeatability. Calibration curves are presented where appropriate in the section on error analysis.

E.1 Error Analysis

The method of estimating the accuracy of the measured quantities and of the calculated results proceeds according to the method of Kline and McClintock [E.1]. The most important results are summarized in Table E.1.

Kline and McClintock [E.1] conclude that, where a "result" R is a function of variables $v_1, v_2, \ldots v_n$ and the "uncertainty interval*" ω_i in any variable v_i is known, or estimated, based on certain "odds" (more about this below), then the uncertainty interval ω_R in the result should be obtained from

$$\omega_R = \left[\left(\frac{\partial R}{\partial v_1} \omega_1 \right)^2 + \left(\frac{\partial R}{\partial v_2} \omega_2 \right)^2 + \ldots + \left(\frac{\partial R}{\partial v_n} \omega_n \right)^2 \right]^{1/2} \quad \text{(E.1)}$$

CONT. ON NEXT PAGE

*In the terminology of Kline and McClintock [E.1], "uncertainty" is the possible value the "error" might have; the "error" is the difference between the true and observed value for a single observation. In the present appendix, this terminology is generally followed. In the body of the thesis and in the other appendices, however, as is common usage, "error" is used synonymously with "uncertainty".

or in alternate form,

CONT. FROM PREVIOUS PAGE

$$\frac{\omega_R}{R} = \{[\omega_1 \frac{\partial}{\partial v_1}(\ln R)]^2 + [\omega_2 \frac{\partial}{\partial v_2}(\ln R)]^2 + \ldots + [\omega_n \frac{\partial}{\partial v_n}(\ln R)]^2\}^{1/2} \quad \text{(E.1)}$$

The "odds" mentioned above are the odds that the experimenter is willing to wager that any given reading lies within $\pm\omega_i$ of the true value. In the present case the uncertainty interval in each variable is quoted for odds of approximately 20 to 1. In equation (E.1) the odds on the variables and in the result are the same.

Table E.1 Summary of Estimated Uncertainties in the Main Measured Variables

Variable	Uncertainties (±)
Mean heat-transfer coefficient, $\bar{\alpha}$	For $\bar{\alpha} < 3000$ Btu/ft^2 h deg. F (92% of the data): 4 - 10% *
Barbotage-rate, $\dot{V}''_g$	$\dot{V}''_g \geq 0.025$ ft/s: 3.7% $\dot{V}''_g < 0.025$ ft/s: 10% or less
Water velocity, u_f	2.5%
Gas velocity in the channel at entrance to the heated porous section, $u_{g,i}$	3.2%

* See footnote next page.

Uncertainty in the mean heat-transfer coefficient $\bar{\alpha}$.

Equation (E.1) may be applied to each of the equations used in calculating the heat-transfer coefficient; the uncertainty interval ω_i for each of the variables and the resulting uncertainty intervals in the intermediate results (e.g. $\dot{q}''_{elec}$) and in the mean heat-transfer coefficient $\bar{\alpha}$ are shown in Table E.2.

The range of uncertainty in the mean heat-transfer coefficients is between approximately 4 and 20%. The largest uncertainties are for large values of the heat-transfer coefficient (the uncertainty increasing with heat-transfer coefficient); for these conditions the uncertainty in k_{eff} dominates the error in $\bar{\alpha}$. The smallest uncertainties are for small heat-transfer coefficients in combination with small $\dot{V}''_g$. For 92% of the data ($\bar{\alpha}$ < 3000 Btu/ft^2 h deg F) the uncertainty is between approximately 4 and 10% for $\bar{\alpha}$.

---

*The uncertainty generally increases with increasing $\bar{\alpha}$; for the worst case ever ($\bar{\alpha}$ ≈ 7100 Btu/ft^2 h deg F), the uncertainty is approximately 20%.

Table E.2 Uncertainty Intervals in the Variables Affecting the Mean Heat-transfer Coefficient

Variable v_i	Uncertainty interval based on approximately 20 to 1 odds ω_i or $\frac{\omega_i}{v_i}$ (±)	Comment
$\Delta E_{overall}$	1 1/2%	Voltmeter calibrated against standard Weston Model S68, No. W91610 dynamometer voltmeter (accuracy 1/2% of full scale deflection); over the range of scale used, the worst accuracy was approximately 1 1/2%. The voltmeter calibration curve is given in Fig. E.1.
I	1 1/2%	Ammeter calibrated against standard Weston Model S69, No. AD 48243 dynamometer ammeter (accuracy 1/4% of full scale deflection); calibration set-up involved Weston Model 461, No. 4601 current transformer (accuracy 1/4%); worst combined accuracy of standard ammeter and current transformer over the range of scale used was approximately 1 1/2%. The ammeter calibration is given in Fig. E.2.
F_E	1%	See evidence in Fig. D.6.
L	0.01 in.	
b	0.001 in.	
δ	0.0005 in.	
x	0.005 in.	
Y	30%	See evidence in Fig. D.5.

Table E.2 (Cont.)

Variable v_i	Uncertainty interval based on approximately 20 to 1 odds ω_i or $\frac{\omega_i}{v_i}$ (±)	Comment
$T_{O,app}$	0.2 deg F	Thermocouple wire was calibrated by the author, (see Section 3.2.3). Uncertainty quoted includes any uncertainty due to dc component in the main ac heating circuit (see Appendix C) and uncertainties due to the measuring circuit.
k_{eff}	12%	See Appendix B.
$T_{B,i}$	0.2 deg F	Thermocouples calibrated by author. Uncertainty quoted includes any variations in inlet water temperature and uncertainties due to the measuring circuit. The uncertainty mentioned does not include any error due to heat gain from the ambient to the water traversing the test section; for the worst case (the lowest liquid velocity, u_f = 0.084 ft/s) the error in $\bar{\alpha}$ due to this effect would be approximately 3/4%. When combined with other uncertainties, the resulting uncertainty in $\bar{\alpha}$ is practically unchanged compared with neglecting this effect.
$T_{B,e}$	0.2 deg F	Comment as for $T_{B,i}$.
$[\alpha/\alpha_{app}]$	2%	See evidence in Fig. D.8.
Resulting uncertainties.		
$\dot{q}''_{elec}$	2.38%	From equation (E.1) applied to equation (D.33).
$\dot{q}''_S$	2.38%	See equation (D.18); error in $\dot{q}''_{elec}$ completely dominates.

Table E.2 (Cont.)

Variable v_i	Uncertainty interval based on approximately 20 to 1 odds ω_i or $\frac{\omega_i}{v_i}$ (±)	Comment
Resulting uncertainties (cont.)		
$\dot{q}''_{net}$	2.38 - 7.60%	In equation (D.32), only the uncertainties in Y and $\dot{q}''_S$ are significant. The uncertainty of 7.60% is the worst possible and occurs for the combination of highest $\dot{V}'''_g$ and lowest heat-transfer coefficient.
$T_{S,app}$	0.20 - 0.71 deg F	From equation (E.1) applied to equation (D.5). The smallest uncertainties are for small heat fluxes (and small heat-transfer coefficients) where the uncertainty in $T_{S,app}$ is dominated by the uncertainty in $T_{O,app}$; the largest uncertainties are for the largest heat fluxes (and heat-transfer coefficients) where the uncertainty in k_{eff} dominates the uncertainty in $T_{S,app}$. At the highest heat-transfer coefficients it wasn't possible to maintain 10 deg. F difference between the wall and bulk temperatures because of the power limitation of the voltage stabilizer (constant-voltage transformer). In the extreme case, the difference between the wall and bulk temperatures at the various thermocouple locations ranged between 2.24 and 4.57 deg F. The range of uncertainties quoted here include any errors due to using equation (D.5), derived from equation (A.5) as opposed to using an equation, the analog of (D.5), but derived from the slightly more rigorous equation (A.4). (See short discussion at the end of Appendix A.)

Table E.2 (Cont.)

Variable v_i	Uncertainty interval based on approximately 20 to 1 odds. ω_i or $\frac{\omega_i}{v_i}$ (±)	Comment
Resulting uncertainties (cont.)		
T_B	0.2 deg. F	From equation (E.1) applied to equation (D.8).
α_{app}	3.70 - 20.4%	From equation (E.1) applied to equation (D.6). The smallest uncertainties in α_{app} occur when the heat-transfer coefficient is the smallest in combination with small $\dot{V}''_g$, in which case uncertainties in $T_{O,app}$, T_B and $\dot{q}''_{elec}$ control the uncertainties in α_{app}; the largest uncertainties in α_{app} occur when the heat-transfer coefficient is the largest, in which case the uncertainty in α_{app} is dominated by the uncertainty in k_{eff}. The larger value quoted at the left is for a heat-transfer coefficient of 7104 Btu/ft^2 h deg. F, the highest value of the mean heat-transfer coefficient encountered in this investigation.
α	4.2 - 20.5%	From equation (E.1) applied to equation (D.7). Comment as for α_{app} except that for the smallest uncertainties in α, the uncertainty in $[\alpha/\alpha_{app}]$ is also significant.
$\bar{\alpha}$	approximately 4 - 20%	For the conditions tested, the uncertainties in $\bar{\alpha}$ are approximately the same as for α.

○ INCREASING VOLTAGE FIRST TIME
△ DECREASING " " "
□ INCREASING VOLTAGE SECOND TIME
▽ DECREASING " " "

E_{std} = VOLTAGE READ ON STANDARD VOLT METER
E = VOLTAGE ON VOLTMETER USED IN APPARATUS, AS READ

CALIBRATED VOLT METER DESCRIBED IN ITEM 29, TABLE F.2, APPENDIX F

STANDARD VOLTMETER: WESTON MODEL S68, NO. W91610 DYNAMOMETER TYPE 0/3, 0/7.5, 0/15 VOLTS
ACCURACY ±1/2% FULL SCALE VALUE.

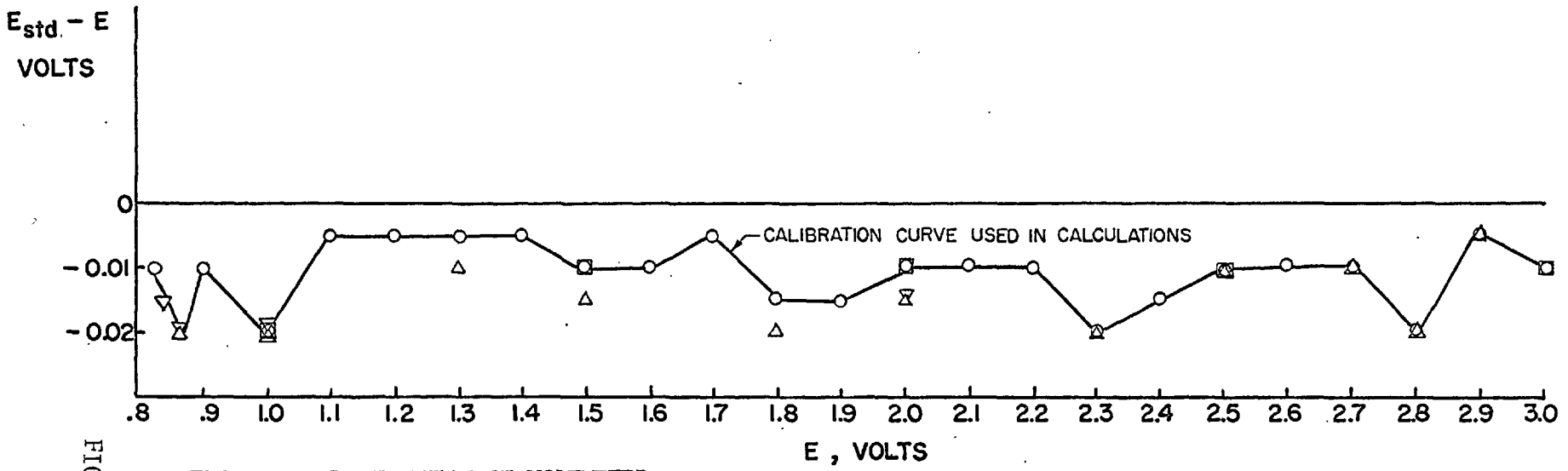

FIG. E.1 CALIBRATION OF VOLTMETER

FIG. E.1

CALIBRATED AMMETER DESCRIBED IN ITEM 28, TABLE F.2, APPENDIX F.

STANDARD AMMETER:
WESTON MODEL S69, NO. AD48243
DYNAMOMETER TYPE, 0/2.5, 0/5 AMPS,
ACCURACY ±1/4% OF FULL SCALE VALUE.
STANDARD CURRENT TRANSFORMER:
WESTON MODEL 461, NO. 4601
ACCURACY ± 1/4 % .

I_{std} = AMPERAGE READ ON STANDARD AMMETER
I = AMPERAGE READ ON AMMETER USED IN APPARATUS

SYMBOL	CURRENT TRANSFORMER RATIO	RANGE ON STD. AMMETER	INCREASING OR DECREASING AMPERAGE
○	4	5	INC.
□	10	5	ISOLATED PT.
△	10	2.5	INC.
◔	10	5	INC.
◒	10	5	DEC.
◑	4	5	DEC.
▣	4	2.5	INC.

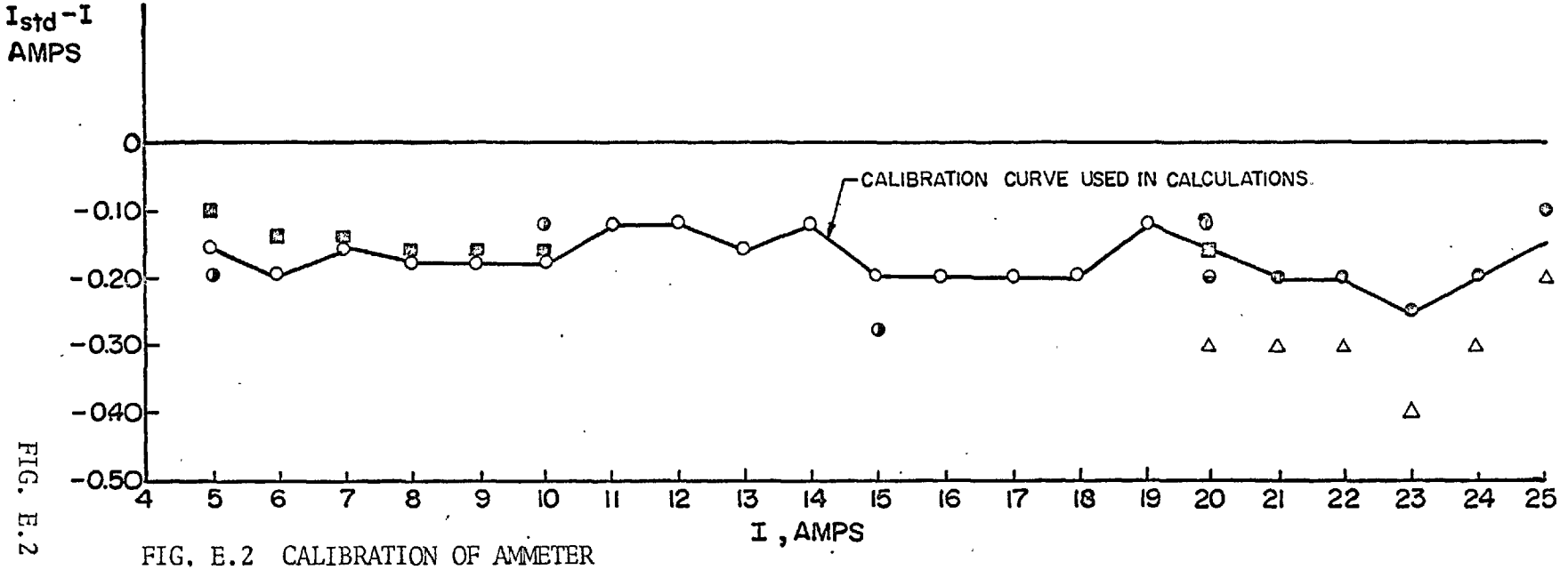

FIG. E.2 CALIBRATION OF AMMETER

FIG. E.2

Uncertainty in the barbotage-rate $\dot{V}''_g$.

Gas (air and vapour mixture, or loosely "air") flow rates to the test section were measured by means of a 1/16 in. orifice. The calculation procedure outlined in British Standard 1042 [E.2] was followed and generally the terminology from that document is used below. The gas flow rate ($\dot{m}_{g,0}$ of Section D.8) in lb/h is given by

$$\dot{m}_{g,0} = 359.1\ C\ Z\ d_{or}^2\ E\ \sqrt{h\rho_{or}} \qquad \text{(E.2)}$$

where:

$$Z = C_D\ C_{Re}\ \varepsilon$$

$$E = \frac{1}{\sqrt{1 - m^2}}$$

$$m = \left(\frac{d_{or}}{d_{pipe}}\right)^2$$

C is the coefficient of discharge,

C_D is the correction for pipe size,

C_{Re} is the Reynolds number correction,

ε is the correction for expansion,

d_{or} is the diameter of the orifice (in inches in equation (E.2)),

d_{pipe} is the diameter of the pipe in which the orifice is installed,

h is the pressure drop across the orifice, inches of water at 60°F,

ρ_{or} is the gas density at the high-pressure orifice tapping, lb/ft^3,

E is the velocity of approach factor.

The factors C, C_D and E depend only on the geometry of the orifice arrangement, while C_{Re} depends on the geometry and Re_{or} the Reynolds number based on the orifice diameter; these may be combined thus

$$K \equiv C\, C_D\, E\, C_{Re}$$

in which case equation (E.2) becomes

$$\dot{m}_{g,O} = 359.1\, K\, \varepsilon\, d_{or}^2 \sqrt{h\rho_{or}} \qquad \text{(E.3)}$$

The orifice was calibrated using a "wet-meter" (Alex Wright, 1/12 ft^3/rev, No. AW 1685, accuracy 1/4 to 1/2% depending on flow rate), the results being shown in Fig. E.3. For computer calculations, equations were fitted by hand to the data and are

$$\left.\begin{aligned} 0 < Re_{or} < 300, \quad & K = 0.00066\, Re_{or} + 0.464 \\ Re_{or} \geqslant 300, \quad & K = 0.646 - (2.1 \times 10^{-6}) Re_{or} + \frac{5.0}{Re_{or}} \end{aligned}\right\} \qquad \text{(E.4)}$$

In Ref. E.3 examples are shown of orifice curves which qualitatively have the same shape (but smoothed, of course).

Consider first the case for $\dot{V}''_g \geqslant 0.025$ ft/s; this covers all the data (453 data points) except for nine data points. For

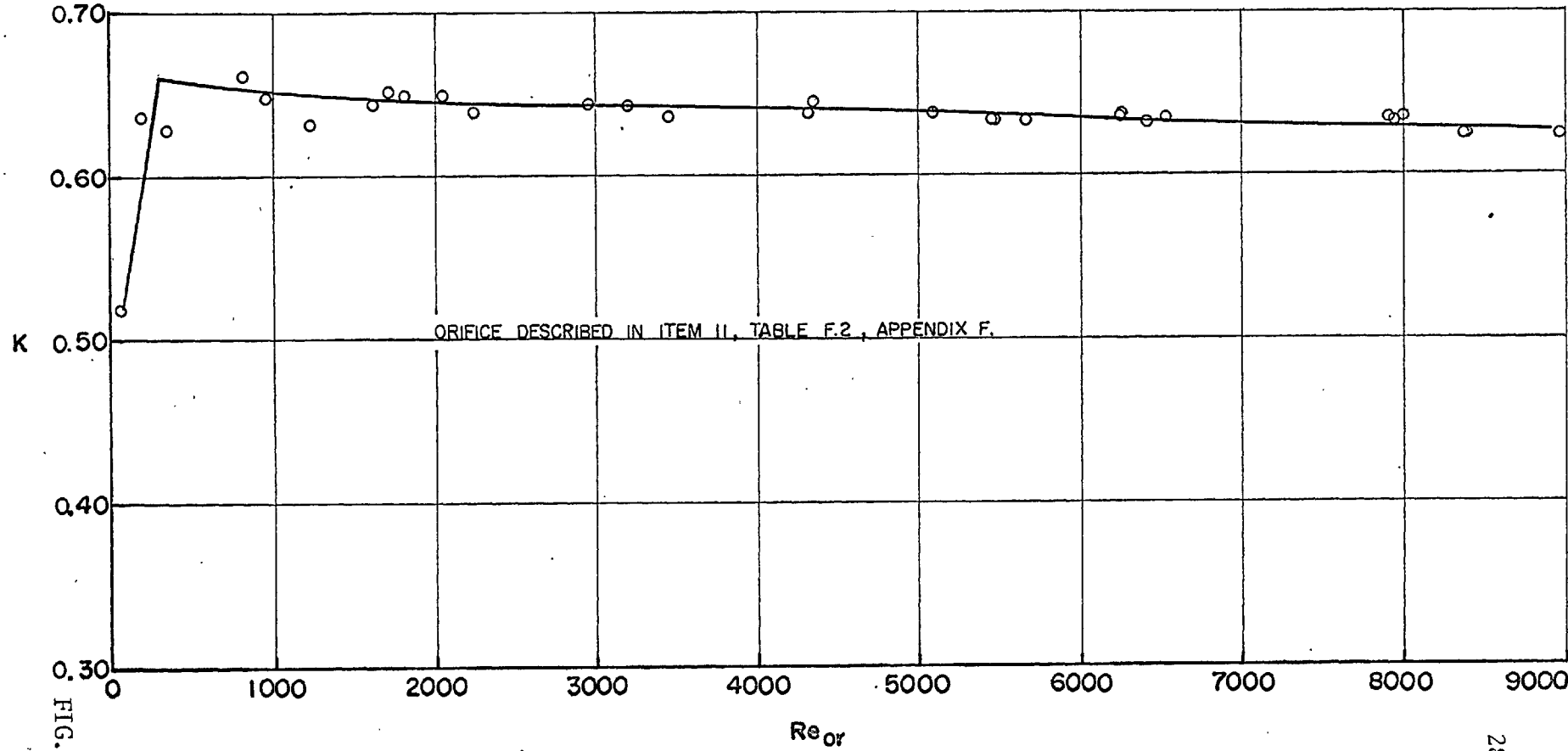

FIG. E.3 CALIBRATION OF ORIFICE FOR MEASURING BARBOTAGE GAS FLOWS

FIG. E.3

these conditions ($Re_{or} > 380$), it is estimated that the uncertainty in K is approximately 2%. In using equation (E.3) for calculating $\dot{m}_{g,O}$, the only significant uncertainties are in K and h (h was read on a vertical water manometer or on a micromanometer depending on the gas flow rate). The uncertainty in h depends on the magnitude of h. For $\dot{V}''_g \geq 0.025$ ft/s, this uncertainty is less than 4%. Applying equation (E.1) to (E.3) and combining with an uncertainty of 2% in K yields an uncertainty in $\dot{m}_{g,O}$ of 2.83%. For an uncertainty of 0.01 in. in the length, and 0.001 in. in the width of the porous heater, this produces an uncertainty of 0.43% in the projected area A_p. On applying equation (E.1) to (D.38), with no significant uncertainty in ρ_g (ρ_g was evaluated using relations for dry air, but see further details below) and with the uncertainties in $\dot{m}_{g,O}$ and A_p mentioned above, there results an uncertainty in $\dot{V}''_g$ of 2.9%.

For $\dot{V}''_g < 0.025$, a case which includes only nine of the 453 data points, the estimated uncertainty in $\dot{V}''_g$ is of the order of 9 1/2% or less.

In the above analysis, reference has been made to the uncertainties in the measurements for $\dot{V}''_g$; no mention was made of the effect on $\dot{V}''_g$ of evaporation into the air at the S-surface, i.e. at the solid-liquid interface (it is at the S-surface conditions that we are attempting to evaluate $\dot{V}''_g$). Evaporation affects both gas density and the gas flow rate. It is impossible to know how much

evaporation occurs at the S-surface, but the worst possible error due to this effect in the flow rate would be 1.9% and in the gas density would be 1.3% (this corresponds to the condition of air saturated with vapour at the S-surface temperature). If these are included in the uncertainty analysis for $\dot{V}''_g \geq 0.025$ ft/s there results the uncertainties: in the mass flow rate of 3.4%, in the gas density of 1.3% and in the projected area of 0.43% (as before); when these are combined in the appropriate manner, the resulting uncertainty in $\dot{V}''_g$ is 3.7%. The uncertainty in $\dot{V}''_g$ for $\dot{V}''_g < 0.025$ ft/s would be approximately 10% or less.

Uncertainty in the liquid velocity u_f.

The water flow rate to the test section was measured on one of two Rotameters in parallel, depending on the flow rate. The Rotameters were calibrated at the flow rates corresponding to the liquid velocities used in the experimental program. The method of calibration was to accurately time the flow of a known weight of water using an open tank situated on a weigh-scale (itself calibrated) for the collection and weighing of the water. The results of the calibration are shown in Figs. E.4 and E.5. It is estimated that the uncertainty in the individual volumetric flow rates (i.e. each datum point shown) is approximately 1 1/2%.

The uncertainty in the cross-sectional area is 2.0%

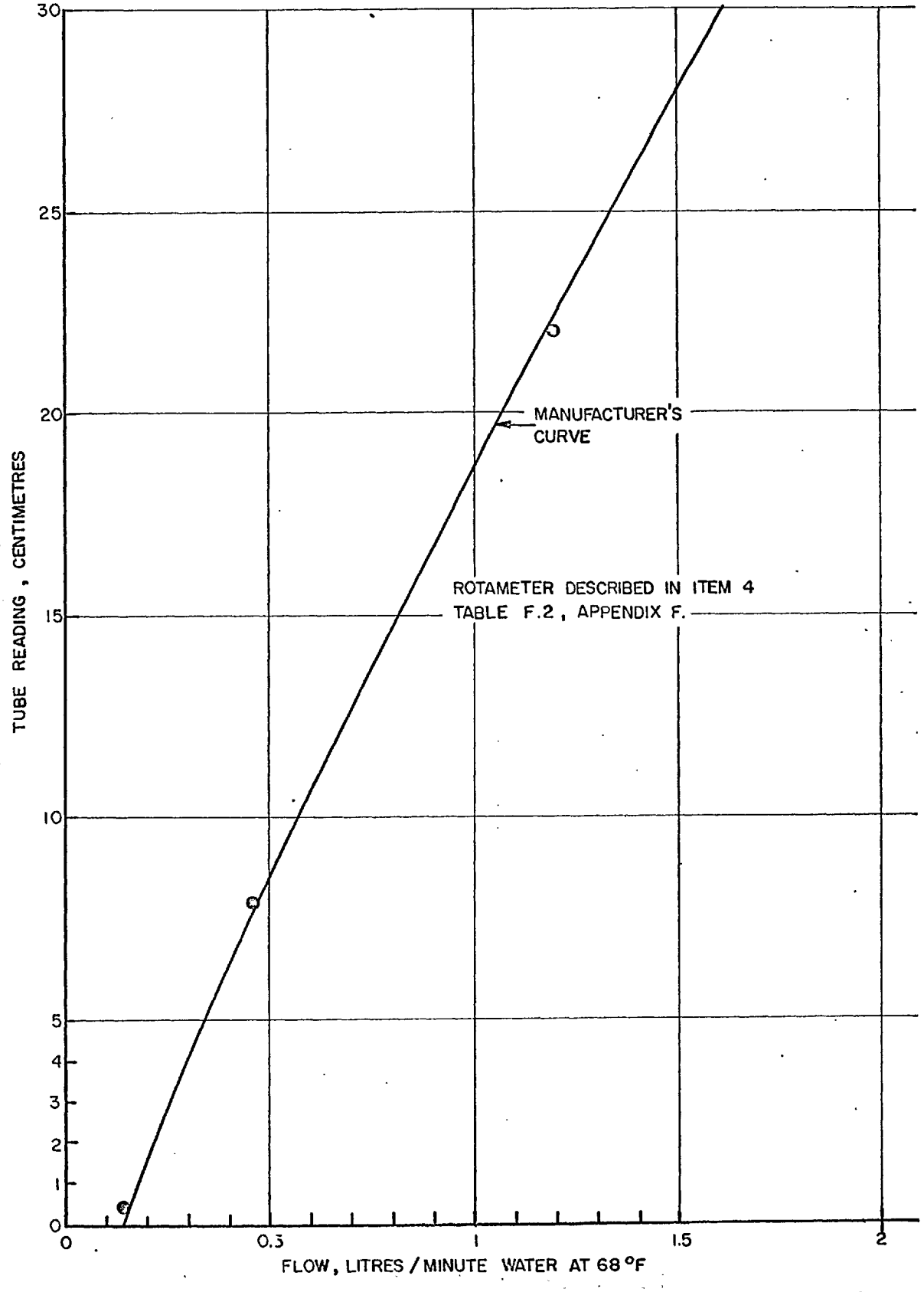

FIG. E.4

FIG. E.4 CALIBRATION OF SMALL WATER ROTAMETER

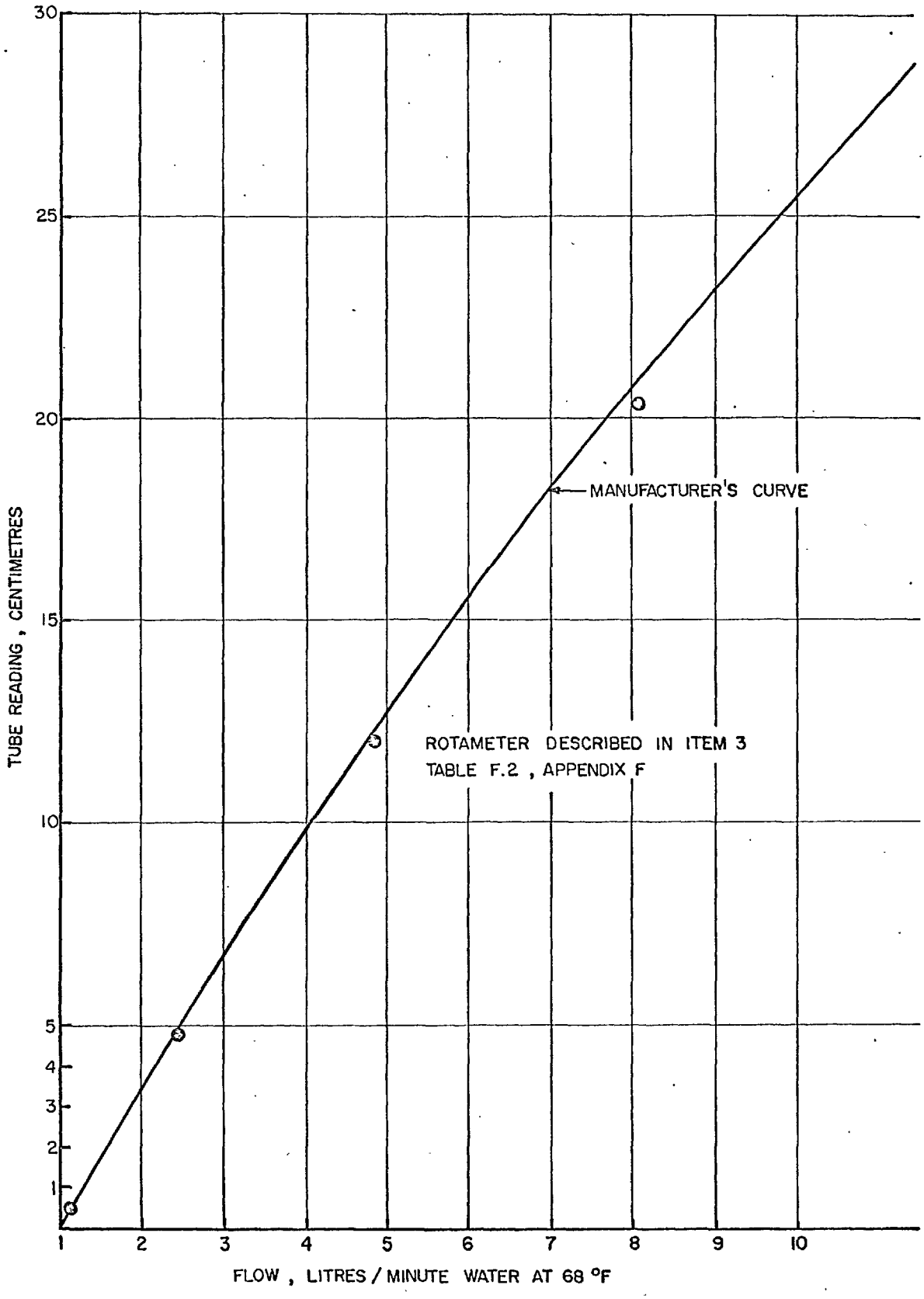

FIG. E.5 CALIBRATION OF LARGE WATER ROTAMETER

FIG. E.5

(for an uncertainty of 0.01 in. and 0.001 in the height and width of the channel respectively). Application of equation (E.1) to (D.39) yields an uncertainty of 2.5% in the water velocity.

The effect of evaporation into the air has negligible effect on the water velocity, the worst change being 0.3% because of evaporation.

Uncertainty in $u_{g,i}$ the gas velocity at entrance to the heated porous section.

The gas flow rate to the upstream injector was measured on one of two Rotameters in parallel depending on the flow rate. The small Rotameter was calibrated using a "wet-meter" (Alex Wright, 1/12 ft^3/rev, No. AW 1685, accuracy 1/4 to 1/2% depending on flow rate). The large Rotameter was calibrated using a "bubble column" (described in Ref. E.4). For the calibration, pressures of 10, 20 and 30 psig were used in the Rotameters. Subsequently, in the experimental program practically all the data were taken using a pressure of 20 psig in the Rotameters. The calibration results for 20 psig are shown in Figs. E.6 and E.7 for the small and large Rotameters respectively. The lines marked "manufacturer's curve" were obtained using the appropriate manufacturers curve for air at 15°C and 760mmHg abs pressure and corrected according to the instructions in Ref. E.5. It is estimated that the uncertainty in flow rate $\dot{m}_{g,3}$ using the calibration curves of Figs. E.6 and E.7 is approximately 2%.

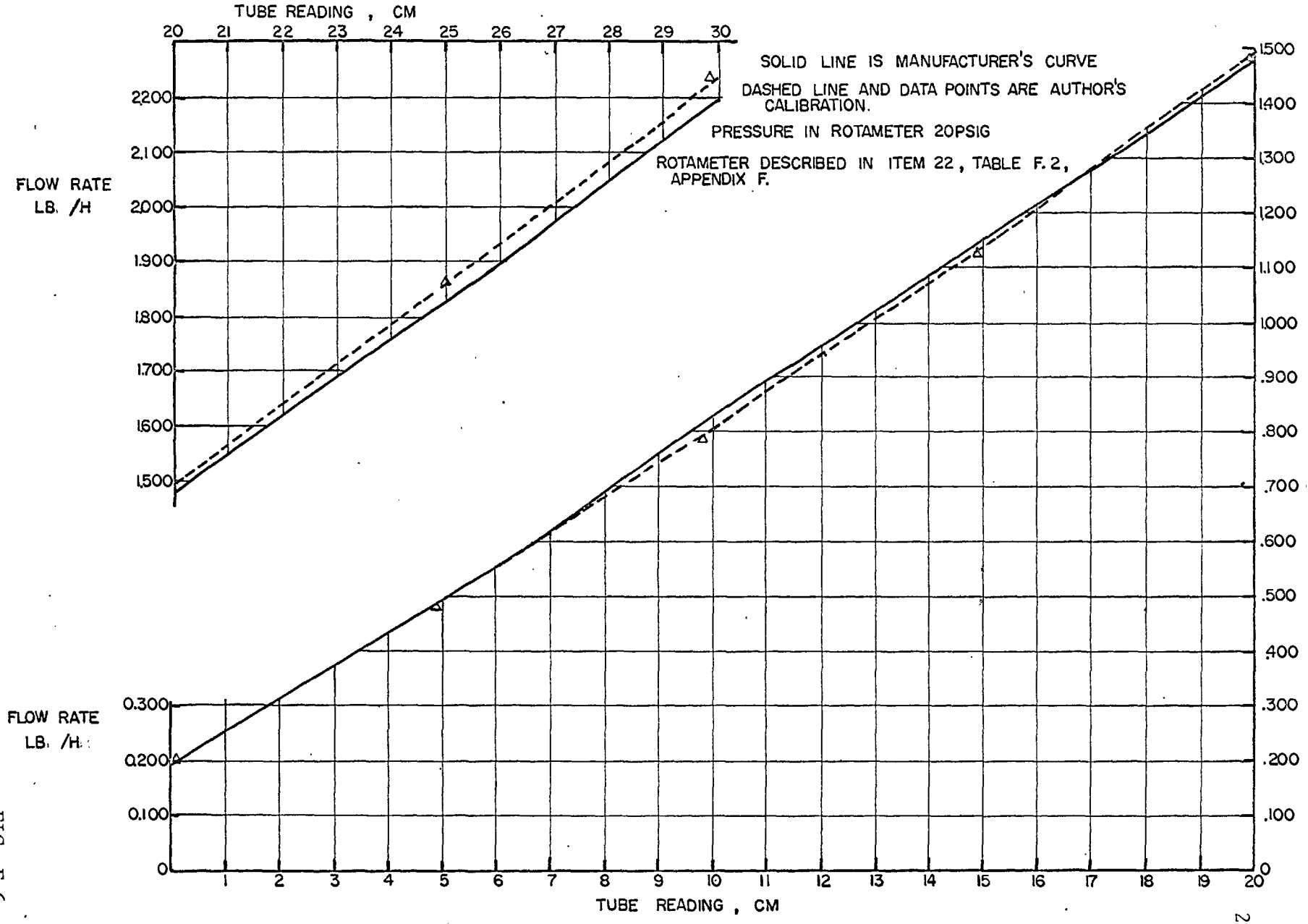

FIG. E.6 CALIBRATION OF SMALL AIR ROTAMETER

FIG. E.6

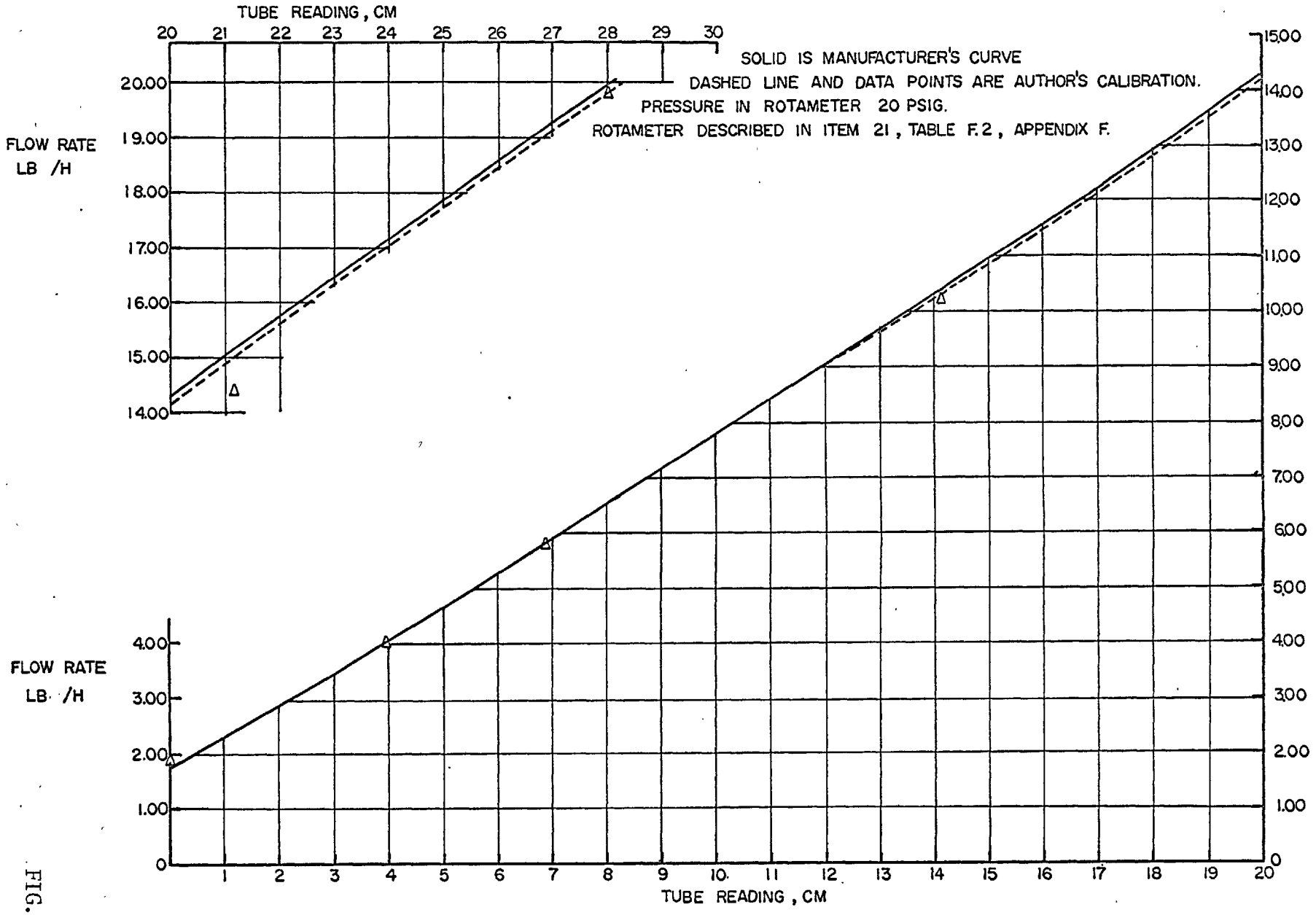

FIG. E.7 CALIBRATION OF LARGE AIR ROTAMETER

For insignificant uncertainties in the gas density at entrance to the heated porous section $\rho_{g,i}$ and an uncertainty of 2% in the cross-sectional area A_T, equation (E.1) applied to (D.40) yields an uncertainty of 2.8% in $u_{g,i}$.

In the above analysis the effect of evaporation into the air between the upstream injector and the entrance to the heated porous section was not considered(evaporation affects both the gas flow rate and the gas density). The maximum error due to this effect would be 1.1% in the gas flow rate and 0.9% in the gas density (this corresponds to the condition of air saturated with vapour at the bulk water temperature). If these are included in the uncertainty analysis there results the uncertainties: in the mass flow rate of 2.3%, in the gas density of 0.9% and in the flow area of 2% (as before); when these are combined in the appropriate manner the resulting uncertainty in $u_{g,i}$ is 3.2%.

E.2 Repeatability

The rms repeatability for the present investigation was 5.4%. The repeatability tests were of two types.

(i) After the original series of zero-inlet-quality tests were run, certain specific conditions of u_f and $\dot{V}''_g$ were selected for the repeat runs. Table E.3 presents the original data and these repeat data, the latter marked with an asterisk. At the end of the test program some of the same specific conditions were repeated. These

Table E.3 Repeat of Specific Data Points in the Original Tests With Zero-Inlet-Quality

u_f ft/s	Nominal $\dot{V}''_g$ ft/s	Original (O) or repeat (R) run	Datum no.	Actual $\dot{V}''_g$ ft/s	$\bar{\alpha}$ $\frac{Btu}{ft^2 h degF}$	$[\frac{\text{Repeat } \bar{\alpha}}{\text{Original } \bar{\alpha}} - 1] \times 100$ %
0.72	0.54	0	40-8	0.540	1484	
		R*	52-1	0.545	1481	-0.1
	0.35	0	40-12	0.360	1502	
		R*	52-2	0.349	1528	1.6
	0.11	0	40-20	0.110	1413	
		R*	52-3	0.108	1437	1.6
1.55	0.53	0	41-8	0.530	1682	
		R*	50-2	0.524	1667	-1.0
		R**	86-3	0.533	1564	-7.1
	0.36	0	41-13	0.370	1728	
		R*	50-3	0.354	1620	-6.2
	0.20	0	41-18	0.196	1648	
		R*	50-4	0.192	1652	0.2
		R**	86-1	0.199	1647	0.3
	0.11	0	41-23	0.113	1490	
		R*	50-5	0.111	1549	4.0
		R**	86-2	0.104	1467	-1.6

* Repeat data after the original series of zero-inlet-quality tests.

** Repeat data at the end of the experimental program.

Table E.4 For Tests with Finite Inlet-Quality, Comparison of $u_{g,i} = 0$ Data with Smoothed Results from Original Zero-Inlet-Quality Tests

u_f ft/s	Nominal $\hat{V}''_g$ ft/s	Datum no.	Actual $\hat{V}''_g$ ft/s	$\bar{\alpha}$ for $u_{g,i} = 0$ $\frac{Btu}{ft^2 hdegF}$	$\bar{\alpha}_o$ from smoothed curves Figs. 6.2 or 6.3 $\frac{Btu}{ft^2 hdegF}$	$[\frac{\bar{\alpha}(col.5)}{\bar{\alpha}_o(col.6)} - 1] \times 100$ %
1	2	3	4	5	6	7
Injector Arrangement 1						
0.29	0	75-2	0	140	130	7.6
	0.05	70-1	0.052	1002	975	3.0
	0.1	72-1	0.099	1362	1320	3.2
	0.2	71-1	0.203	1465	1380	6.2
	0.4	73-1	0.384	1409	1330	5.7
	0.6	69-1	0.585	1271	1275	-0.2
1.55	0	74-2	0	527	535	1.3
	0.05	67-2	0.051	1285	1120	14.8
	0.1	68-1	0.102	1526	1450	5.2
	0.2	64-1	0.204	1797	1660	8.3
	0.4	65-1	0.404	1660	1720	-3.4
	0.6	66-1	0.593	1678	1680	-0.1
5.1	0	82-2	0	1664	1512	10.0
	0.05	77-1	0.051	2070	1960	5.5
	0.1	80-2	0.101	2141	2100	2.0
	0.2	76-2	0.196	2227	2170	2.5
	0.4	81-1	0.419	2076	2190	-5.2
Injector Arrangement 2						
1.55	0	87-1	0	531	535	0.7
	0.05	85-2	0.053	1227	1140	7.6
	0.6	84-1	0.599	1538	1675	-8.0
		*	0.597*	1573*	1675	-6.2

*Average of Data 84-1, -2, -10 and -11 for this condition.

data are also included in the table and marked with two asterisks. (ii) During the finite-inlet-quality tests the first datum point taken for each fixed u_f and $\dot{V}''_g$ was with $u_{g,i} = 0$, i.e. with zero inlet-quality. For the fixed values of $\dot{V}''_g$ used in the finite-inlet-quality tests there was not necessarily a datum point at that $\dot{V}''_g$ in the original zero-inlet-quality tests. Therefore comparison was made with the smoothed results of the original zero-barbotage tests of Figs. 6.2 and 6.3. This comparison is shown in Table E.4.

An examination of the two tables shows that the range of deviation of repeat from original data, except for two points, is -8.0% to +8.3%. The rms deviation is 5.4% which is considered satisfactory.

It was noted that toward the end of the program the pressure drop across the Rigid Mesh porous material increased, possibly indicating some plugging of the porous material. This appeared to reduce the heat-transfer coefficient at the highest values of $\dot{V}''_g$ (see Table E.3, datum no. 86-3; Table E.4, data nos. 84-1, that marked with an asterisk and 81-1). The data at the end of the program for high $\dot{V}''_g$ appeared to be about 7% lower than that taken at the beginning of the program. The 7% is only marginally outside the rms repeatability of 5.4% for all the data. It is mentioned here mainly because, in comparing the effect of Injector Arrangements 1 and 2 for $u_f = 1.55$ ft/s and $\dot{V}''_g = 0.6$ ft/s, it

should therefore be kept in mind that the data for Injector Arrangement 2 (taken at the end of the program) might be raised about 7% on Fig. 6.13 to effect the comparison. The conclusions drawn would not, however, change.

For zero inlet-quality a few (a total of 11 with finite barbotage-rate) readings were taken at liquid velocities of 1.55, 3.1 and 5.1 ft/s using the observation section as entry to the porous heated section. These readings were taken after a set of repeatability runs for the normal entry. The differences in the mean heat-transfer coefficient between observation-section-entry runs and the repeatability normal-entry runs ranged from +9.1% to -19.3% (worst ever) with an algebraic mean difference of -6.6%. These differences were very small indeed compared with the changes (up 1000% in the mean heat-transfer coefficient) which were produced by varying the barbotage-rate or the inlet-quality for otherwise fixed conditions; for this reason no further tests were performed with the observation section as entry nor was an analysis attempted to explain the small existing differences. However, a paragraph of speculation does follow.

Possibly there were non-uniformities in the barbotage-rate, over and above any caused by the pressure drop in the flow channel (see Section D.8), along the length of the porous element. This would mean that for a given distance from the beginning of the

porous section, the local barbotage rate and the local quality would be different depending on the flow direction, so giving different local heat-transfer coefficients which could affect the mean heat-transfer coefficient. From the photographs of conditions in the flow channel for the normal entry it was impossible to detect any differences in local barbotage-rates as, at all but the smallest barbotage-rates, conditions near the surface were soon obscured by the two-phase mixture from upstream of the point under consideration.

References for Appendix E

E.1 S.J. Kline and F.A. McClintock, Describing uncertainties in single-sample experiments, Mechanical Engineering, 75, 3-8 (1953).

E.2 Flow Measurement, British Standards Institute, B.S. 1042 (1943).

E.3 Spiers, Technical Data on Fuels, 6th Edition, p.126.

E.4 P.L. Duffield, Diffusion-controlled electrolysis at a porous electrode, with gas injection, Ph.D. Thesis, Dept. of Mechanical Engineering, Imperial College, Univ. of London, 1966, p.206.

E.5 Rotameter Manufacturing Co., Publication No. RP 2345, "CCM Charts".

APPENDIX F DETAILED INFORMATION ON APPARATUS

This appendix gives detailed information on the tap water and apparatus (other than the test section itself) used in this investigation. The information is given for completeness.

Table F.1 presents the information relating to the composition of the water supply [F.1]. Table F.2 lists the manufacturer, model number, serial number, etc. of the equipment used; the item numbers in the table correspond with the numbers appearing in the flow and circuit diagrams, Figs. 3.2, 3.4 and 3.5. The important measuring instruments have been calibrated by the author and are so designated in the table. The accuracy of the instruments is discussed in Appendix E.

A simple wet-and dry-bulb hygrometer.

A simple wet-and dry-bulb hygrometer was manufactured for measuring the moisture content of the air supplied to the test section (see Appendix D for the use of this measurement). The device is shown in Fig. F.1. The impact tube was calibrated *in situ* against a laboratory pitot tube. Operation was at atmospheric pressure; wet and dry bulb readings were taken with an air velocity relative to the thermometers of approximately 20 ft/s or greater. The readings were converted to moisture content using a conventional psychrometric chart [F.2].

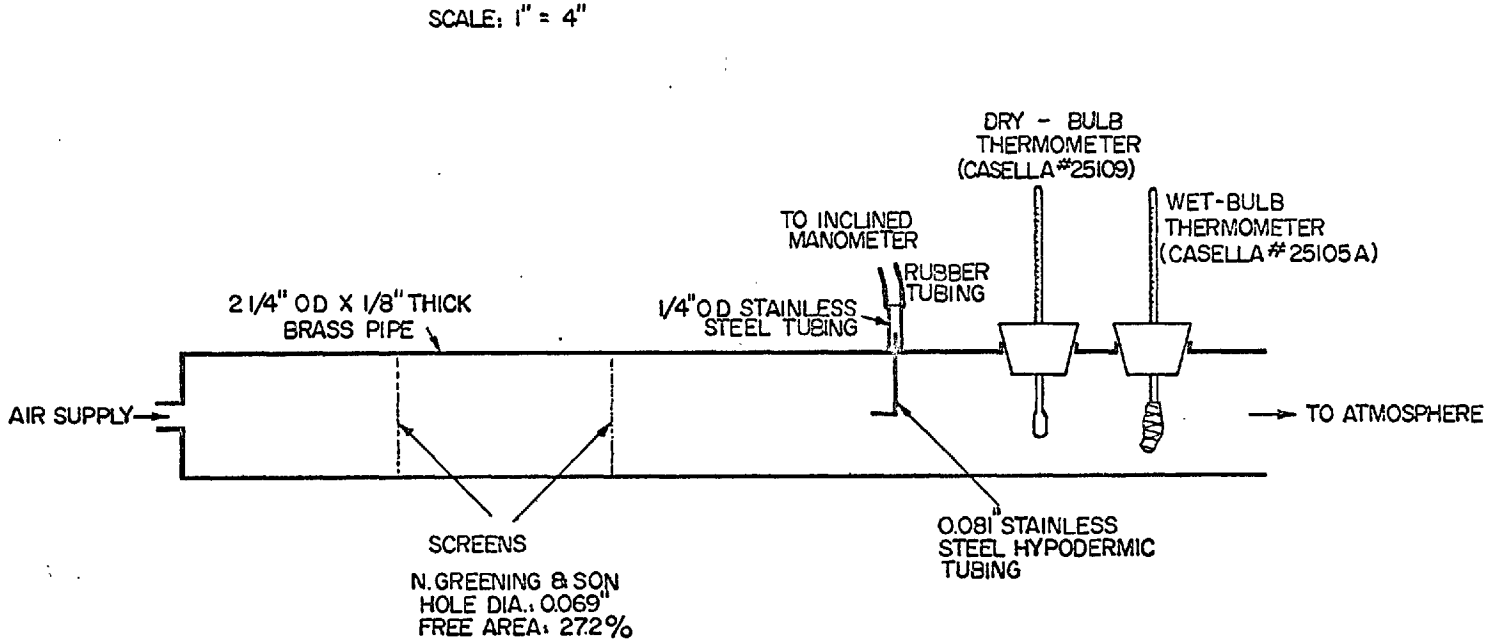

FIG. F.1 A SIMPLE WET- AND DRY-BULB HYGROMETER

References for Appendix F

F.1 E. W. Taylor, Water Examination Department, Metropolitan Water Board, London. Personal Communication.

F.2 Psychrometric chart published by the American Society of Heating, Refrigerating and Air-Conditioning Engineers, Inc. (1963).

Table F.1 Details of Water Supply

	Average for 1964 *	Average for 1965 *
Ammoniacal nitrogen	0.013	0.030
Albumoid nitrogen	0.074	0.085
Nitrate nitrogen	4.8	4.4
Oxygen absorption from $KMnO_4$, 4 hrs at 27°C	1.02	1.04
Hardness (total) $CaCO_3$	264	254
Hardness (non-carbonate) $CaCO_3$	68	68
Chloride as Cl	33	41
Phosphate as PO_4	1.4	1.9
Silicate as SiO_2	9	10
pH value	7.7	7.6
Electrical conductivity (micromhos)	540	550

* Values in mg/l unless otherwise specified.

Table F.2 Detailed Information on Apparatus

Item no. in Figs. 3.2,3.4 or 3.5	Item of equipment	Calib-rated by author	Description
Water supply to test section.			
1	Water heater		Flanged brass tube, 4-in. dia. 25-in. long arranged horizontally with 3 kW Santon Model TIHV 322 domestic immersion heater fitted internally and 2 kW heating cord externally; insulated. Controlled by Items 38 and 39, this table.
2	Water cooler		28 feet length of coiled 1/2-in. dia. copper tubing suspended in galvanized tank 16-in. dia. x 19-in. high. Water to be cooled flowed inside tubes; water and ice mixture on outside of tubes. Insulated.
3	Large Rotameter	x	Rotameter Manufacturing Co. Ltd. Type 101, No. R397147, Metric tube size 18, stainless steel float Type S.
4	Rotameter	x	Rotameter Manufacturing Co. Ltd. Type 124, No. R491680, Metric tube size 10X, stainless steel float Type S.
5	Inlet-water-temperature thermocouple	x	Saxonia Electrical Wire Co., Fe Con 40 S.W.G. (.0048 in.), Type 1A, fibre glass insulated, thermocouple wire supported in stainless steel hypodermic tubing and 1/2-in. brass elbow. Thermocouple junction covered by light coating of epoxy resin.

Table F.2 (Cont.)

Item no. in Figs. 3.2,3.4 or 3.5	Item of equipment	Calib-rated by author	Description
6	Outlet-water-temperature thermocouple	x	As for inlet-water-temperature thermocouple.
7	Vertical manometer		Vertical inverted U-tube 30-in. long. Manometer fluid: water.
8	Vertical manometer		Vertical U-tube 18-in. long. Manometer fluid: Hg, S.G. 13.6
Air supply to test section.			
9	Air filter		Vokes Ltd., Type SPL.9; insert: VAF 57 element 99.9% efficient in eliminating particles down to 5 microns.
10	Pressure-reducing valve		British Oxygen Co. Ltd. Type BHR 12.
11	Orifice	x	British Pitometer Co. Ltd. stainless steel 1/2-in. ID rig with D and D/2 taps, upstream length 8-in., downstream length 3-in. Sharp-edged orifice 1/16-in. dia.
	Manometers used with orifice:		
12	i) Vertical		Vertical U-tube 30-in. long. Manometer fluid: CCl_4, S.G. 1.585
13	ii) Micromanometer		Casella Model T10750, accuracy 0.001-in. on micrometer, 0.002-in. on graduated vertical scale; Manometer fluid: water. I.C. Invent. No. ME1459.

Table F.2 (Cont.)

Item no. in Figs. 3.2,3.4 or 3.5	Item of equipment	Calib-rated by author	Description
14	iii) Vertical		Vertical U-tube 30-in. long. Manometer fluid: Hg, S.G. 13.6
15	Air-temperature thermocouple	x	Honeywell Brown Cu Con Type T 30 B. & S.G. thermocouple wire, arranged similarly to water-temperature thermocouples; assembly insulated with mineral wool.
16	Air filter		Royal Doulton Type F91A with grade F10 element.
17	Air preheater		400 W electrical heater mounted in Sindanyo outer casing, with mixing vanes at exit. Controlled by Item 40, this table.
18	Plenum chamber		Quickfit CA 9/2/1 Type C glass "column adaptor".
19	Thermocouple in plenum chamber	x	Cu Con wire as for Item 15, this table; supported in stainless steel hypodermic tubing.
20	Manometer for plenum pressure		Vertical U-tube 30-in. long. Manometer fluid: Hg, S.G. 13.6
Air supply to upstream injector.			
21	Large Rotameter	x	Rotameter Manufacturing Co. Ltd. Type 125, No. R492886, Metric tube size 18X, Duralumin float Type A.
22	Small Rotameter	x	Rotameter Manufacturing Co. Ltd. Type 125, No. R492884, Metric tube size 7X, Duralumin, float Type A.

Table F.2 (Cont.)

Item no. in Figs. 3.2,3.4 or 3.5	Item of equipment	Calib-rated by author	Description
23	Pressure gauge	x	Budenburg zero to 60 psig, 5 1/4-in. face, No. 7889019.
24	Air temperature thermocouple	x	Honeywell Brown Fe Con Type J, 30 B. & S.G. thermocouple wire suspended at ℄ of 1/2-in. ID brass tube; insulated.
Power supply to test section.			
25	Constant-voltage transformer		Advance Components Ltd., "Volt-stat" Model CVN75/A, input 190-260 V, freq. 50 cps, output 240 V rms ± 1%, load 75 watts, sine wave output.
26	Variable auto-transformer		Zenith 2 kW, 8 amp, 230 V.
27	Transformer		2 kVA, single phase, air cooled, double wound, turns ratio 20:1, 100 amp rating on secondary.
28	Ammeter	x	Crompton Parkinson Ltd., 8-in. LKD Portable moving iron No. 1570473; ranges 0/25, 0/50, 0/100 amps.
29	Voltmeter	x	Crompton Parkinson Ltd., 8-in. LDR Portable, moving-coil rectifier type, No. 1572724, ranges 0/3, 0/10, 0/30 and 0/100 volts, sensitivity 1000 ohms/volt.

Table F.2 (Cont.)

Item no. in Figs. 3.2,3.4 or 3.5	Item of equipment	Calib-rated by author	Description
Thermocouple circuit.			
30	Thermocouples	x	i) Honeywell Brown Cu Con 30 B. & S.G. Type T, Model No. 9B1C5; fibre glass insulated.
31		x	ii) Honeywell Brown Fe Con 30 B. & S.G. Type J, Model No. 9B3C5; fibre glass insulated.
32	Selector switch		Croydon Precision Instrument Co. thermocouple switch Type SP1/P/B/1T, No. 7256 double pole, 24 position.
33	Inductance		Radio Servicing Co., Type C10/300, 300 henries, resistance 850 ohms.
34	Capacitance		Telegraph Condenser Co. Ltd., Type NL 50 microfarads.
35	Potentiometer		H. Tinsley and Co. Ltd., Type 4025, 2 dial precision potentio-meter, Serial No. 157811.
36	Galvanometer		Pye Scalamp Model EF-201
37	Standard cell		H. Tinsley and Co. Ltd., Weston Type 1268, No. 86925.
Water heater circuits.			
38	Constant-voltage transformers		Three. Advance Components Ltd., Type No. CVH1500A, input 190 - 260 V, 50 cps, output 230 V rms, load 1500 W at pf 1.0, Serial Nos. i) 127, ii) 114, iii) 115.

Table F.2 (Cont.)

Item no. in Figs. 3.2,3.4 or 3.5	Item of equipment	Calib-rated by author	Description
39	Variable auto-transformer		Two. Service Trading Co., 2 kW 230 V, 8 amp.
1	Water heater		See above in "Water supply to test section".
Air preheater circuit.			
40	Variable auto-transformer		Service Trading Co., 2 kW, 230 V, 8 amp.
17	Air preheater		See above in "Air supply to porous section".
Photographic equipment.			
	Camera		Micro Precision Products Ltd., Micro Technical Camera, 5X4, Mk VII Lens: Schneider-Kreuznach, Xenar f/4.5/150 mm focal length, No. 7402124.
	Microflash unit		Dawe Microflash Jr., Type 1722A, Serial No. 104, flash duration approx. 5 μsec, 12 joules output.
Stroboscopic equipment.			
	Stroboscopes		Two. Dawe Instruments Ltd., Stroboflash Type 1200D, 250 to 18,000 cpm; Serial Nos: (i) 1244, (ii) 14603.
	Portable flash heads		Two. Dawe Instruments Ltd., Type 1200/2, Serial Nos: (i) 6556, (ii) 378.

APPENDIX G TABULATED DATA

This appendix gives the tabulated results of the present investigation. In all cases, the heat-transfer coefficient quoted is the mean (see Section D.1). Table G.1 presents the single-phase data, Table G.2 presents the data for tests with zero inlet-quality and Table G.3 presents the data for tests with finite inlet-quality.

In Tables G.2 and G.3 the order in which the data are presented for the individual runs is as follows:

Table G.2 Zero-inlet-quality tests,

runs in order of increasing liquid velocity.

Table G.3 Finite-inlet-quality tests,

Injector Arrangement 1,

u_f = 0.29 ft/s, runs in order of increasing $\dot{V}''_g$,

u_f = 1.55 ft/s, runs in order of increasing $\dot{V}''_g$,

u_f = 5.1 ft/s, runs in order of increasing $\dot{V}''_g$,

Injector Arrangement 2,

u_f = 1.55 ft/s, runs in order of increasing $\dot{V}''_g$.

Table G.1 Single-Phase Data

u_f ft/s	Re_f at $T_{B,i}$	Datum no.	$T_{B,i}$ °F	$T_{B,e}$ °F	α_{SP} $\frac{Btu}{ft^2 hdegF}$
0.084	221	44-20	67.4_5	69.3	112
0.292	774	43-29	67.7_5	68.3	130
	778	75-2	68.1^5	68.9	140
	779	75-3	68.1_5	68.9_5	138
	783	75-4	68.6^5	69.3^5_5	140
	761	75-26	66.4_5	66.9^5_5	147
	761	75-27	66.5^5	67.5^5_5	145
0.718	1,903	40-32	67.8_5	68.0_5	297
1.55	4,126	41-31	67.9	68.1_5	535
	4,117	74-2	67.7_5	67.9^5_5	527
	4,011	74A-19	65.8^5	66.0^5	527
	4,111	87-1	67.6_5	67.9_5	531
	4,110	87-2	67.6^5	67.9^5	534
	4,106	87-15	67.5_5	67.8	540
3.08	8,134	42-35	67.7	67.8_5	960
5.08	13,460	45-32	67.8	67.9_5	1,512
	13,740	82-2	69.3_5	69.5^5_5	1,664
	13,740	82-3	69.3^5_5	69.4^5_5	1,651
	13,810	82-27	69.7^5_5	69.9^5_5	1,673
	13,810	82-28	69.7^5_5	69.8^5_5	1,654

Table G.2 Data for Tests with Zero Inlet-Quality

Datum no.	$T_{B,i}$ °F	$T_{B,e}$ °F	$\dot{V}_g''$ ft/s	α_0 $\frac{Btu}{ft^2\,h\,degF}$	P_i psia	ΔP_{chan} psi
u_f = 0.084 ft/s		Run no. 44				
44 - 1	68.1	75.3	0.654	1047	14.89	*
44 - 2	67.6	74.0	0.703	1024	14.89	
44 - 3	67.8_5	75.0	0.602	1051	14.89	
44 - 6	67.7^5	75.0_5	0.505	1068	14.91	
44 - 7	67.7	75.0^5	0.400	1099	14.89	
44 - 8	67.6	75.1^5_5	0.297	1082	14.89	
44 - 9	67.6	74.7^5	0.199	1140	14.87	
44 - 10	67.6	75.6	0.126	1169	14.87	
44 - 13	68.1	75.6_5	0.096	1184	14.87	
44 - 14	68.1	76.0^5	0.072	1155	14.87	
44 - 15	68.0	75.9	0.056	1080	14.87	
44 - 16	68.0	74.8_5	0.041	885	14.86	
44 - 17	68.5	73.8^5	0.027	635	14.86	
44 - 18	68.1	73.0	0.0133	430	14.86	
44 - 19	67.7_5	71.2	0.0066	288	14.85	
44 - 20	67.4^5_5	69.3	0	112	14.85	
Range of Re_f at $T_{B,i}$:		221 - 224				

* Less than 0.10 psi

Table G.2 Continued

Datum no.	$T_{B,i}$	$T_{B,e}$	$\dot{V}_g''$	α_0	P_i	ΔP_{chan}
u_f = 0.292 ft/s	Run no. 43					
43 - 2	67.9	70.6_5	0.613	1320	14.89	*
43 - 6	67.8	70.5^5	0.677	1252	14.89	
43 - 7	67.7_5	70.4_5	0.652	1240	14.89	
43 - 8	67.7^5	70.5^5	0.583	1264	14.90	
43 - 9	67.7	70.4_5	0.554	1265	14.89	
43 - 10	67.7	70.4^5	0.527	1269	14.89	
43 - 11	67.6_5	70.4	0.481	1283	14.89	
43 - 12	67.6_5^5	70.3_5	0.444	1294	14.89	
43 - 13	67.6^5	70.3_5^5	0.403	1290	14.89	
43 - 14	67.6_5	70.3_5^5	0.349	1357	14.89	
43 - 15	67.7_5^5	70.3_5^5	0.306	1370	14.90	
43 - 16	67.7^5	70.2^5	0.261	1382	14.92	
43 - 17	67.6_5	70.2	0.219	1379	14.96	
43 - 18	67.7^5	70.3_5	0.177	1395	14.93	
43 - 19	67.6_5	70.3_5^5	0.145	1401	14.90	
43 - 20	67.6^5	70.3_5^5	0.123	1387	14.90	
43 - 23	67.7	70.3^5	0.096	1309	14.86	
43 - 24	67.6	70.2	0.076	1191	14.83	
43 - 25	67.7	70.0_5	0.054	1056	14.83	
43 - 26	67.8	69.6^5	0.033	741	14.80	
43 - 27	67.9	69.2	0.0182	521	14.80	
43 - 28	67.8	68.7	0.0068	301	14.80	
43 - 29	67.7_5	68.3	0	130	14.80	
Range of Re_f at $T_{B,i}$:		773 - 778				

* Less than 0.10 psi

Table G.2 Continued

Datum no.	$T_{B,i}$	$T_{B,e}$	$\dot{V}_g''$	α_0	P_i	ΔP_{chan}
u_f = 0.718 ft/s		Run no. 40				
40 - 2	67.6	68.7_5	0.600	1437	15.09	*
40 - 5	67.7_5	68.9_5	0.621	1454	15.09	
40 - 6	67.7_5	68.9_5	0.643	1435	15.09	
40 - 7	67.7_5	68.9_5	0.565	1468	15.10	
40 - 8	67.8_5	69.0_5	0.540	1484	15.10	
40 - 9	67.9_5	69.0_5	0.497	1465	15.09	
40 - 10	67.9	69.0_5	0.449	1473	15.10	
40 - 11	67.8	69.0_5	0.390	1488	15.15	0.10
40 - 12	67.7_5	68.9_5	0.360	1502	15.20	0.10
40 - 13	67.8_5	68.9_5	0.316	1534	15.20	0.10
40 - 14	67.8_5	68.9_5	0.290	1515	15.20	0.10
40 - 15	67.8_5	68.9_5	0.263	1553	15.19	0.10
40 - 16	67.8	69.0_5	0.234	1542	15.18	*
40 - 17	67.8	68.8	0.210	1541	15.15	
40 - 18	67.7	68.7	0.177	1527	15.10	
40 - 19	67.6	68.7	0.158	1508	15.07	
40 - 20	67.6	68.7	0.110	1413	15.00	
40 - 24	67.7_5	68.3_5	0.136	1515	15.05	
40 - 25	67.8_5	68.6_5	0.135	1529	15.05	
40 - 26	67.8_5	68.7	0.093	1371	14.99	
40 - 27	67.9_5	68.7	0.076	1294	14.95	
40 - 28	67.9_5	68.9	0.061	1137	14.90	
40 - 29	67.9_5	68.7	0.040	905	14.89	
40 - 30	67.8	68.6	0.0297	760	14.89	
40 - 31	67.8_5	68.4	0.0164	587	14.89	
40 - 32	67.8_5	68.0_5	0	297	14.82	
Range of Re_f at $T_{B,i}$: 1896 - 1906						

* Less than 0.10 psi

Table G.2 Continued

Datum no.	$T_{B,i}$	$T_{B,e}$	$\dot{V}_g''$	α_0	P_i	ΔP_{chan}
u_f = 1.55 ft/s Run no. 41						
41 - 2	67.8	68.4	0.605	1724	15.35	0.17
41 - 5	67.9	68.4	0.650	1658	15.36	0.17
41 - 6	67.9	68.5	0.626	1674	15.36	0.17
41 - 7	67.7_5	68.3_5	0.570	1693	15.35	0.17
41 - 8	67.8^5	68.4^5	0.530	1682	15.35	0.17
41 - 9	67.8_5	68.4^5	0.499	1618	15.38	0.17
41 - 10	67.8^5	68.5^5	0.466	1711	15.40	0.17
41 - 11	67.8_5	68.5	0.440	1716	15.45	0.16
41 - 12	67.9^5	68.4_5	0.403	1715	15.50	0.16
41 - 13	67.9	68.5^5	0.370	1728	15.50	0.16
41 - 14	67.9_5	68.5	0.334	1715	15.49	0.15
41 - 15	67.9^5	68.4_5	0.298	1693	15.45	0.14
41 - 16	67.8_5	68.3^5_5	0.257	1681	15.38	0.13
41 - 17	67.8^5_5	68.3^5_5	0.220	1658	15.33	0.12
41 - 18	67.8^5_5	68.3^5	0.196	1648	15.28	0.11
41 - 20	68.0^5	68.6_5	0.161	1637	15.20	*
41 - 21	67.7	68.2^5_5	0.134	1561	15.18	
41 - 23	67.9	68.2^5_5	0.113	1490	15.10	
41 - 26	67.7	68.1^5_5	0.084	1373	15.05	
41 - 27	67.7	68.1^5_5	0.082	1251	15.01	
41 - 28	67.7_5	68.1^5_5	0.052	1146	15.01	
41 - 29	67.7^5	68.1^5	0.0294	862	14.99	
41 - 30	67.6_5	67.9	0.0109	681	14.97	
41 - 31	67.9^5	68.1_5	0	535	14.90	
Range of Re_f at $T_{B,i}$: 4111 - 4134						

* Less than 0.10 psi

Table G.2 Continued

Datum no.	$T_{B,i}$	$T_{B,e}$	$\dot{V}_g''$	α_0	P_i	ΔP_{chan}
u_f = 3.08 ft/s Run no. 42						
42 - 2	68.0	68.3	0.581	1906	15.70	0.27
42 - 5	67.6_5	67.9_5	0.643	1890	15.72	0.28
42 - 6	67.7^5	68.0^5	0.621	1911	15.72	0.27
42 - 7	68.0	68.3_5	0.607	1891	15.71	0.27
42 - 8	68.0	68.3_5	0.592	1886	15.70	0.27
42 - 10	67.8	68.5^5	0.559	1935	15.70	0.27
42 - 12	67.7	68.0	0.525	1895	15.70	0.27
42 - 13	68.0	68.2_5	0.485	1920	15.77	0.27
42 - 14	68.0	68.3_5^5	0.441	1916	15.80	0.26
42 - 15	67.7_5	68.0_5^5	0.412	1889	15.80	0.25
42 - 16	67.7_5^5	68.1^5	0.380	1861	15.72	0.25
42 - 17	67.9^5	68.2	0.350	1905	15.65	0.24
42 - 18	67.8	68.1	0.304	1904	15.55	0.22
42 - 19	67.7_5	68.1	0.276	1903	15.38	0.21
42 - 20	67.9^5	68.1_5	0.238	1906	15.22	0.19
42 - 21	67.7	67.9_5^5	0.200	1865	15.10	0.18
42 - 23	67.9	68.2^5	0.167	1869	15.35	0.16
42 - 24	67.7	68.0_5	0.138	1805	15.22	0.14
42 - 25	67.6_5	68.0^5	0.123	1760	15.23	0.13
42 - 28	67.7_5^5	68.1	0.097	1684	15.19	0.11
42 - 30	67.8^5	68.0_5	0.075	1632	15.15	0.10
42 - 31	67.8_5	68.1^5	0.058	1515	15.10	*
42 - 32	68.0^5	68.2_5	0.049	1433	15.10	↓
42 - 33	67.8	68.0^5	0.0323	1318	15.09	
42 - 34	67.8_5	68.0	0.0138	1160	15.01	
42 - 35	67.7^5	67.8_5	0	960	14.75	
Range of Re_f at $T_{B,i}$: 8130 - 8179						

* Less than 0.10 psi

Table G.2 Continued

Datum no.	$T_{B,i}$	$T_{B,e}$	$\dot{V}_g''$	α_0	P_i	ΔP_{chan}
u_f = 5.08 ft/s Run no. 45						
45 - 1	67.9_5	67.9_5	0.648	2211	16.65	0.47
45 - 2	68.0^5	68.0^5	0.667	2223	16.65	0.48
45 - 3	68.1_5	68.1_5	0.628	2201	16.62	0.48
45 - 4	68.0_5^5	68.1^5	0.608	2194	16.62	0.48
45 - 5	67.9_5^5	68.0	0.588	2196	16.55	0.48
45 - 6	68.0_5^5	68.2	0.564	2220	16.55	0.47
45 - 7	67.8_5^5	68.0	0.544	2215	16.53	0.47
45 - 10	68.2_5^5	68.5	0.511	2174	16.58	0.46
45 - 11	67.8_5^5	68.1	0.514	2192	16.66	0.45
45 - 12	68.0_5^5	68.3_5	0.476	2213	16.62	0.44
45 - 13	67.7^5	67.8_5^5	0.430	2143	16.55	0.43
45 - 14	67.7	68.0^5	0.388	2177	16.48	0.42
45 - 15	67.9_5	68.2_5	0.348	2182	16.35	0.39
45 - 17	67.9^5	68.1_5^5	0.267	2182	16.15	0.35
45 - 18	68.1	68.3_5^5	0.232	2165	16.66	0.35
45 - 19	67.9	68.1^5	0.195	2166	15.99	0.29
45 - 20	67.9_5	68.1	0.157	2121	15.89	0.26
45 - 21	67.9^5	68.0_5	0.140	2124	15.80	0.25
45 - 22	67.7_5	68.0^5	0.115	2104	15.73	0.22
45 - 25	67.8_5^5	68.0	0.113	2142	15.73	0.21
45 - 26	67.9^5	68.0	0.104	2101	15.65	0.20
45 - 27	67.7	67.8_5	0.079	2056	15.56	0.17
45 - 28	67.8	68.0^5	0.056	1995	15.49	0.15
45 - 29	67.9	68.0_5	0.0313	1837	15.20	0.12
45 - 30	67.5_5	67.8^5	0.0202	1736	15.17	0.10
45 - 31	67.6^5	67.8	0.0049	1583	15.10	*
45 - 32	67.8	67.9_5	0	1512	15.08	*
Range of Re_f at $T_{B,i}$: 13,410 - 13,520						

* Less than 0.10 psi

Table G.3 Data for Tests with Finite Inlet Quality

Datum no.	$T_{B,i}$ °F	$T_{B,e}$ °F	$\dot{V}_g''$ ft/s	$u_{g,i}$ ft/s	$\frac{u_{g,i}}{u_f}$	α_{TP} Btu/ft^2 h degF	$\frac{\alpha_{TP}}{\alpha_{SP}}$ **	P_i psia	ΔP_{chan} psi
Injector Arrangement 1									
u_f = 0.292 ft/s; $\dot{V}_g''$ = 0 Run no. 75									
75 - 2	68.1	68.9	0	0	0	140		14.78	*
75 - 3	68.1$_5$	68.9$_5$		0	0	138		14.78	
75 - 4	68.6	69.3$_5$		0	0	140		14.78	
75 - 5	68.6$_5$	69.4		0.443	1.514	263	1.85	14.78	
75 - 6	68.5$_5$	69.7		0.712	2.44	357	2.51	14.78	
75 - 7	69.0$_5$	70.3$_5$		1.113	3.81	423	3.01	14.78	
75 - 8	69.0	70.3$_5$		1.802	6.16	529	3.72	14.78	
75 - 9	68.2	69.6$_5$		2.79	9.52	350	2.46	14.79	
75 - 10	68.3	69.7$_5$		1.772	6.06	531	3.74	14.79	
75 - 11	68.2	69.6$_5$		2.38	8.13	408	2.87	14.78	
75 - 12	67.7$_5$	69.1$_5$		3.55	12.12	366	2.58	14.82	
75 - 13	67.7$_5$	69.1$_5$		4.69	16.04	399	2.81	14.79	
75 - 14	67.1$_5$	68.5$_5$		7.34	25.1	445	3.13	14.79	
75 - 15	66.8$_5$	68.1		10.43	35.6	499	3.51	14.79	
75 - 16	65.8	68.6$_5$		45.8	156.7	1138	8.01	14.98	
75 - 17	64.2	67.7$_5$		77.7	265	1522	10.72	15.23	
75 - 18	64.5	68.0		73.8	252	1478	10.40	15.23	
75 - 19	64.7$_5$	68.3$_5$		59.5	203	1326	9.34	15.09	
75 - 20	65.7$_5$	68.7$_5$		45.0	154.0	1146	8.07	14.99	
75 - 21	66.3	69.3		30.2	103.5	950	6.69	14.89	
75 - 22	66.4$_5$	69.5$_5$		21.5	73.6	738	5.19	14.85	
75 - 23	66.4$_5$	68.2$_5$		14.6	50.1	582	4.10	14.79	
75 - 24	66.5$_5$	67.7$_5$		10.6	36.2	504	3.55	14.79	
75 - 25	66.3$_5$	67.7		3.51	12.0	379	2.67	14.79	
75 - 26	66.4$_5$	66.9$_5$		0	0	147		14.78	
75 - 27	66.5$_5$	67.5$_5$		0	0	145		14.78	
Re_f at $T_{B,i}$: 738 - 788									

* Less than 0.10 psi

** α_{SP} is the average (= 142 Btu/ft^2 h degF) of Data 75 - 2, -3, -4, -26 and -27.

Table G.3 Continued

Datum no.	$T_{B,i}$ °F	$T_{B,e}$ °F	$\dot{V}_g''$ ft/s	$u_{g,i}$ ft/s	$\frac{u_{g,i}}{u_f}$	c $\frac{\text{Btu}}{\text{ft}^2\ \text{h degF}}$	P_i psia	ΔP_{chan} psi
Injector Arrangement 1								
u_f = 0.292 ft/s; nominal $\dot{V}_g''$ = 0.05 ft/s Run no. 70								
70 - 1	67.6	69.9_5	0.052	0	0	1002	14.98	*
70 - 2	67.2_5	69.7_5	0.050	0.448	1.531	1046	14.97	
70 - 3	67.3_5	69.8_5	0.051	0.720	2.46	1081	14.98	
70 - 4	67.4_5	69.9_5	0.050	1.402	4.79	1090	14.98	
70 - 5	67.4_5	69.9_5	0.053	2.33	8.00	1056	14.97	
70 - 6	67.5_5	70.0_5	0.052	3.90	13.34	1047	14.97	
70 - 7	67.3_5	69.8_5	0.051	6.89	23.6	1064	15.08	
70 - 8	67.3_5	69.7_5	0.051	8.87	30.3	1079	15.08	
70 - 9	67.4_5	69.9_5	0.051	11.95	40.8	1117	15.08	
70 - 10	65.5_5	67.5_5	0.052	73.1	250	1605	15.38	0.12
70 - 11	65.5_5	67.5_5	0.051	74.7	256	1601	15.43	0.11
70 - 12	66.0	68.1	0.050	58.2	199	1537	14.79	*
70 - 13	66.5	68.6_5	0.051	43.7	149.6	1497	15.19	
70 - 14	66.9_5	69.2_5	0.050	29.5	100.8	1375	15.18	
70 - 15	67.5_5	69.8_5	0.051	14.33	49.0	1180	15.08	
70 - 16	67.3_5	69.5_5	0.053	21.3	72.8	1299	15.08	
Re_f at $T_{B,i}$: 751 - 773								

* Less than 0.10 psi

Table G.3 Continued

Datum no.	$T_{B,i}$ °F	$T_{B,e}$ °F	$\dot{V}_g''$ ft/s	$u_{g,i}$ ft/s	$\frac{u_{g,i}}{u_f}$	α $\frac{Btu}{ft^2\ h\ degF}$	P_i psia	ΔP_{chan} psi
Injector Arrangement 1								
u_f = 0.292 ft/s; nominal $\dot{V}_g''$ = 0.1 ft/s Run no. 72								
72 - 1	67.5_5	70.2	0.099	0	0	1362	15.07	*
72 - 2	67.6^5	70.2_5	0.100	0.435	1.487	1371	15.05	
72 - 3	67.5_5	70.2^5_5	0.100	1.882	6.44	1325	15.05	
72 - 4	66.6^5_5	69.3^5	0.100	1.872	6.40	1369	15.05	
72 - 5	66.6^5	69.4_5	0.100	3.98	13.59	1351	15.03	
72 - 6	66.6	69.4^5	0.099	6.47	22.1	1351	15.05	
72 - 7	66.5_5	69.2_5	0.098	13.55	46.3	1413	15.06	
72 - 8	66.1^5_5	68.7^5	0.099	29.1	99.6	1497	15.08	
72 - 9	65.8^5	68.3	0.099	43.7	149.4	1553	15.19	
72 - 10	65.5_5	67.8_5	0.098	58.6	200	1567	15.29	0.10
72 - 11	65.2^5_5	67.3^5_5	0.098	72.0	246	1615	15.42	0.12
Re_f at $T_{B,i}$: 749 - 772								

* Less than 0.10 psi

Table G.3 Continued

Datum no.	$T_{B,i}$ °F	$T_{B,e}$ °F	$\dot{V}_g''$ ft/s	$u_{g,i}$ ft/s	$\frac{u_{g,i}}{u_f}$	α $\frac{Btu}{ft^2\ h\ degF}$	P_i psia	ΔP_{chan} psi
Injector Arrangement 1								
u_f = 0.292 ft/s; nominal $\dot{V}_g''$ = 0.2 ft/s Run no. 71								
71 - 1	68.0	70.8_5	0.203	0	0	1465	14.97	*
71 - 2	67.9_5	70.8_5	0.202	0.440	1.506	1400	14.97	
71 - 3	67.8_5	70.7_5	0.201	0.998	3.41	1413	14.97	
71 - 4	67.9_5	70.7_5	0.200	1.834	6.27	1373	14.96	
71 - 5	68.0	70.8_5	0.202	2.98	10.18	1400	14.96	
71 - 6	70.7	70.5_5	0.201	5.58	19.07	1414	14.99	
71 - 7	67.6	70.4_5	0.202	7.37	25.2	1439	14.99	
71 - 8	67.5	70.3_5	0.202	10.51	35.9	1463	15.0	
71 - 9	67.2	70.1	0.200	13.08	44.7	1479	15.05	
71 - 10	66.8	69.6_5	0.201	28.3	96.7	1502	15.0	
71 - 11	66.5_5	69.1_5	0.201	42.8	146.4	1510	15.10	
71 - 12	66.0_5	68.5_5	0.200	57.9	198.0	1487	15.21	
71 - 13	65.4_5	68.0_5	0.198	72.0	246	1515	15.35	
71 - 14	65.4_5	67.8_5	0.198	77.7	266	1514	15.39	
Re_f at $T_{B,i}$: 751 - 777								

* Less than 0.10 psi

Table G.3 Continued

Datum no.	$T_{B,i}$ °F	$T_{B,e}$ °F	$\dot{V}_g''$ ft/s	$u_{g,i}$ ft/s	$\frac{u_{g,i}}{u_f}$	α $\frac{Btu}{ft^2\ h\ degF}$	P_i psia	ΔP_{chan} psi
Injector Arrangement 1 u_f = 0.292 ft/s; nominal $\dot{V}_g''$ = 0.4 ft/s Run no. 73								
73 - 1	65.3	67.7	0.384	69.9	239	1409	15.46	0.13
73 - 2	65.7_5	68.3_5	0.384	55.2	188.6	1399	15.30	0.12
73 - 3	66.2^5	68.9^5	0.386	40.9	139.7	1386	15.26	0.10
73 - 4	66.5	69.3	0.388	26.6	90.7	1396	15.16	*
73 - 5	66.9	69.8	0.389	11.59	39.6	1362	15.10	⋮
73 - 6	67.3	70.2	0.392	3.85	13.18	1291	15.15	⋮
73 - 7	67.2_5	70.2_5	0.391	1.357	4.64	1322	15.09	⋮
73 - 8	67.2^5_5	70.2^5_5	0.392	0	0	1342	15.06	↓
Re_f at $T_{B,i}$: 749 - 770								

* Less than 0.10 psi

Table G.3 Continued

Datum no.	$T_{B,i}$ °F	$T_{B,e}$ °F	$\dot{V}_g''$ ft/s	$u_{g,i}$ ft/s	$\frac{u_{g,i}}{u_f}$	α $\frac{Btu}{ft^2\ h\ degF}$	P_i psia	ΔP_{chan} psi
Injector Arrangement 1								
u_f = 0.292 ft/s; nominal $\dot{V}_g''$ = 0.6 ft/s Run no. 69								
69 - 1	68.9	71.5_5	0.585	0	0	1271	14.90	*
69 - 2	67.3_5	70.1^5	0.579	0.445	1.522	1289	14.95	
69 - 3	67.4_5^5	70.2_5	0.579	1.1129	3.86	1285	14.99	
69 - 4	67.4^5	70.3_5^5	0.578	2.26	7.72	1263	15.00	
69 - 5	67.4_5	70.2^5	0.577	4.05	13.84	1274	15.00	
69 - 6	67.4_5^5	70.3	0.575	5.57	19.03	1282	15.00	
69 - 7	67.5_5^5	70.3	0.574	7.15	24.4	1285	15.00	
69 - 8	67.3_5^5	70.1	0.574	10.04	34.3	1309	15.00	
69 - 9	66.8_5^5	69.4_5	0.575	24.8	84.8	1356	15.05	
69 - 10	66.3^5	68.7^5	0.572	40.9	139.8	1348	15.15	0.12
69 - 11	65.9_5	68.2_5	0.573	56.1	191.9	1325	15.25	0.12
69 - 12	65.4^5	67.6^5	0.566	71.1	243	1341	15.38	0.13
69 - 13	65.1_5	67.5_5	0.561	74.8	256	1353	15.45	0.14
Range of Re_f at $T_{B,i}$: 747 - 786								

* Less than 0.10 psi

Table G.3 Continued

Datum no.	$T_{B,i}$ °F	$T_{B,e}$ °F	$\dot{V}_g''$ ft/s	$u_{g,i}$ ft/s	$\frac{u_{g,i}}{u_f}$	α_{TP} Btu / ft² h degF	$\frac{\alpha_{TP}}{\alpha_{SP}}$	P_i psia	ΔP_{chan} psi
Injector Arrangement 1									
u_f = 1.55 ft/s; $\dot{V}_g''$ = 0 (Increasing inlet quality) Run no. 74									
74 - 2	67.7_5	67.9_5	0	0	0	527	1	14.93	*
74 - 3	67.5_5	67.8_5	↓	0.388	0.250	669	1.27	15.05	↓
74 - 4	67.6^5	68.1^5		2.18	1.34	1140	2.16	15.16	
74 - 5	67.6_5	68.1_5		6.01	3.86	1148	2.17	15.16	
74 - 6	67.6^5_5	68.1^5_5		9.24	5.94	1306	2.47	15.16	0.13
74 - 7	67.6^5	68.4^5		13.81	8.88	1554	2.95	15.30	0.12
74 - 8	67.3_5	68.0		17.04	10.96	1644	3.12	15.38	0.12
74 - 10	67.5^5_5	68.1_5		23.1	14.83	1827	3.44	15.51	0.15
74 - 11	67.8^5	68.4^5_5		35.6	22.9	2281	4.33	15.75	0.18
74 - 12	67.4	68.2		52.3	33.6	2904	5.51	16.25	0.23
74 - 13	67.9_5	68.7		66.3	42.6	3510	6.65	16.74	0.27
74 - 14	68.6^5_5	69.4		71.5	45.9	3594	6.81	16.95	0.29
74 - 15	68.8^5_5	69.6		58.4	37.6	3173	6.01	16.40	0.25
74 - 16	68.3^5_5	69.1	↓	45.0	28.9	2790	5.29	16.05	0.21
Re_f at $T_{B,i}$: 4177 - 4094. For this test, one pressure tap plugged; ΔP_{chan} were obtained during the test below for the same conditions.									
(Decreasing inlet quality) Run no. 74A									
74A -1	67.3	68.1	0	71.2	45.8	3434	6.51	16.85	0.29
74A -2	67.4	68.1_5	↓	66.3	42.7	3346	6.34	16.68	0.27
74A -4	67.6	68.4^5_5		52.5	33.8	2922	5.54	16.15	0.22
74A -12	66.3_5	66.7^5_5		6.00	3.86	1173	2.22	15.08	*
74A -13	66.1^5	66.5^5_5		4.84	3.11	1193	2.26	15.56	*
74A -14	66.1	66.6^5		3.35	2.16	1397	2.65	15.20	0.11
74A -15	65.8_5	66.3_5		2.24	1.44	1106	2.10	15.10	*
74A -16	65.9^5_5	66.6^5		1.508	0.970	860	1.63	14.99	↓
74A -17	66.2^5	66.5_5		1.045	0.672	718	1.36	14.93	
74A -18	65.8	66.2^5_5		0.536	0.345	732	1.39	14.99	
74A -19	65.8	66.0^5	↓	0	0	527	1	14.87	↓
Re_f at $T_{B,i}$: 4109 - 4011									

* Less than 0.10 psi

Table G.3 Continued

Datum no.	$T_{B,i}$ °F	$T_{B,e}$ °F	$\dot{V}_g''$ ft/s	$u_{g,i}$ ft/s	$\frac{u_{g,i}}{u_f}$	α $\frac{\text{Btu}}{\text{ft}^2\ \text{h degF}}$	P_i psia	ΔP_{chan} psi
Injector Arrangement 1 u_f = 1.55 ft/s; nominal $\dot{V}_g''$ = 0.05 ft/s Run no. 67								
67 - 2	67.3_5	67.8_5	0.051	0	0	1285	14.92	*
67 - 3	67.4_5	67.9_5	0.050	0.311	0.200	1359	14.99	*
67 - 4	67.6_5	68.0_5	0.049	0.591	0.380	1400	14.99	*
67 - 5	67.6_5	68.0_5	0.049	1.925	1.238	1748	15.18	0.10
67 - 6	67.4_5	67.9_5	0.051	3.00	1.930	1877	15.23	0.11
67 - 7	67.5_5	68.0_5	0.051	5.75	3.70	1632	15.13	*
67 - 8	67.5	68.0_5	0.050	9.15	5.88	1736	15.20	0.10
67 - 9	67.4	68.0_5	0.049	12.74	8.19	1866	15.28	0.12
67 - 10	67.4	68.0_5	0.050	16.74	10.77	1983	15.37	0.12
67 - 11	67.6	68.2_5	0.050	16.80	10.80	1967	15.37	0.12
67 - 12	67.6	68.0_5	0.050	23.47	15.09	2105	15.46	0.14
67 - 13	67.3_5	67.9_5	0.049	35.0	22.5	2406	15.70	0.15
67 - 14	67.3_5	68.0_5	0.049	44.6	28.7	2640	15.95	0.18
67 - 15	67.2_5	68.0_5	0.050	51.1	32.8	2729	16.15	0.19
67 - 16	67.2_5	67.9_5	0.048	58.8	37.8	2824	16.35	0.22
67 - 17	67.1_5	67.9	0.049	66.9	43.0	2963	16.65	0.27
67 - 18	66.9_5	67.6_5	0.049	69.0	44.4	3049	16.83	0.31
Re_f at $T_{B,i}$: 4073 - 4111								

* Less than 0.10 psi

Table G.3 Continued

Datum no.	$T_{B,i}$ °F	$T_{B,e}$ °F	$\dot{V}_g''$ ft/s	$u_{g,i}$ ft/s	$\frac{u_{g,i}}{u_f}$	α $\frac{Btu}{ft^2\ h\ degF}$	P_i psia	ΔP_{chan} psi
Injector Arrangement 1 u_f = 1.55 ft/s; nominal $\dot{V}_g''$ = 0.1 ft/s Run no. 68								
68 - 1	67.5	68.0	0.102	0	0	1526	15.10	*
68 - 2	67.5_5	68.0_5	0.102	0.387	0.249	1635	15.17	
68 - 3	67.4_5^5	68.0_5^5	0.101	0.629	0.404	1635	15.19	
68 - 4	67.3_5^5	67.8_5^5	0.101	1.342	0.863	1708	15.26	
68 - 5	67.7_5^5	68.3^5	0.101	1.420	0.913	1752	15.26	
68 - 6	68.0^5	68.5	0.101	2.51	1.615	1876	15.36	0.11
68 - 7	67.9	68.4_5	0.101	5.27	3.39	1870	15.27	0.11
68 - 8	67.9_5	68.5^5	0.101	8.42	5.42	1906	15.35	0.11
68 - 9	67.9_5^5	68.4	0.099	12.57	8.09	1983	15.38	0.12
68 - 10	67.6^5	68.2_5	0.102	15.90	10.22	2090	15.48	0.13
68 - 11	67.6_5	68.2_5^5	0.099	22.2	14.29	2190	15.55	0.14
68 - 12	67.0_5^5	67.8^5	0.101	35.5	22.8	2419	15.85	0.17
68 - 13	66.8_5^5	67.6	0.100	43.8	28.2	2532	16.04	0.20
68 - 14	67.1_5^5	68.0	0.101	51.1	32.9	2646	16.23	0.22
68 - 15	67.3_5^5	68.0_5	0.099	59.5	38.29	2729	16.45	0.26
68 - 16	67.3_5^5	68.0_5^5	0.098	65.9	42.4	2821	16.70	0.30
68 - 17	67.3^5	68.0_5^5	0.098	71.6	46.1	2912	16.95	0.34
Re_f at $T_{B,i}$: 4067 - 4130								

* Less than 0.10 psi

Table G.3 Continued

Datum no.	$T_{B,i}$ °F	$T_{B,e}$ °F	$\dot{V}_g''$ ft/s	$u_{g,i}$ ft/s	$\frac{u_{g,i}}{u_f}$	α $\frac{Btu}{ft^2\ h\ degF}$	P_i psia	ΔP_{chan} psi
Injector Arrangement 1								
u_f = 1.55 ft/s; nominal $\dot{V}_g''$ = 0.2 ft/s Run no. 64								
64 - 1	67.2	67.7	0.204	0	0	1797	14.95	0.10
64 - 2	67.2	67.7	0.203	0.397	0.255	1851	14.99	0.11
64 - 3	67.0_5	67.5	0.202	0.564	0.362	1850	15.00	0.11
64 - 4	67.0^5	67.5	0.203	1.694	1.089	2022	15.17	0.12
64 - 5	66.9_5	67.4_5	0.201	4.08	2.62	2026	15.19	0.14
64 - 6	66.9^5_5	67.4^5_5	0.202	7.10	4.57	2088	15.06	0.16
64 - 7	67.0^5	67.5^5	0.205	7.14	4.59	1986	15.00	0.15
64 - 8	67.0	67.5	0.201	11.21	7.21	2043	15.10	0.17
64 - 9	66.9_5	67.4_5	0.205	15.00	9.65	2142	15.18	0.14
64 - 11	66.6^5_5	67.1^5_5	0.200	20.74	13.34	2205	15.25	0.15
64 - 12	68.3^5	68.8^5_5	0.200	36.7	23.6	2496	15.65	0.22
64 - 13	68.2	68.7^5_5	0.205	44.8	28.8	2497	15.85	0.24
64 - 14	68.0_5	68.6^5	0.198	52.0	33.4	2614	15.95	0.26
64 - 15	67.9^5	68.4_5	0.202	59.3	38.1	2767	16.37	0.31
64 - 16	67.9_5	68.5^5	0.196	66.2	42.6	2755	16.52	0.34
64 - 17	67.8^5_5	68.4	0.201	70.6	45.4	2762	16.63	0.38
64 - 18	68.3^5	68.8_5	0.205	12.82	8.25	2145	15.18	0.23
64 - 19	68.2_5	68.7^5_5	0.202	0.953	0.613	1888	15.10	0.14
64 - 20	68.3^5	68.8^5	0.202	2.16	1.392	1917	15.15	0.16
64 - 21	68.3_5	68.8_5	0.204	5.86	3.77	1963	15.05	0.16
Re_f at $T_{B,i}$: 4057 - 4149								

Table G.3 Continued

Datum no.	$T_{B,i}$ °F	$T_{B,e}$ °F	$\dot{V}_g''$ ft/s	$u_{g,i}$ ft/s	$\frac{u_{g,i}}{u_f}$	α $\frac{Btu}{ft^2\ h\ degF}$	P_i psia	ΔP_{chan} psi
Injector Arrangement 1								
u_f = 1.55 ft/s; nominal $\dot{V}_g''$ = 0.4 ft/s Run no. 65								
65 - 1	68.0	68.5$_5$	0.404	0	0	1660	15.20	0.14
65 - 2	67.9$_5$	68.5^5	0.401	0.412	0.265	1718	15.20	0.16
65 - 3	68.0^5	68.6^5	0.404	0.993	0.638	1758	15.20	0.16
65 - 4	68.3$_5$	68.9	0.408	0.997	0.641	1758	15.15	0.15
65 - 5	68.2^5	68.7$_5$	0.391	2.21	1.421	1874	15.20	0.16
65 - 6	68.2	68.8^5	0.406	2.65	1.701	1902	15.15	0.16
65 - 7	68.1$_5$	68.7^5	0.406	5.71	3.67	1902	15.09	0.15
65 - 8	68.1^5	68.6$_5$	0.402	8.91	5.73	1951	15.16	0.17
65 - 9	68.0$_5$	68.6^5	0.398	13.99	9.00	2021	15.25	0.18
65 - 10	67.9^5	68.5	0.400	19.78	12.72	2097	15.36	0.19
65 - 11	67.6$_5$	68.3	0.395	32.8	21.1	2178	15.66	0.23
65 - 12	67.9$_5$	68.5$_5$	0.388	41.2	26.5	2245	15.85	0.27
65 - 13	67.6^5	68.2^5	0.391	40.9	26.3	2233	15.87	0.27
65 - 14	67.8	68.4	0.382	49.1	31.6	2266	16.11	0.30
65 - 15	67.9	68.5	0.384	50.6	32.5	2349	16.35	0.35
65 - 16	67.8	68.4	0.380	62.9	40.42	2381	16.63	0.37
65 - 17	67.7	68.3	0.376	69.4	44.6	2446	16.78	0.41
Re_f at $T_{B,i}$: 4151 - 4107								

Table G.3 Continued

Datum no.	$T_{B,i}$ °F	$T_{B,e}$ °F	$\dot{V}_g''$ ft/s	$u_{g,i}$ ft/s	$\frac{u_{g,i}}{u_f}$	α $\frac{Btu}{ft^2\ h\ degF}$	P_i psia	ΔP_{chan} psi
Injector Arrangement 1 u_f = 1.55 ft/s; nominal $\dot{V}_g''$ = 0.6 ft/s Run no. 66								
66 - 1	67.7_5	68.3_5	0.593	0	0	1678	15.15	0.19
66 - 2	67.6^5	68.2^5	0.591	0.389	0.250	1743	15.18	0.20
66 - 3	67.5_5	68.2	0.590	0.923	0.594	1815	15.18	0.21
66 - 4	67.5^5	68.2	0.590	2.30	1.476	1899	15.25	0.23
66 - 5	68.0^5	68.6	0.595	2.28	1.466	1991	15.25	0.22
66 - 6	67.9	68.5	0.594	3.91	2.51	1929	15.25	0.20
66 - 7	67.8_5	68.4_5	0.590	6.11	3.93	1920	15.33	0.25
66 - 8	67.8^5_5	68.5^5	0.587	8.43	5.42	1946	15.34	0.22
66 - 9	67.8^5	68.5	0.585	12.32	7.92	1997	15.44	0.23
66 - 10	67.8_5	68.4_5	0.577	18.07	11.62	2057	15.55	0.24
66 - 11	67.8^5	68.4^5	0.571	30.3	19.50	2107	15.78	0.27
66 - 12	67.7_5	68.3_5	0.564	38.7	24.9	2137	16.40	0.29
66 - 13	67.6^5_5	68.3^5_5	0.560	46.4	29.9	2229	16.26	0.32
66 - 14	67.6^5	68.3^5_5	0.542	53.4	34.4	2307	16.45	0.35
66 - 15	67.4_5	68.2^5_5	0.542	61.7	39.7	2365	16.73	0.39
66 - 16	67.5^5_5	68.2^5	0.541	63.1	40.6	2355	16.75	0.50
66 - 17	67.2^5_5	67.9_5	0.538	66.9	43.0	2268	16.95	0.45
Re_f at $T_{B,i}$: 4090 - 4126								

Table G.3 Continued

Datum no.	$T_{B,i}$ °F	$T_{B,e}$ °F	$\dot{V}_g''$ ft/s	$u_{g,i}$ ft/s	$\frac{u_{g,i}}{u_f}$	α_{TP} Btu/ft² h degF	$\frac{\alpha_{TP}}{\alpha_{SP}}$ **	P_i psia	ΔP_{chan} psi
Injector Arrangement 1									
u_f = 5.08 ft/s; $\dot{V}_g''$ = 0 Run no. 82									
82 - 2	69.3_5	69.5_5	0	0	0	1664		15.26	*
82 - 3	69.3_5	69.4_5		0	0	1651		15.25	*
82 - 4	69.8_5	70.1^5		56.7	11.15	7104	4.27	21.22	0.75
82 - 5	69.9^5	70.1		55.3	10.89	6608	3.97	21.00	0.74
82 - 6	69.8_5	70.0_5		44.3	8.73	5509	3.31	19.80	0.62
82 - 7	69.9^5	70.0^5_5		35.5	6.99	4784	2.87	19.00	0.53
82 - 8	69.6_5	69.8^5_5		35.5	6.99	4839	2.91	19.00	0.58
82 - 9	69.8^5_5	70.1^5		29.7	5.85	4395	2.64	18.50	0.46
82 - 10	69.8^5	70.0_5		23.6	4.65	4134	2.48	18.00	0.41
82 - 11	69.8	70.0^5_5		17.99	3.54	3910	2.35	17.53	0.37
82 - 12	69.7_5	70.0^5		13.16	2.59	3506	2.11	17.10	0.31
82 - 13	69.8^5	70.0_5		10.39	2.05	3278	1.97	16.83	0.28
82 - 14	69.9_5	70.2^5_5		8.66	1.704	3180	1.91	16.68	0.26
82 - 15	70.0^5_5	70.3^5		6.50	1.28	3020	1.82	16.45	0.24
82 - 16	70.0^5_5	70.3		5.80	1.142	2947	1.77	16.35	0.24
82 - 17	70.1^5	70.3_5		5.11	1.006	2933	1.76	16.35	0.24
82 - 18	70.1	70.3^5_5		4.50	0.886	2865	1.72	16.33	0.23
82 - 19	70.0_5	70.3^5		3.93	0.774	2794	1.68	16.33	0.21
82 - 20	70.0^5_5	70.3		3.19	0.628	2664	1.60	16.23	0.20
82 - 21	70.0^5_5	70.2_5		2.50	0.492	2503	1.50	16.12	0.18
82 - 22	70.0^5	70.2^5_5		1.875	0.369	2311	1.39	16.00	0.16
82 - 23	69.95	70.2^5_5		1.241	0.244	2112	1.27	15.86	0.13
82 - 24	69.9_5	70.2^5_5		0.790	0.155	1994	1.20	15.76	0.11
82 - 25	69.7^5_5	70.0^5		0.600	0.118	1887	1.13	15.68	0.10
82 - 26	69.7^5_5	69.9_5		0.457	0.090	1820	1.09	15.65	*
82 - 27	69.7^5_5	69.9^5_5		0	0	1673		15.55	*
82 - 28	69.7^5_5	69.8^5_5	↓	0	0	1654		15.55	*
Re_f at $T_{B,i}$: 13,740 - 13,880									

* Less than 0.10 psi

** α_{SP} is the average (= 1661 Btu/ft² h degF) of Data 82 - 2, -3, -27 and -28.

Table G.3 Continued

Datum no.	$T_{B,i}$ °F	$T_{B,e}$ °F	$\dot{V}_g''$ ft/s	$u_{g,i}$ ft/s	$\frac{u_{g,i}}{u_f}$	α $\frac{Btu}{ft^2\ h\ degF}$	P_i psia	ΔP_{chan} psi
Injector Arrangement 1								
u_f = 5.08 ft/s; nominal $\dot{V}_g''$ = 0.05 ft/s Run no. 77								
77 - 1	67.2_5	67.5_5	0.051	0	0	2070	15.25	0.13
77 - 2	67.7_5	68.0	0.052	0.481	0.095	2137	15.30	0.14
77 - 3	65.4_5	65.6_5	0.052	1.260	0.248	2370	15.50	0.18
77 - 4	64.5	64.7_5	0.051	3.01	0.592	2621	15.85	0.24
77 - 5	65.0	65.3_5	0.052	4.69	0.922	2859	16.00	0.28
77 - 6	66.0	66.3	0.051	7.36	1.449	2905	16.15	0.30
77 - 7	65.5	65.8	0.051	11.86	2.33	3173	16.82	0.35
77 - 8	65.6	65.9	0.052	20.0	3.94	3398	17.30	0.41
77 - 9	65.7_5	66.0_5	0.051	45.1	8.88	4062	19.40	0.65
77 - 10	67.4_5	67.7_5	0.051	58.6	11.53	4400	20.00	0.74
77 - 11	65.8	66.1	0.059	29.8	5.86	3622	18.15	0.51
77 - 12	65.8	66.1	0.052	29.8	5.88	3738	18.10	0.51
77 - 13	65.8	66.1	0.053	11.98	2.36	3192	16.65	0.35
77 - 14	65.2	65.4_5	0.052	1.238	0.244	2378	15.55	0.18
Re_f at $T_{B,i}$: 12,870 - 13,450								

Table G.3 Continued

Datum no.	$T_{B,i}$ °F	$T_{B,e}$ °F	$\dot{V}_g''$ ft/s	$u_{g,i}$ ft/s	$\frac{u_{g,i}}{u_f}$	α $\frac{Btu}{ft^2\ h\ degF}$	P_i psia	ΔP_{chan} psi
Injector Arrangement 1 u_f = 5.08 ft/s; nominal $\dot{V}_g''$ = 0.1 ft/s Run no. 80								
80 - 2	66.8	67.0_5	0.101	0	0	2141	15.87	0.19
80 - 3	67.7	67.9^5	0.101	0	0	2161	15.83	0.20
80 - 4	67.6_5	67.9	0.101	0	0	2170	15.83	0.19
80 - 7	66.3^5_5	66.6_5	0.100	58.6	11.54	3923	21.50	0.91
80 - 8	66.7^5_5	67.0^5	0.101	55.0	10.83	3909	21.22	0.89
80 - 9	66.5^5	66.8	0.101	42.8	8.42	3696	19.85	0.75
80 - 10	66.4	66.6_5	0.102	28.8	5.67	3383	18.43	0.59
80 - 11	66.0	66.3^5_5	0.103	19.47	3.83	3137	17.73	0.50
80 - 12	65.8	66.0^5	0.101	10.56	2.08	2954	17.03	0.42
80 - 13	65.7	66.0	0.102	6.57	1.29	2839	16.65	0.36
80 - 14	65.6_5	66.0	0.101	4.00	0.788	2763	16.55	0.34
80 - 15	65.7^5_5	66.1	0.102	2.52	0.496	2632	16.33	0.31
80 - 16	65.9^5	66.2_5	0.102	0.84	0.165	2342	16.05	0.24
Re_f at $T_{B,i}$: 13,080 - 13,440								

Table G.3 Continued

Datum no.	$T_{B,i}$ °F	$T_{B,e}$ °F	$\dot{V}_g''$ ft/s	$u_{g,i}$ ft/s	$\frac{u_{g,i}}{u_f}$	α $\frac{Btu}{ft^2\ h\ degF}$	P_i psia	ΔP_{chan} psi
Injector Arrangement 1								
u_f = 5.08 ft/s; nominal $\dot{V}_g''$ = 0.2 ft/s Run no. 76								
76 - 2	67.2_5	67.6	0.196	0	0	2227	16.05	0.27
76 - 3	67.3_5	67.6	0.195	0.442	0.087	2318	16.20	0.28
76 - 4	67.4_5	67.7	0.201	57.2	11.26	3597	21.60	0.93
76 - 5	66.9_5	67.3_5	0.198	45.6	8.97	3326	20.20	0.85
76 - 6	67.0_5	67.2_5	0.196	30.3	5.96	3140	18.80	0.75
76 - 7	67.2_5	67.5_5	0.195	19.37	3.81	3026	17.90	0.63
76 - 8	67.0_5	67.4_5	0.204	10.16	2.00	2840	17.20	0.55
76 - 9	66.7_5	66.9_5	0.192	6.10	1.20	2758	16.85	0.50
76 - 10	67.2_5	67.6	0.198	3.47	0.68	2639	16.70	0.43
76 - 11	67.1_5	67.5	0.196	1.777	0.350	2556	16.45	0.41
Re_f at $T_{B,i}$: 13,270 - 13,380								

Table G.3 Continued

Datum no.	$T_{B,i}$ °F	$T_{B,e}$ °F	$\dot{V}_g''$ ft/s	$u_{g,i}$ ft/s	$\frac{u_{g,i}}{u_f}$	α $\frac{Btu}{ft^2\ h\ degF}$	P_i psia	ΔP_{chan} psi
Injector Arrangement 1								
u_f = 5.08 ft/s; nominal $\dot{V}_g''$ = 0.4 ft/s Run no. 81								
81 - 1	66.2_5	66.5	0.419	0	0	2076	16.45	0.43
81 - 2	66.3_5	66.5_5	0.418	0	0	2073	16.45	0.43
81 - 3	65.6_5^5	65.9_5^5	0.418	1.563	0.308	2264	16.83	0.53
81 - 4	65.0_5^5	65.3^5	0.418	3.93	0.774	2368	17.00	0.58
81 - 5	65.6^5	65.9	0.414	8.31	1.636	2432	17.15	0.60
81 - 6	65.3_5	65.6_5	0.414	16.57	3.26	2565	17.82	0.70
81 - 7	64.5^5	64.7_5^5	0.414	26.4	5.20	2658	18.60	0.80
81 - 8	64.0	64.3_5^5	0.408	41.2	8.11	2828	19.80	0.97
81 - 9	64.2	64.4^5	0.408	53.8	10.61	2978	21.30	
81 - 10	64.5	64.8	0.408	0	0	2124	16.40	0.43
Re_f at $T_{B,i}$: 12,780 - 13,200								

Table G.3 Continued

Datum no.	$T_{B,i}$ °F	$T_{B,e}$ °F	$\dot{V}_g''$ ft/s	$u_{g,i}$ ft/s	$\frac{u_{g,i}}{u_f}$	α_{TP} Btu/ft^2 h degF	$\frac{\alpha_{TP}}{\alpha_{SP}}$ **	P_i psia	ΔP_{chan} psi
Injector Arrangement 2									
u_f = 1.55 ft/s; $\dot{V}_g''$ = 0				Run no. 87					
87 - 1	67.6_5	67.9_5	0	0	0	531		14.81	*
87 - 2	67.6^5	67.9^5	↓	0	0	534		14.80	↓
87 - 3	67.3_5	67.7		0.961	0.618	726	1.36	14.86	
87 - 4	67.0^5_5	67.5_5		0.961	0.618	711	1.33	14.86	
87 - 5	67.5^5_5	67.9^5_5		1.45	0.933	779	1.46	14.93	
87 - 6	67.8^5_5	68.2^5_5		2.38	1.530	848	1.58	14.92	
87 - 7	67.6^5	68.0^5		3.43	2.21	877	1.64	14.99	
87 - 8	67.2_5	67.6		4.89	3.15	981	1.83	15.05	
87 - 9	67.1^5	67.5		6.11	3.93	1013	1.89	15.10	
87 - 10	67.2	67.9		9.19	5.91	1241	2.32	15.25	
87 - 11	67.2	67.9		23.6	15.21	1942	3.63	15.45	0.13
87 - 12	67.0_5	67.8		51.6	33.2	2821	5.28	16.12	0.24
87 - 13	66.8^5	67.5		66.6	42.9	3261	6.10	16.60	0.32
87 - 14	66.7_5	67.6		73.1	47.0	3464	6.48	16.83	0.34
87 - 15	67.5^5_5	67.8	↑	0	0	540		14.85	*
Re_f at $T_{B,i}$: 4060 - 4120									

* Less than 0.10 psi

** α_{SP} is the average (= 535 Btu/ft^2 h degF) from Data 87-1, -2, and -15.

Table G.3 Continued

Datum no.	$T_{B,i}$ °F	$T_{B,e}$ °F	$\dot{V}_g''$ ft/s	$u_{g,i}$ ft/s	$\frac{u_{g,i}}{u_f}$	α $\frac{Btu}{ft^2\ h\ degF}$	P_i psia	ΔP_{chan} psi
Injector Arrangement 2								
u_f = 1.55 ft/s; nominal $\dot{V}_g''$ = 0.05 ft/s Run no. 85								
85 - 2	68.1_5	68.6	0.053	0	0	1227	14.63	*
85 - 3	67.8_5	68.2_5	0.052	0	0	1196	14.63	*
85 - 4	67.7_5	68.5^5	0.050	72.8	46.8	3094	16.60	0.38
85 - 5	67.8^5	68.5	0.050	59.5	38.2	2815	16.05	0.30
85 - 6	67.9	68.7	0.052	35.5	22.8	2490	15.45	0.19
85 - 7	68.0	68.7_5	0.054	24.8	15.94	2190	14.08	0.15
85 - 8	68.1_5	68.9^5	0.053	12.92	8.31	1868	15.05	0.12
85 - 9	68.1^5	68.7	0.053	5.88	3.78	1445	14.80	0.10
85 - 10	67.9_5	68.5_5	0.053	2.08	1.338	1300	14.70	*
85 - 11	68.1_5^5	68.5_5^5	0.053	0	0	1175	14.68	*
Re_f at $T_{B,i}$: 4120 - 4140								

* Less than 0.10 psi

Table G.3 Continued

Datum no.	$T_{B,i}$ °F	$T_{B,e}$ °F	$\dot{V}_g''$ ft/s	$u_{g,i}$ ft/s	$\frac{u_{g,i}}{u_f}$	α $\frac{Btu}{ft^2\ h\ degF}$	P_i psia	ΔP_{chan} psi
Injector Arrangement 2								
u_f = 1.55 ft/s; nominal $\dot{V}_g''$ = 0.6 ft/s Run no. 84								
84 - 1	68.0	68.6	0.599	0	0	1538	15.28	0.14
84 - 2	67.9	68.5	0.594	0	0	1575	15.28	0.14
84 - 3	67.1	67.8	0.548	66.3	42.6	2222	17.13	0.52
84 - 4	67.3	68.1_5	0.556	52.8	34.0	2095	16.63	0.43
84 - 5	67.0_5	67.8_5	0.582	29.9	19.2	1844	16.00	0.31
84 - 6	67.8_5	68.7	0.586	17.96	11.55	1808	15.70	0.25
84 - 7	67.7_5	68.5_5	0.597	6.05	3.89	1481	15.50	0.18
84 - 8	67.8_5	68.5_5	0.606	2.24	1.444	1488	15.30	0.15
84 - 9	67.7_5	68.5	0.602	0.92	0.592	1557	15.30	0.15
84 - 10	67.6_5	68.4_5	0.599	0	0	1600	15.25	0.16
84 - 11	67.7	68.4_5	0.594	0	0	1581	15.28	0.15
Re_f at $T_{B,i}$: 4080 - 4130								

Reprinted from

International Journal of
HEAT and MASS
TRANSFER

PERGAMON PRESS

OXFORD · LONDON · NEW YORK · PARIS

Int. J. Heat Mass Transfer. Vol. 6, pp. 531–535. Pergamon Press 1963. Printed in Great Britain.

SHORTER COMMUNICATION

SIMULATION OF POOL BOILING HEAT TRANSFER BY GAS INJECTION AT THE INTERFACE

G. E. SIMS,* U. AKTÜRK† and K. O. EVANS-LUTTERODT†
Mechanical Engineering Department, Imperial College, London

NOMENCLATURE

A, a dimensionless constant;
g, gravitational acceleration, ft/h²;
g_0, constant in Newton's Second Law of Motion, $4{\cdot}17 \times 10^8$ lbm ft/lbf h²;
h, heat-transfer coefficient between the heated wall and the bulk liquid, Btu/ft² h degF;
k, thermal conductivity of the liquid, Btu/ft h degF;
K_1, Kutateladze's criterion for the critical heat flux, equation (4);
n, exponent of the Reynolds number in equations (1), (2) and (3);
N_{Nu}, Nusselt number
N_{Pr}, Prandtl number
N_{Re}, Reynolds number
} see equations (1) and (2);
p, system pressure, lbf/ft²;
P, dimensionless pressure term in equation (2);
$\dot{q}''$, heat flux measured through a control surface just on the wall side of the solid–fluid interface, Btu/ft² h;
$\dot{q}''_{cr}$, critical heat flux measured as for $\dot{q}''$, Btu/ft² h;
$\dot{V}''$, gas volume injected per unit time and unit area of heating surface or superficial gas-injection velocity, ft³/ft² h or ft/h;
$\dot{V}''_{cr}$, critical superficial gas-injection velocity corresponding to the critical superficial vapour velocity in boiling, ft³/ft² h or ft/h.

Greek symbols

α, thermal diffusivity of the liquid, ft²/h;
λ, latent heat of vaporization of the fluid, Btu/lbm;
γ, kinematic viscosity of the liquid, ft²/h;
ρ_G, density of injected gas, lbm/ft³;
ρ_L, density of liquid (saturated for boiling), lbm/ft³;
ρ_V, density of saturated vapour, lbm/ft³;
σ, surface tension for the liquid–vapour interface, lbf/ft;
σ_{LG}, surface tension for the liquid–gas interface, lbf/ft.

INTRODUCTION

IN A RECENT experimental investigation Gose, Acrivos and Petersen [1] simulated nucleate pool boiling at saturation temperature by bubbling a gas through a heated porous or drilled surface into a pool of liquid, the gas being insoluble in the liquid.

We are carrying out similar investigations, measuring both heat- and mass-transfer coefficients with a view to comparing the results with boiling heat transfer in general, and Kutateladze's [2] theory in particular. In connection with this study we have examined the data of Gose *et al.* in the light of Kutateladze's theory; with the results contained in the present note.

The comparison of the experimental results with correlations developed for boiling heat transfer will be made in two parts, closely following Kutateladze's presentation. The first part of the comparison will be made for saturation pool boiling at moderate heat fluxes and pressures; the second part for the critical heat flux (burnout).

In this note the following terms require qualification: "porous" will describe only metal plates manufactured by sintering metal powders; "drilled" will describe only solid metal plates with holes drilled through them; "incipient boiling range" will describe the region where the predominant mechanism of boiling heat transfer changes from free convection to nucleate boiling.

MODERATE HEAT FLUXES

Kutateladze obtained the following dimensionless equation for nucleate pool boiling at saturation temperature:

$$\frac{h}{k}\left[\frac{\sigma g_0}{g(\rho_L - \rho_V)}\right]^{\frac{1}{2}} = A\left(\frac{\gamma}{\alpha}\right)^{0{\cdot}35} \times \left\{\frac{\dot{q}''}{\lambda\rho_V\gamma}\left[\frac{\sigma g_0}{g(\rho_L - \rho_V)}\right]^{\frac{1}{2}}\right\}^n \left\{\frac{p g_0^{\frac{1}{2}} \cdot 10^{-4}}{[\sigma g(\rho_L - \rho_V)]^{\frac{1}{2}}}\right\}^{0{\cdot}7} \quad (1)$$

where $A = 0{\cdot}44$ and $n = 0{\cdot}7$. It will be noted that the group

$$\left[\frac{\sigma g_0}{g(\rho_L - \rho_V)}\right]^{\frac{1}{2}}$$

has the dimension of length so that the dimensionless group

$$\frac{h}{k}\left[\frac{\sigma g_0}{g(\rho_L - \rho_V)}\right]^{\frac{1}{2}}$$

* Research Assistant.
† Research Student.

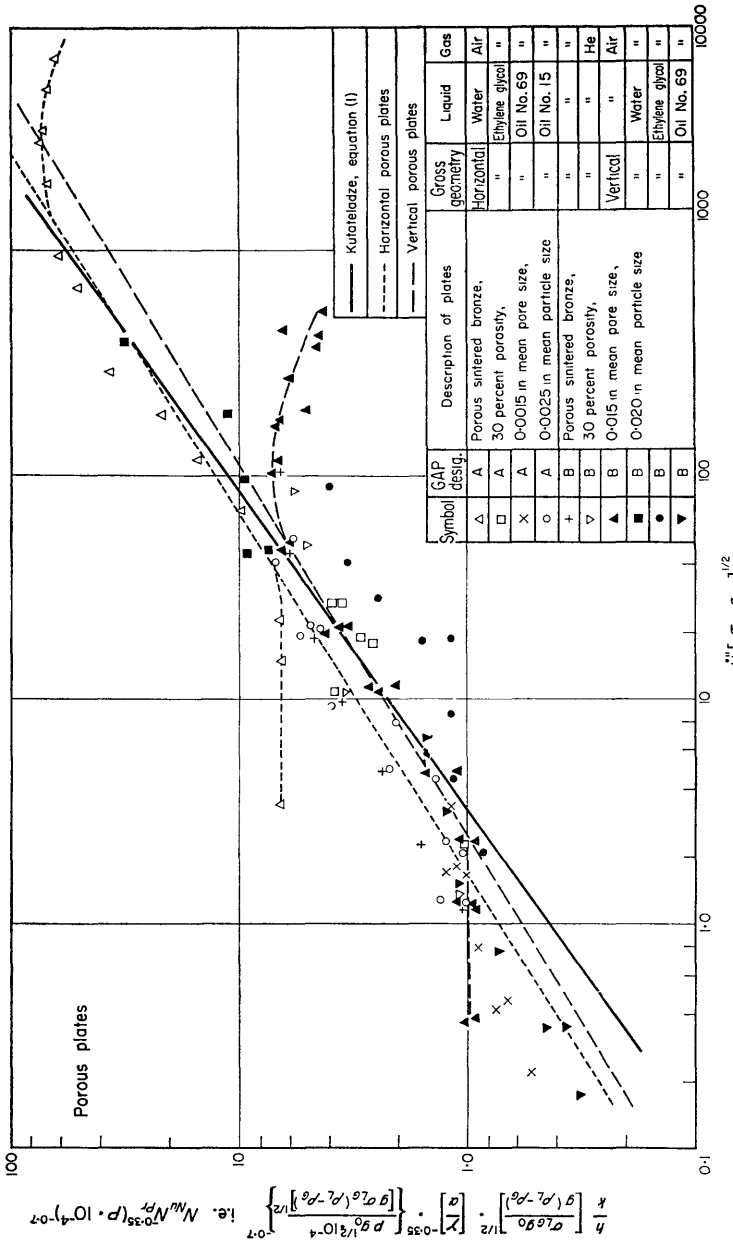
Kutateladze, equation (1)
Horizontal porous plates
Vertical porous plates
Porous plates
Symbol | GAP desig. | Description of plates | Gross geometry | Liquid | Gas
△ | A | Porous sintered bronze, | Horizontal | Water | Air
□ | A | 30 percent porosity, | " | Ethylene glycol | "
× | A | 0·0015 in mean pore size, | " | Oil No. 69 | "
○ | A | 0·0025 in mean particle size | " | Oil No. 15 | "
+ | B | Porous sinfered bronze, | " | " | He
▽ | B | 30 percent porosity, | " | " | Air
▲ | B | 0·015 in mean pore size, | Vertical | " | "
■ | B | 0·020 in mean particle size | " | Water | "
● | B | | " | Ethylene glycol | "
▼ | B | | " | Oil No. 69 | "
100
10
1·0
0·1
1·0
10
100
1000
10000
$\frac{\nu''}{\nu}\left[\frac{\sigma_{Lg}\, g_0}{g(\rho_L-\rho_0)}\right]^{1/2}$ i.e. N_{Re}
$\frac{h}{k}\left[\frac{\sigma_{Lg} g_0}{g(\rho_L-\rho_0)}\right]^{1/2}\cdot\left[\frac{\nu}{a}\right]^{-0.35}\cdot\left\{\frac{\rho\, g_0^{1/3}10^{-4}}{[g\,\sigma_{Lg}(\rho_L-\rho_0)]^{1/2}}\right\}^{-0.7}$ i.e. $N_{Nu}N_{Pr}^{-0.35}(P\cdot 10^{-4})^{-0.7}$

Fig. 1a.

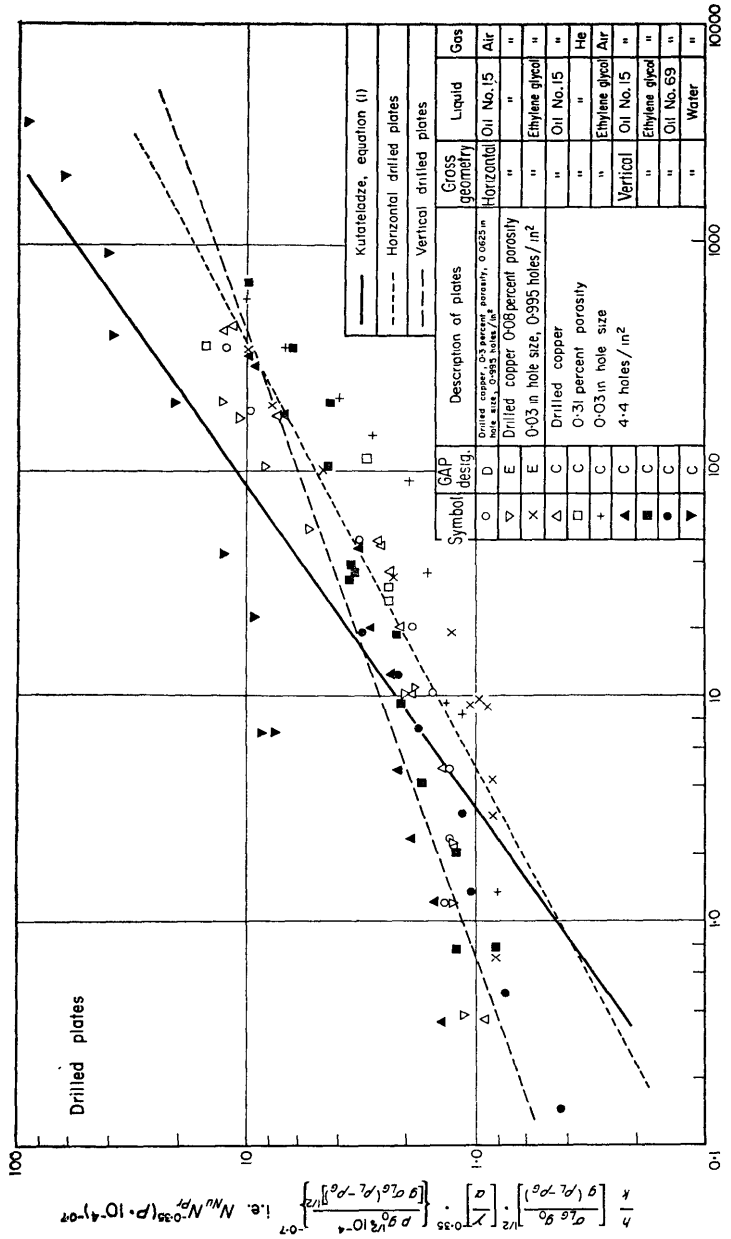

Fig. 1b.

FIG. 1. Gas injection compared to saturation pool boiling at moderate heat fluxes.

is a form of Nusselt number, N_{Nu}, and the dimensionless group

$$\frac{\dot{q}''}{\lambda\rho_V\gamma}\left[\frac{\sigma g_0}{g(\rho_L-\rho_V)}\right]^{\frac{1}{2}}$$

is a form of Reynolds number, N_{Re}, since the group $\dot{q}''/\lambda\rho_V$ has the dimensions of velocity. The group γ/α is the usual Prandtl number, N_{Pr}, and the group

$$\frac{pg_0^{\frac{1}{2}}}{[\sigma g(\rho_L-\rho_V)]^{\frac{1}{2}}}$$

is a dimensionless pressure term, P. Equation (1) then, can be rewritten as

$$N_{Nu} = A \,.\, N_{Pr}^{0\cdot35} \,.\, N_{Re}^{n} \,.\, (P \,.\, 10^{-4})^{0\cdot7} \qquad (2)$$

The group $\dot{q}''/\lambda\rho_V$ is the volume time rate of vapour production by boiling per unit area of heating surface or the "superficial" vapour velocity; in the gas-injection case it is replaced by the term $\dot{V}''$, the gas volume injected per unit time and area of heating surface; $\dot{V}''$ is equal to the "superficial" gas velocity. For the latter case, equation (1) becomes

$$\frac{h}{k}\left[\frac{\sigma_{LG}g_0}{g(\rho_L-\rho_G)}\right]^{\frac{1}{2}} = A\left(\frac{\gamma}{\alpha}\right)^{0\cdot35} \times \left\{\frac{\dot{V}''}{\gamma}\left[\frac{\sigma_{LG}g_0}{g(\rho_L-\rho_G)}\right]^{\frac{1}{2}}\right\}^{n}\left\{\frac{pg_0^{\frac{1}{2}}\,.\,10^{-4}}{[\sigma_{LG}g(\rho_L-\rho_G)]^{\frac{1}{2}}}\right\}^{0\cdot7} \qquad (3).$$

Equation (3) can also be rewritten as equation (2).

A plot of $N_{Nu} \,.\, N_{Pr}^{-0\cdot35} \,.\, (P \,.\, 10^{-4})^{-0\cdot7}$ vs. N_{Re} is shown in Fig. 1. The various systems of heated surfaces, gross geometry, liquids and gases are given in the key to the symbols. All the tests were performed at atmospheric pressure; the fluid properties were evaluated at the heated surface temperature.

In Figs. 1a and b straight lines have been drawn for the points corresponding to horizontal porous plates, vertical porous plates, horizontal drilled plates and vertical drilled plates. Kutateladze's relationship, equation (1), has also been drawn for the comparison. The values of the constant, A, and the exponent of the Reynolds number, n, appearing in equation (3) were were found from Fig. 1 to be:

	A	n
Porous plates, horizontal,	0·72	0·62
vertical,	0·58	0·60
Drilled plates, horizontal,	0·43	0·53
vertical,	1·14	0·36

Kutateladze used $A = 0{\cdot}44$ and $n = 0{\cdot}7$ for nucleate pool boiling at saturation temperature.

Inspection of Fig. 1a shows that Kutateladze's equation for moderate heat fluxes correlates the porous-plate data. On the other hand, it is seen from Fig. 1b that the slopes of the lines for the drilled plates are quite different from that proposed by Kutateladze; there is also considerable scatter of data points.

For the porous plates, the curves of h vs. $\dot{V}''$ exhibited maxima beyond which h decreased with increasing $\dot{V}''$. For the drilled plates, no such maxima existed.

In Fig. 1a, the data points in the vicinity of maximum heat-transfer coefficients and beyond them, also those corresponding to the incipient boiling range have not been included. However, the results for the complete range of gas-injection rates for two porous-plate systems have been included in order to illustrate the type of data points rejected, and in particular to illustrate the existence of maximum heat-transfer coefficients. Kutateladze's correlation does not fit, and indeed is not meant to fit, the region corresponding to incipient boiling and the region of maximum heat-transfer coefficients. The complete range of drilled-plate results have been included because the rejection of any data points corresponding to the region of incipient boiling would have not been justified as this region was not well defined; nor did maximum heat-transfer coefficients exist.

The drilled-plate systems are unlike boiling in the existence of very few centres of gas injection (nucleating sites in boiling) and in the constancy of the number of sites throughout the range of injection rates. The absence of maxima in the h vs. $\dot{V}''$ curves is probably related to this. Gose *et al.* suggest the following tentative explanation ". . . the velocity of the gas leaving the drilled holes is much greater than the velocity of the gas leaving the pores, and these jets of gas can penetrate the layer of gas tending to form an insulating film near the wall".

CRITICAL HEAT FLUXES

Kutateladze, postulating that the critical heat flux (burnout) is a hydrodynamic phenomenon, derived, by a combination of physical reasoning and dimensional analysis, the following relationship for saturation pool boiling:

$$\frac{\dot{q}''_{cr}}{\lambda\rho_V^{\frac{1}{2}}\,[gg_0\sigma(\rho_L-\rho_V)]^{\frac{1}{4}}} = K_1 = \text{constant} = 0{\cdot}16 \pm 0{\cdot}03. \qquad (4)$$

The value of the constant was determined from existing experimental data on boiling.

The quantity $\dot{q}''_{cr}/\lambda\rho_V$ represents the superficial vapour velocity under burnout conditions; in the gas-injection case this group is replaced by $\dot{V}''_{cr}$, the critical superficial gas velocity. For the latter case, equation (4) becomes

$$\frac{\dot{V}''_{cr}\rho_G^{\frac{1}{2}}}{[gg_0\sigma_{LG}\,(\rho_L-\rho_G)]^{\frac{1}{4}}} = K_1. \qquad (5)$$

K_1 has been evaluated from the data of Gose *et al.* and the results are shown in Table 1. The values of $\dot{V}''_{cr}$ used in equation (5) were the superficial gas velocities at which the maximum heat-transfer coefficients occurred.

In Table 1 the values of K_1 are certainly of the correct

Table 1. Kutateladze's critcal heat flux criterion applied to gas injection.

G, A and P plate designation	Gross geometry	Liquid	Injected gas	K_1, equation (5)
A	Horizontal	Water	Air	0·13
A	Horizontal	Shell Tellus oil No. 15	Air	0·14
B	Horizontal	Shell Tellus oil No. 15	Air	0·16
A	Horizontal	Ethylene glycol	Air	0·23
A	Horizontal	Shell Tellus oil No. 69	Air	0·02
B	Vertical	Shell Tellus oil No. 69	Air	0·05
B	Vertical	Water	Air	0·05
B	Vertical	Ethylene glycol	Air	0·10
B	Vertical	Shell Tellus oil No. 15	Air	0·12

NOTE: A description of the porous plates is given in the key to the symbols in Fig. 1.

order of magnitude and three of the values are within the range 0·13–0·19 as determined by Kutateladze. If the effect of heater orientation is taken into account, then the results are even better than they at first appear.

The values of K_1 obtained by Kutateladze were for heaters having a horizontal orientation. Bernath [3], in assessing the effect of heater orientation, found that the critical heat fluxes for heaters with vertical orientation were approximately three-quarters of those for horizontal. The only system tested by Gose *et al.* in the horizontal and vertical positions was that of oil No. 15, air and plate B; K_1 for the vertical position ($K_1 = 0{\cdot}12$) is indeed three-quarters of that for the horizontal position ($K_1 = 0{\cdot}16$). The values of K_1 for the vertical position of heaters could then be expected to fall between $\frac{3}{4}$ (0·13) and $\frac{3}{4}$ (0·19), i.e. between 0·10 and 0·14. Considering the effect of heater orientation, then, three of the five horizontal systems and two of the four vertical systems give values of K_1 within the expected ranges.

However, there were some sources of error in evaluating K_1; for certain systems there was difficulty in assessing the value of $\dot{V}''_{cr}$ because of the lack of data points near the maximum h. This was especially true for the system of vertical plate B, with water and air ($K_1 = 0{\cdot}05$). But, for the system which had the lowest value of K_1 (0·02), the selection of the $\dot{V}''_{cr}$ was comparatively easy as the curve was well defined. This system involved oil No. 69, the most viscous liquid tested, which may account for part of the large discrepancy.

The critical superficial *gas* velocity has been used to correspond to the critical superficial *vapour* velocity. This might have introduced a source of discrepancy since in boiling the superficial vapour velocities at the maximum heat-transfer coefficient and at the critical heat flux are not necessarily the same.

CONCLUSIONS

Kutateladze's relationships for moderate heat fluxes and for the critical heat flux correlate satisfactorily the porous-plate results of Gose, Acrivos and Petersen. Porous-plate systems therefore appear to simulate nucleate pool boiling at saturation temperature.

The results of Gose, Acrivos and Petersen for the drilled plates are not correlated by Kutateladze's relationship for moderate heat fluxes and no phenomenon corresponding to the critical heat flux in boiling occurred. Thus, as a simulation of boiling, the use of drilled plates is not satisfactory.

REFERENCES

1. E. E. GOSE, A. ACRIVOS and E. E. PETERSEN, Heat transfer to liquids with gas evolution at the interface, presented at the Mexico City meeting of the A.I.Ch.E. (1960).
2. S. S. KUTATELADZE, Heat transfer in condensation and boiling, (1952); translated as U.S. Atomic Energy Commission report, A.E.C.-tr-3770 (1959).
3. L. BERNATH, A theory of local boiling burnout and its application to existing data, *Chem. Engng. Progr. Symp. Ser.* **56**, No. 30, 95–116 (1960).